

A BEAM TEST FOR ADHESIVES

by

Valerie F. Fior

Thesis submitted to the Faculty of the
Virginia Polytechnic Institute and State University
in partial fulfillment of the requirements for the degree of
Master of Science
in
Engineering Mechanics

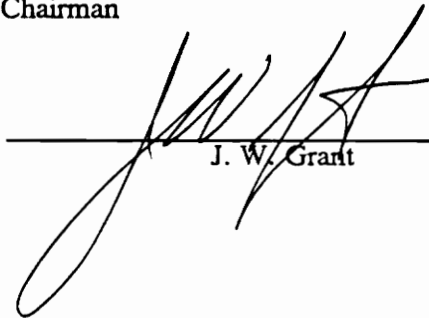
APPROVED:



H. F. Brinson, Chairman



D. A. Dillard



J. W. Grant

July, 1988

Blacksburg, Virginia

LD
5655
V855
1988

F567

c.2

A BEAM TEST FOR ADHESIVES

by

Valerie F. Fior

H. F. Brinson, Chairman

Engineering Mechanics

(ABSTRACT)

The strength of materials solution for a new bonded cantilever beam test specimen to determine adhesive shear properties is reviewed and discussed. A parametric analysis for the adhesive shear stress and for the end deflection reveals the specimen dimensions required for reliable bonded adhesive shear properties determination. Recommendations are provided for conducting reproducible tests. A pure and quasi-uniform shear test for stiff adhesives is proposed.

Analytical solutions are compared with Finite Element solutions from VISTA and NOVA for the stresses in the adhesive. It appears that the assumption of pure shear is nearly valid even for very stiff and/or very thick adhesives. In order to increase the end point deformations for stiff adhesives, a modified specimen is proposed. Three-dimensional effects through the thickness of the adhesive layer are studied with the program ABAQUS.

Experiments were performed using the two methods derived from theory and good correlation between theory and experiment were obtained with some restrictions. For both methods, experimental results underlined the need for defining proper specimen geometry prior to testing. Simple numerical codes are proposed to facilitate this purpose.

Acknowledgements

The author is grateful to the Office of Naval Research which provided the funding for this work.

Dr Hal F. Brinson is acknowledged for his advising and his help for writing this report.

Many thanks are extended to the to faculty, staff and students of the Center for Adhesion Science (VPI) and the Engineering Science and Mechanics Department (VPI) for their suggestions, help and encouragement throughout this work.

Table of Contents

1 - INTRODUCTION	1
2 - LITERATURE REVIEW	8
3 - OPTIMIZATION OF THE BMC THEORY	23
3.1 - DEFINITION OF SPECIMEN GEOMETRY	24
3.1.1 - Slenderness ratio l/h	24
3.1.2 - Thickness ratio t/h	24
3.2 - FROM THE SHEAR DEFORMATION TO THE SHEAR MODULUS	30
3.2.1 - Parametric analysis	38
3.2.2 - Example of the specimen dimension determination	44
3.2.3 - Proposal for a unique specimen dimension	47
3.2.4 - Definition of a specimen dimension for property measurement with Scanning Electron Microscopy (SEM)	49
3.3 - A LOAD DEFLECTION TEST TO DETERMINE THE ADHESIVE SHEAR MODULUS	51
3.3.1 - Influence of the adherend shear deformation on deflection	52

3.3.2 - Parametric analysis	55
4 - FINITE ELEMENTS METHODS (FEM) APPLIED TO THE ANALYSIS OF THE BMC SPECIMEN	59
4.2 - EXTENSION OF THE BMC THEORY TO PLANE STRAIN	60
4.2.1 - Shear stress distribution in a state of plane strain	60
4.2.2 - Deflection of the beam in a state of plane strain	61
4.3 - DESCRIPTION OF THE FEM CODES AVAILABLE	62
4.3.1 - Influence of the Finite Element mesh on the stress distribution	63
4.4 - COMPARISON OF BMC THEORY WITH FEM RESULTS	66
4.5 - STRESS ANALYSIS WITHIN THE ADHESIVE	73
4.5.1 - Effects of the adhesive thickness on the stress state	73
4.5.2 - Three-dimensional stress analysis in the adhesive	83
4.5.2.1 - Boundary conditions	86
4.5.2.2 - Results and discussion	88
4.5.3 - Comparison of the stress state in the adhesive between the BMC test specimen and a modified BMC specimen	114
4.5.3.1 - Finite Element model	114
4.5.3.2 - Results and discussion	114
5 - EXPERIMENTAL APPROACH	121
5.1 - SPECIMEN PREPARATION	121
5.2 - EXPERIMENTAL SET-UP	122
5.3 - SHEAR DEFORMATION MEASUREMENTS	128
5.4 - DEFLECTION MEASUREMENTS	141
5.5 - DISCUSSION OF THE RESULTS	156
5.5.1 - Determination of the adhesive shear modulus from the shear deformation measure- ments	156

5.5.2 - Evaluation of the adhesive shear modulus from the end deflection measurements .	166
6 - CONCLUSION AND RECOMMENDATIONS	176
BIBLIOGRAPHY	182
Appendix A. Supplements to the parametric analysis	184
Listing of the program for computing the data points of the curves alpha bar versus E/Ga.	185
Listing of the program for computing the data points of the curves beta versus E/Ga. . . .	186
Execs for plotting outputs	188
Vita	197

List of Illustrations

Figure 1. BMC test specimen.	2
Figure 2. Comparison of the BMC specimen behavior with the limit cases.	3
Figure 3. Comparison of the BMC specimen deflection with the limit cases.	5
Figure 4. Shear strain determination for the case of no adhesion.	5
Figure 5. Bondline shear stresses in lap shear specimen (from reference 9).	11
Figure 6. Bondline tensile stresses in lap shear specimen (from reference 9).	11
Figure 7. Torsion test geometry.	12
Figure 8. Iosipescu shear test (from reference 12).	12
Figure 9. Arcan specimen showing (a) the loading frame and (b) the butterfly specimen (from reference 14).	14
Figure 10. Variation of the shear stress along the adhesive for various values of alpha bar.	16
Figure 11. Dependence of the end deflection of the BMC on the beam deformability for various geometries (from reference 6).	18
Figure 12. Determination of the adhesive shear stiffness by measuring the end deflection (from reference 6).	19
Figure 13. Shear strain versus load.	20
Figure 14. End deflection versus load.	21
Figure 15. Definition of the slenderness ratio.	25
Figure 16. Definition of the thickness ratio.	27
Figure 17. Definition of the thickness ratio - refinement for thin adhesives.	27
Figure 18. Definition of the thickness ratio - refinement for very thin adhesives.	28
Figure 19. Variation of the maximum shear stress with adherend-adhesive stiffnesses for $l/h = 96$, $t/h = 0.02$ - limitations of the BMC shear deformation test.	31

Figure 20.	Variation of the maximum shear stress with adherend-adhesive stiffnesses for $l/h = 192$, $t/h = 0.04$ - limitations of the BMC shear deformation test.	33
Figure 21.	Variation of the maximum shear stress with adherend-adhesive stiffnesses for $l/h = 24$, $t/h = 0.02$ - limitations of the BMC shear deformation test.	34
Figure 22.	Variation of the shear strain with the stiffness ratio for various geometries (from reference 6).	36
Figure 23.	Three situations for adhesive shear stiffness determination.	39
Figure 24.	Variation of alpha bar as a function of the stiffness ratio. From left to right, each curve is associated with a value of ℓ/h which varies from 10 to 160 in steps of 10.	42
Figure 25.	Variation of alpha bar with x/ℓ	43
Figure 26.	Alpha bar versus E/Ga with $\ell/h = 10$ and $t/h = 0.05$. Example of specimen dimension determination from an estimate of the stiffness ratio.	45
Figure 27.	Influence of the shear term on the end deflection. From left to right, ℓ/h varies from 1 to 10 in steps of 1 between each curve.	54
Figure 28.	Variation of beta versus E/Ga . From left to right, ℓ/h varies from 20 to 170 in steps of 10 between each curve.	56
Figure 29.	Variation of beta versus E/Ga . From left to right, ℓ/h varies from 20 to 170 in steps of 10 between each curve.	57
Figure 30.	Variation of beta versus E/Ga . Example of specimen determination from an estimate of the stiffness ratio.	58
Figure 31.	Finite Element mesh used with VISTA.	64
Figure 32.	Finite Element mesh used with NOVA.	64
Figure 33.	Influence of the mesh refinement on the stress singularity at the tip. Solid curve : mesh with 16 elements in the length direction. Triangles : mesh with 24 elements in the length direction.	65
Figure 34.	Comparison of the beam deflection obtained with VISTA (triangles), NOVA (diamonds) in plane stress. Solid curve : plane stress BMC theory. Dashed curve : plane strain BMC theory.	69
Figure 35.	Comparison of numerical and theoretical dimensionless end deflections for the cases computed with NOVA in plane stress.	70
Figure 36.	Comparison of numerical and theoretical dimensionless end deflections for the cases computed with VISTA in plane strain.	71
Figure 37.	Analysis of the mid-plane shear stress distribution for the SEM specimen. Solid curve : theory. Triangles : FE with NOVA. $P = 100$ Lb. $E/Ga = 260$ $l = 3$ in. $h = 0.125$ in. $2t = 0.005$ in.	72
Figure 38.	Iso-stress curves in the adhesive layer with $2t = 0.005$ in..	74
Figure 39.	Iso-stress curves in the adhesive layer with $2t = 0.01$ in..	75

Figure 40. Iso-stress curves in the adhesive layer with $2t = 0.025$ in..	76
Figure 41. Iso-stress curves in the adhesive layer with $2t = 0.05$ in..	77
Figure 42. Iso-stress curves in the adhesive layer with $2t = 0.25$ in..	78
Figure 43. Stress diagrams at $x/\ell = 0.5$ for $\ell/h = 10$, $t/h = 0.10$ and $E/Ga = 260,000$	80
Figure 44. Stress diagrams at $x/\ell = 0.5$ for $\ell/h = 10$, $t/h = 0.10$ and $E/Ga = 260$	81
Figure 45. Three-dimensional element with node numbering.	84
Figure 46. Three-dimensional mesh of the BMC specimen.	85
Figure 47. Load distribution at $x = \ell$ and $y = \pm(h + t)$	89
Figure 48. Locations in the adhesive where numerical results with ABAQUS are presented.	91
Figure 49. Beam deflection from three-dimensional analysis. $P = 100$ Lb., $E/Ga = 26000$, $\ell/h = 10$ and $t/h = 0.1$	93
Figure 50. Beam deflection from three-dimensional analysis. $P = 100$ Lb., $E/Ga = 26000$, $\ell/h = 10$ and $t/h = 0.05$	94
Figure 51. Beam deflection from three-dimensional analysis. $P = 100$ Lb., $E/Ga = 260$, $\ell/h = 10$ and $t/h = 0.1$	95
Figure 52. Beam deflection from three-dimensional analysis. $P = 100$ Lb., $E/Ga = 260$, $\ell/h = 10$ and $t/h = 0.05$	96
Figure 53. Shear stress in the adhesive layer from three-dimensional analysis. $P = 100$ Lb., $E/Ga = 26000$, $\ell/h = 10$ and $t/h = 0.1$	97
Figure 54. Shear stress in the adhesive layer from three-dimensional analysis. $P = 100$ Lb., $E/Ga = 26000$, $\ell/h = 10$ and $t/h = 0.05$	98
Figure 55. Shear stress in the adhesive layer from three-dimensional analysis. $P = 100$ Lb., $E/Ga = 260$, $\ell/h = 10$ and $t/h = 0.1$	99
Figure 56. Shear stress in the adhesive layer from three-dimensional analysis. $P = 100$ Lb., $E/Ga = 260$, $\ell/h = 10$ and $t/h = 0.05$	100
Figure 57. Tensile stress σ_x in the adhesive layer from three-dimensional analysis. $P = 100$ Lb., $E/Ga = 26000$, $\ell/h = 10$ and $t/h = 0.1$	101
Figure 58. Tensile stress σ_x in the adhesive layer from three-dimensional analysis. $P = 100$ Lb., $E/Ga = 26000$, $\ell/h = 10$ and $t/h = 0.05$	102
Figure 59. Tensile stress σ_x in the adhesive layer from three-dimensional analysis. $P = 100$ Lb., $E/Ga = 260$, $\ell/h = 10$ and $t/h = 0.1$	103
Figure 60. Tensile stress σ_x in the adhesive layer from three-dimensional analysis. $P = 100$ Lb., $E/Ga = 260$, $\ell/h = 10$ and $t/h = 0.05$	104
Figure 61. Tensile stress σ_y in the adhesive layer from three-dimensional analysis. $P = 100$ Lb., $E/Ga = 26000$, $\ell/h = 10$ and $t/h = 0.1$	105

Figure 62. Tensile stress σ_y in the adhesive layer from three-dimensional analysis. $P = 100$ Lb., $E/Ga = 26000$, $\ell/h = 10$ and $t/h = 0.05$	106
Figure 63. Tensile stress σ_y in the adhesive layer from three-dimensional analysis. $P = 100$ Lb., $E/Ga = 260$, $\ell/h = 10$ and $t/h = 0.1$	107
Figure 64. Tensile stress σ_y in the adhesive layer from three-dimensional analysis. $P = 100$ Lb., $E/Ga = 260$, $\ell/h = 10$ and $t/h = 0.05$	108
Figure 65. Tensile stress σ_z in the adhesive layer from three-dimensional analysis. $P = 100$ Lb., $E/Ga = 26000$, $\ell/h = 10$ and $t/h = 0.1$	109
Figure 66. Tensile stress σ_z in the adhesive layer from three-dimensional analysis. $P = 100$ Lb., $E/Ga = 26000$, $\ell/h = 10$ and $t/h = 0.05$	110
Figure 67. Tensile stress σ_z in the adhesive layer from three-dimensional analysis. $P = 100$ Lb., $E/Ga = 260$, $\ell/h = 10$ and $t/h = 0.1$	111
Figure 68. Tensile stress σ_z in the adhesive layer from three-dimensional analysis. $P = 100$ Lb., $E/Ga = 260$, $\ell/h = 10$ and $t/h = 0.05$	112
Figure 69. Finite elements mesh used with VISTA for the analysis of a short adhesive.	115
Figure 70. Comparison of the shear stress distribution between a short adhesive and a long adhesive. Solid curve : results from VISTA for short adhesive. Dashed curve : results from theory for long adhesive.	117
Figure 71. Iso-stress curves in the short adhesive layer with $2t = 0.05$ in..	118
Figure 72. Tensile stress σ_x at different locations in the short adhesive layer.	119
Figure 73. Tensile stress σ_y at different locations in the short adhesive layer.	120
Figure 74. Specimen configuration.	123
Figure 75. Experimental set-up.	127
Figure 76. Krieger gage on the BMC specimen.	129
Figure 77. Shear strain versus load. Specimen RB1. Comparison of theory (solid curve) with experiments (triangles).	130
Figure 78. Shear strain versus load. Specimen RB2. Comparison of theory (solid curve) with experiments (triangles).	131
Figure 79. Shear strain versus load. Specimen RB3. Comparison of theory (solid curve) with experiments (triangles).	132
Figure 80. Shear strain versus load. Specimen RB4. Comparison of theory (plane and slashed lines) with experiments (triangles and diamonds) for two measurement locations on the beam.	133
Figure 81. Shear strain versus load. Specimen RB5. Comparison of theory (solid curve) with experiments (triangles).	134

Figure 82. Shear strain versus load. Specimen RB6. Comparison of theory (solid and dashed curves) with experiments (triangles, diamonds, squares).	135
Figure 83. Shear strain versus load. Specimen RB7. Comparison of theory (solid and dashed curves) with experiments (triangles and diamonds).	136
Figure 84. Shear strain versus load. Specimen ARB1. Comparison of theory (solid curve) with experiments (triangles).	137
Figure 85. Shear strain versus load. Specimen ARB2. Comparison of theory (solid curve) with experiments (triangles).	138
Figure 86. Shear strain versus load. Specimen ARB3. Comparison of theory (solid curve) with experiments (triangles).	139
Figure 87. Shear strain versus load. Specimen ARB4. Comparison of theory (solid curve) with experiments (triangles).	140
Figure 88. End deflection versus load. Specimen RB3. Comparison of theory (solid curve) with experiments (triangles).	142
Figure 89. End deflection versus load. Specimen RB4. Comparison of theory (solid curve) with experiments (triangles).	143
Figure 90. End deflection versus load. Specimen RB5. Comparison of theory (solid curve) with experiments (triangles).	144
Figure 91. End deflection versus load. Specimen RB6. Comparison of theory (solid curve) with experiments (triangles).	145
Figure 92. End deflection versus load. Specimen RB7. Comparison of theory (solid curve) with experiments (triangles).	146
Figure 93. End deflection versus load. Specimen ARB1. Comparison of theory (solid curve) with experiments (triangles).	147
Figure 94. End deflection versus load. Comparison of theory (solid curves) with experiments for specimen ARB2 (triangles) and specimen ARB3 (diamonds).	148
Figure 95. End deflection versus load. Specimen ARB4. Comparison of theory (solid curve) with experiments (triangles).	149
Figure 96. End deflection versus load. Specimen EAL1. Comparison of theory (solid curve) with experiments (triangles).	150
Figure 97. End deflection versus load. Specimen EAL2. Comparison of theory (solid curve) with experiments (triangles).	151
Figure 98. End deflection versus load. Specimen EAL3. Comparison of theory (solid curve) with experiments (triangles).	152
Figure 99. End deflection versus load. Specimen EAL4. Comparison of theory (solid curve) with experiments (triangles).	153
Figure 100. End deflection versus load. Specimen EAL5. Comparison of theory (solid curve) with experiments (triangles).	154

Figure 101.	End deflection versus load. Specimen EAL6. Comparison of theory (solid curve) with experiments (triangles).	155
Figure 102.	Shear strain versus stiffness ratio. Graphical comparison between theory and experiments. Top : specimen RB1. Bottom : specimen RB2.	159
Figure 103.	Shear strain versus stiffness ratio. Graphical comparison between theory and experiments. Top : specimen RB3. Bottom : specimen RB4.	160
Figure 104.	Shear strain versus stiffness ratio. Graphical comparison between theory and experiments. Top : specimen RB5. Bottom : specimen RB6.	161
Figure 105.	Shear strain versus stiffness ratio. Graphical comparison between theory and experiments for specimen RB7.	162
Figure 106.	Shear strain versus stiffness ratio. Graphical comparison between theory and experiments. Top : specimen ARB1. Bottom : specimen ARB2.	163
Figure 107.	Shear strain versus stiffness ratio. Graphical comparison between theory and experiments. Top : specimen ARB3. Bottom : specimen ARB4.	164
Figure 108.	Dimensionless end deflection versus stiffness ratio. Graphical comparison between theory and experiments. Top : specimen RB3. Bottom : specimen RB4.	168
Figure 109.	Dimensionless end deflection versus stiffness ratio. Graphical comparison between theory and experiments. Top : specimen RB5. Bottom : specimen RB6.	169
Figure 110.	Dimensionless end deflection versus stiffness ratio. Graphical comparison between theory and experiments for specimen RB7.	170
Figure 111.	Dimensionless end deflection versus stiffness ratio. Graphical comparison between theory and experiments. Top : specimen ARB1. Bottom : specimen ARB2.	171
Figure 112.	Dimensionless end deflection versus stiffness ratio. Graphical comparison between theory and experiments. Top : specimen ARB3. Bottom : specimen ARB4.	172
Figure 113.	Dimensionless end deflection versus stiffness ratio. Graphical comparison between theory and experiments. Top : specimen EAL1. Bottom : specimen EAL2.	173
Figure 114.	Dimensionless end deflection versus stiffness ratio. Graphical comparison between theory and experiments. Top : specimen EAL3. Bottom : specimen EAL4.	174
Figure 115.	Dimensionless end deflection versus stiffness ratio. Graphical comparison between theory and experiments. Top : specimen EAL5. Bottom : specimen EAL6.	175
Figure 116.	Parametric analysis for alpha bar versus E/Ga with $t/h = 0.1$. From left to right, ℓ/h varies from 10 to 170 in steps of 10 between each curves.	189
Figure 117.	Parametric analysis for alpha bar versus E/Ga with $t/h = 0.2$. From left to right, ℓ/h varies from 10 to 170 in steps of 10 between each curves.	190
Figure 118.	Parametric analysis for alpha bar versus E/Ga with $t/h = 0.02$. From left to right, ℓ/h varies from 10 to 170 in steps of 10 between each curves.	191
Figure 119.	Parametric analysis for alpha bar versus E/Ga with $t/h = 0.04$. From left to right, ℓ/h varies from 10 to 170 in steps of 10 between each curves.	192

Figure 120. Parametric analysis for beta versus E/Ga with $t/h = 0.1$. From left to right, ℓ/h varies from 20 to 170 in steps of 10 between each curves.	193
Figure 121. Parametric analysis for beta versus E/Ga with $t/h = 0.2$. From left to right, ℓ/h varies from 20 to 170 in steps of 10 between each curves.	194
Figure 122. Parametric analysis for beta versus E/Ga with $t/h = 0.01$. From left to right, ℓ/h varies from 20 to 170 in steps of 10 between each curves.	195
Figure 123. Parametric analysis for beta versus E/Ga with $t/h = 0.02$. From left to right, ℓ/h varies from 20 to 170 in steps of 10 between each curves.	196

List of Tables

Table 1.	Comparison of the BMC model with the limit cases (P = 10 Lb.).	22
Table 2.	Variety of valuable beam lengths.	26
Table 3.	Review of literature of adhesive material properties.	37
Table 4.	Definition of a unique specimen geometry for BMC shear deformation test applied to stiff adhesives (limit of validity : $E/Ga \leq 1000$).	48
Table 5.	Definition of a specimen dimension for SEM application with $2t = 0.005$ in. and $l = 3$ in.	50
Table 6.	Definition of geometrical and material properties used as input data for the numerical analysis.	67
Table 7.	Numerical results from FEM codes VISTA and NOVA compared with BMC theory (P = 100 Lb.).	68
Table 8.	Definition of geometrical and material properties used as input data for the numerical analysis with ABAQUS.	90
Table 9.	Rubber-to-steel specimens.	124
Table 10.	Rubber-to-aluminum specimens.	125
Table 11.	Epoxy-to-aluminum specimens.	126
Table 12.	Comparison between experiments and theory for the calculation of the adhesive shear modulus from shear deformation measurements (P = 10 Lb.).	157
Table 13.	Comparison between experiments and theory for the calculation of the adhesive shear modulus from the end deflection measurements.	167

List of Symbols

BMC	bonded cantilever beams method named by its three inventors Brinson, H. F., Moussiaux, E. and Cardon, A. H.
P	load
h	adherend's thickness
t	half adhesive's thickness
ℓ	beam's length
b	beam's width
E	Young's modulus of the adherends
ν	Poisson's ratio of the adherends
G	shear modulus of the adherends
E_a	Young's modulus of the adhesive
ν_a	Poisson's ratio of the adhesive
G_a	shear modulus of the adhesive
v	beam deflection
δ	beam end deflection
u	longitudinal displacement
τ, τ_{xy}	shear stress

γ, γ_{xy}	shear strain
σ_x	tensile stress in the x direction
σ_y	tensile stress in the y direction
σ_z	tensile stress in the z direction
$\bar{\alpha}$	geometrical and material properties dependent parameter
β	dimensionless end deflection
ξ	one-dimensional local coordinate system
N_i	interpolation functions
f_i	nodal force contribution

1 - INTRODUCTION

In bonded structures adhesives are intended to carry shear loads and hence most test specimen geometries have been designed and oriented towards the determination of shear properties which could be used in the design of joints. However, many test specimens such as the single lap or thick adherend have complex stress distributions in the adhesive layer and failures are often related to peel stresses and the high stress concentration at the bond terminations [1]. Other specimens such as the Iosipescu or the Arcan do have nearly uniform pure shear in the adhesive layer. However, their shapes are complex and, therefore, do not lend themselves to routine testing. Hence, the ideal test for adhesives should be one which eliminates the drawbacks mentioned above and the cantilever beam to be discussed herein seems to be a reasonable approach.

Recently, Brinson and collaborators [2-5] have suggested the need of better test specimen geometries especially for durability predictions. The cantilever beam shear test specimen (BMC) is suggested as a better means of obtaining shear properties and is made by bonding together two thin plates. When concentrated and equal loads act on the free end of each adherend (fig.1), the state of stress is pure shear in the adhesive layer.

In order to emphasize the reason for the interest of the so-called BMC specimen, three cantilever beams subjected to a total load P are presented in fig.2. The three beams are all the same

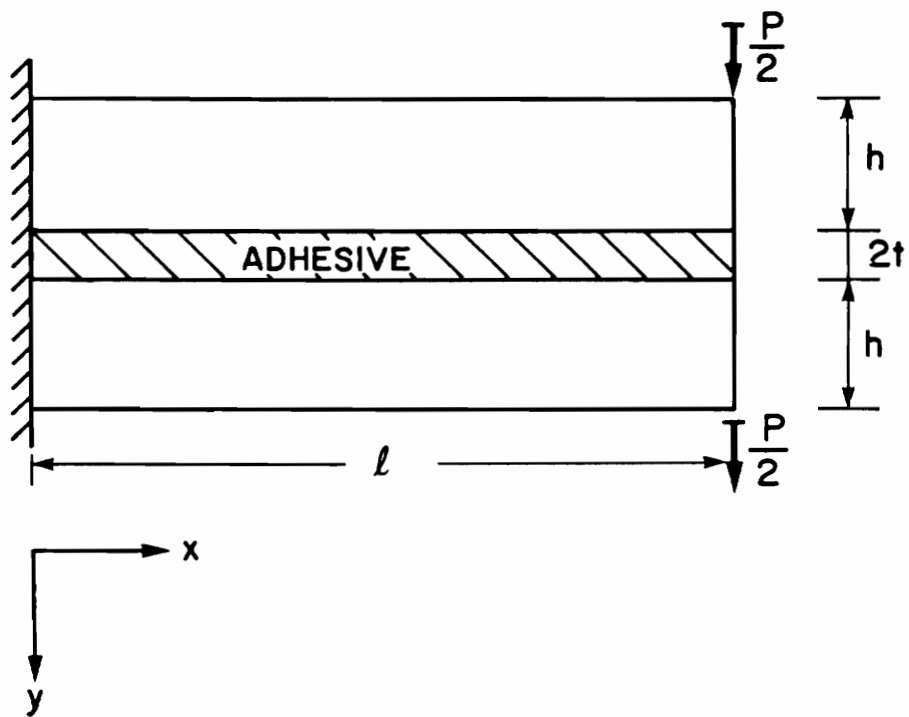
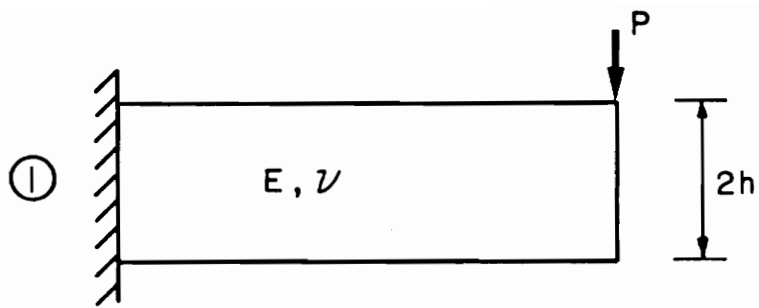
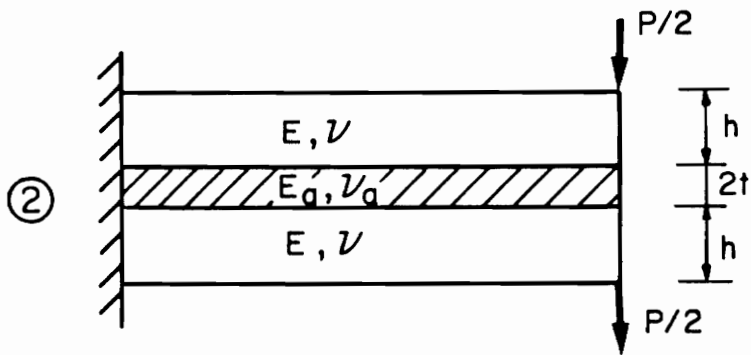


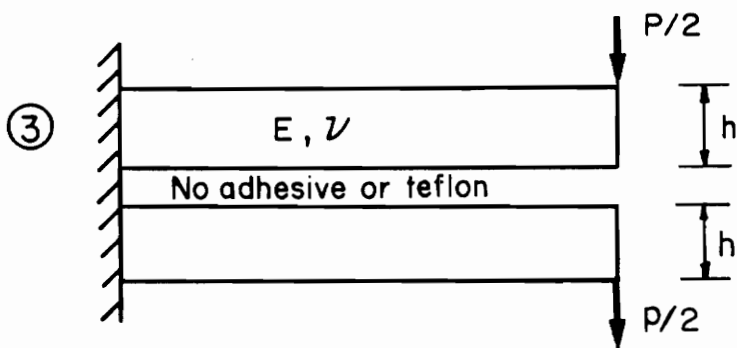
Figure 1. BMC test specimen.



Monolithic beam



BMC specimen



Beams with no adhesive

Figure 2. Comparison of the BMC specimen behavior with the limit cases.

length and thickness to permit a comparison of the deflections. The bonded beam deflects more than the monolithic beam $2h$ and less than the third (fig.3) when there is no adhesive.

In the case of the monolithic beam shown in fig.2, which could be thought of as a case of perfect adhesion, the maximum deflection at the beam tip equals,

$$\delta_1 = \frac{2P\ell^3}{Ebh^3} \quad (1)$$

and the shear stress given by strength of materials is :

$$\tau = \frac{3P}{4bh} \quad (2)$$

Assuming a linear elastic material, the shear strain is as follows :

$$\gamma = \frac{\tau}{G} \quad (3)$$

or,

$$\gamma_1 = \frac{3P}{4Gb} \quad (4)$$

For the third case when there is no adhesion, the maximum deflection is,

$$\delta_3 = \frac{16P\ell^3}{Ebh^3} \quad (5)$$

Examining case three more closely reveals that the displacement of points A and point B on the top and bottom beams as shown in fig.4 are,

$$u_A = \frac{3P}{2Eb} \left(\frac{\ell}{h} \right)^2 \quad (6)$$

$$u_B = -\frac{3P}{2Eb} \left(\frac{\ell}{h} \right)^2 \quad (7)$$

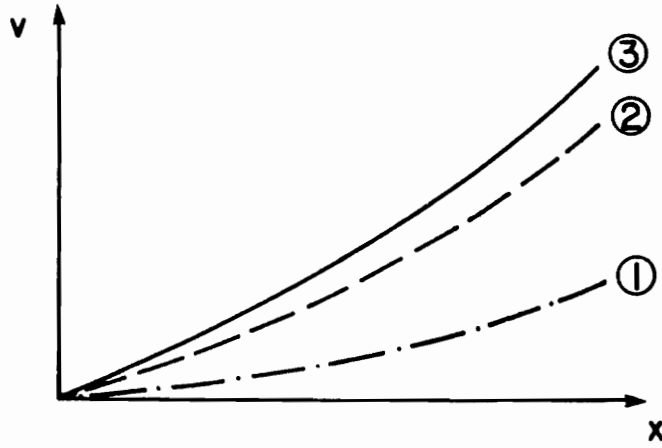


Figure 3. Comparison of the BMC specimen deflection with the limit cases.

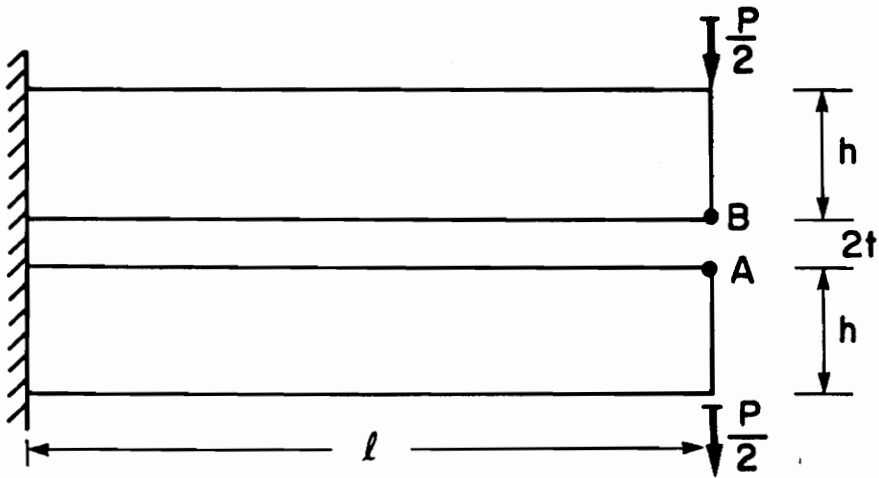


Figure 4. Shear strain determination for the case of no adhesion.

The relative motion divided by the space between the beams is,

$$\gamma = \frac{u_A - u_B}{2t} \quad (8)$$

which yields the following apparent strain for the case of no adhesion,

$$\gamma_3 = \frac{3P}{2Eb} \left(\frac{\ell}{h} \right)^2 \quad (9)$$

Obviously, case two shown in fig.2 for two adhesively bonded beams would have a maximum deflection between that of the limiting cases one and three given by equations (1) and (5), respectively. A relative comparison of the three cases is shown in fig.3. Further, it is intuitively obvious that case two would be a case of pure shear and the magnitude of the strains for this case would be bounded by the strains given above for cases one (equation 4) and three (equation 9) which represent the cases of perfect adhesion and zero adhesion, respectively.

E. Moussiaux [6] has developed a strength of materials type stress analysis to model the behavior of the bonded cantilever beam. Our purpose herein is to carry on the analysis of the BMC specimen. The theoretical model and the first suggestions to determine the adhesive shear modulus are reviewed, analyzed and optimized. Due to the complexity of the stress equation and the beam deflection equation as well, a parametric analysis is generated and gives important conclusions about the use of the theory to design a proper test specimen.

Next, numerical methods give more information about the stress state in the adhesive layer and the conditions required for a pure shear state. Two finite-elements codes (VISTA, NOVA) are used to verify the solution obtained by Moussiaux. It should be noted that Moussiaux's simple theory is for the case of plane stress while the Finite Element code VISTA is for the case of plane strain. The former theory has thus been extended to obtain a complete comparison between the simple beam theory and the finite element numerical results. In addition, three-dimensional effects on the state of stresses are studied in the adhesive layer and at the interface between adherend and adhesive using the Finite Element code ABAQUS.

An experimental program is also outlined and presented to verify analytical solutions. Both steel and aluminum adherends and neoprene rubber and epoxy resin adhesives are investigated. Measurements of shear deformation in the adhesive layer and end deflection of the beam allow us to compare the experimental results to analytical predictions.

2 - LITERATURE REVIEW

The use of adhesive bonding as a joining technique has become an attractive alternative due to a number of disadvantages with conventional fastening techniques especially for non-metallic materials. For example, traditional connectors such as bolts, rivets, welds and screws do not distribute loads uniformly. High stress concentrations occur and reduce the strength of the connection at comparatively small loads. These become serious problems when the components are made of polymeric or composite materials.

Compared to traditional fasteners, adhesive bonds provide a greater uniformity in load distribution and some other potential advantages:

- higher joint strength, damage tolerance and fatigue life,
- no reduced strength of composites due to fastener holes,
- lower part count,
- reduced weight,
- easier processing,
- cost saving for operation, maintenance and fuel,
- reduced corrosion problems.

Despite these advantages, some factors have caused the adhesive joints to be considered sensitive and unpredictable, and hence, wider usage of adhesives has been limited. Some of these disadvantages are given below:

- the complexity of stress and failure analyses of adhesives,
- the difficulty of analyzing the quality and reliability of adhesives,
- the lack of an acceptable standard design and testing methodology for mechanical characterization,
- the disparity between bulk adhesive properties and adhesive properties in the bonded state that often make the former unusable in predicting the response of a full scale structural elements.

The basic features of the adhesive bond problems were examined in the classic analysis of Goland and Reissner [7]. In their work, the adherends were assumed to deform as thin plates when bonded by an elastic adhesive layer. In addition to the resulting shear stress, τ_{xy} , a significant normal or out-of-plane (peel) tensile stress, σ_{zz} , was shown to develop in the bondline. As the adhesive layer was assumed to be very thin, the resulting stress distribution from this model was assumed to not vary through the thickness of the adhesive. Actually, the maximum stress in the bondline almost always occurs at the interface and differs drastically from the average through the thickness.

Some studies [8-13] have demonstrated the influence of several factors such as specimen geometry, material stiffness, experimental processing, etc. on the distribution of stress. Their combined effect is a non-uniform and non-pure shear state in the adhesive layer with stress concentrations at the bimaterial tips. These variations in stress magnitude and distribution make difficult the measurement of deformation properties inside the bond. They have led to the existence of a wide variety of specimen geometries and loading procedures for in-situ adhesive testing. Their main purpose is to minimize the stress concentration at bond termination and to allow an accurate determination of shear properties at the same time. The ideal test would contain a constant and pure shear stress state throughout the adhesive.

The lap shear test and its variants have been and are still the most commonly used shear tests because of their simple geometry and because they give insight to bonded shear properties using only tensile loads. For example, the thick adherend specimen, based on the the assumptions of rigid adherends and no rotation, is assumed to be a case of constant and pure shear for the adhesive. However, in practice, equilibrium and the fact that the adherends are elastic with rotations due to moments gives rise to very high peel stresses and non-uniform shear stresses. Some authors [8-10] have used the Finite Element technique to perform a stress analysis inside the joint which does correctly identify the large shear and peel stresses at the bond termination of lap joints. This is illustrated in fig.5 and 6 in the case of the modified single lap shear specimen analyzed in reference [9]. The high peel stresses near the bond termination tends to dominate the fracture behavior of the joint. On the other hand, it is difficult to experimentally verify the high stresses and, as a result, often the failure stress is calculated as the load divided by the bonding area even though a non-uniform state of stress occurs in the joint. Obviously, the lap shear test is deficient in producing data design for mechanical structures.

An alternate to lap shear testing is provided by the napkin ring torsion test specimen. Even in this specimen, though, stress concentrations exist at edges. However, for adherends with rounded corners loaded in tension, stress concentrations are reduced as shown by Liechti [15].

In the three point bending test [11], the adhesive is again supposed to be in a pure shear state. Finite Element analysis, however, shows the presence of large cleavage stresses at the bond termination even though the shear stress does appear to be more uniformly distributed in the adhesive. But once more the average stress is very different from the actual stress acting at the extremities .

In a torsion test such as the one shown in fig.7, the adhesive is subjected to a more homogeneous stress distribution, since the stress concentrations at the bond ends are less significant. However, a uniform stress is obtained only for small rotations.

The Iosipescu shear test [12] utilizes a notched specimen in bending as a shear test for composite materials (fig.8). This test induces a state of uniform shear stress at the midsection of the specimen by creating two counteracting moments which are produced by the applied load. The use

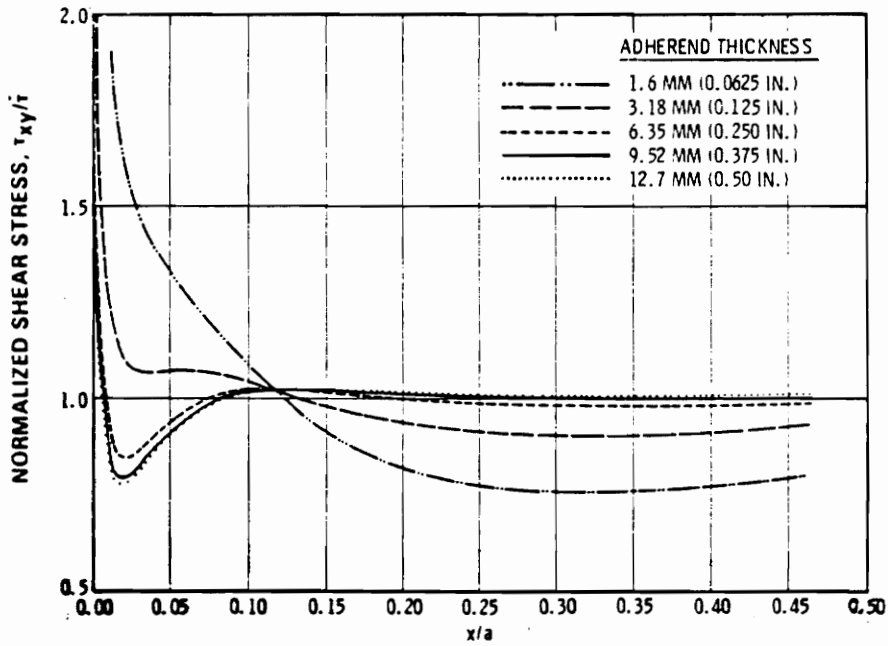


Figure 5. Bondline shear stresses in lap shear specimen (from reference 9).

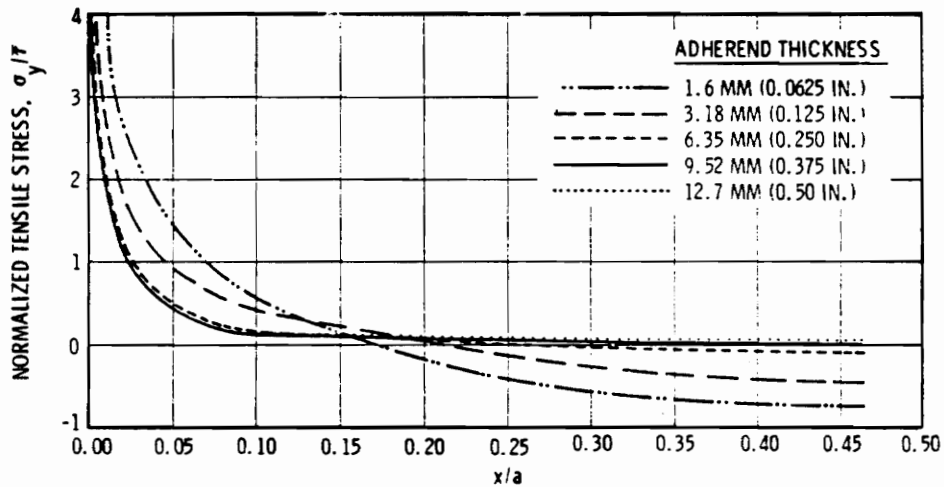


Figure 6. Bondline tensile stresses in lap shear specimen (from reference 9).

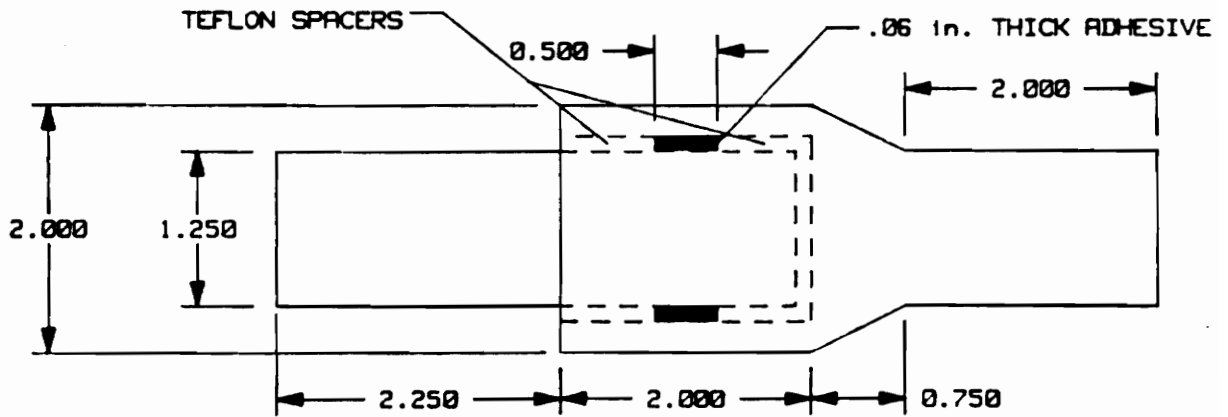


Figure 7. Torsion test geometry.

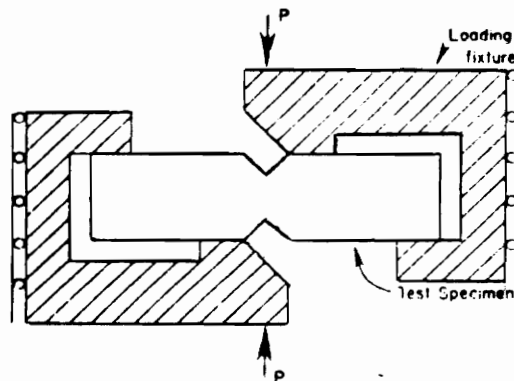


Figure 8. Iosipescu shear test (from reference 12).

of this test is still limited, because of the need for precision notches in order to achieve a uniform shear state. The test fixture requires strict dimensional tolerance but according to its inventors, the optimization of this test could lead to a definitive form of experimental shear test for adhesive joints.

Another promising new test for adhesive joints is the ARCAN specimen [13-15], the geometry of which is shown in fig.9-a and 9-b. It uses round stiff adherends which are notched and bonded in such a way as to produce a pure shear state. Loading can be applied to obtain any combination of tension or shear.

The so-called BMC test or the bonded cantilever beams test is the most recently developed adhesive shear test. Using the geometry of two cantilever beams bonded together with an adhesive layer, and applying equally acting loads on both adherends, H.F. Brinson [2-5] assumed that the specimen should develop a uniform and constant shear state in the adhesive layer. H.F. Brinson and E. Moussiaux [6] used a strength of materials type solution developed by H. Beck [16] in 1962 to model the stress state inside the bonded joint of the BMC specimen. As this new shear test is the topic of this report, the main results from the analytical solution are reviewed next.

An expression of the shear stress was found and was shown to be a function of the x-coordinate only and of a parameter $\bar{\alpha}$.

$$\tau_{xy} = \frac{3P(1 + 2t/h)}{bh(1 + 3(1 + 2t/h)^2)} \left(1 - \cosh \bar{\alpha} \frac{x}{\ell} + \tanh \bar{\alpha} \sinh \bar{\alpha} \frac{x}{\ell} \right) \quad (10)$$

or,

$$\tau_{xy} = \bar{\tau} \left(1 - \cosh \bar{\alpha} \frac{x}{\ell} + \tanh \bar{\alpha} \sinh \bar{\alpha} \frac{x}{\ell} \right) \quad (10a)$$

where,

$$\bar{\alpha} = \sqrt{\frac{3G_a}{E} \left(\frac{\ell}{h} \right)^2 \frac{(1 + 2t/h)^2}{t/h} \left(1 + \frac{1}{3(1 + 2t/h)^2} \right)} \quad (11)$$

The shear stress is uniform through the thickness of the bondline at any constant distance from the end, but varies from zero at the fixed end to a maximum value at the free end :

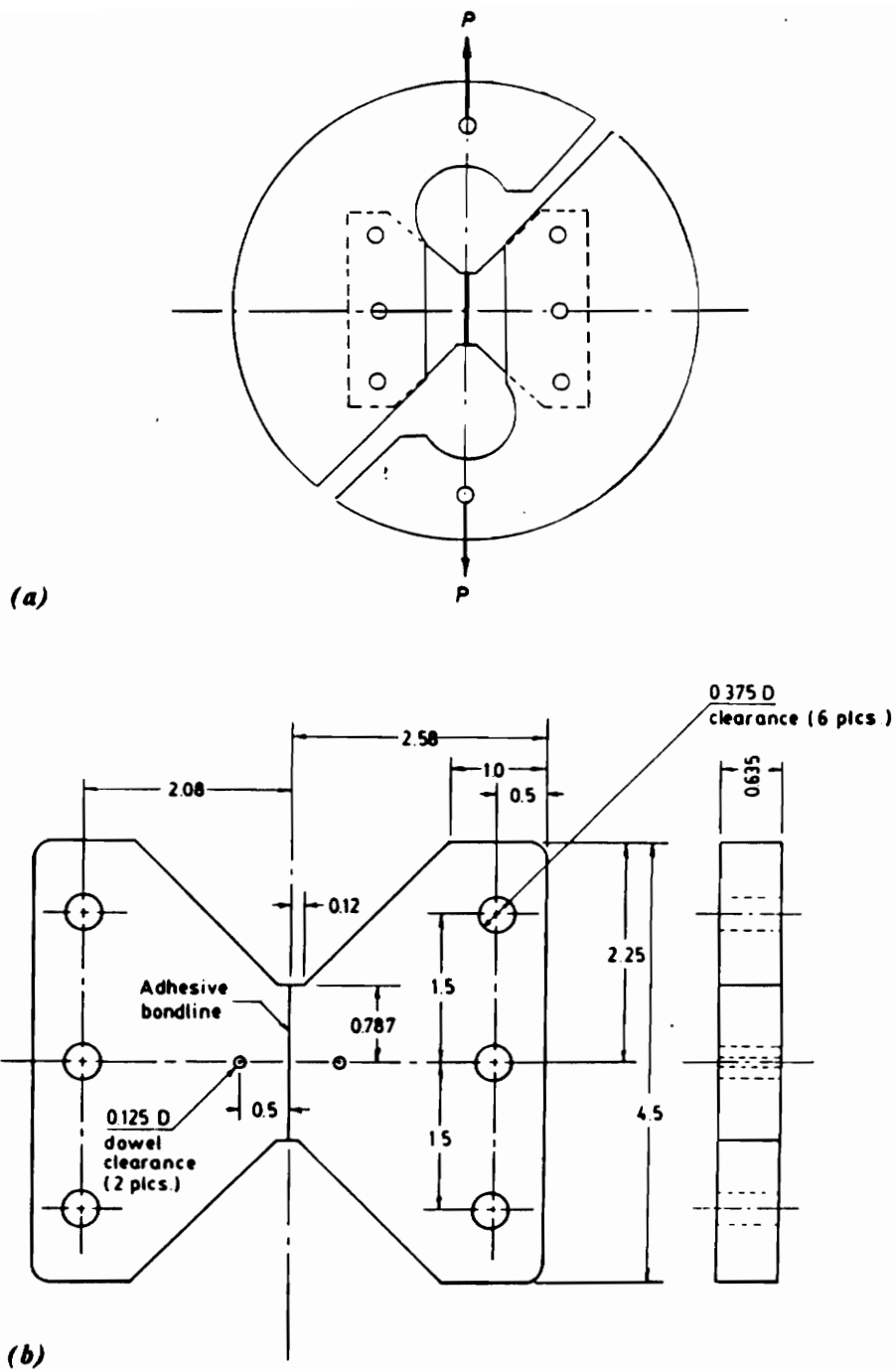


Figure 9. Arcan specimen showing (a) the loading frame and (b) the butterfly specimen (from reference 14).

$$\tau_{xy}^{\max} = \frac{3P(1 + 2t/h)}{bh(1 + 3(1 + 2t/h)^2)} \left[1 - \frac{1}{\cosh \bar{\alpha}} \right] \quad (12)$$

The larger the parameter $\bar{\alpha}$, the faster the shear stress reaches its maximum, and so, the more constant is the stress along the beam length (fig.10). Hence, for an experimental use, a measurement of the shear strain in the zone where the stress is constant, can easily yield the adhesive shear modulus by using,

$$\tau_{xy}^{\max} = G_a \gamma_{xy}^{\max} \quad (13)$$

which assumes a linear elastic behavior of the adhesive.

Along the length, the beam mid-plane deflects as follows :

$$v(x) = \frac{6P}{Eb h^3} \left[\frac{\ell x^2}{2} - \frac{x^3}{6} \right] + \frac{3Px}{4bhG} - \frac{6P}{Eb h^3 \gamma^2} \left[\frac{\ell x^2}{2} - \frac{x^3}{6} + \left(\frac{\ell}{\bar{\alpha}} \right)^3 \sinh \frac{\bar{\alpha} x}{\ell} - \left(\frac{\ell}{\bar{\alpha}} \right)^2 x - \left(\frac{\ell}{\bar{\alpha}} \right)^3 \tanh \bar{\alpha} \cosh \frac{\bar{\alpha} x}{\ell} + \left(\frac{\ell}{\bar{\alpha}} \right)^3 \tanh \bar{\alpha} \right] \quad (14)$$

with,

$$\gamma^2 = 1 + \frac{1}{3(1 + 2t/h)^2} \quad (15)$$

The end deflection, obtained at $x = \ell$ is :

$$\delta = \frac{P\ell^3}{2Eb(h+t)^3} (1 + t/h)^3 \left[4 \left(1 - \frac{1}{\gamma^2} \right) + \frac{3E}{2G} \left(\frac{h}{\ell} \right)^2 + \frac{12}{\gamma^2} \left(\frac{1}{\bar{\alpha}^2} - \frac{1}{\bar{\alpha}^3} \tanh \bar{\alpha} \right) \right] \quad (16)$$

Or,

$$\delta = \beta \frac{P\ell^3}{2Eb(h+t)^3} \quad (18)$$

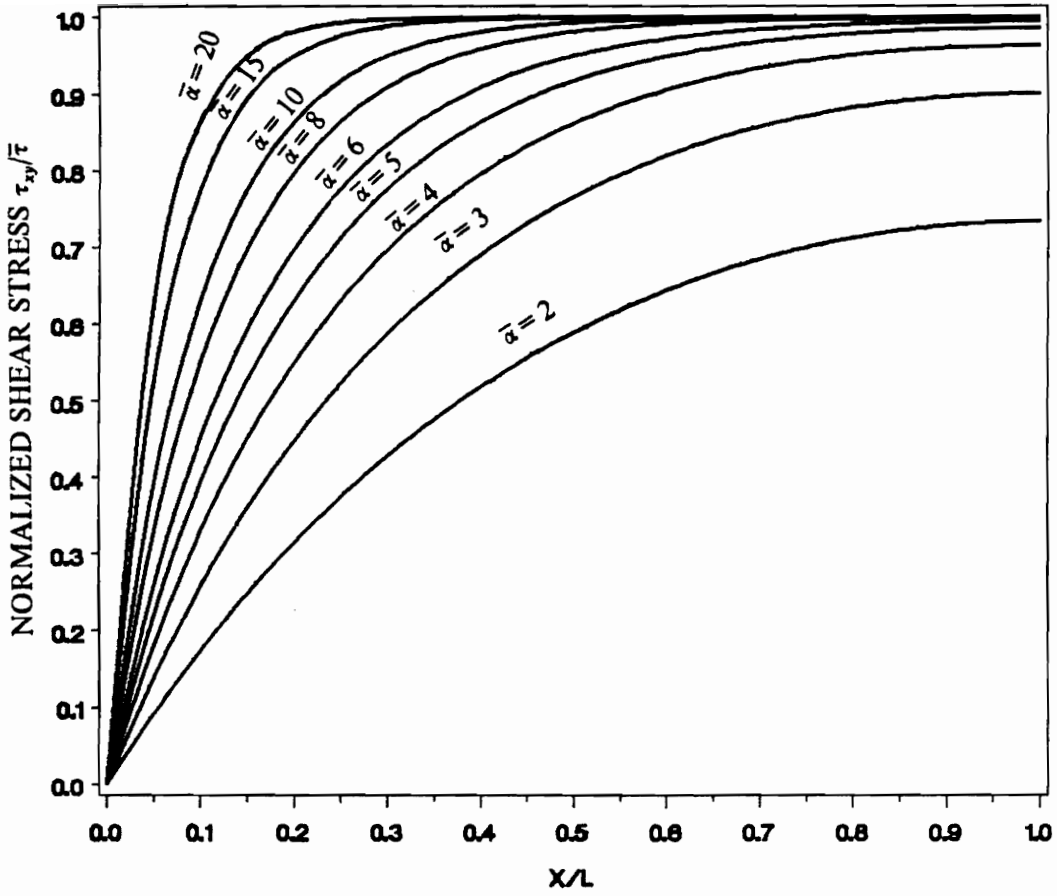


Figure 10. Variation of the shear stress along the adhesive for various values of alpha bar .

where β is the dimensionless end deflection which can be used to determine the adhesive shear modulus :

$$\beta = (1 + t/h)^3 \left[4 \left(1 - \frac{1}{y^2} \right) + \frac{3E}{2G} \left(\frac{h}{\ell} \right)^2 + \frac{12}{y^2} \left(\frac{1}{\bar{\alpha}^2} - \frac{1}{\bar{\alpha}^3} \tanh \bar{\alpha} \right) \right] \quad (18)$$

From the variation of β versus the stiffness ratio (fig.11), the ratio E/G_a of a bonded beam can be evaluated only if the end deflection measured lies in the fast increasing middle zone of the curve (fig.12). In this particular region, β exhibits maximum sensitivity to the specimen deformability and the best accuracy for G_a is obtained in this manner.

In fig.13 and 14, the solutions for shear strain and end deflection derived from BMC theory are compared with the limiting cases of perfect and zero adhesion discussed in chapter 1. For that purpose, we used aluminum adherends ($E = 10^7$ Psi, $\nu = 0.3$) of 3 in. long, 0.125 in. thick and 1 in. wide. Bondline thickness was 0.005 in.. As shown on the figure, we used three types of adhesives : $G_a = 1,000$ Psi - 10,000 Psi - 100,000 Psi. In fig.14, one can see that for stiff bonded adhesives, end deflections are very close to each other for these three cases and therefore its measurement must be very precise in order to accurately determine G_a . Table 1 also gives a summary of the numerical results. In the following section, the BMC method is analyzed with a view of understanding and controlling every parameter that may influence the experimental application and the collection of data.

Since Moussiaux's effort, a new finite-element code called NOVA is now available for the stress analysis of in-situ adhesives [10]. The program NOVA can be used for plane stress as well as plane strain analyses while an older code, VISTA, gives only data for plane strain and has been extensively used for the stress analysis through the adhesive thickness. Finally, some experimental results for adhesive shear moduli are presented which have been found using the BMC theory.

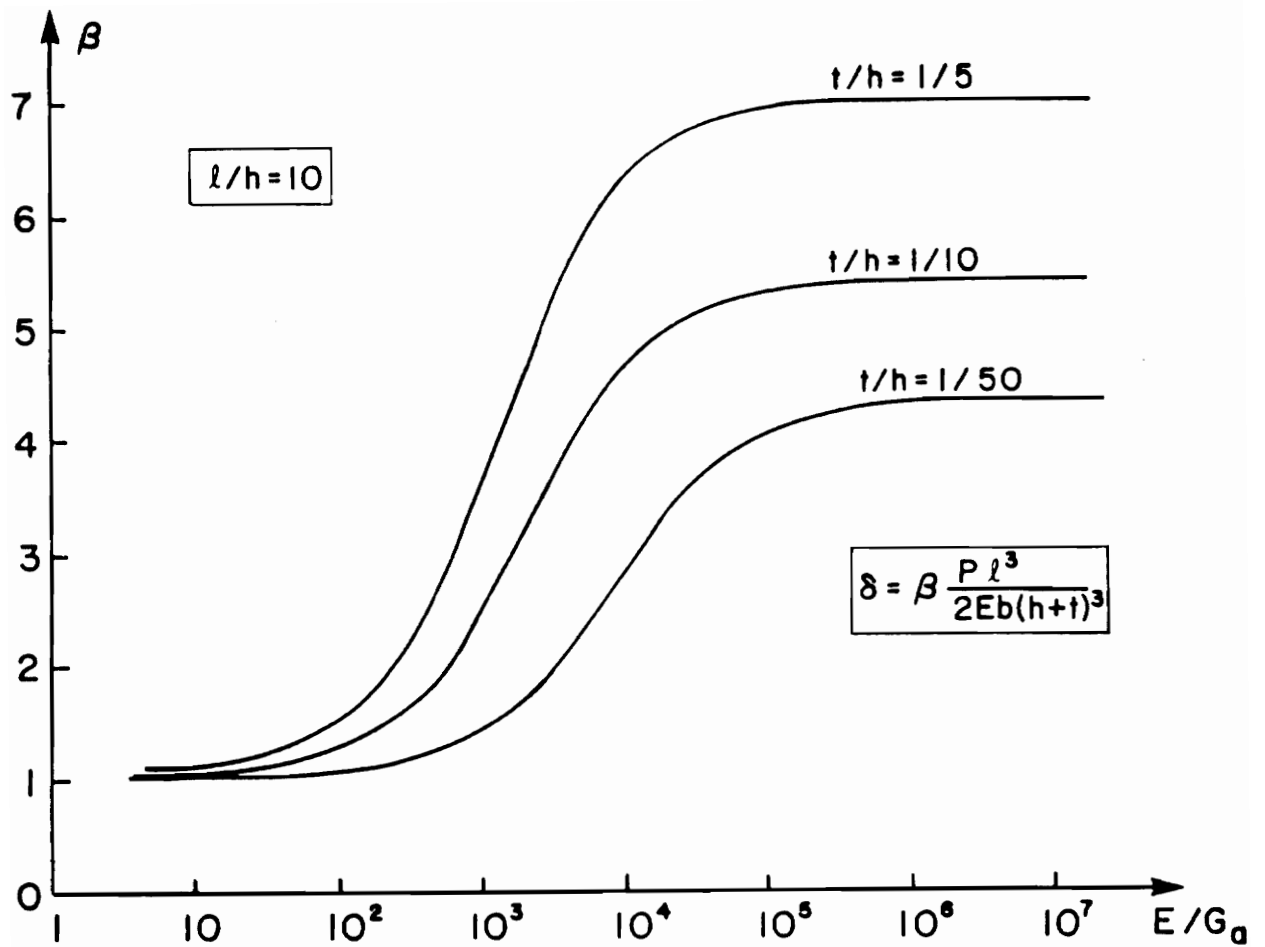


Figure 11. Dependence of the end deflection of the BMC on the beam deformability for various geometries (from reference 6).

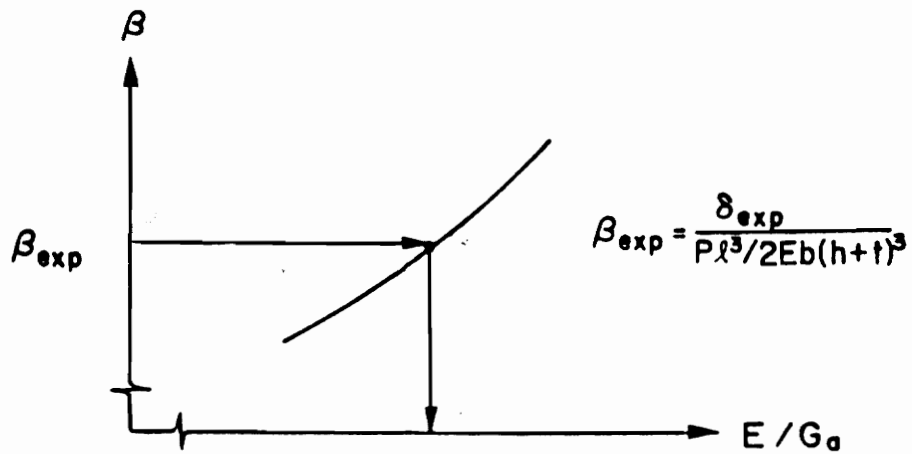


Figure 12. Determination of the adhesive shear stiffness by measuring the end deflection (from reference 6).

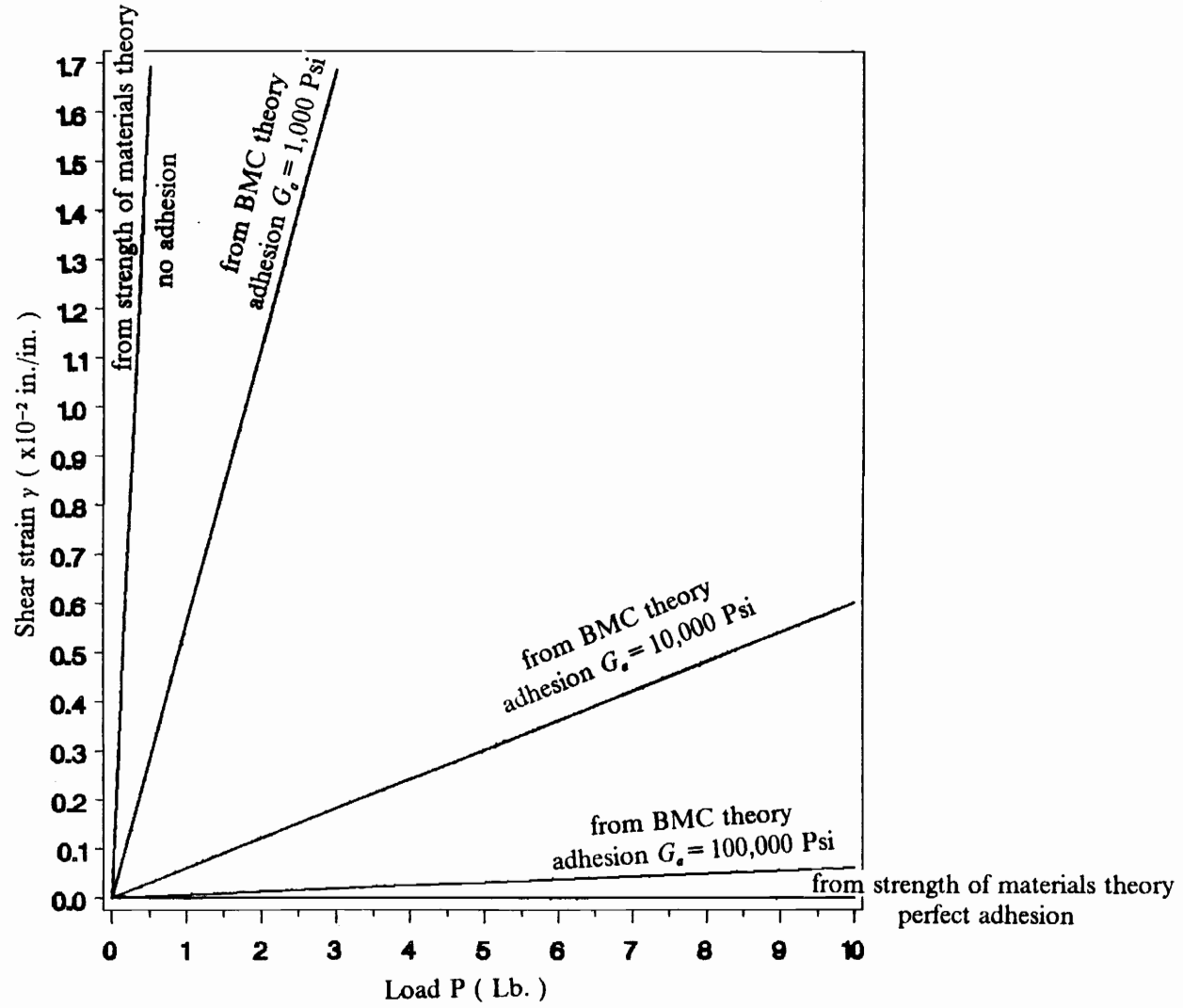


Figure 13. Shear strain versus load .

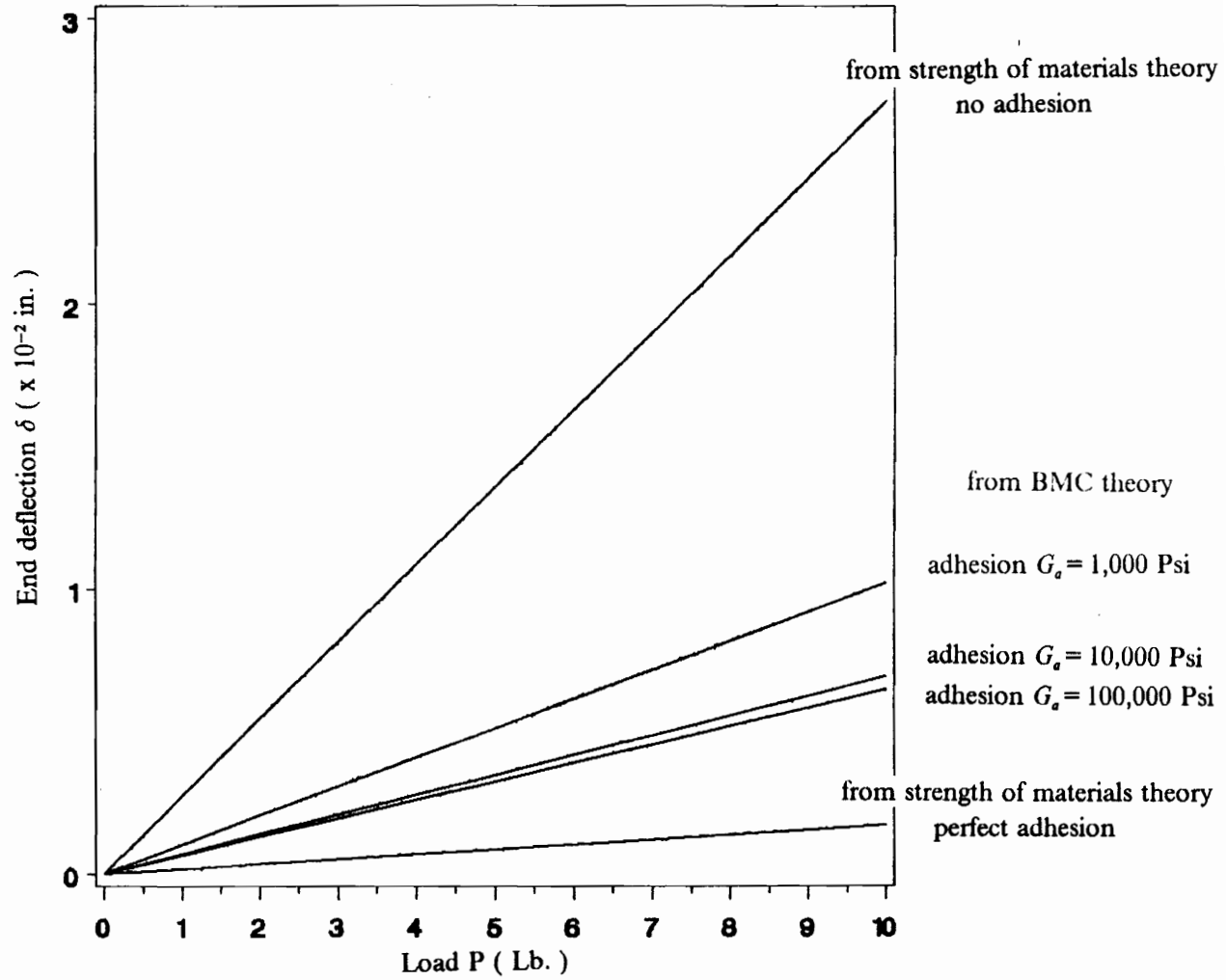


Figure 14. End deflection versus load .

Table 1. Comparison of the BMC model with the limit cases (P = 10 Lb.).

CASE DEFINITION	END DEFLECTION (x 0.01 in.)	SHEAR STRAIN (x 0.01)
no adhesion (1)	2.710	33.8820
adhesion $G_a = 1,000$ Psi	1.019	5.6237
adhesion $G_a = 10,000$ Psi	0.691	0.6015
adhesion $G_a = 100,000$ Psi	0.648	0.0601
perfect adhesion (2)	0.169	1.564E-04

- (1) adhesive's shear modulus approaches zero
- (2) adhesive thickness approaches zero

3 - OPTIMIZATION OF THE BMC THEORY

The analytical solution of the BMC test for stress (or strain) and deflection distribution can be used in conjunction with experimental data to determine the mechanical properties of adhesives in the bonded state. However, limitations occur because the shear stress state in the adhesive as well as the beam deflection are sensitive to the choice of specimen geometry and to the type of the adhesive and the adherend which are tested. It is therefore necessary to make a parametric analysis of the beam geometry for gaining a better understanding of the beam response.

For this purpose, we first defined the range of lengths and thicknesses for which this study must be limited. Then, the two approaches for the BMC test are analyzed independently. If the adhesive is characterized from the measurement of the adhesive shear deformation, the influence of geometry on the stress distribution is studied. If the bonded joint is characterized from the end deflection, the influence of geometry on the magnitude of the parameter β is discussed. For each case, a procedure is presented to define the BMC specimen geometry.

3.1 - DEFINITION OF SPECIMEN GEOMETRY

3.1.1 - Slenderness ratio ℓ/h

The choice of specimen dimensions is oriented towards two directions: the beam should have a "realistic" length and the geometry should not violate the hypotheses from which the theoretical model is derived. To design a specimen with realistic dimensions, the beam length should be roughly less than 12 inches. It can be seen in fig.15 that the slenderness ratio must not exceed 100 if the adherends thickness h is 0.125 in.. When a smaller ratio can be used, it is possible to have several combinations of beam lengths and adhesive thicknesses. This gives more flexibility to the user. However, in order to satisfy the basic assumptions of the underlying BMC theory, the slenderness ratio should always be above 10 [6]. Table 2 summarizes the possible lengths as a function of adherend thicknesses.

3.1.2 - Thickness ratio t/h

The adhesive thicknesses commonly used vary from 0.005 in. in aircraft industry up to 0.2 in. in automotive industry. Therefore, the choice of the bond thickness of a BMC specimen should be bounded by these two values. In accordance with the definition of the BMC specimens dimensions, we define that the adhesive thickness is $2t$ and that the thickness ratio t/h deals with half the adhesive thickness. As discussed in [6], the smaller the thickness ratio, the more uniform is the shear stress along the beam. For a given adherend thickness h , t/h is minimized by making the adhesive thinner. Conversely, for a given adhesive thickness, t/h is minimized by using a thicker adherend. Figures 16 to 18 show the possible combinations of adherend and adhesive thicknesses.

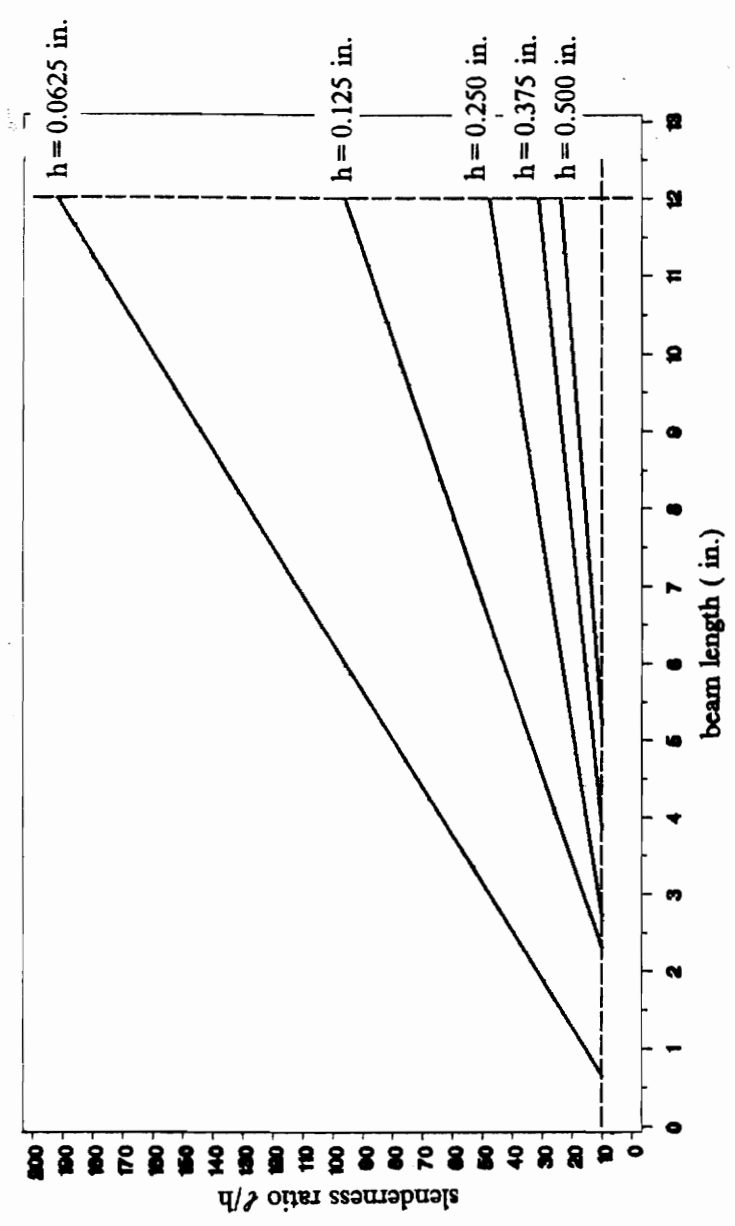


Figure 15. Definition of the slenderness ratio .

Table 2. Variety of valuable beam lengths.

h (in.)	$(\ell/h)_{\min}$	ℓ_{\min} (in.)	$(\ell/h)_{\max}$	ℓ_{\max} (in.)
0.0625	10	0.625	192	12
0.125	10	1.25	96	12
0.250	10	2.50	48	12
0.375	10	3.75	32	12
0.500	10	5.00	24	12
0.625	10	6.25	19	12
0.750	10	7.50	16	12
0.875	10	8.75	14	12
1.000	10	10.0	12	12

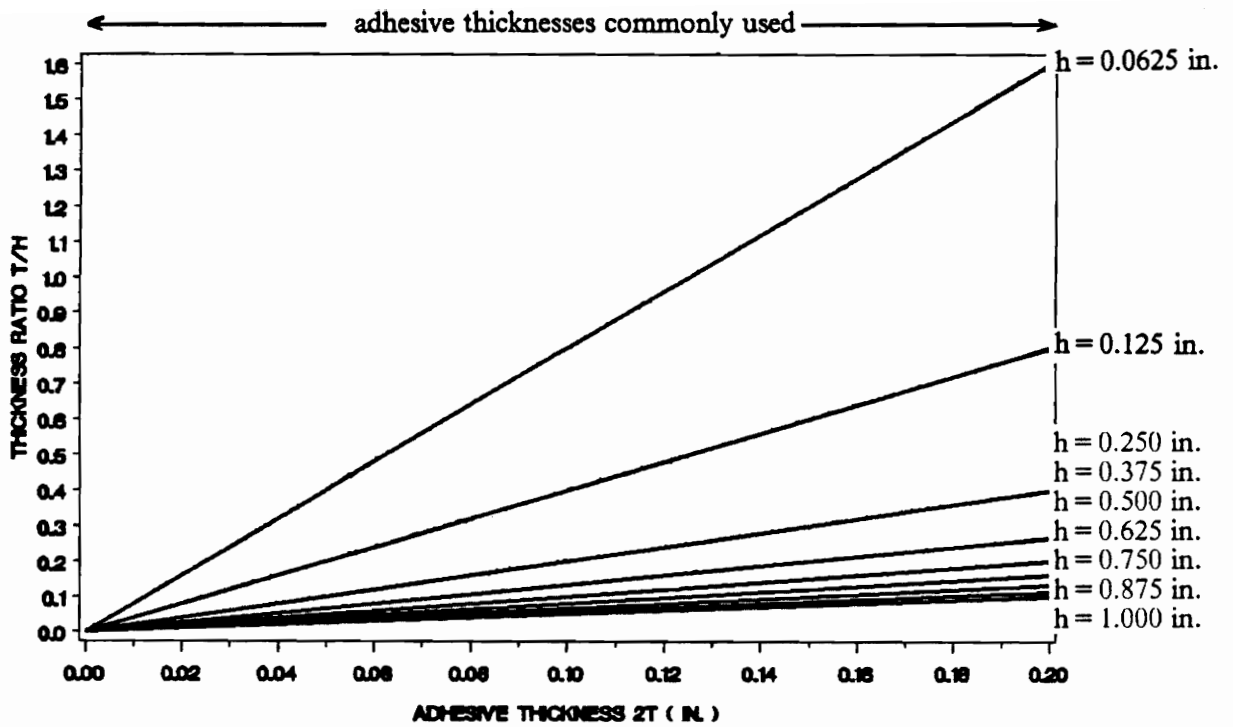


Figure 16. Definition of the thickness ratio.

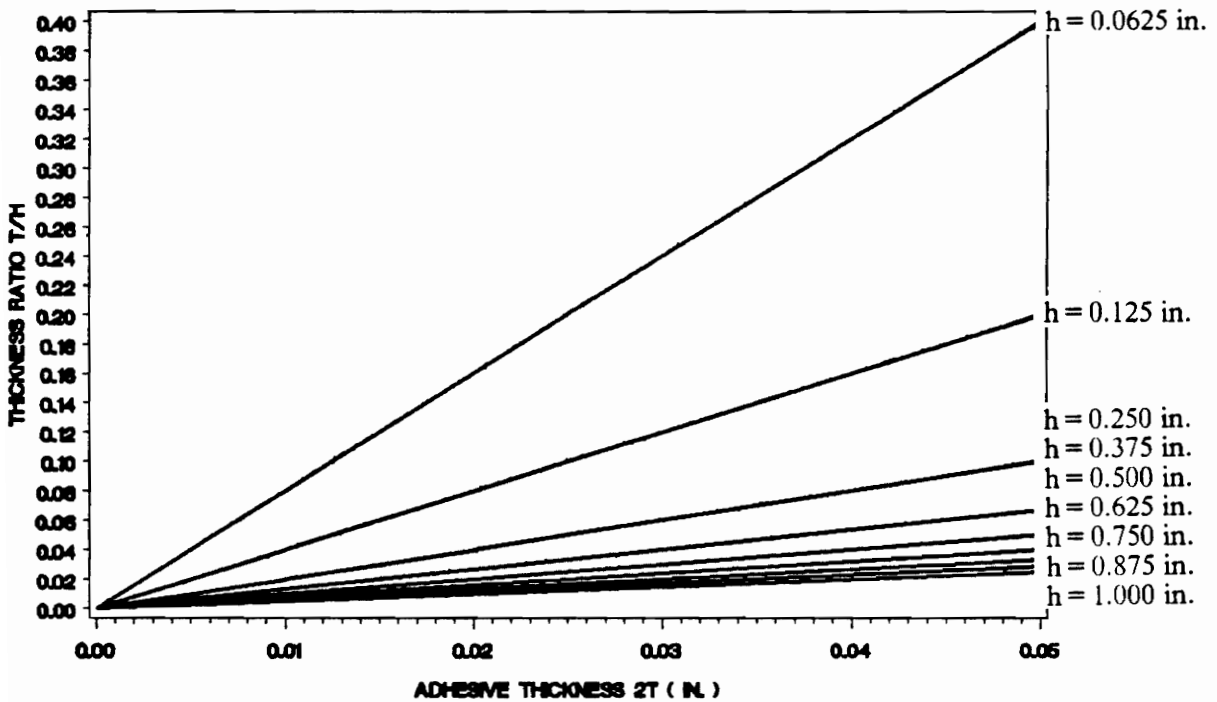


Figure 17. Definition of the thickness ratio - refinement for thin adhesives.

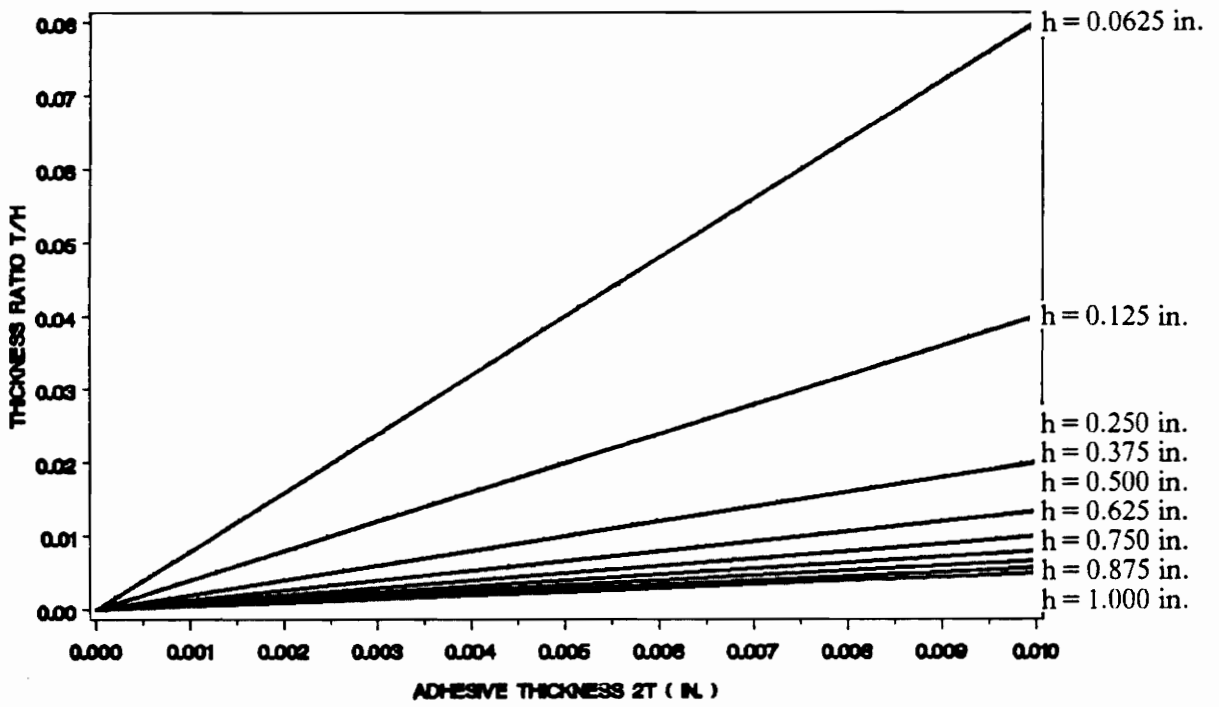


Figure 18. Definition of the thickness ratio - refinement for very thin adhesives .

In conclusion, if a parametric analysis is performed in order to discuss the capabilities of the BMC method, it should account for the geometric limitations mentioned above. The beam length remains a realistic quantity if it does not exceed 12 inches. In agreement with practical use of adhesives, the thickness ratio can vary up to 1.6. After the definition of geometrical limitations, the next step would consist in reducing the number of the parameters involved :

- the measurement location x/ℓ which determine the stress magnitude,
- the slenderness ratio which involves the beam length ℓ and the thickness h ,
- the thickness ratio which involves the adhesive and the adherend thicknesses t and h ,
- the adherend stiffness E ,
- the adhesive shear stiffness G_a .

From a practical point of view, a BMC test specimen must be designed to allow for reliable and convenient determination of in-situ adhesive properties. In the following, it is shown that a compromise can be found for stiff adhesives and shear deformation data. However, finding a unique specimen oriented towards end deflection measurements is more uncertain.

3.2 - FROM THE SHEAR DEFORMATION TO THE SHEAR MODULUS

As seen in reference [6], under certain conditions, it is possible to obtain the adhesive shear properties by measuring the shear deformation: "...if a measurement of the shear strain in the adhesive can be obtained at the place of maximum stress, the shear modulus can be easily found."

The determination of the shear modulus G_a following the procedure mentioned in [6] requires that the shear stress be constant over the adhesive length where the shear deformation is measured. The uniformity of the stress is also interesting because it eliminates one parameter in the analysis: the measurement location x/ℓ . Such a situation can be found for large values of the coefficient $\bar{\alpha}$, involving a large ℓ/h ratio and a small t/h ratio. In addition, another useful finding is the variation of the maximum shear stress value with increasing stiffness ratio E/G_a and various geometries. The maximum shear stress is:

$$\tau_{xy}^{\max} = \frac{3P(1 + 2t/h)}{bh(1 + 3(1 + 2t/h)^2)} \left[1 - \frac{1}{\cosh \bar{\alpha}} \right] \quad (12)$$

If the parameter $\bar{\alpha}$ is large enough to cause $\cosh \bar{\alpha}$ to go to infinity and consequently to cause $(1 - 1/\cosh \bar{\alpha})$ to approach 1, the value of the maximum shear stress becomes a function of the geometry and the loading only. This situation occurs for $\bar{\alpha}$ values greater than 6. The variation of τ_{xy}^{\max} versus E/G_a shown in fig.19 indicates that the shear test is also limited to particular material properties. For the geometry shown, the maximum stress is independent of material properties and $\bar{\alpha}$ is larger than 6 if the ratio E/G_a is below 30,000. If material properties combined with geometrical properties make the parameter $\bar{\alpha}$ equals to 6, then the shear stress reaches its maximum at the loaded end of the beam only. Increasing the uniformity of the shear stress to eliminate the measurement location dependence, reduces the range of stiffness ratio because this requires a larger $\bar{\alpha}$.

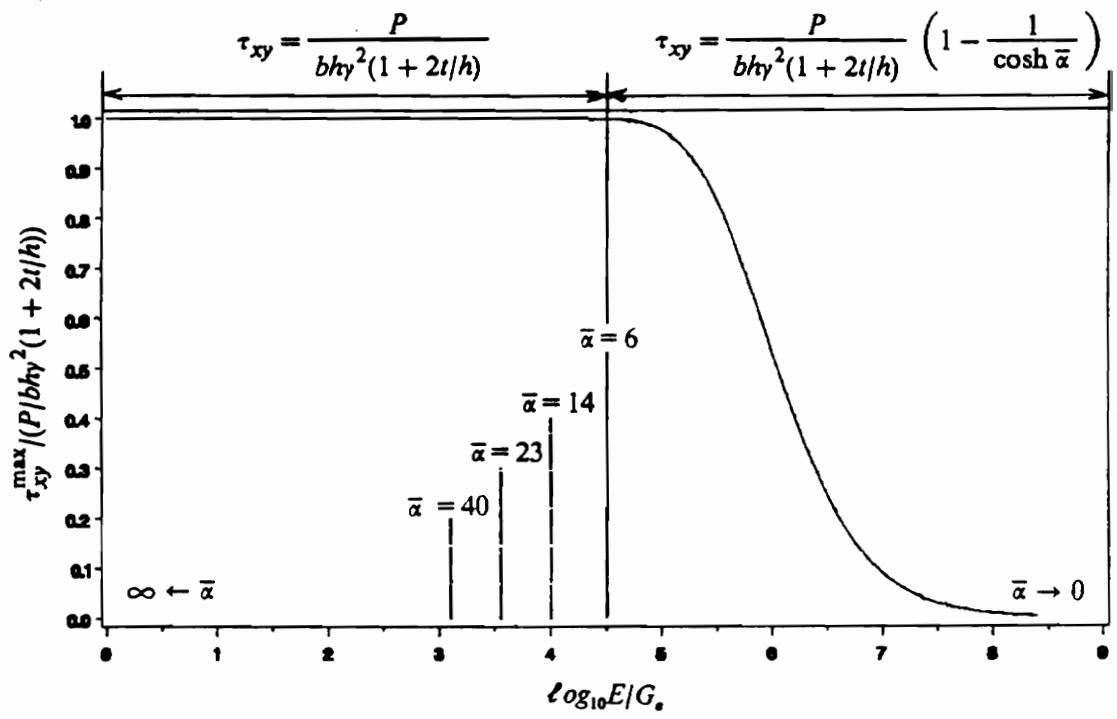


Figure 19. Variation of the maximum shear stress with adherend-adhesive stiffnesses for $l/h = 96$, $t/h = 0.02$ - limitations of the BMC shear deformation test.

However, without modifying the stiffness range, it is also possible to vary the beam geometry in order to obtain higher $\bar{\alpha}$ for a more uniform stress along the adhesive (fig.20 and 21). If the BMC specimen is assumed to have a slenderness ratio of 96 and a thickness ratio of 0.02, then as shown in fig.19, the test is valid if $1 \leq E/G_a \leq 30,000$. Using this latter relationship for three adherends, steel ($E = 3 \times 10^7$ Psi), aluminum ($E = 10^7$ Psi) and titanium ($E = 1.65 \times 10^7$ Psi), yields the additional condition in that the adhesive shear modulus be bounded as follows for a valid test.

<i>Adherend</i>	<i>Adhesive modulus range (for valid test)</i>
Steel	$10^3 \leq G_a \leq 3 \times 10^7$ Psi
Aluminum	$3 \times 10^2 \leq G_a \leq 10^7$ Psi
Titanium	$5 \times 10^2 \leq G_a \leq 1.65 \times 10^7$ Psi

For the smallest adhesive shear moduli, $\bar{\alpha}$ is equal to 6 and the shear stress reaches its maximum at the beam end only. As discussed previously, the stress uniformity is increased by defining a larger $\bar{\alpha}$. This reduces the range of adhesive shear moduli as shown by the following discussion. If $\bar{\alpha}$ equals 14, the shear stress is constant along 70 % of the adhesive and again from fig.19, the test is valid if $1 \leq E/G_a \leq 10,000$. This condition yields,

<i>Adherend</i>	<i>Adhesive modulus range (for valid test)</i>
Steel	$3 \times 10^3 \leq G_a \leq 3 \times 10^7$ Psi
Aluminum	$10^3 \leq G_a \leq 10^7$ Psi
Titanium	$1.65 \times 10^3 \leq G_a \leq 1.65 \times 10^7$ Psi

For the conditions shown above, the adhesive shear stress can be calculated from the geometry and loading alone. However it should be noted that, in this instance, the technique does not work well for very soft adhesives.

The relative displacement of the adherends can be measured at the place of known stress and the shear modulus can be determined, assuming linear elastic adhesive behavior :

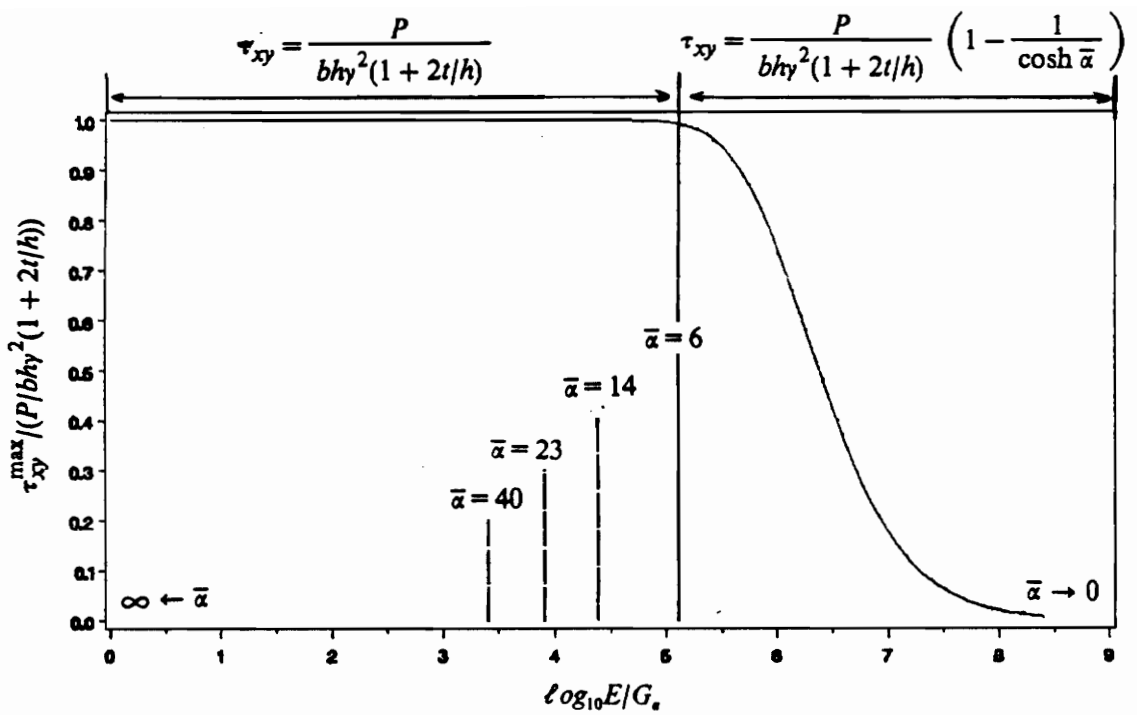


Figure 20. Variation of the maximum shear stress with adherend-adhesive stiffnesses for $l/h = 192$, $t/h = 0.04$ - limitations of the BMC shear deformation test.

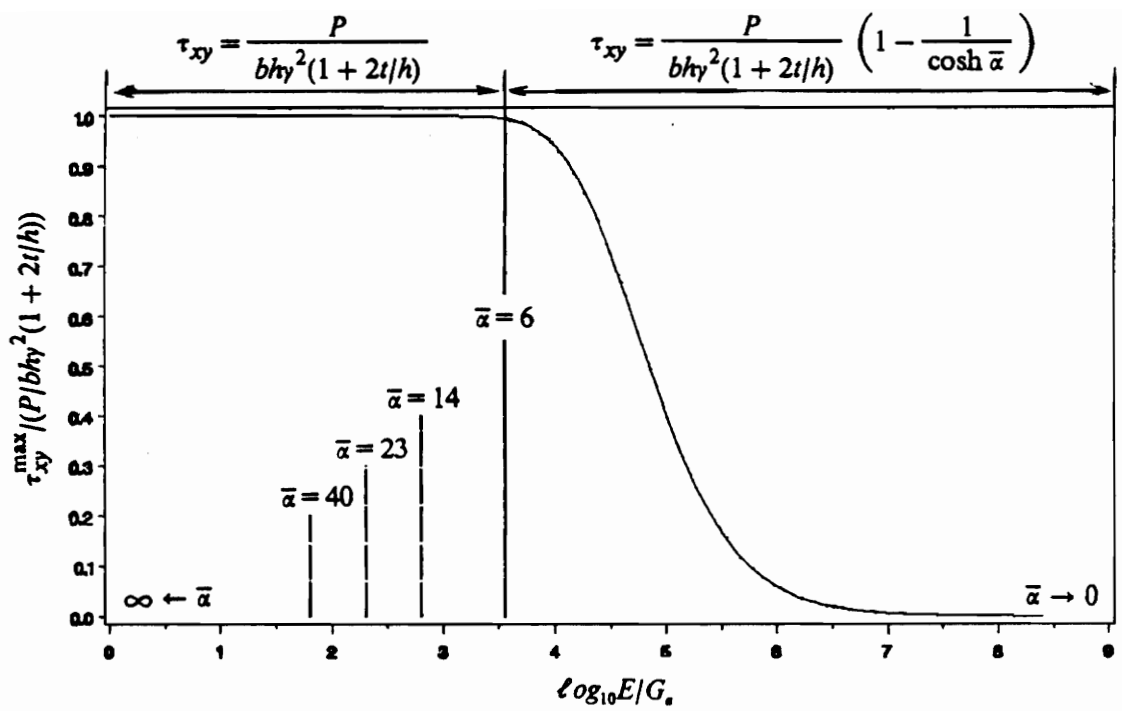


Figure 21. Variation of the maximum shear stress with adherend-adhesive stiffnesses for $l/h = 24$, $t/h = 0.02$ - limitations of the BMC shear deformation test .

$$\tau_{xy}^{\max} = G_a \gamma_{xy}^{\max} \quad (13)$$

where γ_{xy}^{\max} is from experimental data and τ_{xy}^{\max} is calculated from the BMC theory :

$$\tau_{xy}^{\max} = \frac{3P(1 + 2t/h)}{bh(1 + 3(1 + 2t/h)^2)} \quad (12a)$$

Moussiaux pointed out in reference [6] that the maximum shear strain rather than the maximum shear stress can be used as an indicator of the proper conditions for a good test. This approach is shown in fig.22 and illustrates that the maximum shear strain varies linearly with stiffness ratio when the maximum shear stress is constant and determined by geometry and load alone. In other words, the examples given above are taken for the condition of linear shear strain variations. Fundamentally, the linear shear strain zone or the conditions for a good test increases with increasing beam length and with decreasing adhesive thickness.

Table 3 gives a survey of several adhesives found in the literature which demonstrates that a broad range of typical commercial structural adhesives are within the range of stiffness of the examples given above. That the BMC specimen can be used for these combinations of adhesives and adherends.

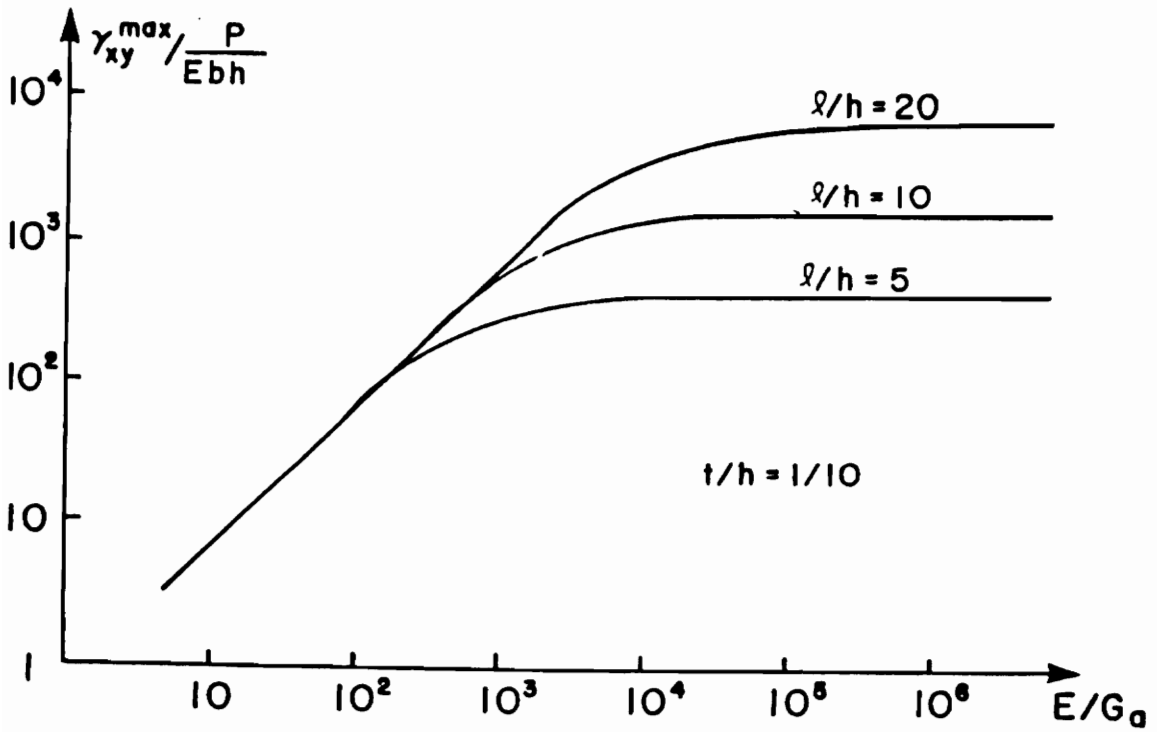


Figure 22. Variation of the shear strain with the stiffness ratio for various geometries (from reference 6).

Table 3. Review of literature of adhesive material properties.

ADHESIVE	YOUNG'S MODULUS E_e (Psi)	POISSON'S RATIO ν_e	SHEAR MODULUS G_e (Psi)
FM 1018 ref. (a)	1.0×10^6	0.35	$3.5-4.0 \times 10^5$
FM 73	0.2437×10^6	0.32	9.231×10^4
FM 355 ref. (a)	4.5×10^5	0.35	1.5×10^5
FM 300 ref. (a)	4.0×10^5	0.35	1.2×10^5
320/322 ref. (b)	1.18×10^5	0.37	4.3×10^4
rubber	290	0.49	97
polyurethane ref. (c)	600	0.50	2.0×10^2

ref.(a) : American Cyanamid, Inc.
 ref.(b) : Lord Corporation, Inc.
 ref.(c) : Measurement Group, Inc.

3.2.1 - Parametric analysis

The choice of geometry should take into account the preceding restrictions in order to obtain an extension of the uniform shear stress zone and to facilitate the test procedure. Ideally, in the calculation of the shear modulus, γ_{xy} is measured, τ_{xy} is calculated from geometry and loading, and the adhesive is assumed to be linear elastic such that :

$$G_a = \frac{\gamma_{xy}}{\tau_{xy}} \quad (13a)$$

In case the shear stress is not equal to its maximum, it is a function of G_a through the parameter $\bar{\alpha}$:

$$\tau_{xy}(x) = \frac{3P(1 + 2t/h)}{bh(1 + 3(1 + 2t/h)^2)} \left(1 - \cosh \bar{\alpha} \frac{x}{\ell} + \tanh \bar{\alpha} \sinh \bar{\alpha} \frac{x}{\ell} \right) \quad (10)$$

This gives rise to three types of situations which are illustrated in fig.23.

case 1 :

The kind of shear stress distribution obtained for high values of parameter $\bar{\alpha}$ is referred to as case 1. In this case, τ_{xy} is constant over almost the entire beam length. Thus, as shown in fig.23, if the shear strain is measured at either points A or B, the adhesive modulus can be determined simply from equation (13a) in which τ_{xy} is not a function of $\bar{\alpha}$ and is determined only from the geometry and the applied load.

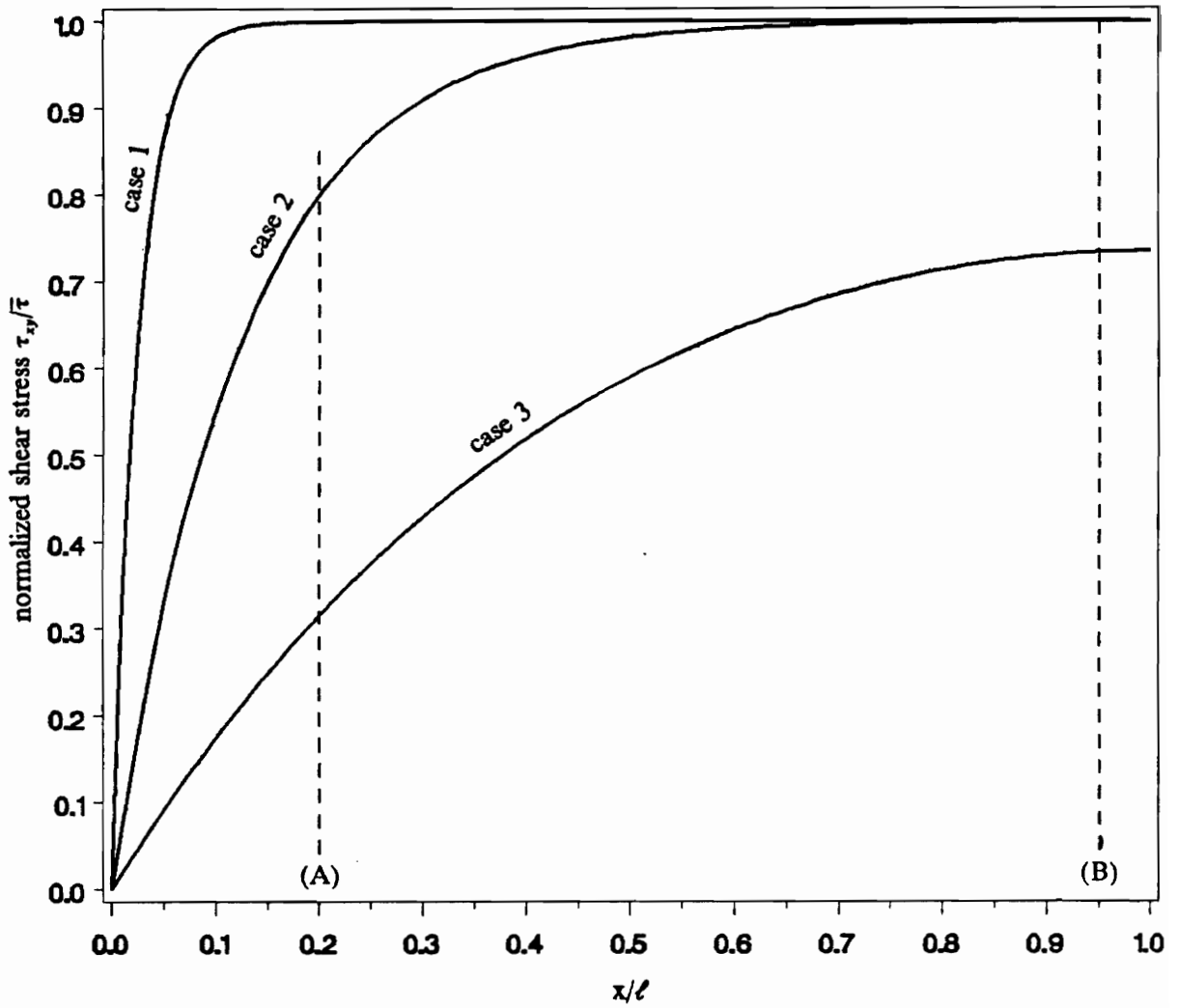


Figure 23. Three situations for adhesive shear stiffness determination.

case 2 :

If the shear strain is measured at point B, then again the shear modulus, G_a , can be obtained easily as in case 1. However, if the shear strain is measured at point A then the shear stress will be given by :

$$\tau_{xy,a}(x) = \frac{3P(1 + 2t/h)}{bh(1 + 3(1 + 2t/h)^2)} (1 - \cosh \bar{\alpha}x_a + \tanh \bar{\alpha} \sinh \bar{\alpha}x_a) \quad (10a)$$

In equation (10a), all quantities are known except for $\bar{\alpha}$ which is a function of G_a , the parameter investigated. In this instance, the adhesive shear modulus must be calculated in an iterative fashion as discussed below in case 3.

case 3 :

Case 3 is defined by an $\bar{\alpha}$ lower than 6. This upper bound was calculated so that the shear stress never reaches a maximum as defined in equation (12a) because $0 < (\cosh \bar{\alpha}x/\ell - \tanh \bar{\alpha} \sinh \bar{\alpha}x/\ell) \leq 1$. It follows that in this case, the stress is a function of the unknown G_a and no mathematical transformation exists to eliminate the dependence of τ_{xy} on G_a . Regardless of the position of measurement, case 3 is similar to case 2 when a measurement is made at $x/\ell = x_a$. That is, knowledge of the adhesive shear modulus is required to predict the adhesive shear stress magnitude, and the adhesive shear stress is needed to compute the adhesive shear modulus. Therefore, it becomes impossible to obtain the required shear modulus unless a numerical method is used. Solving for G_a numerically would consist of seeking a solution to the following equation :

$$G_a(1 - \cosh \bar{\alpha} \frac{x}{\ell} + \tanh \bar{\alpha} \sinh \bar{\alpha} \frac{x}{\ell}) = \frac{3\gamma_{xy}P(1 + 2t/h)}{bh(1 + 3(1 + 2t/h)^2)} \quad (19)$$

While such a procedure can be used, it would not be as direct and useful as for case 1 above. As a result, this study emphasizes the fact that we need to predict the appropriate specimen dimensions

in order to create a known shear stress in the adhesive layer when we test an adhesive. Both the geometry and the material properties of the specimen are included in the expression for $\bar{\alpha}$ which, in turn, is directly related to the distribution of shear stress in the joint. In fig.24, $\bar{\alpha}$ is plotted versus E/G_a with $t/h = 0.05$ and using several values of the ratio ℓ/h . The horizontal curve for $\bar{\alpha} = 6$ is given and characterizes the limit below which the shear stress becomes sensitive to the material properties. Used in conjunction with the (τ_{xy} vs. x/ℓ) curve such as that shown in fig.23, this set of curves represents a very useful tool to define the BMC specimen dimensions.

From the stress equation :

$$\tau_{xy}(x) = \frac{3P(1 + 2t/h)}{bh(1 + 3(1 + 2t/h)^2)} \left(1 - \cosh \bar{\alpha} \frac{x}{\ell} + \tanh \bar{\alpha} \sinh \bar{\alpha} \frac{x}{\ell} \right) \quad (10)$$

and the parameter $\bar{\alpha}$ equation :

$$\bar{\alpha} = \sqrt{\frac{3G_a}{E} \left(\frac{\ell}{h} \right)^2 \frac{(1 + 2t/h)^2}{t/h} \left(1 + \frac{1}{3(1 + 2t/h)^2} \right)} \quad (11)$$

we can define a relation between the magnitude of $\bar{\alpha}$ and the beam length over which the shear stress is constant. This relation, obtained numerically, consists of finding the values of x/ℓ associated with the values of $\bar{\alpha}$ which make the term in parenthesis in equation 10 approach one. The curve ($\bar{\alpha}$ vs. x/ℓ) so determined is shown in fig.25 and explicitly defines the values of $\bar{\alpha}$ for which the shear stress is constant over a portion of the beam. In other words, the shear stress is constant in the adhesive layer for all values of $\frac{x}{\ell}$ above and to the right of the curve. Thus, constant shear stress over the entire beam can be obtained for very high values of $\bar{\alpha}$ which also implies either a very large slenderness ratio, a small thickness ratio and/or a small stiffness ratio (fig.24).

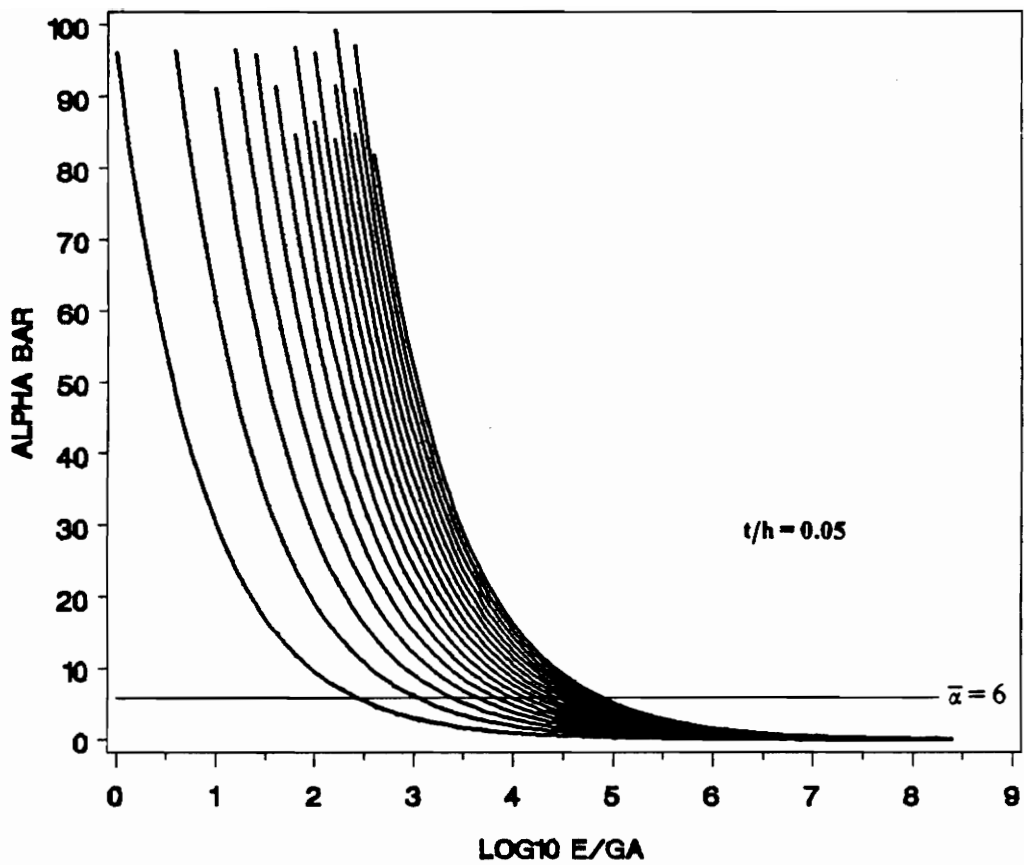


Figure 24. Variation of alpha bar as a function of the stiffness ratio. From left to right, each curve is associated with a value of l/h which varies from 10 to 160 in steps of 10

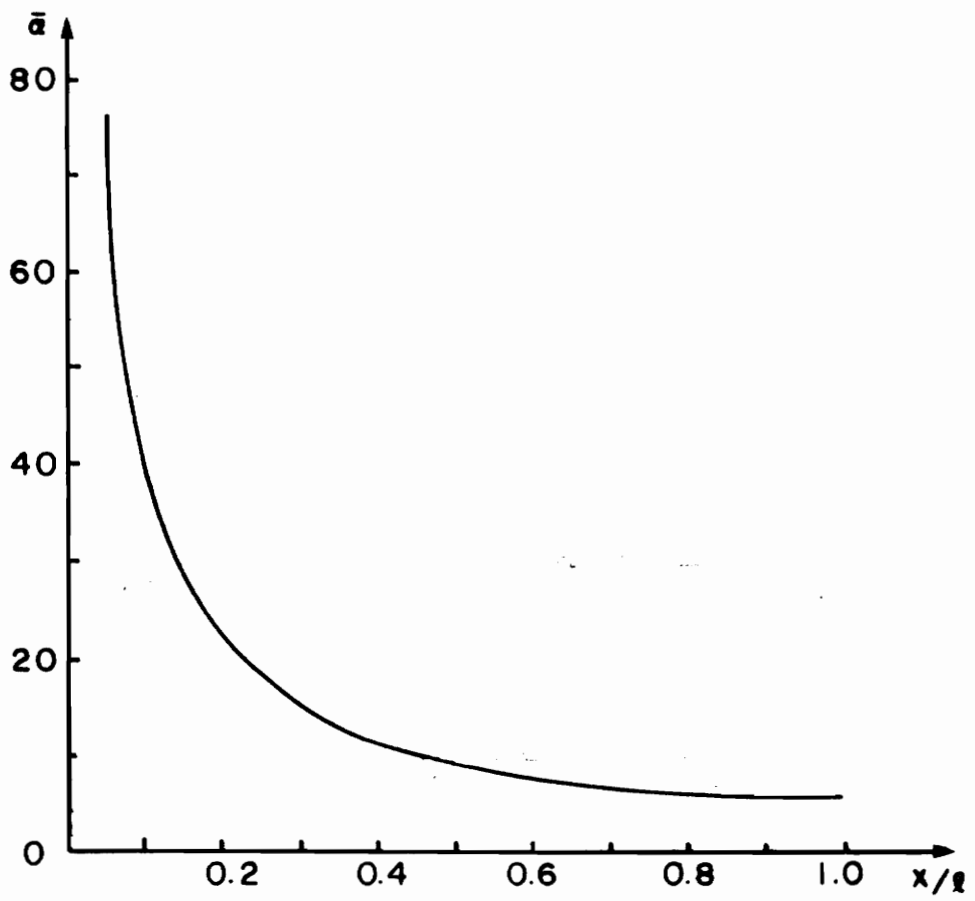


Figure 25. Variation of alpha bar with x/l .

Practically speaking, the choice of a BMC specimen geometry is based on the use of fig.24 and 25. In fig.24 the estimate of the stiffness ratio to be investigated is found and the beam geometry is adjusted to make the beam as short as possible for practical reasons, and at the same time, to make the parameter $\bar{\alpha}$ as large as possible. From fig.25, $\bar{\alpha}$ is determined by the desired location for making a convenient strain measurement. If a uniform shear stress zone does not exist, it means that the geometry chosen is not good, relatively to the stiffness ratio investigated. Other guidelines similar to fig.24 are given in appendix, with different values of thickness ratios t/h . It may be useful to draw these guidelines for other geometries when we want to extend the limits of validity of the model to the category of soft adhesives. However, as discussed at the beginning of section 3.2, the simplicity of the test for soft adhesives would lead to an unrealistic beam length and a very thin adhesive thickness. A compromise will be presented in section 3.3.

3.2.2 - Example of the specimen dimension determination

Our purpose herein, is to emphasize the sensitivity of the method when a geometry is chosen and an estimate of E/G_a is known.

Let us now consider the case when the stiffness ratio is estimated to lie between 10^2 and 10^3 . We set the thickness ratio to 0.05 and we find the variation of $\bar{\alpha}$ versus E/G_a for $\ell/h = 10$ in fig.24. As pictured in fig.26, if E/G_a is 10^2 and if $\bar{\alpha}$ is 10, 50 % of the beam is under a constant shear stress in the adhesive (fig.25). This gives a lot of space for the experimental measurement. However, if $E/G_a = 10^3$, $\bar{\alpha} = 3$, no beam area is available where the stress is a simple constant function of loading and geometry. Therefore, the limits of validity of the BMC shear deformation test are exceeded and it is not possible to characterize the adhesive shear properties other than numerically as mentioned previously. Hence, the uniform stress zone changes from 50 % to 0 % when E/G_a increases from 10^2 to 10^3 . At the limit point, ($\bar{\alpha} = 6$, $E/G_a = 200$), the stress reaches its maximum at the end only. The slenderness ratio chosen is obviously not appropriate for this particular case. If by chance, the real E/G_a investigated is below 200, the measurement location should be defined very precisely. In

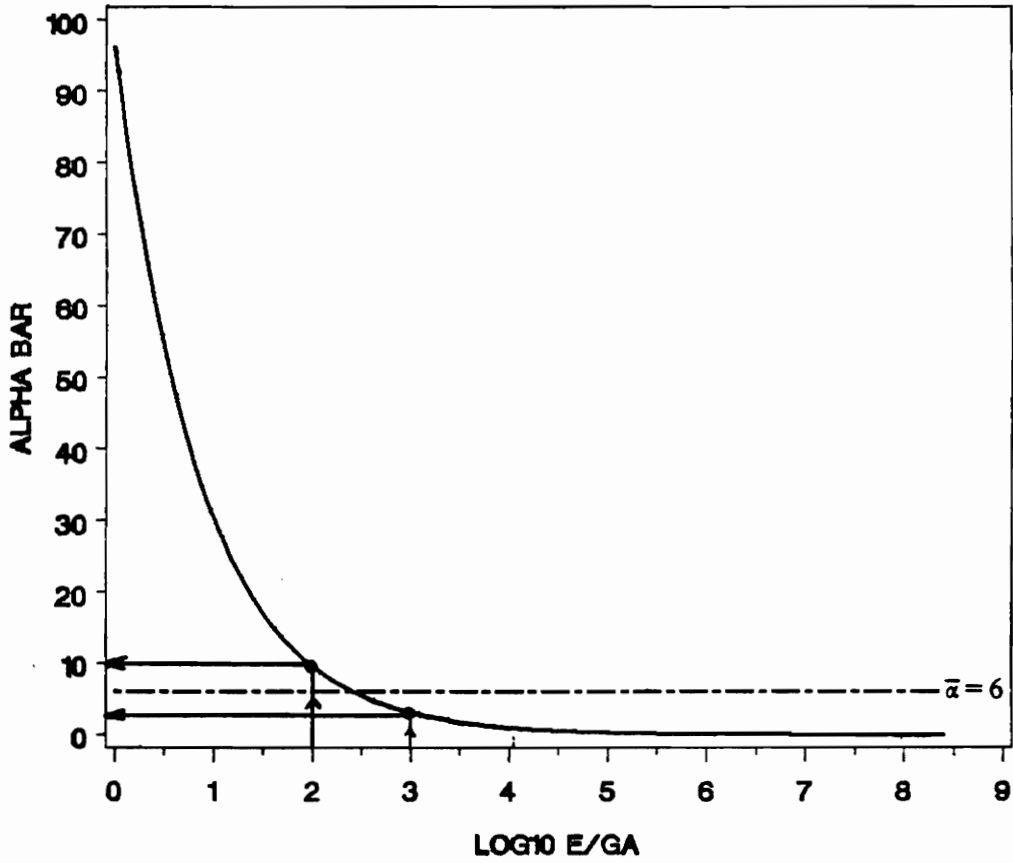


Figure 26. Alpha bar versus E/Ga with $l/h = 10$ and $t/h = 0.05$. Example of specimen dimension determination from an estimate of the stiffness ratio.

this example, we can also see that to remain on the conservative side, the choice of a BMC specimen should be based on an overestimate of the stiffness ratio.

For convenience, a computer program has been written that can help the user to optimize the BMC specimen geometry. The program has the capability of making a geometrical parametric analysis. It computes the data points of the variation of $\bar{\alpha}$ versus E/G_a for various geometries. To run the program, the user has to input a value for the thickness ratio only. The result is a set of guidelines similar to those shown in fig.24. The listing of the program is presented in appendix A and the basic steps of the procedure are described below .

user part :

- define t/h

computer part :

- do loop ℓ/h
- do loop E/G_a
- plot $\bar{\alpha} = f (E/G_a)$ varying ℓ/h

user part :

- analyze the plot
- define ℓ/h , according to the estimate of E/G_a and the adherend thicknesses available.

3.2.3 - Proposal for a unique specimen dimension

The BMC shear deformation test is convenient and easy to perform as long as the stress is not a function of material parameters E and G_a . This condition occurs only for stiff adhesives such that the stiffness ratio is below 10^4 depending on the geometry. When we look at the variation of the maximum shear stress versus the stiffness ratio, the entire domain of this type of adhesives is covered for the highest slenderness ratio ℓ/h and the smallest thickness ratio t/h (fig.20). For practical convenience, the smallest slenderness ratio would be more suitable but it would imply a reduction of the adhesive stiffness range that can be tested. However, from the information presented previously in table 3 where some adhesive properties are listed, it can be seen that the definition of stiff adhesives can be limited to $E/G_a = 10^3$, instead of 10^4 . It follows that ℓ/h can be reduced to seek a specimen geometry which will produce stress uniformity covering the entire stiff adhesive domain. Several solutions are proposed for a unique BMC shear deformation test specimen. Results are presented in table 4 in terms of percent stress uniformity along the beam.

Table 4. Definition of a unique specimen geometry for BMC shear deformation test applied to stiff adhesives (limit of validity : $E/Ga \leq 1000$).

percentage of constant shear stress	t/h	ℓ/h	h (in.)	2t (in.)	ℓ (in.)
70 %	0.02	40	0.0625	0.02500	2.5
	0.02	40	0.1250	0.00500	5.0
	0.05	50	0.0625	0.00625	3.125
	0.05	50	0.1250	0.01250	6.2
	0.10	70	0.0625	0.01250	4.375
	0.10	70	0.1250	0.02500	8.75
	0.20	80	0.0625	0.02500	5.0
	0.20	80	0.1250	0.05000	10.0
80 %	0.01	40	0.0625	0.00125	2.5
	0.01	40	0.1250	0.00250	5.0
	0.01	40	0.2500	0.00500	10.0
	0.02	50	0.0625	0.00250	3.125
	0.02	50	0.1250	0.00500	6.25
	0.04	70	0.0625	0.00500	4.375
	0.04	70	0.1250	0.01000	8.75
	0.05	80	0.0625	0.00625	5.0
	0.05	80	0.1250	0.01250	10.0
	0.10	100	0.0625	0.01250	6.25
	0.10	100	0.1250	0.02500	12.5
	0.15	120	0.0625	0.01875	7.5
	0.20	130	0.0625	0.02500	8.125
85 %	0.02	70	0.0625	0.00250	4.375
	0.02	70	0.1250	0.00500	8.75
	0.05	100	0.0625	0.00625	6.25

3.2.4 - Definition of a specimen dimension for property measurement with Scanning Electron Microscopy (SEM)

One of the long range objectives in the study of adhesives is to find a means to measure and observe properties and related deformation mechanisms at micron or submicron levels especially near the adhesive/adherend interface. To accomplish this task, it is essential to have a simple specimen with a pure shear stress state which can be tested in an SEM. The BMC specimen appears to be a good candidate for such a specimen and such a test. However, the dimensions of the vacuum chamber requires that a relatively short specimen be used. If the beam length does not exceed 3 in., 50% to 60% of the total adhesive length can be analyzed, starting from the loaded end. If the beam length is one inch longer, only 25% of the adhesive length can be analyzed. Therefore, there is a limitation on the beam length and we present herein possible specimen geometries for this particular application. For this purpose, we start with the limitation that $\ell = 3$ in. and we arbitrary chose an adhesive thickness $2t = 0.005$ in.. The parametric analysis is presented in table 5. Knowing t and ℓ , various magnitudes of adherend thickness and the associated ratios are calculated. Then, the analysis is limited to the range of stiff adhesives such that $E/G_a \leq 10^3$ to compute the minimum slenderness ratio required for a given state of shear stress within the bondline. Under these conditions, several specimen configurations are suitable one of which is given below.

$$h = 0.125 \text{ in.}, \ell = 3 \text{ in.}, 2t = 0.005 \text{ in.}$$

The dimensionless ratios are :

$$t/h = 0.02, \ell/h = 24$$

And the test is defined for stiffness ratios varying from 1 to 10^3 . In this example, the shear stress is constant over 50 % of the specimen's length which is well within the range of travel of many SEMs.

Table 5. Definition of a specimen dimension for SEM application with $2t = 0.005$ in. and $\ell = 3$ in.

h (in.)	0.0625	0.125	0.250
t/h	0.04	0.02	0.01
ℓ/h	48	24	12
$(\ell/h)_{\min \text{ required}}$ 80 % *	70	50	40
$(\ell/h)_{\min \text{ required}}$ 70 % *	40	40	30
$(\ell/h)_{\min \text{ required}}$ 60 % *	35	30	25
$(\ell/h)_{\min \text{ required}}$ 50 % *	30	20	20

(*) minimum slenderness required by theory to get the percentage of uniform shear stress indicated.

3.3 - A LOAD DEFLECTION TEST TO DETERMINE THE ADHESIVE SHEAR MODULUS

The end point deflection of the BMC cantilever beam adhesive bond test can also be used as a means to characterize adhesive shear properties. The method is convenient and simple because it consists in measuring the end deflection and calculating the shear modulus using equation (18) given in chapter 2. This method uses the dimensionless value β reported in the graph presented in fig.12 (chapter 2) as a function the stiffness ratio.

Several ways can be used to handle the data generated with this test. First of all, from the measurement of the end deflection δ , Moussiaux [6] suggested that equation (16) be solved numerically for $\bar{\alpha}$ and then use the result to calculate G_a :

$$\delta = \frac{P\ell^3}{2Eb(h+t)^3} (1+t/h)^3 \left[4 \left(1 - \frac{1}{\gamma^2} \right) + \frac{3E}{2G} \left(\frac{h}{\ell} \right)^2 + \frac{12}{\gamma^2} \left(\frac{1}{\bar{\alpha}^2} - \frac{1}{\bar{\alpha}^3} \tanh \bar{\alpha} \right) \right] \quad (16)$$

$$\bar{\alpha} = \sqrt{\frac{3G_a}{E} \left(\frac{\ell}{h} \right)^2 \frac{(1+2t)^2}{t/h} \left(1 + \frac{1}{3(1+2t/h)^2} \right)} \quad (11)$$

and,

$$\gamma^2 = 1 + \frac{1}{3(1+2t/h)^2} \quad (15)$$

On the other hand, a graphical determination of G_a using the curves given by Moussiaux in fig.11 (chapter 2) is more direct and easier to use. However, for low beam deformability (low ratio E/G_a), the dimensionless end deflection tends to an asymptotic value equal to unity. In that case, the coefficient β is not sensitive to the variations of the stiffness ratio. As the ratio decreases, the adherend-adhesive combination tends to constitute a system with a resulting stiffness which approaches that of the adherend itself. As a consequence, the beam behaves like a monolithic isotropic beam of thickness $2(h+t)$. For large stiffness ratios, the same phenomenon occurs with a different

physical meaning. For soft adhesives, the adherends can develop their full deformation like two independent monolithic beams of thickness h . The shear strain is maximum but it also becomes insensitive to material properties variations as seen in fig.22. In these domains where the deflection is not sensitive to the material stiffnesses, the adhesive shear properties cannot be extracted. It follows that the bond properties can be evaluated only if the stiffness ratio investigated lies where β increases rapidly with the stiffness ratio E/G_a .

We can see in fig.11 that the domain of large β variations always covers two orders of magnitude of variation in the stiffness ratio. This is a rather narrow range but does clearly indicate that a unique test specimen can be designed to test adhesives with a BMC deflection method. In conclusion, adhesive shear properties can be evaluated by measuring the beam end point deflection, provided that the specimen geometry is chosen carefully.

In the next section, in order to study the beam deflection response for various geometrical and material conditions, a parametric analysis has been performed whose purpose is to create guidelines that would help the user predict adequate specimen dimensions. First, the effect of the shear term in the deflection equation is analyzed.

3.3.1 - Influence of the adherend shear deformation on deflection

Close examination of equation (16) on the previous page reveals that the total beam deformation is composed of contributions from the bending of the adherends, shear deformation of the adherends and shear deformation of the adhesive layer. These are respectively represented by each of the three terms in the square bracket.

A properly designed test specimen should minimize the effects of adherend shear deformations. To visualize the proper conditions to minimize this contribution, the value of

$$\beta = (1 + t/h)^3 \left[4 \left(1 - \frac{1}{\gamma^2} \right) + \frac{3E}{2G} \left(\frac{h}{\ell} \right)^2 + \frac{12}{\gamma^2} \left(\frac{1}{\bar{\alpha}^2} - \frac{1}{\bar{\alpha}^3} \tanh \bar{\alpha} \right) \right] \quad (18)$$

is plotted in fig.27 with (dashed line) and without (solid line) the middle or adherend shear term. As can be observed, the solid and dashed curves coincide for large slenderness ratios ℓ/h . As a result, to avoid adherend shear deformation effects requires a large slenderness ratio.

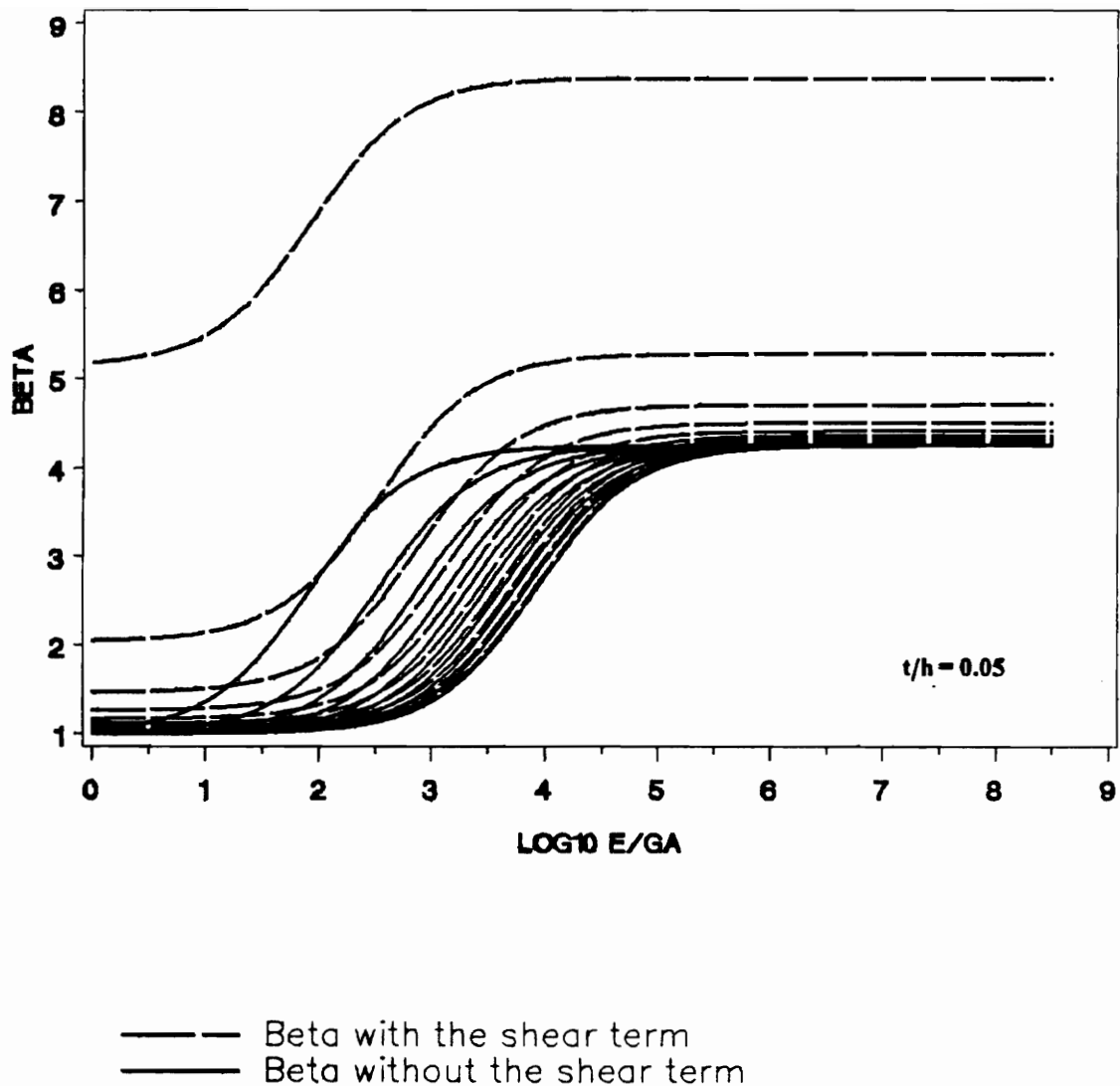


Figure 27. Influence of the shear term on the end deflection. From left to right, l/h varies from 1 to 10 in steps of 1 between each curve.

3.3.2 - Parametric analysis

The preceding discussion has demonstrated that a specimen geometry can be selected to test adhesives with the end deflection method. For each stiffness ratio investigated, the parameter β can only be easily found in the region of rapid variation as seen in fig.28. Therefore, the choice of the geometry is important because the resulting end deflection might be insensitive to materials properties if the experimental data or β lie on the horizontal plateaus of the (β vs. E/G_s) curve. A procedure to select the proper geometry is now proposed and it starts with the assumption that an estimate of the stiffness ratio is available. A computer program was written to determine the variations of the dimensionless end deflection versus beam stiffness ratios. The goal of the procedure is to present on the same figure, the data resulting from the combination of various geometries. In this form, to the user is given an overview of the possible beam geometries that can make the test successful. It is required that the thickness ratio be input to execute the program for various combinations of both the slenderness ratio and the stiffness ratio. The results are shown in fig.28 for $t/h = 0.05$ and fig.29 for $t/h = 0.04$. The values of the slenderness ratio are limited to vary from 20 to 170. Previous discussions have shown that under 10, the slenderness ratio severely influences the beam deflection by making the adherend shear term dominant compared to other terms. The upper limit is due to the fact that the β curves converge for values of ℓ/h around 170 making the use of higher slenderness ratios needless which is in agreement with the conclusions on the parametric study limitations discussed in section 3.1. A listing of the program is reported in appendix with examples computed for varying thickness ratios. An example of the choice of specimen dimension is given in fig.30 for which we assumed that the stiffness ratio was around 10^4 . One can appreciate the simplicity of the evaluation of the proper specimen geometry.

Next, a numerical analysis of the BMC specimen with Finite Element Methods is developed.

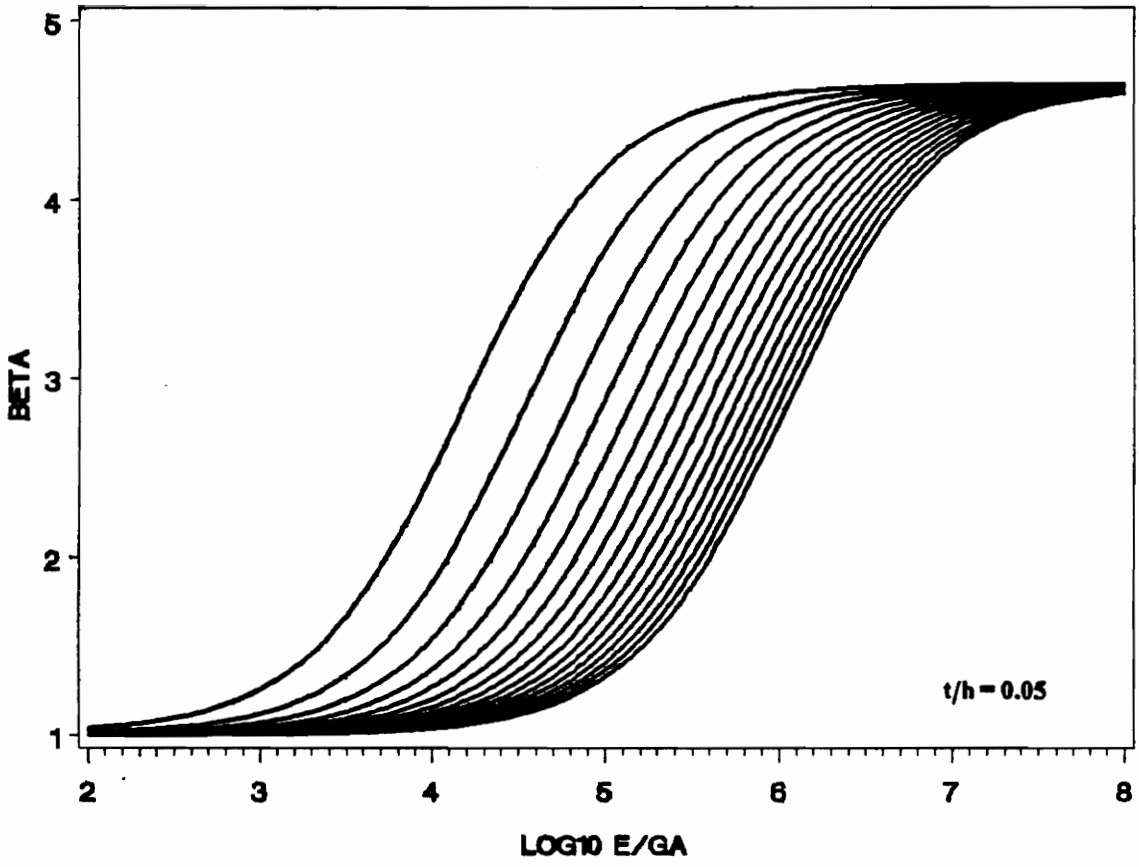


Figure 28. Variation of beta versus E/Ga. From left to right, l/h varies from 20 to 170 in steps of 10 between each curve.

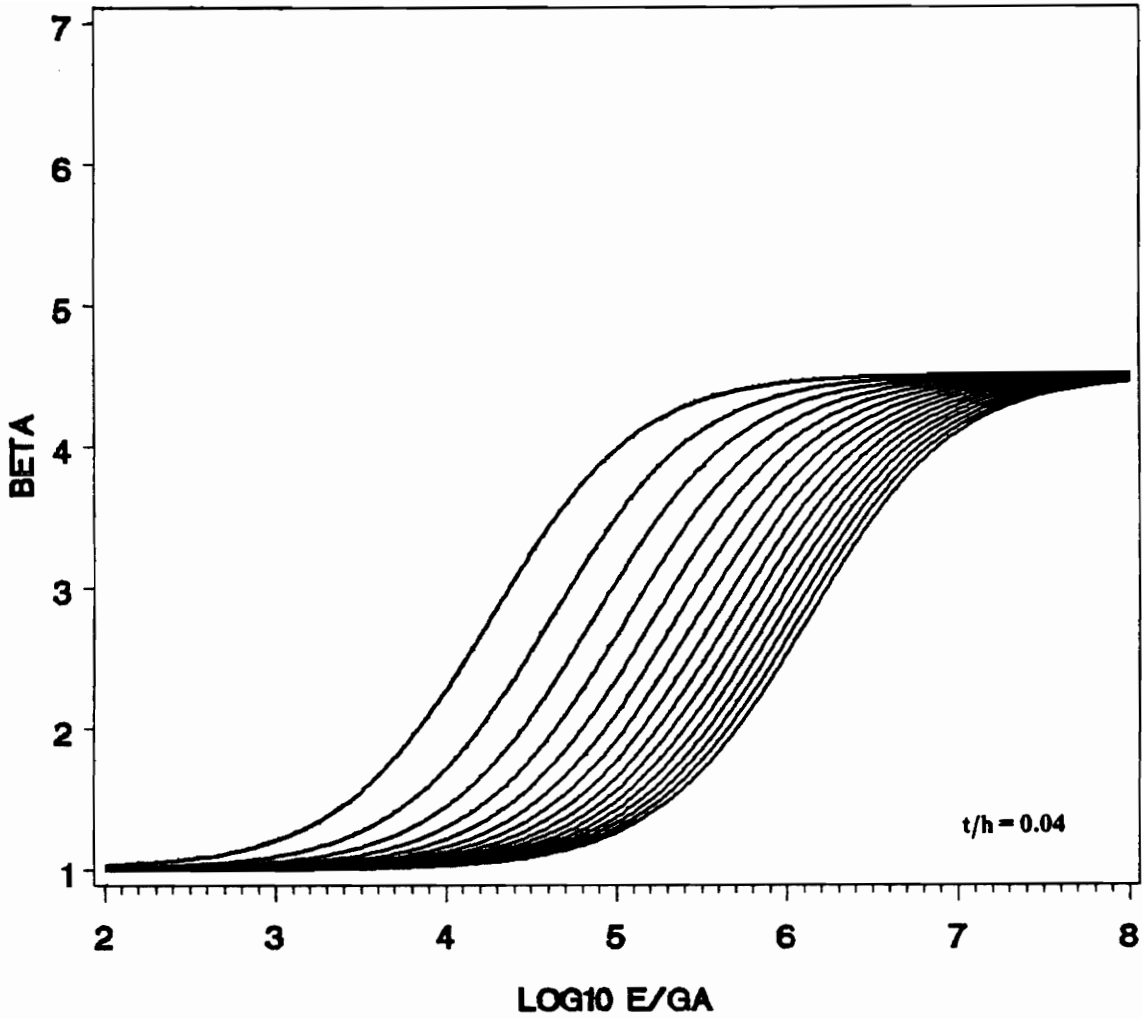


Figure 29. Variation of beta versus E/Ga. From left to right, t/h varies from 20 to 170 in steps of 10 between each curve.

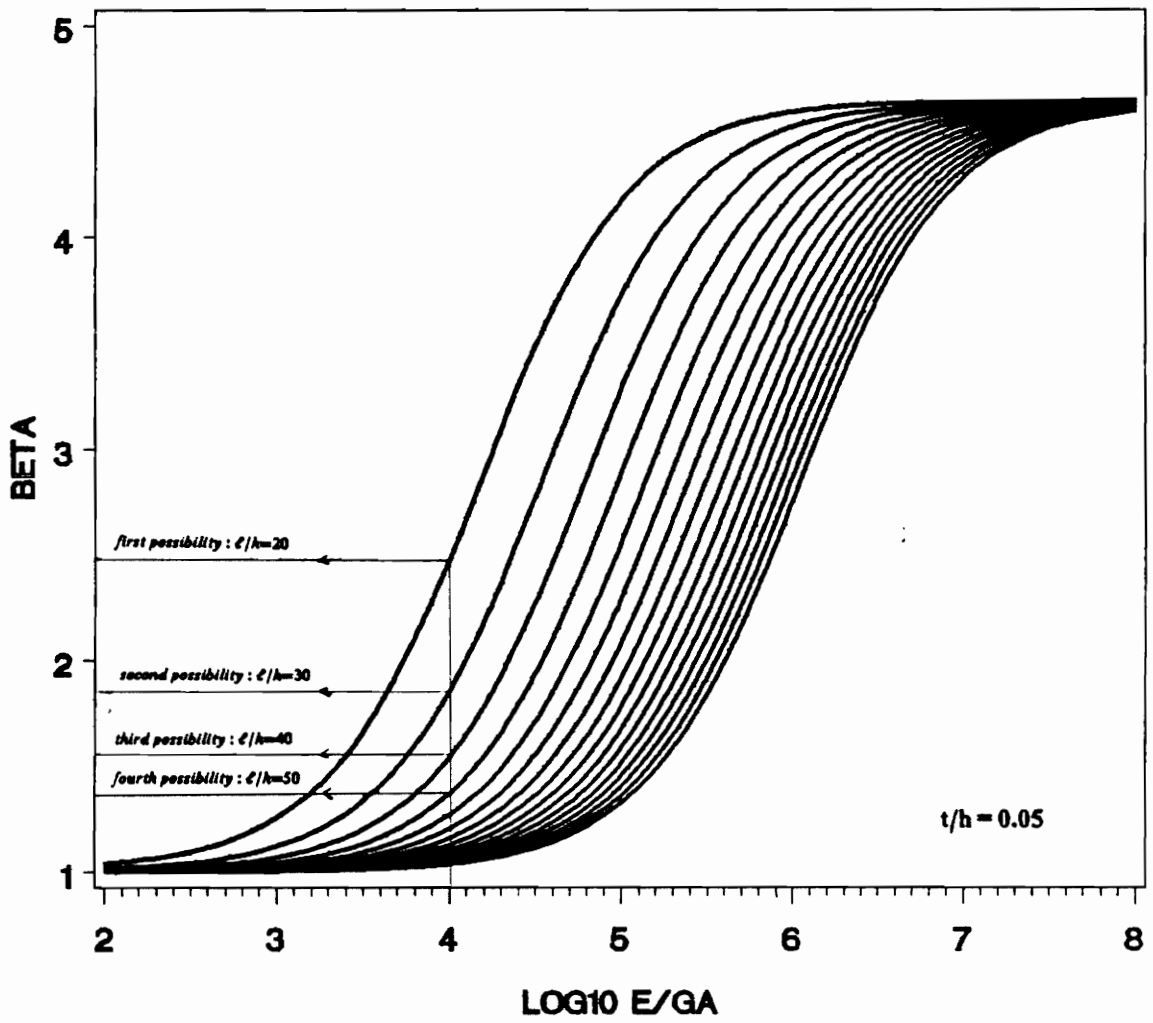


Figure 30. Variation of beta versus E/Ga. Example of specimen determination from an estimate of the stiffness ratio

4 - FINITE ELEMENTS METHODS (FEM) APPLIED TO THE ANALYSIS OF THE BMC SPECIMEN

In reference [6], a numerical evaluation of the BMC model was performed to obtain both the shear stress distribution in the adhesive layer and the beam deflection. The analysis was conducted with the Finite Element code VISTA which permits the study of plane strain problems. For the cases investigated, it was revealed that a uniform and pure shear stress was acting in the adhesive layer. Numerical shear stress singularities occurred close to the loaded end however, for which no consistent explanations were provided. In reference [6], VISTA was also used for the analysis of the beam deflection but no agreement was obtained when the analytical results were compared to the numerical results : each computed case differed by 5 % up to 10 % from theoretical values. These discrepancies may be attributed to the fact that VISTA solves plane strain types of problems only, whereas the theoretical solution was derived from the plane stress Euler-Bernoulli beam theory. When dealing with a plane strain problem, the bending stiffness is larger than that for plane stress, and hence, a smaller deflection is obtained for the same applied load.

In the present work, the numerical analysis of the BMC specimen started by Moussiaux is extended and consists in a numerical parametric analysis. A complete study of the BMC model is possible by using additional FEM codes. First of all, we extend the BMC theory in the case of plane strain in order to complete the numerical evaluation by Moussiaux.

4.2 - EXTENSION OF THE BMC THEORY TO PLANE STRAIN

In Moussiaux's work, plane stress theory has been compared to a plane strain numerical code and discrepancies were found for deflections in the few cases investigated. In this section, we use Theory of Elasticity to transform in plane strain the shear stress equation and the beam deflection equations derived in the BMC theory. Next, solutions will be compared to the code VISTA.

4.2.1 - Shear stress distribution in a state of plane strain

In reference [6], the shear stress solution from the BMC theory has been compared with VISTA and has been validated because of the very good agreement found between numerical and analytical approaches. In the cases investigated, adhesives were relatively stiff and large values of the parameter $\bar{\alpha}$ resulted making the shear stress constant in a large section of the adhesive layer. Our first work has consisted in running cases assuming soft adhesive which implies a small value of the parameter $\bar{\alpha}$ such that the maximum shear stress defined in equation (12a) could never be reached. We found that the shear stress magnitude is always less than that calculated from the original BMC theory. Then, conclusions from [6] were questionable and we tried to rewrite the shear stress equation in order to account for plane strain problems.

For the plane stress situation, the shear stress distribution at the midplane of the BMC specimen is :

$$\tau_{xy}(x) = \bar{\tau} \left(1 - \cosh \bar{\alpha} \frac{x}{\ell} + \tanh \bar{\alpha} \sinh \bar{\alpha} \frac{x}{\ell} \right) \quad (10a)$$

where,

$$\bar{\alpha} = \sqrt{3 \frac{G_a}{E} \left(\frac{\ell}{h} \right)^2 \frac{(1 + 2t/h)^2}{t/h} \left(1 + \frac{1}{3(1 + 2t/h)^2} \right)} \quad (11)$$

Replacing E in the latter equations by $\frac{E}{1 - \nu^2}$ and ν by $\frac{\nu}{1 - \nu}$ transforms the equations to their general form for the plane strain condition. The new solution leaves the adherend and the adhesive shear moduli unchanged, but the coefficient $\bar{\alpha}$ becomes $\bar{\alpha}\sqrt{1 - \nu^2}$.

Therefore, the shear stress distribution for plane strain is as follows:

$$\tau_{xy}^e(x) = \bar{\tau} \left(1 - \cosh \bar{\alpha} \frac{x}{\ell} \sqrt{1 - \nu^2} + \tanh(\bar{\alpha}\sqrt{1 - \nu^2}) \sinh(\bar{\alpha} \frac{x}{\ell} \sqrt{1 - \nu^2}) \right) \quad (23)$$

As shown above, equation (23) differs from equation (10a) by the presence of a factor $\sqrt{1 - \nu^2}$ in the hyperbolic functions. We can see that due to the nature of the variations of the hyperbolic functions \cosh and \sinh , this factor will cause the shear stress to vary differently to its variation calculated from the plane stress theory.

Comparison between the theoretical solution represented in equation (23) and numerical results from VISTA will be presented in section 4.4. Next, we turn to the development of the beam deflection equation in the case of plane strain.

4.2.2 - End Deflection of the beam in a state of plane strain

We recall that the beam deflection derived for plane stress is given by :

$$\delta = \frac{P\ell^3}{2Eb^3} \left[4 + \frac{3E}{2G} \left(\frac{h}{\ell} \right)^2 + \frac{12}{\gamma^2} \left(\frac{1}{\bar{\alpha}^2} - \frac{1}{3} - \frac{1}{\bar{\alpha}^3} \tanh \bar{\alpha} \right) \right] \quad (16)$$

Proceeding as we did for the shear stress, the form of this equation in plane strain becomes as follows:

$$\delta^e = \frac{P\ell^3(1-\nu^2)}{2Ebh^3} \left[4 + \frac{3E}{2G(1-\nu^2)} \left(\frac{h}{\ell} \right)^2 + \right] \left[\frac{12}{\gamma^2} \left(\frac{1}{\bar{\alpha}^2(1-\nu^2)} - \frac{1}{3} - \frac{1}{\bar{\alpha}^3(1-\nu^2)\sqrt{1-\nu^2}} \tanh \bar{\alpha}\sqrt{1-\nu^2} \right) \right] \quad (24)$$

When we look at equation (24), it is clear that a smaller deflection will result in plane strain due to the factor $(1-\nu^2)$ in front and inside the square bracket. Results for deflection will be also presented in section 4.4 in comparison with FEM.

4.3 - DESCRIPTION OF THE FEM CODES AVAILABLE

We first used the finite element code VISTA as prescribed by the work done in [6]. This code may be used for the analysis of axisymmetric bodies or for the plain strain analysis of two-dimensional problems. The material library allows us to model isotropic-linearly elastic, viscoelastic materials, and orthotropic-linearly elastic materials. The element library offers isoparametric quadratic quadrilaterals and triangles as well as subparametric triangle elements. In our study, the specimen was discretized by a two-dimensional plane strain mesh of 8-node isoparametric quadrilateral elements. The mesh, consisting of 633 nodes and 192 elements, is shown in fig.31.

Recently, a new finite-element code called NOVA is available for the stress analysis of in-situ adhesives [10]. NOVA has the capability of solving two-dimensional, planar or axisymmetric problem geometries with either isotropic or anisotropic materials. Routines allow for geometrical nonlinearities and nonlinear viscoelastic behavior in the adhesive. The code was validated by comparison with analytical and experimental results found in the literature for specimens such as the single lap joint, the thick adherend lap joint, rod, viscoelastic adhesive coupon including moisture

diffusion, creep, etc... In our work, NOVA was used for a numerical plane stress analysis of the BMC test specimen. The "NOVA" specimen was discretized into 288 8-node isoparametric and two-dimensional plane stress elements : 24 elements in the x-direction, 12 elements in the y-direction and a total of 937 nodal points. The mesh with NOVA is shown in fig.32.

For each run, we assumed both the adherends and the adhesive to be linear elastic. The Finite Element mesh was gradually refined towards the loaded and the clamped ends in order to describe possible singularities. The loading of the BMC was applied by imposing the following boundary conditions : a symmetric load applied at one end as shown in fig.1 and the other end clamped. The stresses in the adhesive layer and the deflection of the beam were studied for various geometrical and material properties input data in order to analyze the effect of these parameters. Results obtained numerically have been compared to analytical predictions in section 4.4. Before presenting these results, a first study is performed with the code VISTA to provide a better understanding of the numerical shear stress singularities found in reference [6] and recalled at the beginning of this chapter.

4.3.1 - Influence of the Finite Element mesh on the stress distribution

For a more accurate description of the numerical stress gradients near the extremity of the adhesive, a more refined mesh was used for the analysis with VISTA. We divided the adhesive into 24 elements instead of 16 in the x-direction with same refinements close to the edges. The results are shown in fig.33. It can be seen that the stress singularity is shifted to the beam tip as the mesh is refined. Therefore, it appears that the stress singularity occurring when a FEM analysis of the BMC specimen is performed, is sensitive to the degree of refinement of the mesh. By making the mesh even more refined at the edge, the singularity would concentrate in an infinitively small region at the beam extremity. Another comparison with the FEM code NOVA confirms this observation

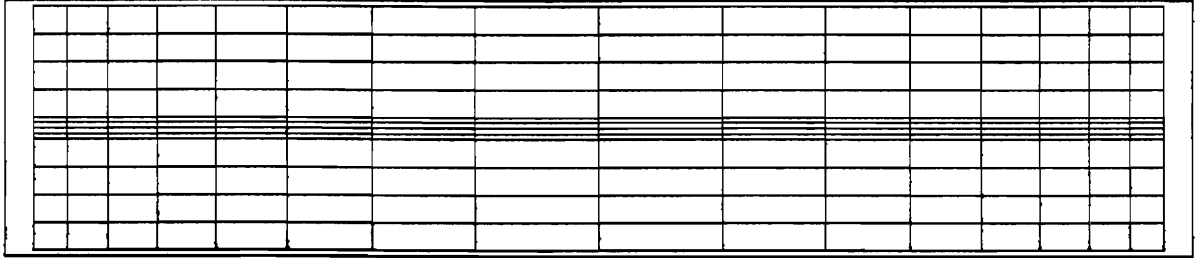


Figure 31. Finite elements mesh used with VISTA

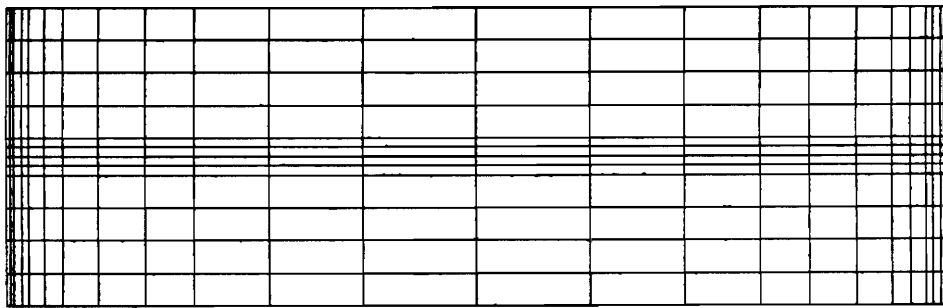


Figure 32. Finite elements mesh used with NOVA

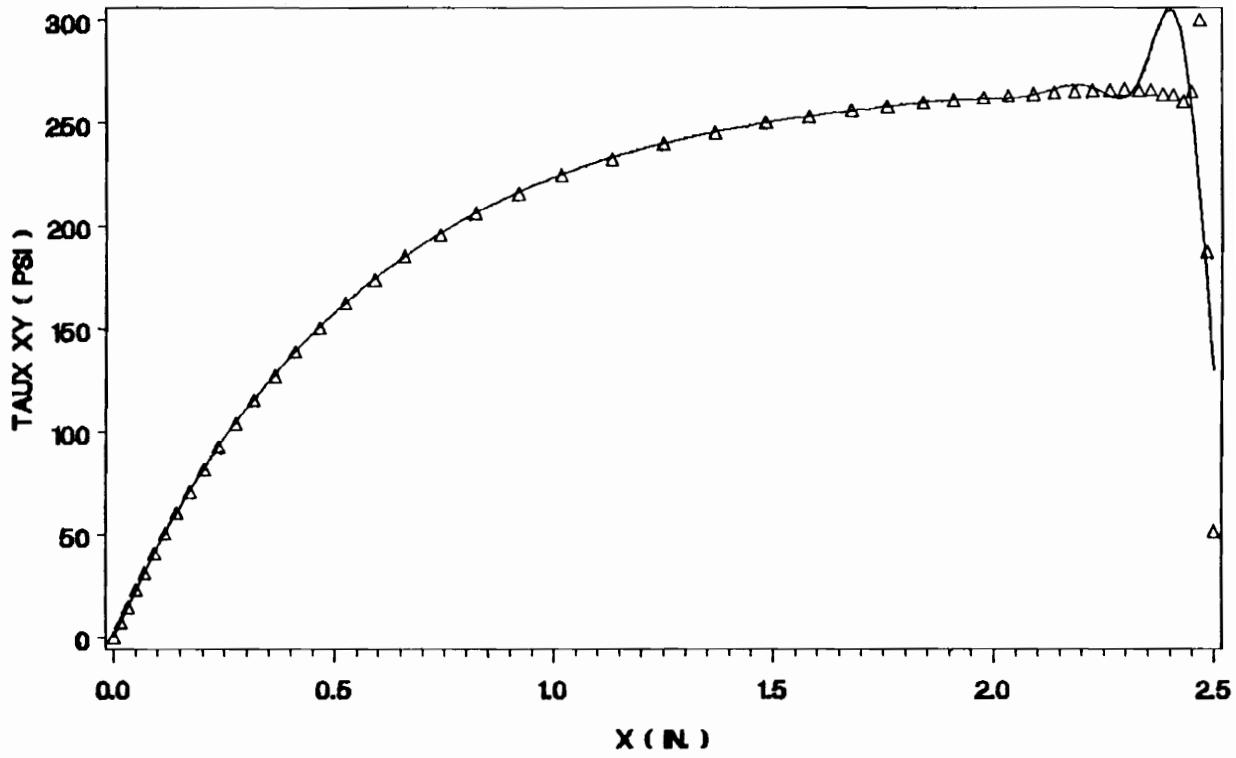


Figure 33. Influence of the mesh refinement on the stress singularity at the tip. Solid curve : mesh with 16 elements in the length direction. Triangles : mesh with 24 elements in the length direction.

with the additional information that the FEM code definition is also involved in the stress numerical singularity observed because it has been noticed in the analysis with NOVA that the stress singularities is smoother than that observed in the analysis with VISTA.

4.4 - COMPARISON OF BMC THEORY WITH FEM RESULTS

Table 6 lists the input data for the comparative FEM analysis. Geometrical and material data are given in terms of parameter $\bar{\alpha}$ in accordance with chapter 3. Numerical results for the maximum shear stress and the end deflection of the beam are printed in table 7, together with the analytical predictions. This allows us to make a comparison between theory and Finite Element results, and also to appreciate the good agreement between them. For a better overview of the quality of the results, a graphical comparison of the beam deflections is shown on fig.34 to 36. Finally, the solution for the shear stress field proposed in chapter 3 for a BMC specimen oriented towards SEM application is checked by numerical analysis. Results are shown in fig.37.

Table 6. Definition of geometrical and material properties used as input data for the numerical analysis.

specimen number	t (in.)	h (in.)	ℓ (in.)	t/h	ℓ/h	E/G_s	$\bar{\alpha}$
1	0.0625	0.25	5.0	0.25	20	100000	0.3
2	0.0625	0.25	5.0	0.25	20	260	6.9
3	0.0250	0.25	2.5	0.10	10	26	14.3
4	0.0250	0.25	2.5	0.10	10	87	7.8
5	0.0250	0.25	2.5	0.10	10	260	4.5
6	0.0250	0.25	2.5	0.10	10	2600	1.4
7	0.0250	0.25	2.5	0.10	10	84000	0.2
8	0.0250	0.25	5.0	0.10	20	260	9.0
9	0.0125	0.25	2.5	0.05	10	26	18.8
10	0.0125	0.25	2.5	0.05	10	87	10.3
11	0.0125	0.25	2.5	0.05	10	260	5.9
12	0.0125	0.25	2.5	0.05	10	2600	1.9
13	0.0125	0.25	2.5	0.05	10	26000	0.6
14	0.0125	0.25	2.5	0.05	10	84000	0.3
15	0.0125	0.25	5.0	0.05	20	84000	0.6
16	0.0050	0.25	2.5	0.02	10	26	28.5
17	0.0050	0.25	2.5	0.02	10	87	15.6
18	0.0050	0.25	2.5	0.02	10	260	9.0
19	0.0050	0.25	2.5	0.02	10	2600	2.8
20	0.0050	0.25	2.5	0.02	10	26000	0.9
21	0.0050	0.25	2.5	0.02	10	84000	0.5

Table 7. Numerical results from FEM codes VISTA and NOVA compared with BMC theory (P = 100 Lb.).

specimen number	VISTA		THEORY (1)		NOVA (2)		THEORY (2)	
	τ_{xy}^{max} (Psi)	δ (in.)	τ_{xy}^{max} (Psi)	δ (in.)	τ_{xy}^{max} (Psi)	δ (in.)	τ_{xy}^{max} (Psi)	δ (in.)
1	13	1.37E-01	12	1.40E-01	14	1.53E-01	14	1.54E-01
2	233	2.62E-02	232	2.60E-02	235	2.84E-02	232	2.85E-02
3	271	3.72E-03	271	3.81E-03	272	4.17E-03	271	4.17E-03
4	271	4.17E-03	270	4.24E-03	271	4.64E-03	271	4.65E-03
5	266	5.27E-03	265	5.30E-03	266	5.75E-03	265	5.81E-03
6	144	1.10E-02	141	1.17E-02	150	1.30E-02	148	1.29E-02
7	8	5.79E-03	8	6.00E-03	10	6.53E-03	8	6.60E-03
8	272	3.16E-02	271	3.16E-02	271	3.49E-02	271	3.47E-02
9	285	4.15E-03	285	4.23E-03	285	4.63E-03	285	4.64E-03
10	285	4.41E-03	285	4.48E-03	285	4.95E-03	285	4.91E-03
11	285	5.08E-03	284	5.12E-03	285	5.67E-03	284	5.61E-03
12	195	1.00E-02	194	1.00E-02	202	1.14E-02	201	1.10E-02
13	42	1.61E-02	41	1.66E-02	45	1.74E-02	44	1.82E-02
14	14	5.75E-03	14	5.93E-03	15	6.28E-03	15	6.51E-03
15	49	4.22E-02	49	4.29E-02	55	5.44E-02	53	4.72E-02
16	295	4.45E-03	294	4.53E-03	295	4.97E-03	294	4.96E-03
17	295	4.57E-03	294	4.64E-03	295	5.10E-03	294	5.08E-03
18	295	4.88E-03	294	4.93E-03	295	5.53E-03	294	5.40E-03
19	258	7.84E-03	256	7.81E-03	260	8.84E-03	260	8.57E-03
20	84	1.47E-02	83	1.49E-02	91	1.59E-02	89	1.64E-02
21	31	5.57E-03	31	5.70E-03	35	6.00E-03	34	6.26E-03

(1) plane strain
(2) plane stress

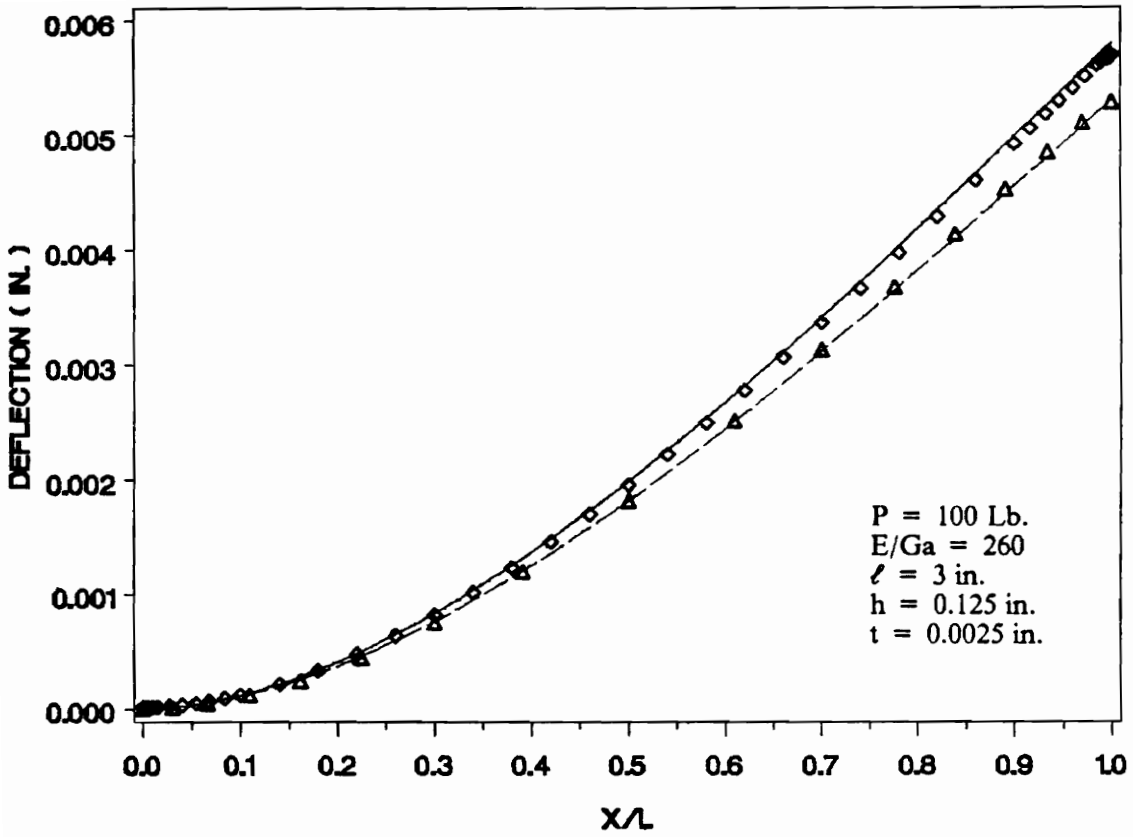
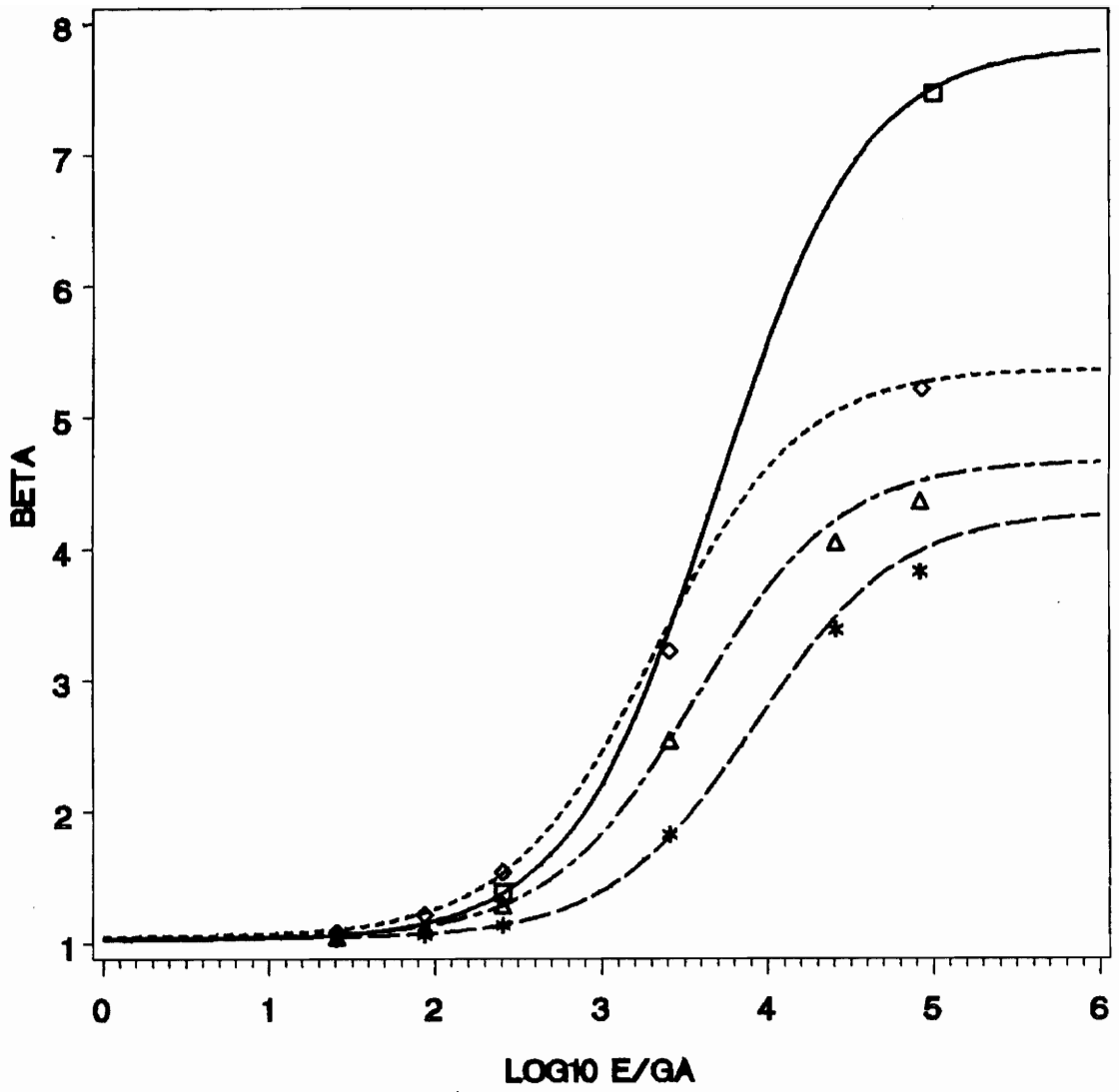
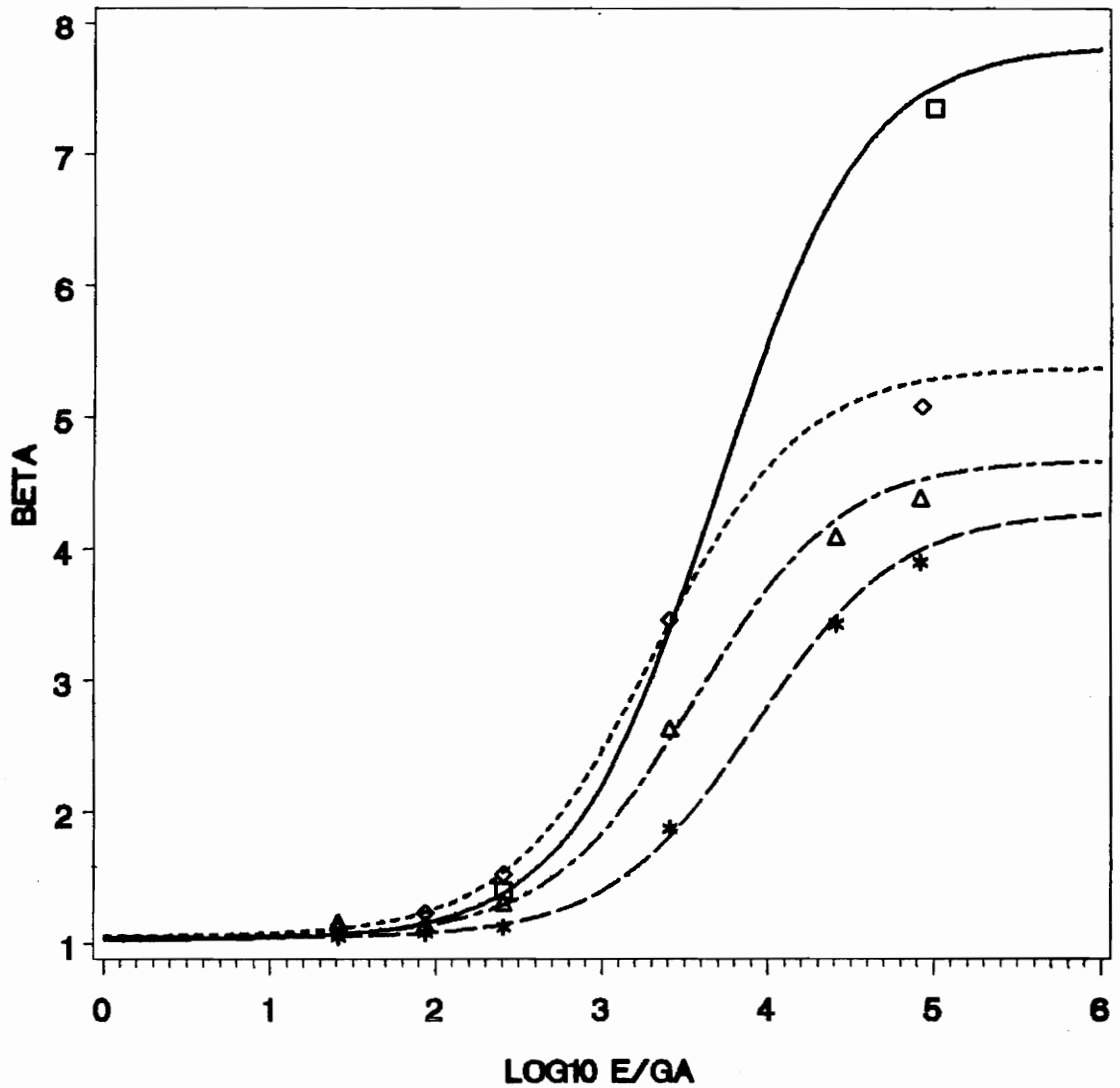


Figure 34. Comparison of the beam deflection obtained with VISTA (triangles), NOVA (diamonds) in plane stress. Solid curve : plane stress BMC theory. Dashed curve : plane strain BMC theory.



BMC THEORY	FEM				
—————	□	□	□	T/H=0.25	L/H=20
- - - - -	◇	◇	◇	T/H=0.10	L/H=10
- · - · -	△	△	△	T/H=0.05	L/H=10
· · · · ·	*	*	*	T/H=0.02	L/H=10

Figure 35. Comparison of numerical and theoretical dimensionless end deflections for the cases computed with NOVA in plane stress.



BMC THEORY	FEM			
—————	□	□	□	T/H=0.25 L/H=20
- - - - -	◇	◇	◇	T/H=0.10 L/H=10
- · - · -	△	△	△	T/H=0.05 L/H=10
- · - - -	*	*	*	T/H=0.02 L/H=10

Figure 36. Comparison of numerical and theoretical dimensionless end deflections for the cases computed with VISTA in plane strain.

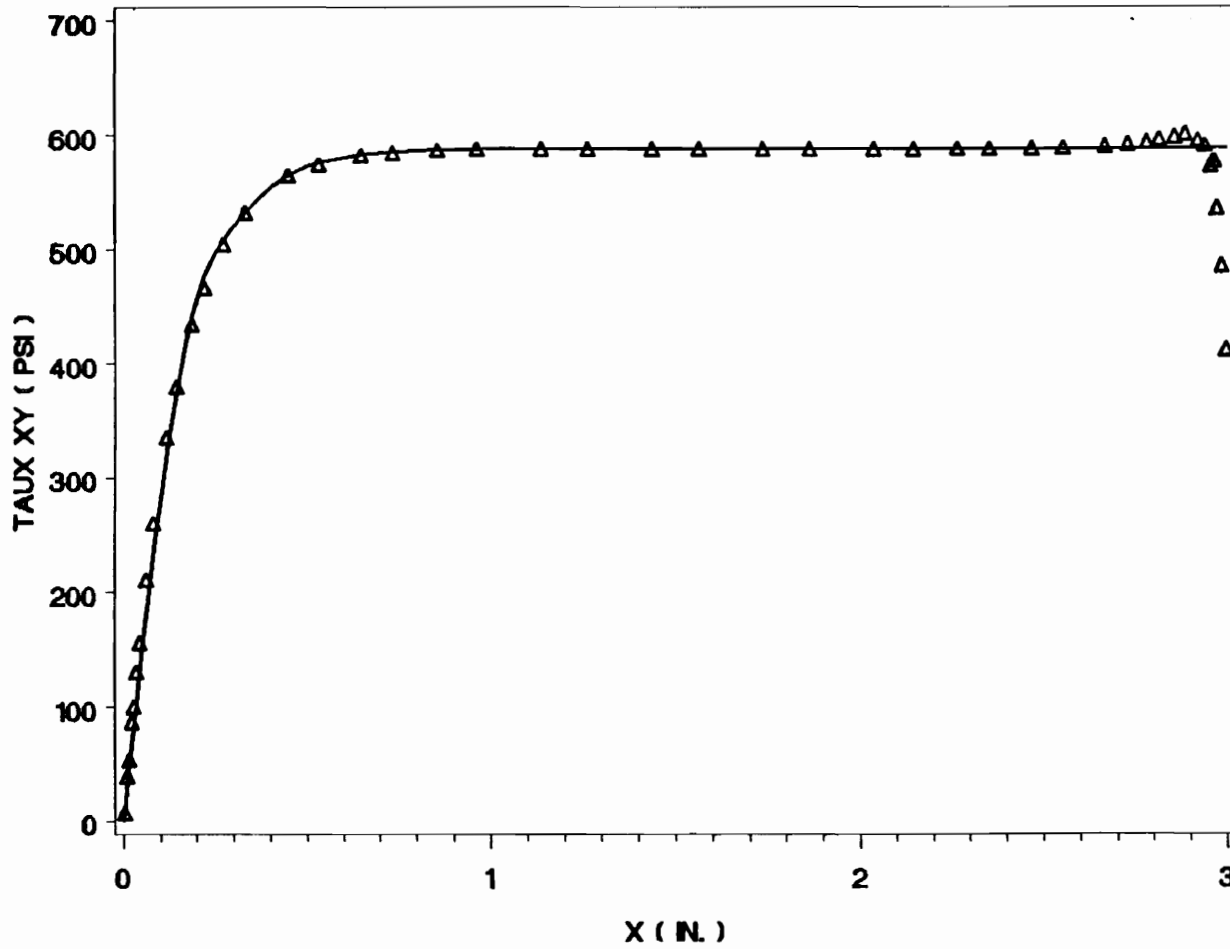


Figure 37. Analysis of the mid-plane shear stress distribution for the SEM specimen- plane line : theory - triangles : numerical with NOVA - $P = 100$ Lb. $E/Ga = 260$ $l = 3$ in. $h = 0.125$ in. $2t = 0.005$ in.

4.5 - STRESS ANALYSIS WITHIN THE ADHESIVE

The FEM codes were used to pursue the analysis of the BMC specimen in greater detail. They provide a further understanding of the role played by modifications in the BMC test specimen in influencing the stresses in the bonded joint. The effect of the loading mode on the stress distribution has already been treated in [6] and it was concluded that the pure shear state within the adhesive layer is severely dependent on the symmetry of the applied load. In the present analysis, the influence of the adhesive thickness on the stress distribution and three-dimensional effects on stresses are studied. A particular BMC specimen with an adhesive layer shorter than the adherends is also analyzed.

4.5.1 - Effects of the adhesive thickness on the stress state

Purity and uniformity of the shear stress state are analyzed for various adhesive thicknesses. For thick adhesives, the purity of the stress state might be perturbed by the development of tensile stresses σ_x and σ_y . In addition, the uniformity of the shear stress distribution can be altered by the increase of the adhesive thickness.

VISTA was used to study the effects of adhesive thickness on the stress distribution within the bondline. Five cases were run and compared for joint thicknesses of 0.005, 0.01, 0.025, 0.05 and 0.25 in.. The material properties used to run these examples were as follows : stiffness ratio $E/G_a = 260$, adherends thicknesses $h = 0.25$ in., and beam lengths $\ell = 2.5$ in.. The only variable was the adhesive thickness $2t$.

Tensile stresses σ_x , σ_y and shear stress τ_x , from the FEM outputs are reported in fig.38 to 42 in the form of iso-stress maps covering all the adhesive layer in the plane x-y. The analysis of these figures revealed that the magnitudes of the tensile stresses do not exceed a few percent of that of the shear stress. This also holds true for the case of thickest adhesive of 0.25 in.. Hence, the shear state

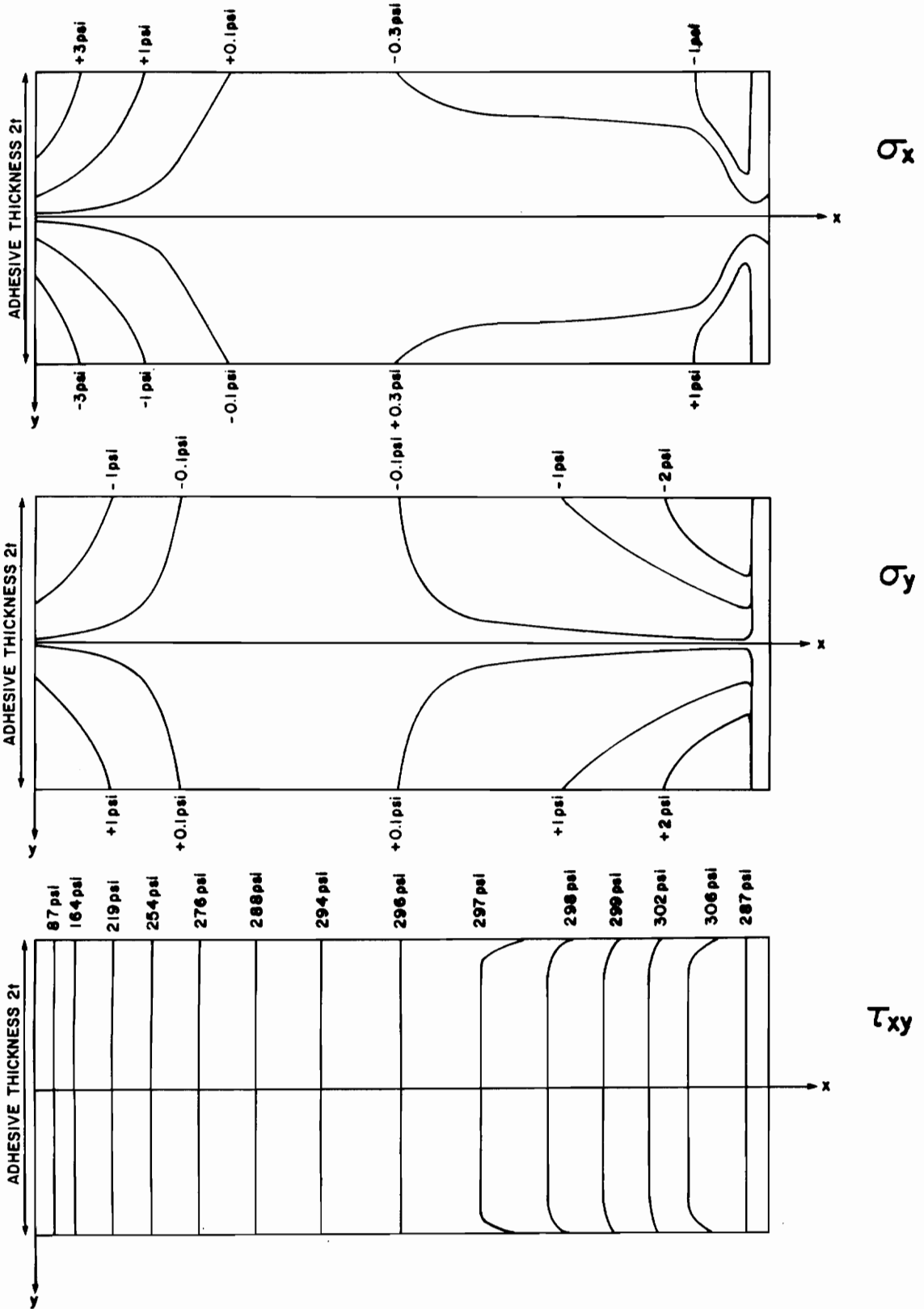


Figure 38. Iso-stress lines in the adhesive layer - $2t = 0.005$ in.

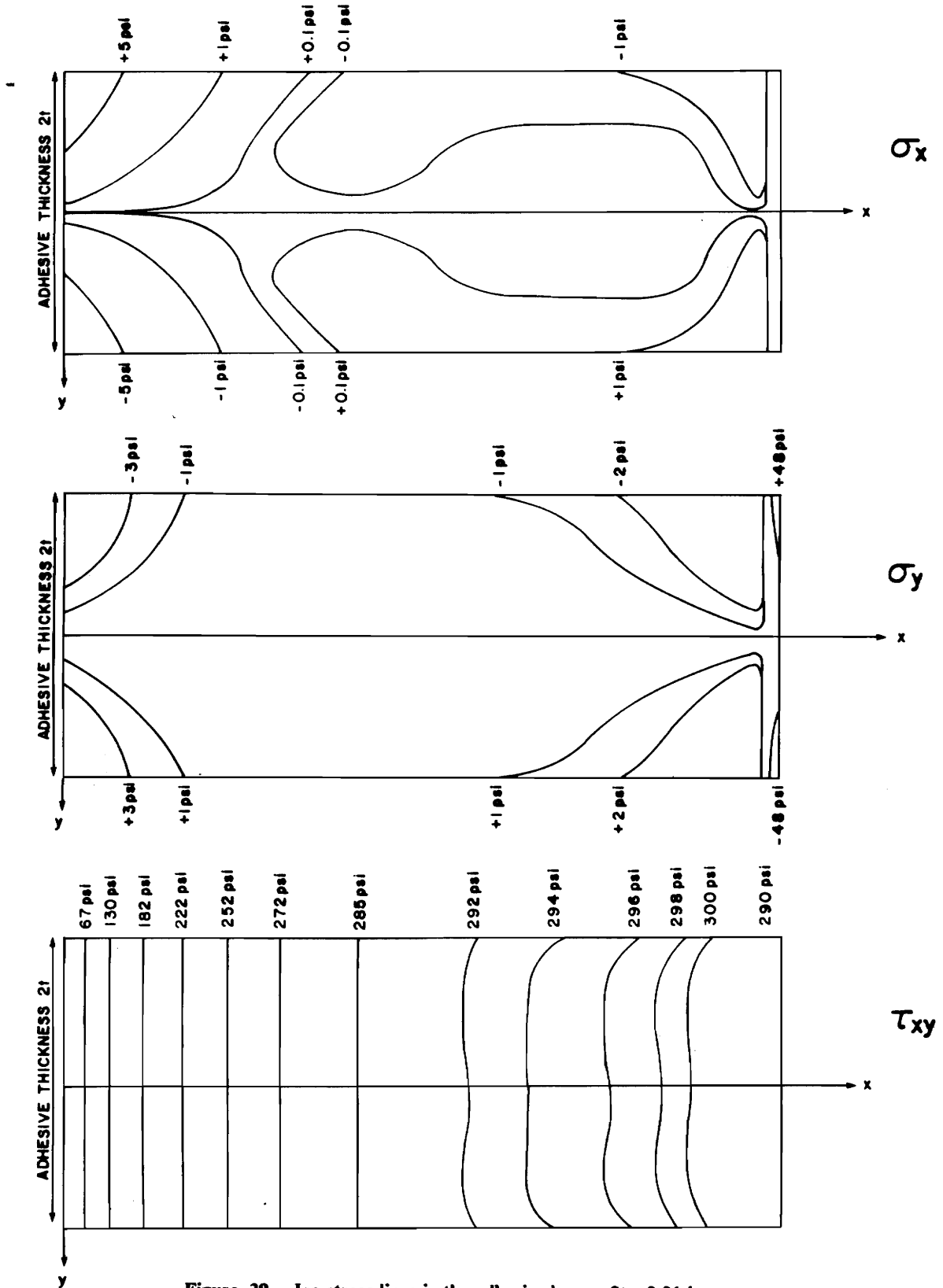


Figure 39. Iso-stress lines in the adhesive layer - $2t = 0.01$ in.

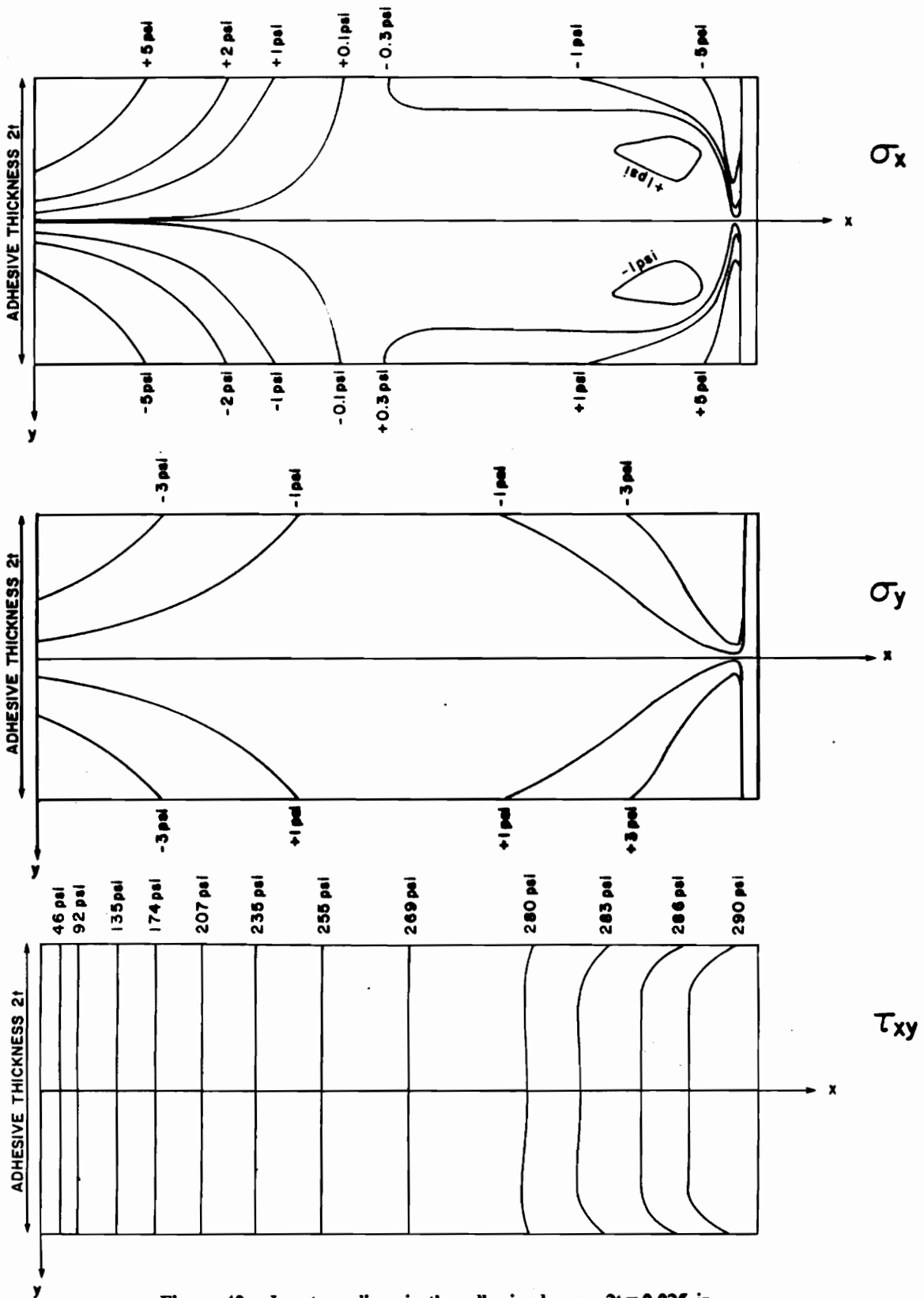


Figure 40. Iso-stress lines in the adhesive layer - $2t = 0.025$ in.

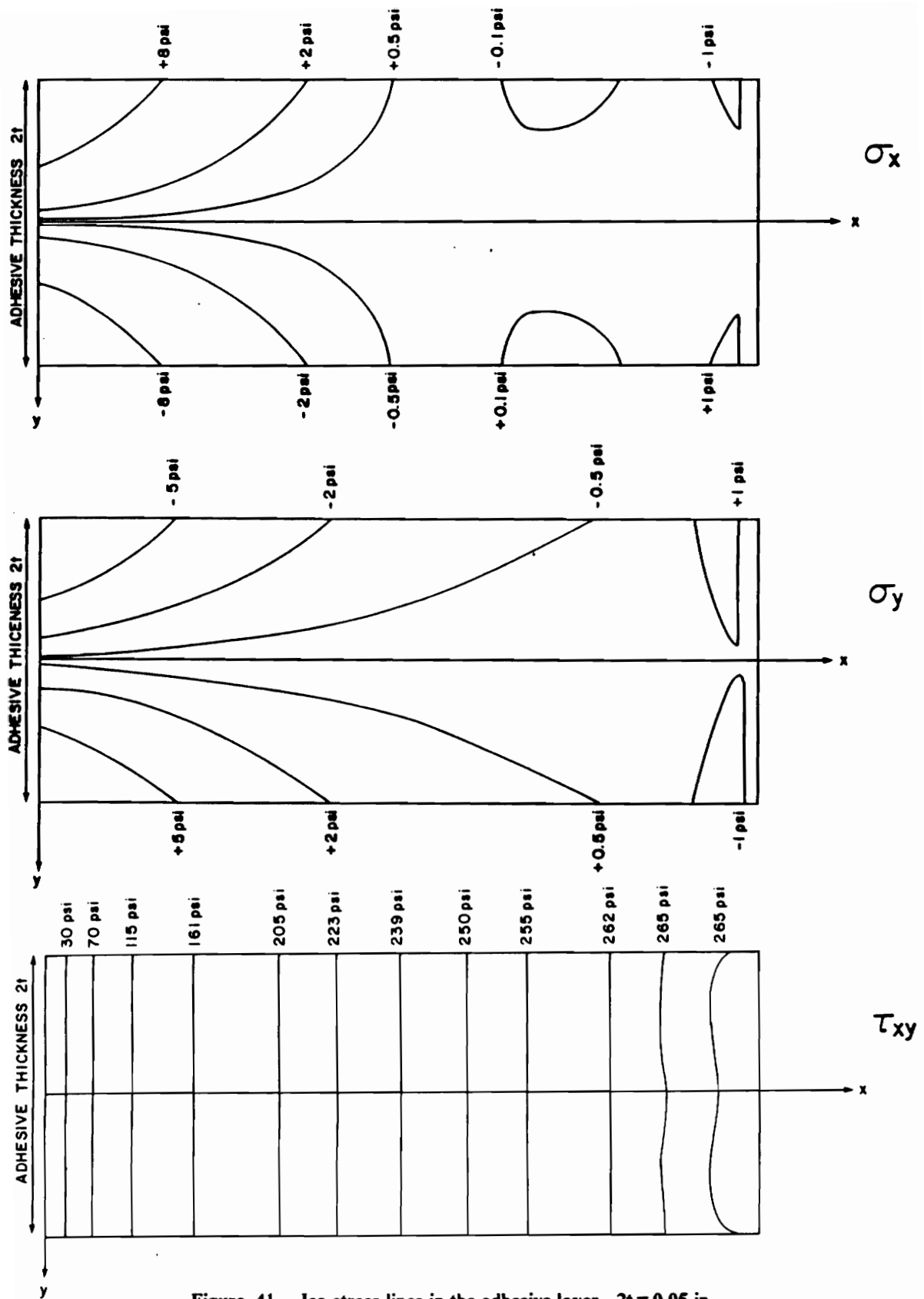


Figure 41. Iso-stress lines in the adhesive layer - $2t = 0.05$ in.

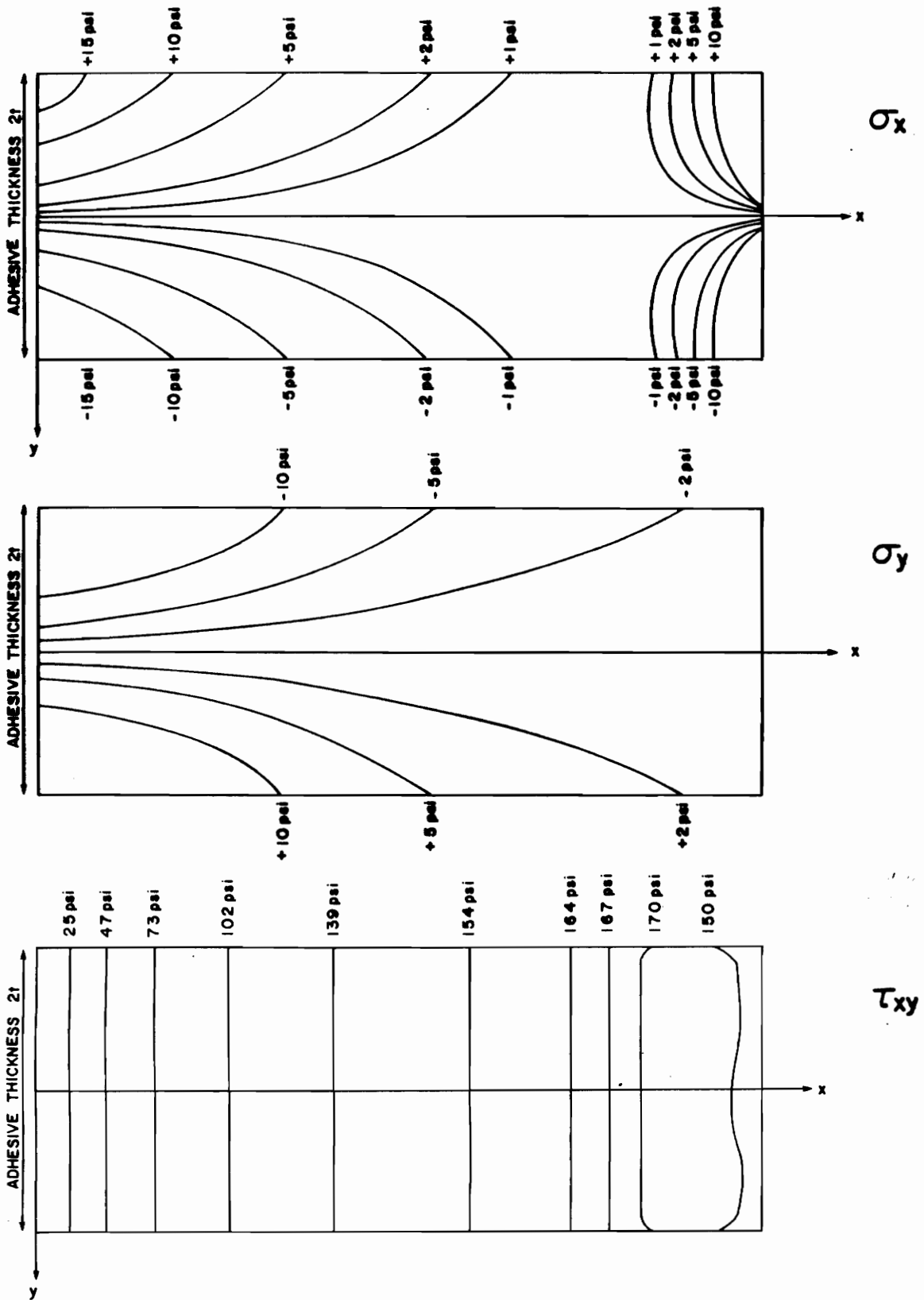


Figure 42. Iso-stress lines in the adhesive layer - $2t = 0.25$ in.

in the adhesive layer is dominant and it is pure at the midplane. The shear stress is also uniform almost everywhere in the y-direction, irrespective of joint thickness. We note however that the shear stress varies in the y-direction in areas such as the adherend-adhesive interface and the loaded end. This fact can be attribute to the discretization of the adhesive layer with VISTA. By refining the mesh in the y-direction and in the x-direction, the intermediate small regions where the shear stress is not constant in the y-direction is expected to be reduced. In conclusion, the thickness of the adhesive layer does have an influence on the stress magnitude but it is not important enough to affect the purity and the uniformity of the shear stress state.

Although their magnitudes are small compared to that of the shear stress, normal stresses do exist in the adhesive layer. Their presence is not acceptable in view of the assumption of pure shear state of the BMC theory. In order to understand the presence of these stresses, a solution is proposed herein for which we turn to the analysis of the adhesive stiffness effect on the adhesive state of stress.

The case of a BMC specimen in which adherends are bonded with a soft adhesive such as rubber has been studied with VISTA. The numerical code showed that the state of stress in the adhesive is pure shear due to the absence of significant tensile stress at any location in the adhesive. Conversely, in the case of a stiff adhesive, the beam tends to act like a monolithic beam and an infinitesimal element of the adhesive experiences tensile stresses σ_x and σ_y in addition to the shear stress τ_{xy} . In fig.43 and 44, we plotted stress fields for two cases studied with FEM. Both cases featured the same specimen geometry and the stresses were picked up at the same location : $x/\ell = 0.5$. Adherends had also the same stiffness and Poisson's ratio. Only the adhesive stiffnesses differed : for one specimen the adhesive Young's modulus was 10^5 Psi and for the second specimen, it was 100 Psi. These properties made the stiffness ratios equal to 260 and 260,000 respectively. The diagrams for the axial stress σ_x clearly reveal the influence of adhesive stiffness on the BMC specimen behavior.

In conclusion, material properties and beam geometry contribute to the magnitude of each stress. FEM showed that in most cases, the state of stress is always shear since the tensile stresses are negligible. Moreover, the pure shear stress state at the midplane of the adhesive is extended to

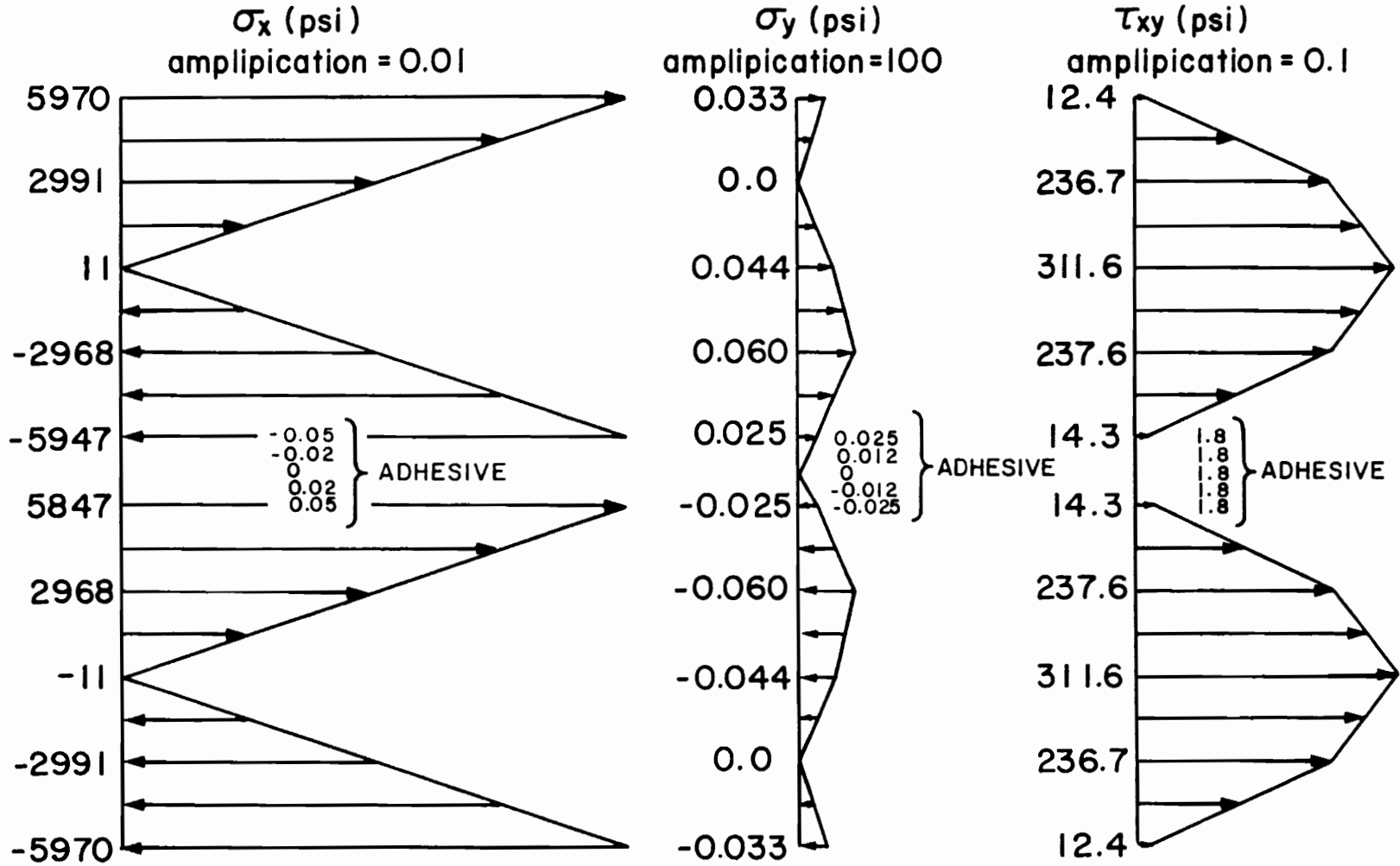


Figure 43. Stress diagrams at $x/\ell = 0.5$ for $\ell/h = 10$, $t/h = 0.10$ and $E/G_a = 260,000$.

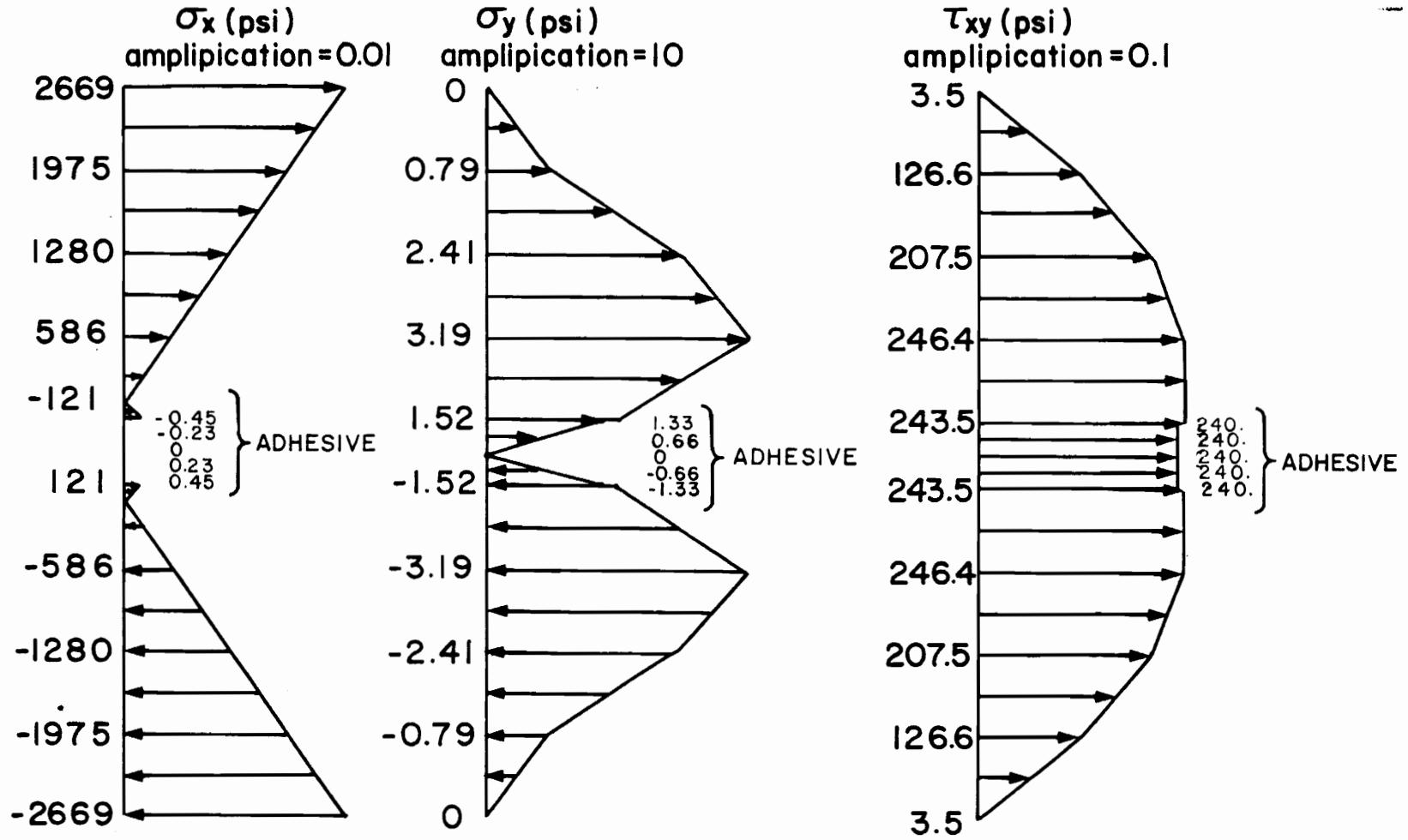


Figure 44. Stress diagrams at $x/l = 0.5$ for $l/h = 10$, $t/h = 0.10$ and $E/Ga = 260$.

the entire bondline when the joint is soft compared to the adherend stiffness. Therefore, the two-dimensional numerical analysis underlines that the BMC theory based on the assumption of pure shear acting in the adhesive, is valid for a category of adhesives with low stiffness. It is also interesting to recall that in reference [6], Moussiaux studied the influence of boundary conditions on the BMC specimen. When a nonsymmetric load is acting, tensile stresses σ_x , σ_y develop at the centerline close to the loaded end, but the magnitude of the shear stress is not affected.

4.5.2 - Three-dimensional stress analysis in the adhesive

The preceding sections have been concerned with two-dimensional numerical analysis of the BMC specimen. The present section is devoted to further analysis based on the understanding of stress state and beam deflection in a modelling closer to the real situation than the two-dimensional analysis when dealing with the experimental use of the BMC specimen.

In order to analyze the in-plane and the out-of-plane stresses in the adhesive layer, we used the 4.5 version of the ABAQUS code made available at Virginia Polytechnic Institute and State University under an academic contract with Hibbit, Karlsson and Sorensen, Inc..

ABAQUS is a Finite Element program, designed for the analysis of structural responses. The program libraries permit a large flexibility and a high degree of generality in modelling both linear and nonlinear problems. The program can solve stress problems divided into static and dynamic responses and offers options for material, geometric and boundary nonlinearities. Specifications for boundary conditions and for history definition are very flexible and the specifications are made even more powerful by the possibility of adding subroutines written by the user to the internal main program. This option makes the program usable for any kind of structural analysis.

The geometric modelling for the three-dimensional analysis of the BMC specimen required the use of twenty-node quadratic elements as shown in fig.45, where the node numbers have been referred to a cartesian coordinate system. In our analysis of the BMC specimen, the Finite Element mesh consisted in 400 elements arranged as follows : 10 elements in the x-direction, 3 elements in each adherend and 4 elements in the adhesive in the y-direction and 4 elements in the z-direction (fig.46). This discretization produced 2189 nodal points and a total of 6567 degrees of freedom. A more refined mesh may have been more suitable in our analysis, especially in the z-direction. However, due to the difficulties of running the program when we tried to define a more refined mesh, we simply optimized the discretization of the beam in order to ensure sufficient storage and maximum accuracy in the output data.

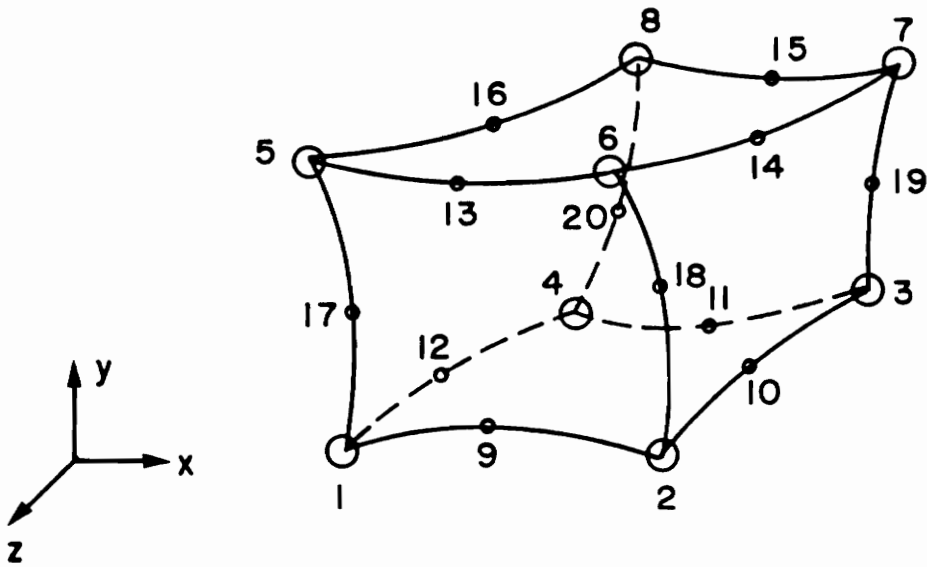


Figure 45. Three-dimensional element with node numbering.

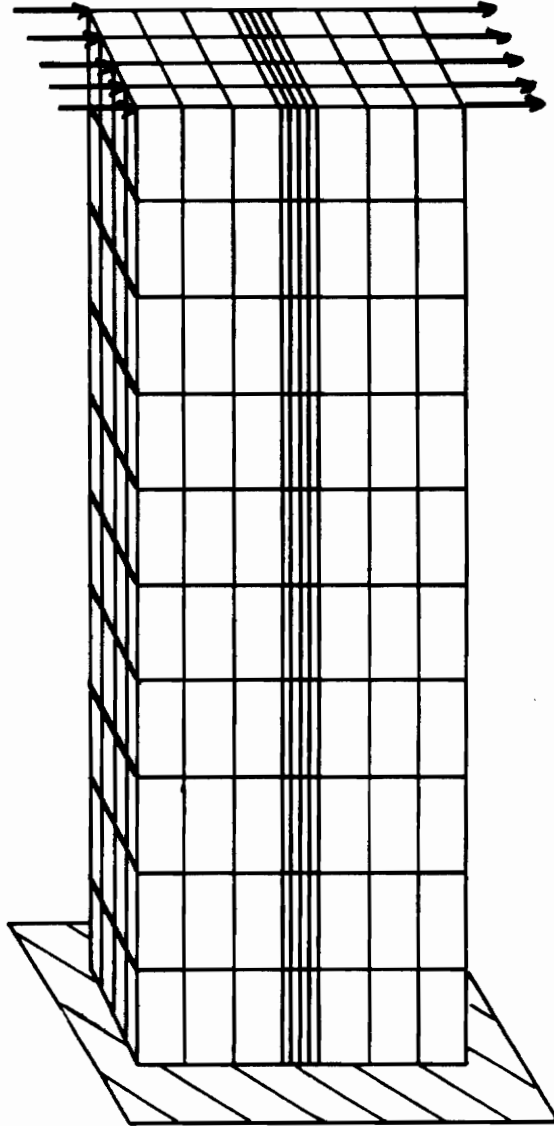


Figure 46. Three-dimensional mesh of the BMC specimen.

4.5.2.1 - Boundary conditions

In the BMC test specimen problem, the first boundary condition is kinematic and consists in specifying fixed displacements at the clamped end of the beam. In the Finite Element modelling with ABAQUS, a node set is assigned the boundary condition. The degrees of freedom of the nodal points in the set are constrained in the 3 directions x, y and z to satisfy the fixed displacement condition.

Extending the two-dimensional BMC analysis to a three-dimensional problem modifies the boundary conditions for loading because the load acting at the extremities is now distributed along the edges. The force is acting parallel to the y-direction and it is distributed uniformly in the z-direction with a resultant equal to $\frac{P}{2}$. The problem then consists in finding the nodal force distribution.

In reference [17], O.C. Zienkiewicz proposed to integrate the appropriate shape functions at the nodal points multiplied by the load, over the volume of an element. However, the mathematical work is simplified by noticing that the forces are acting only at one edge of the elements at the beam tips. Consequently, the problem is equivalent to calculating the force contribution on the three nodes of a one-dimensional quadratic element.

The interpolation functions for a one-dimensional three-nodes element are given by J.N. Reddy in [18]. These functions are constructed by using the linear stretch transformation :

$$\xi = \frac{2x - (x_e + x_{e+1})}{h_e} \quad (25)$$

where ξ is the local coordinate equal to -1 at the left end node and equal to +1 at the right end node. The coordinates x_e and x_{e+1} are referred to the global coordinate system and represent the positions of the left end and the right end nodes respectively. The quantity h is the length of the element and subscript e indicates that the variables are referred to the element.

The interpolation functions are easily derived. Their expressions at nodes 1, 2, 3 of the element are :

$$N_1 = -\frac{1}{2} \xi(1 - \xi) \quad (26a)$$

$$N_2 = 1 - \xi^2 \quad (26b)$$

$$N_3 = \frac{1}{2} \xi(1 + \xi) \quad (26c)$$

In order to obtain the nodal forces equivalent to a distributed load acting on edges of the BMC three-dimensional model, we have to integrate the shape functions N_i multiplied by the acting force, over the length of the one-dimensional quadratic element. Prior to the integration and because a change in coordinate system has been done, we must differentiate the variable x with respect to the local variable ξ , namely :

$$dx = \frac{h_e}{2} d\xi \quad (27)$$

Next, in the local coordinate system ξ , the force acting at node i of element e is given in the general case as follows :

$$f_i^e = \int N_i f \frac{h_e}{2} d\xi \quad (28)$$

In equation 28, f is equal to $\frac{P}{2}$. Due to the choice of the Finite Element mesh, h_e is $\frac{1}{4}$ inch for every element. Finally, for each node, we obtain :

$$f_1^e = \frac{P}{48} \quad (29a)$$

$$f_2^e = \frac{P}{12} \quad (29b)$$

$$f_3^e = \frac{P}{48} \quad (29c)$$

The distribution of the loads at the edge of the BMC specimen characterized by $\frac{x}{\rho} = 1$ was drawn in fig.47.

4.5.2.2 - Results and discussion

The properties of the cases investigated in the three-dimensional Finite Element analysis are listed in table 8. The results for stresses and deflections are presented at the end of this section. Due to symmetry, results are given for only one quarter of the adhesive layer at 9 different locations. These locations are shown in fig.48.

The deflections depicted in fig.49 to 52 show that the numerical results with ABAQUS lie between theoretical predictions in plane stress and in plane strain for any location in the adhesive. This remark was expected because when one uses FEM to analyze a three-dimensional problem, there is no option to define whether the problem should be solved in plane stress or in plane strain. Depending on the choice of the specimen geometry, the numerical solution in 3 dimensions approaches one of the two two-dimensional solutions in plane stress or in plane strain. In reference [19], Timoshenko and Goodier define plane stress and plane strain in terms of the geometry and the loading of a body. On account of geometry, plane stress state is defined qualitatively as thin plates problems whereas plane strain state concerns bodies whose dimension in the z direction is very large. Then, when we compare the beam deflections in fig.49 and 50 for $E/G_a = 26000$ to that shown in fig.51 and 52 for $E/G_a = 260$, we can see that the adhesive thicknesses considered do not influence the convergence of the numerical solution towards either the plane stress or the plane strain theoretical solution. However, for the deflection of the softer adhesive characterized by the highest stiffness ratio, numerical solution approaches the theoretical solution for plane strain. Conversely, in the case of the stiffer adhesive, numerical solution is closer to the analytical predictions in plane

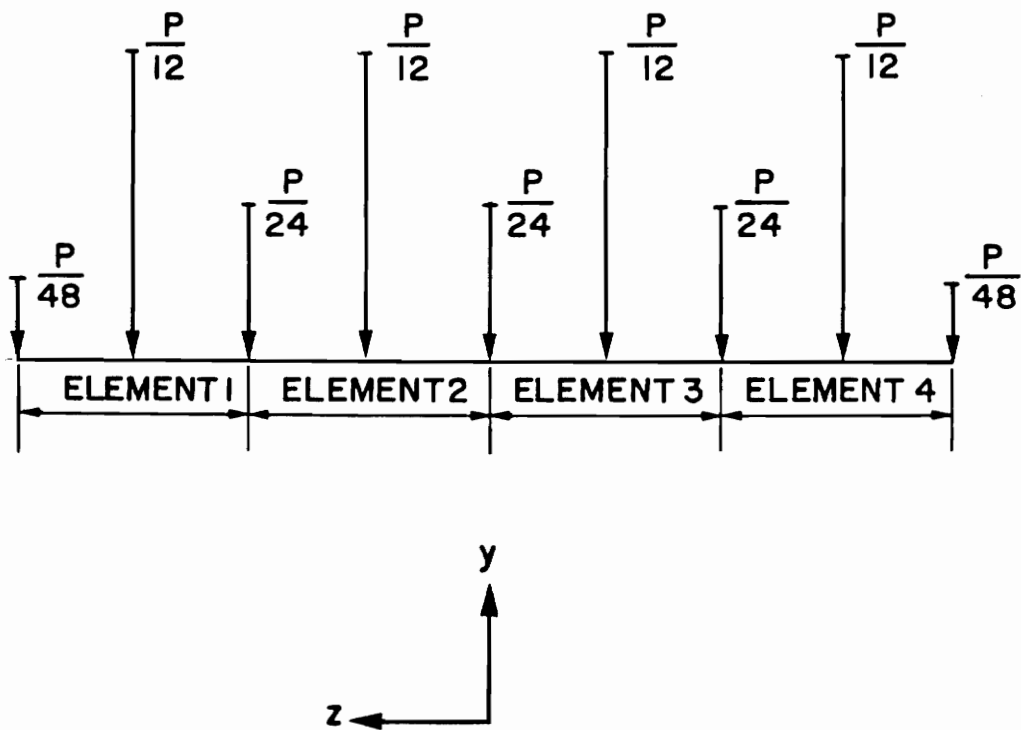


Figure 47. Load distribution at $x=l$ and $y=\pm(h+t)$.

Table 8. Definition of geometrical and material properties used as input data for the numerical analysis with ABAQUS.

case #	t (in.)	h (in.)	ℓ (in.)	t/h	ℓ/h	E (Psi)	ν	E_s (Psi)	ν_s
1	0.025	0.25	2.5	0.10	10	10^7	0.3	10^3	0.3
2	0.0125	0.25	2.5	0.05	10	10^7	0.3	10^3	0.3
3	0.025	0.25	2.5	0.10	10	10^7	0.3	10^5	0.3
4	0.0125	0.25	2.5	0.05	10	10^7	0.3	10^5	0.3

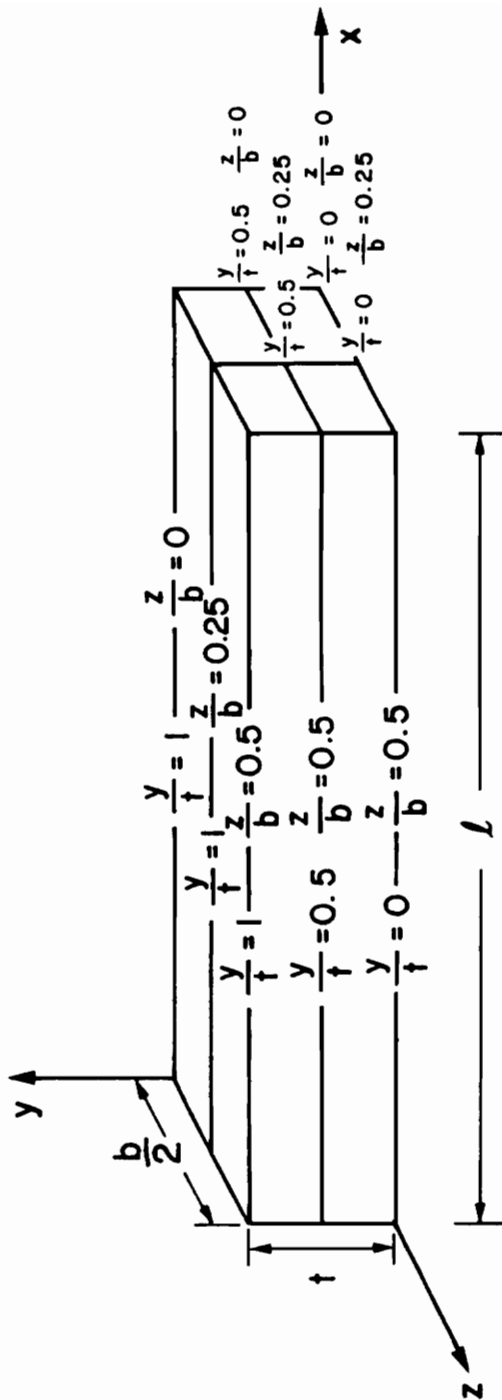


Figure 48. Locations in the adhesive where numerical results with ABAQUS are presented.

stress. An explanation would be that when the adhesive stiffness approaches that of the adherend, the BMC specimen tends to behave like a monolithic beam of thickness $2(h + t)$ but when the adhesive is very soft, the deflection of the specimen is almost due to the bending of the adherend alone whose thickness is h . Then, in the case of the stiff adhesive, the ratio of the beam thickness by the beam width is larger than that in the case of the beam with a soft adhesive. Consequently, regardless to the definition given in [19] for plane stress and plane strain in term of geometry, the deflection in the first case is closer to the deflection calculated analytically in plane stress and the second case favors the deflection to approach the plane strain situation with a dominant dimension in the z direction. On account to an experimental application, the beam deflection measured on the BMC specimen can differ from the theoretical solution for the reasons explained above without going against the validity of the BMC theory.

Next, we turn to the analysis of the stress state in the adhesive layer.

In fig.53 to 68, we plotted the numerical results obtained for stresses σ_x , σ_y , σ_z and τ_{xy} at different locations in the adhesive layer. The locations where the stresses were calculated are listed in the figures. The first remark is that the shear stress is acting alone at the adhesive midplane because all other stresses are zero at this location. In the case of the shear stress distribution, numerical results superpose very well with the analytical solution from the BMC theory reported in fig.53 to 56. The agreement between theory and ABAQUS is perfect for soft adhesive but in the case of stiff adhesive, numerical results differ by a few percent from theory in the z direction for a given x location. However, ABAQUS gives a similar shear stress distribution to theory in the plane $z = 0$. We can see that there is no influence of the adhesive thickness on the quality of the results except, of course, for the magnitude of the resulting shear stress. Stress singularities occur at the loaded end which have already been studied in the two-dimensional FE analysis. In the case of the axial stresses, they all present stress singularities at both the clamped end of the beam and the loaded end with high concentration at the latter location. In addition, the decrease of the adhesive thickness contributes to reduce the magnitude of tensile stresses. The magnitude of the in-plane stresses σ_x and σ_y are significantly increased from soft adhesive with less than 1 Psi to stiff adhesive with less than 10 Psi. The larger in-plane stresses are present at the interface between adherend and adhesive

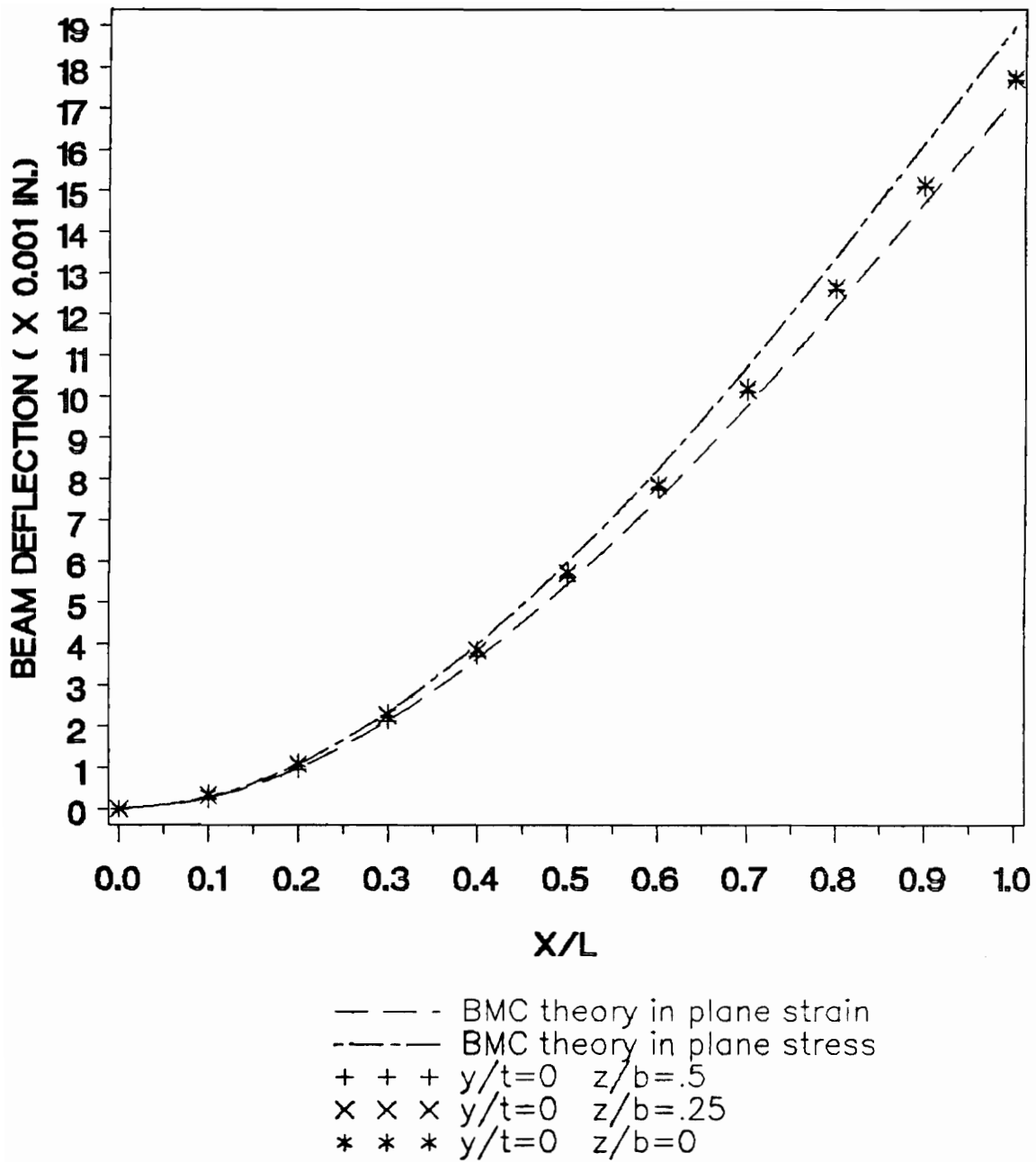


Figure 49. Beam deflection from three-dimensional analysis. $P = 100$ Lb., $E/Ga = 26000$, $l/h = 10$ and $t/h = 0.1$.

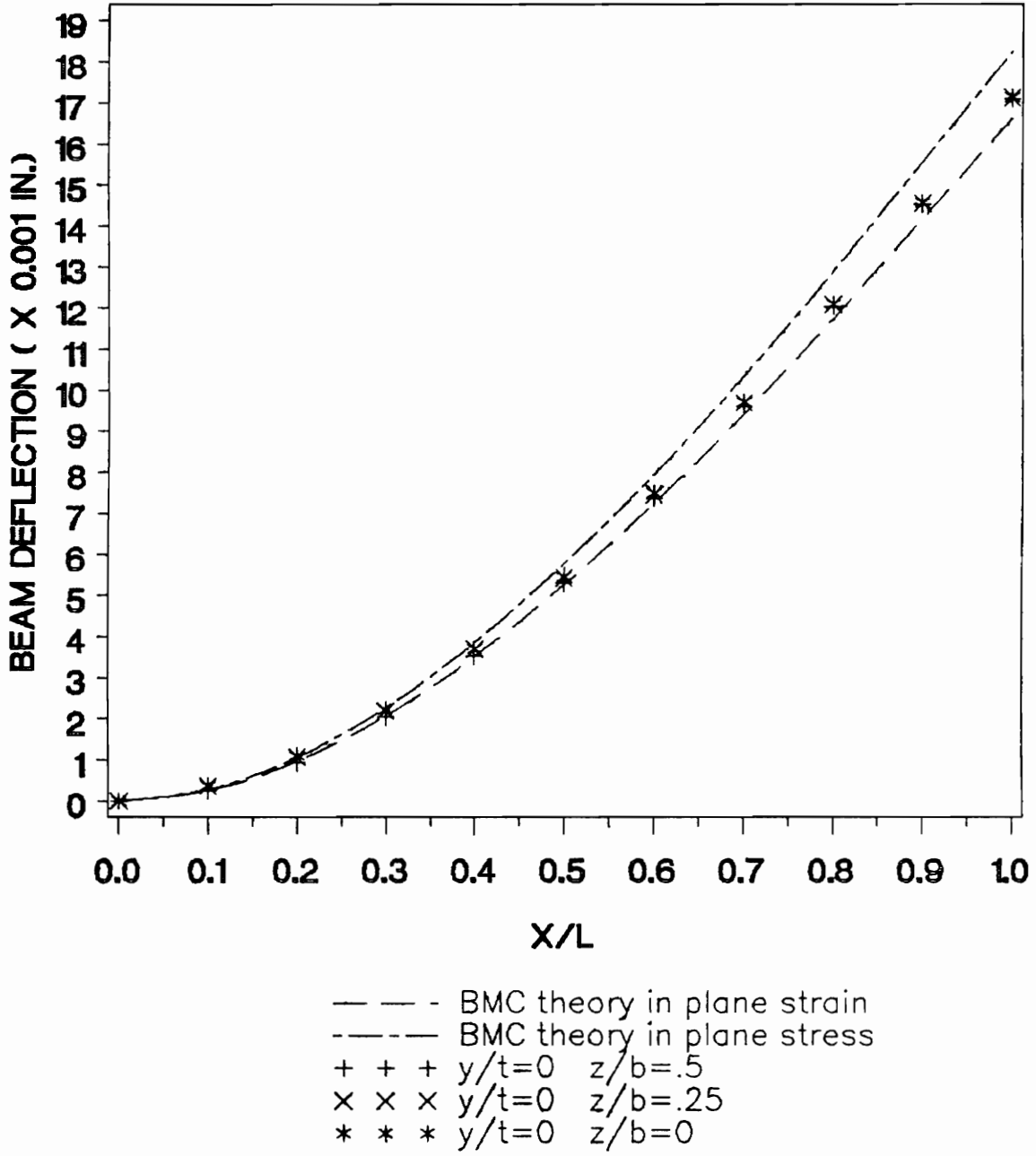


Figure 50. Beam deflection from three-dimensional analysis. $P=100$ Lb., $E/Ga=26000$, $l/h=10$ and $t/h=0.05$.

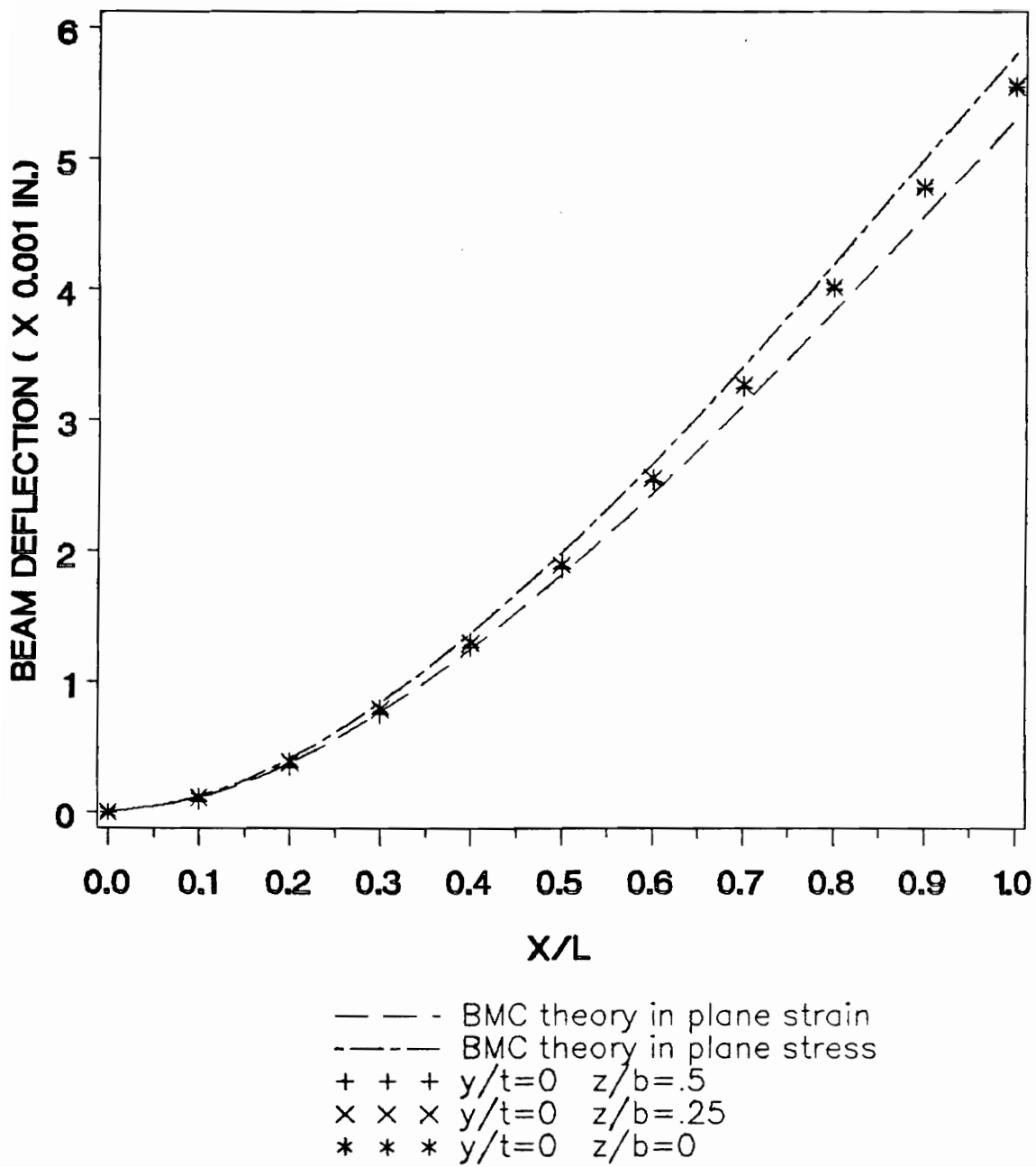


Figure 51. Beam deflection from three-dimensional analysis. $P = 100$ Lb., $E/Ga = 260$, $l/h = 10$ and $t/h = 0.1$.

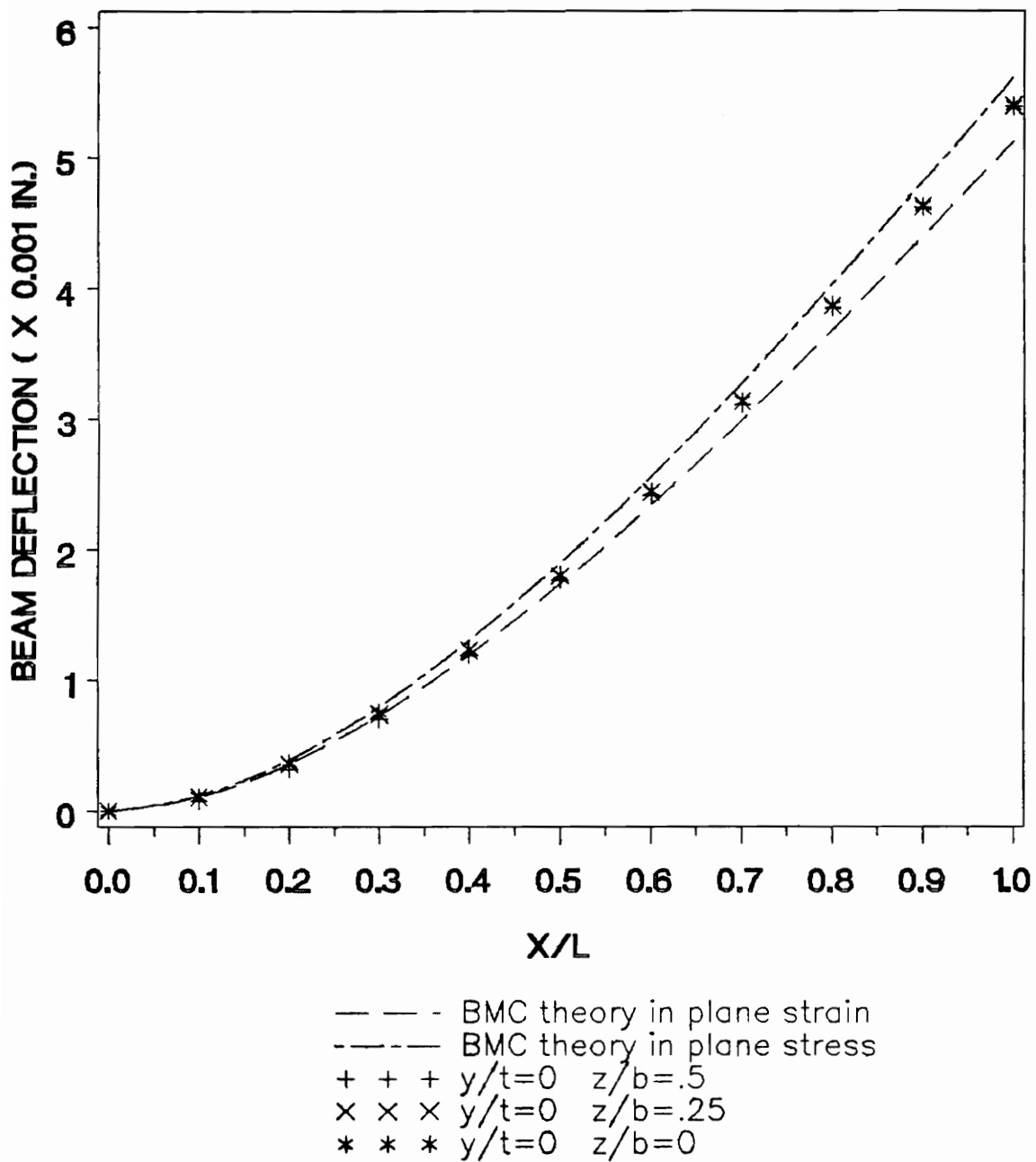


Figure 52. Beam deflection from three-dimensional analysis. $P=100$ Lb., $E/Ga=260$, $l/h=10$ and $t/h=0.05$.

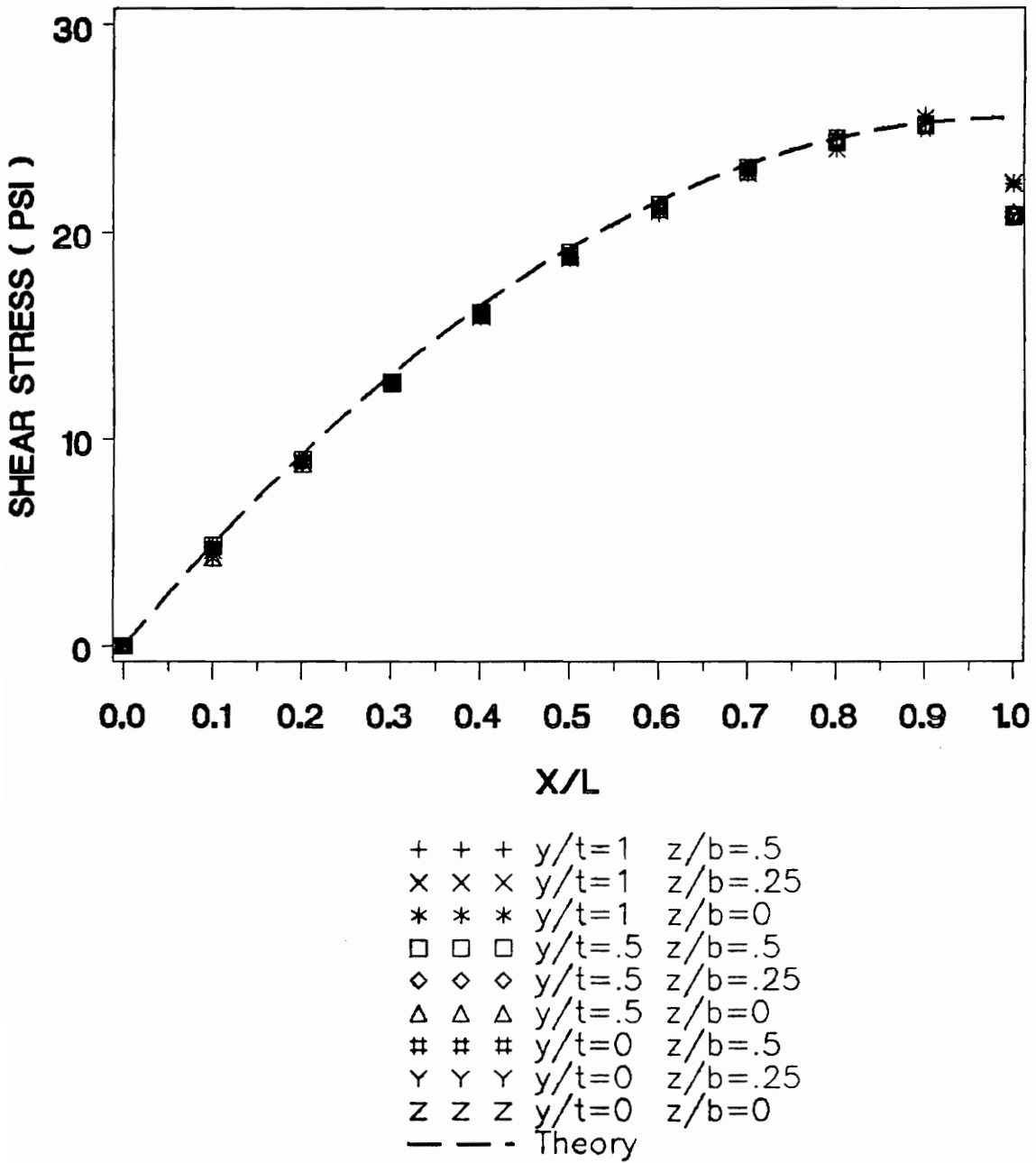


Figure 53. Shear stress in the adhesive layer from three-dimensional analysis. P=100 Lb., E/Ga=26000, l/h=10 and t/h=0.1.

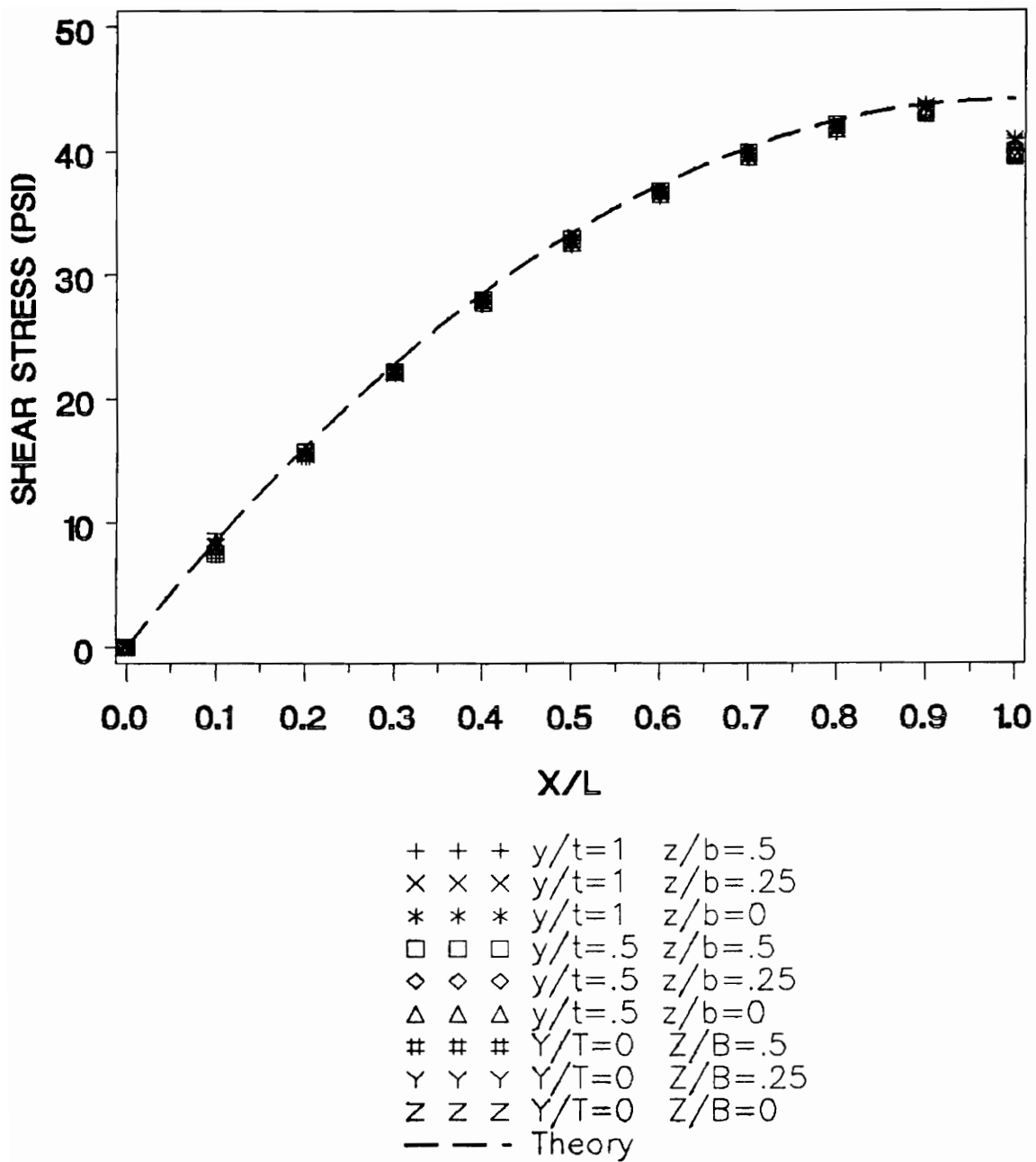


Figure 54. Shear stress in the adhesive layer from three-dimensional analysis. $P = 100$ Lb., $E/G_a = 26000$, $l/h = 10$ and $t/h = 0.05$.

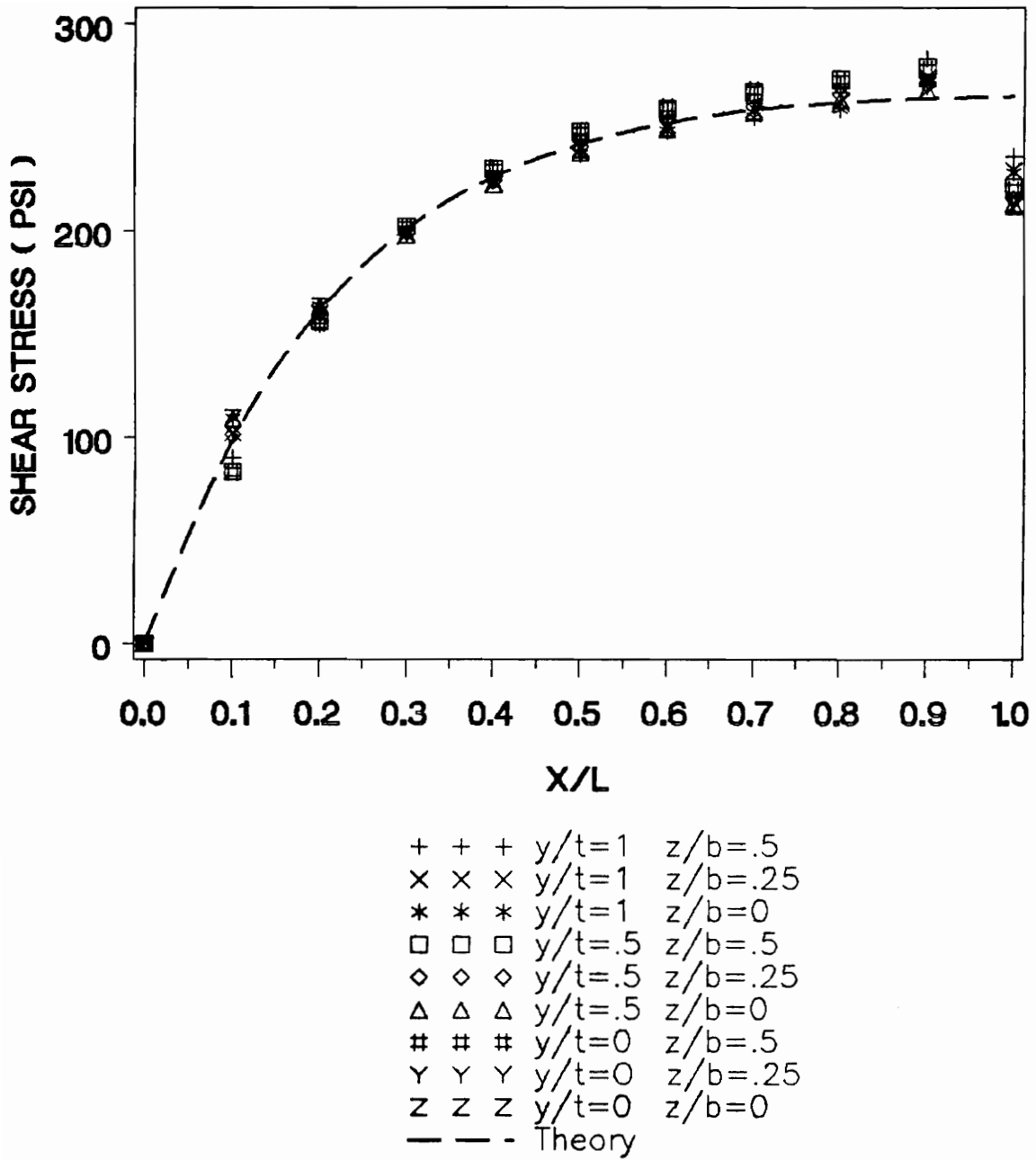


Figure 55. Shear stress in the adhesive layer from three-dimensional analysis. $P = 100$ Lb., $E/Ga = 260$, $l/h = 10$ and $t/h = 0.1$.

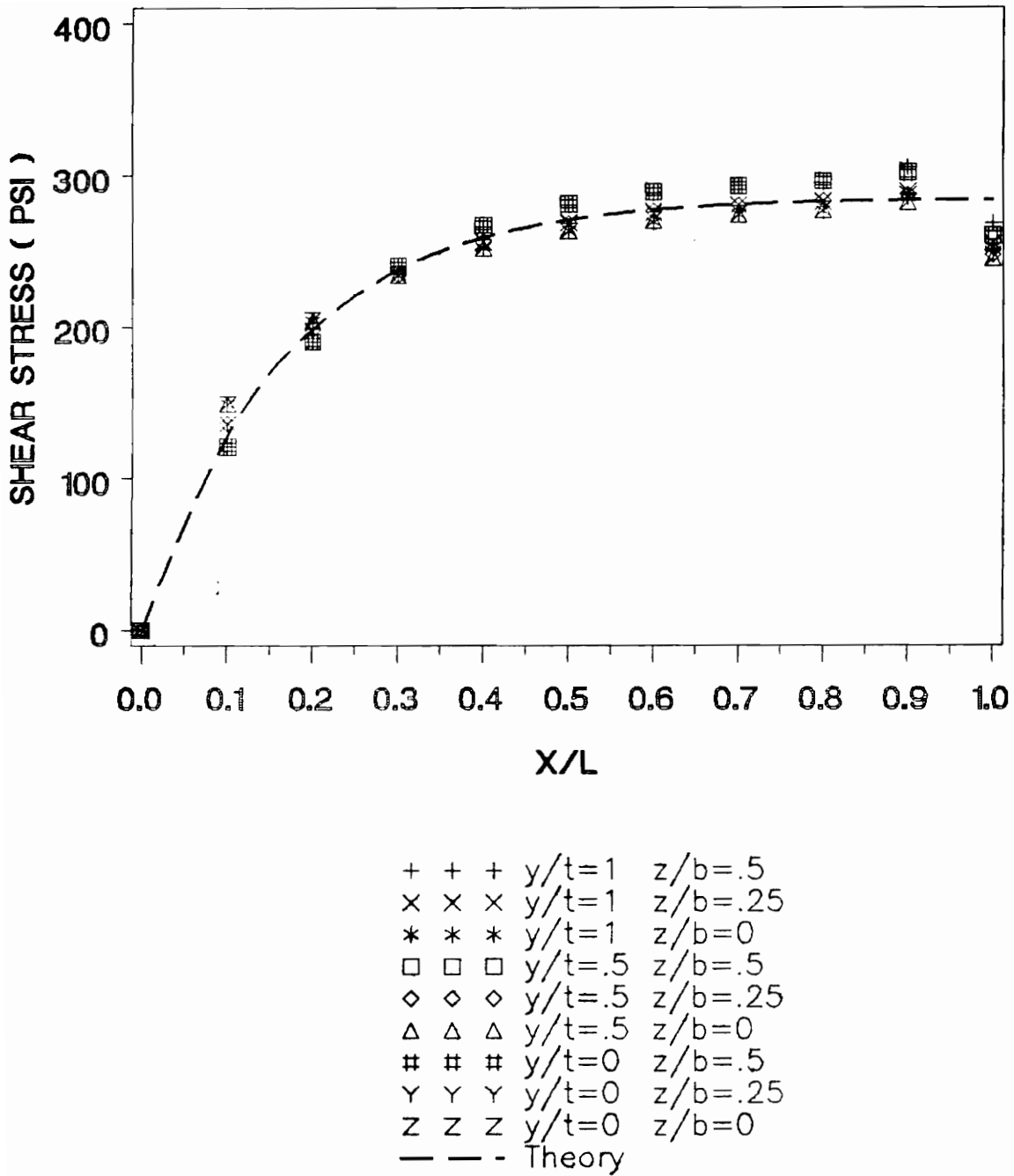


Figure 56. Shear stress in the adhesive layer from three-dimensional analysis. $P = 100$ Lb., $E/Ga = 260$, $l/h = 10$ and $t/h = 0.05$.

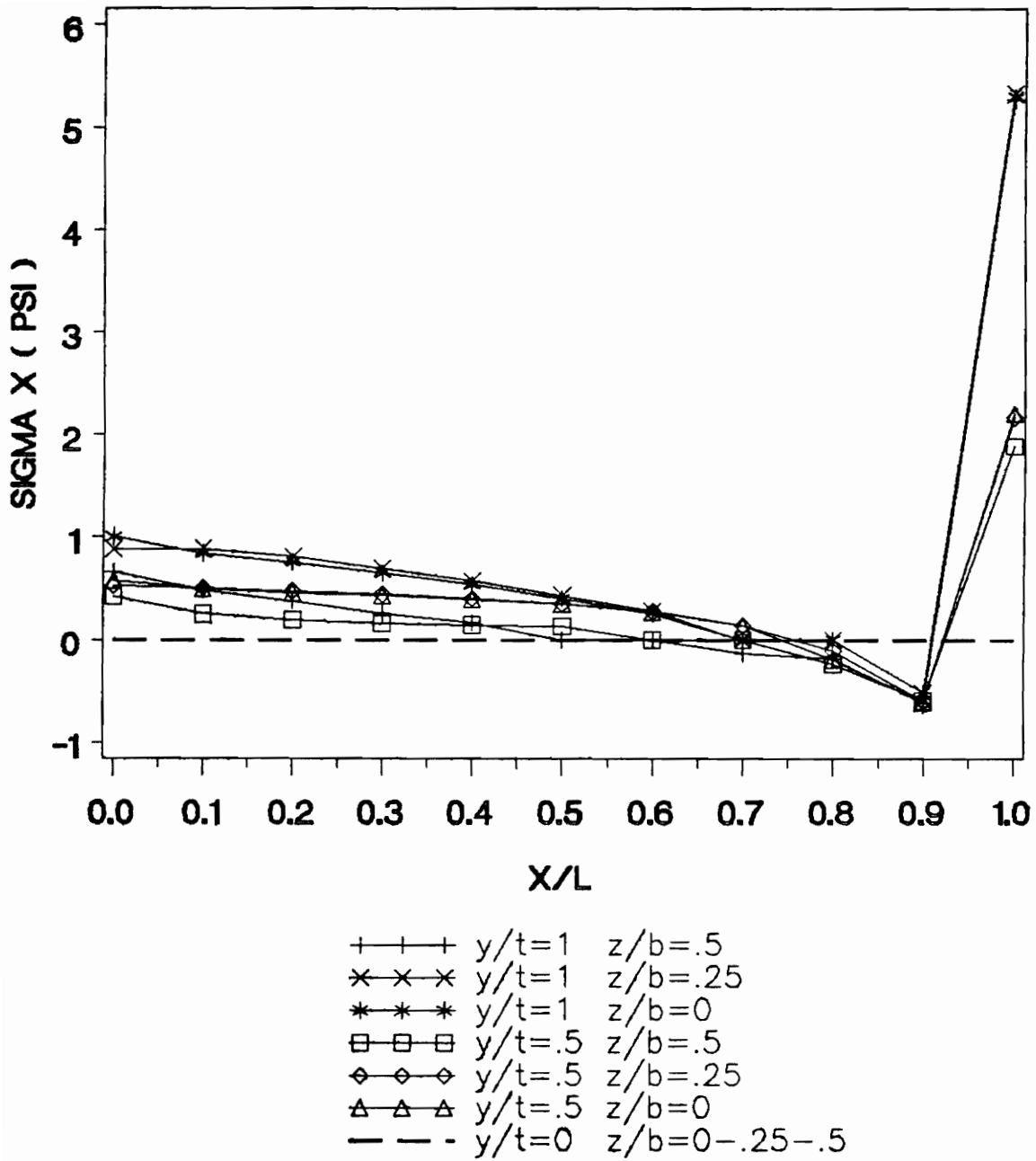


Figure 57. Tensile stress σ_x in the adhesive layer from three-dimensional analysis. $P = 100$ Lb., $E/Ga = 26000$, $\ell/h = 10$ and $t/h = 0.1$.

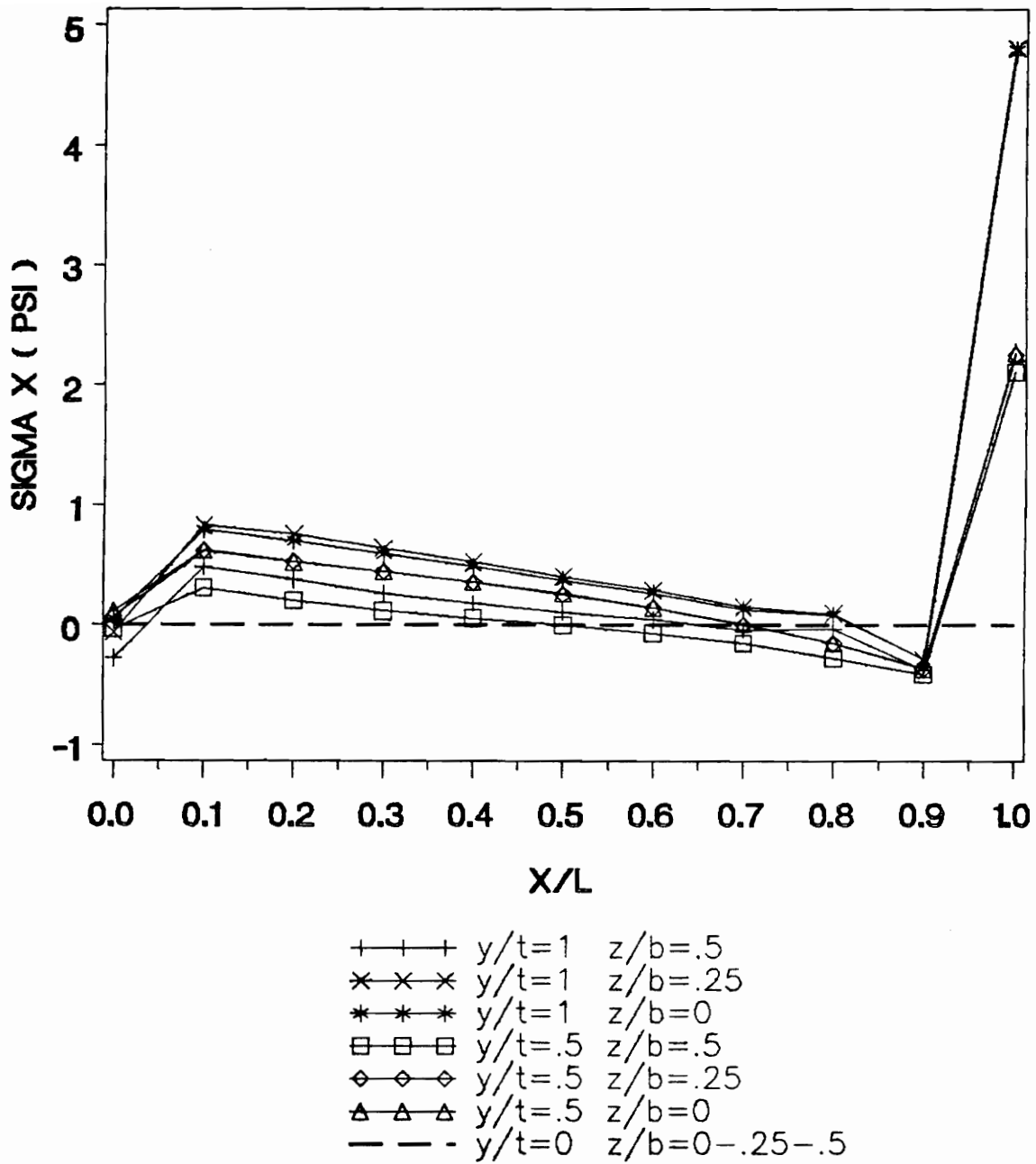


Figure 58. Tensile stress σ_x in the adhesive layer from three-dimensional analysis. $P = 100$ Lb., $E/Ga = 26000$, $l/h = 10$ and $t/h = 0.05$.

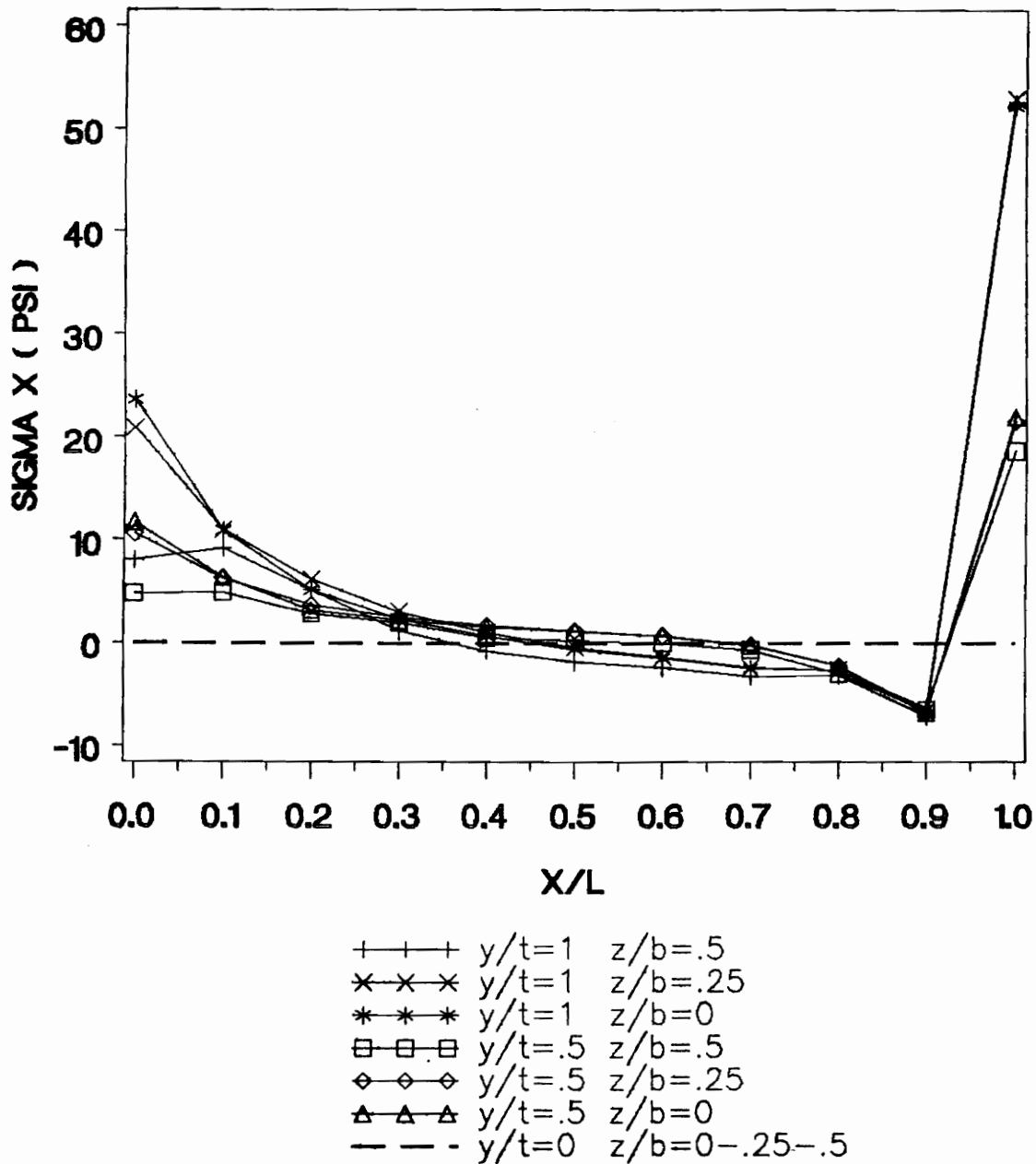


Figure 59. Tensile stress σ_x in the adhesive layer from three-dimensional analysis. $P=100$ Lb., $E/Ga=260$, $l/h=10$ and $t/h=0.1$.

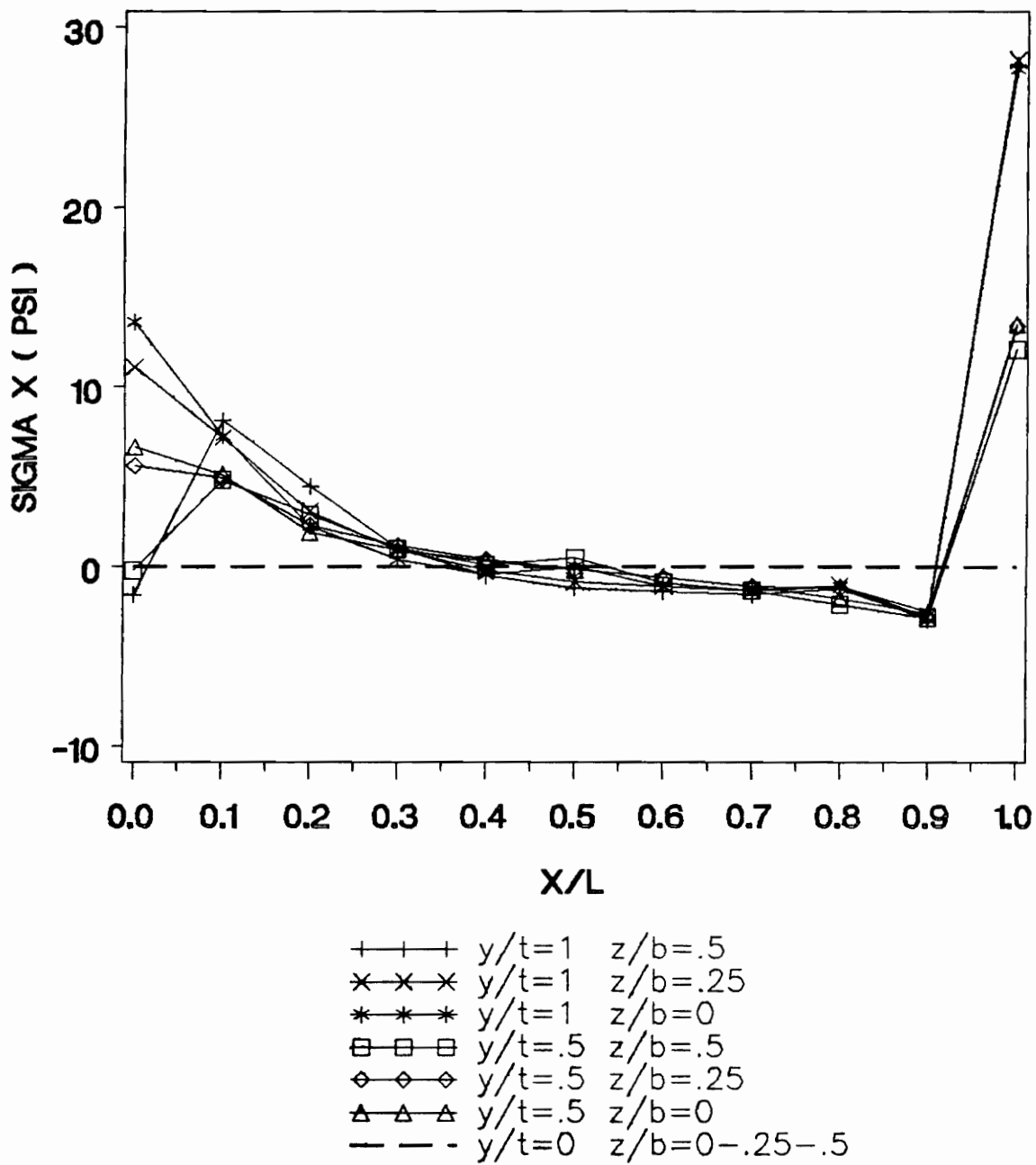


Figure 60. Tensile stress sigma x in the adhesive layer from three-dimensional analysis. P=100 Lb., E/Ga=260, l/h=10 and t/h=0.05.

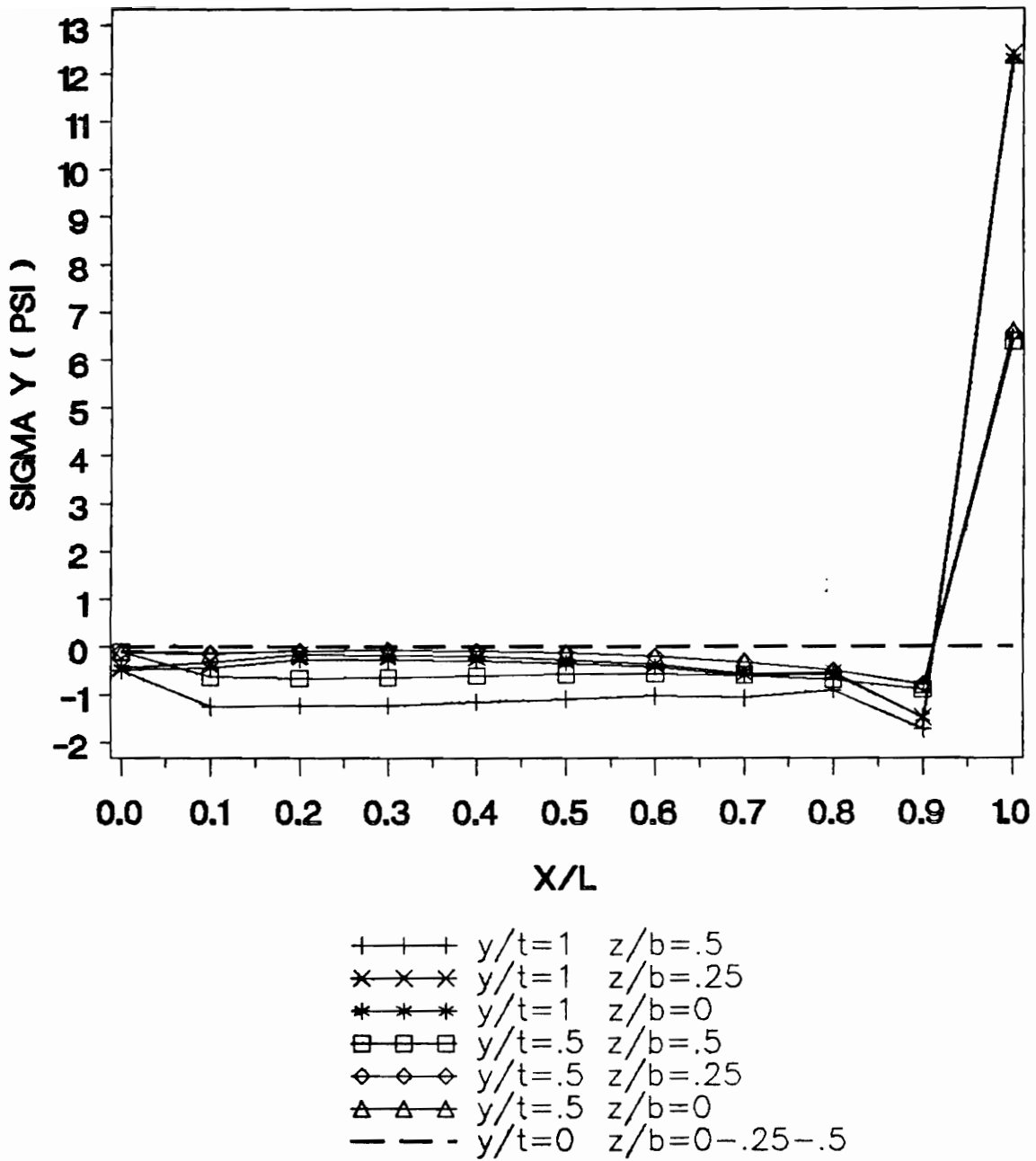


Figure 61. Tensile stress sigma y in the adhesive layer from three-dimensional analysis. P = 100 Lb., E/Ga = 26000, l/h = 10 and t/h = 0.1.

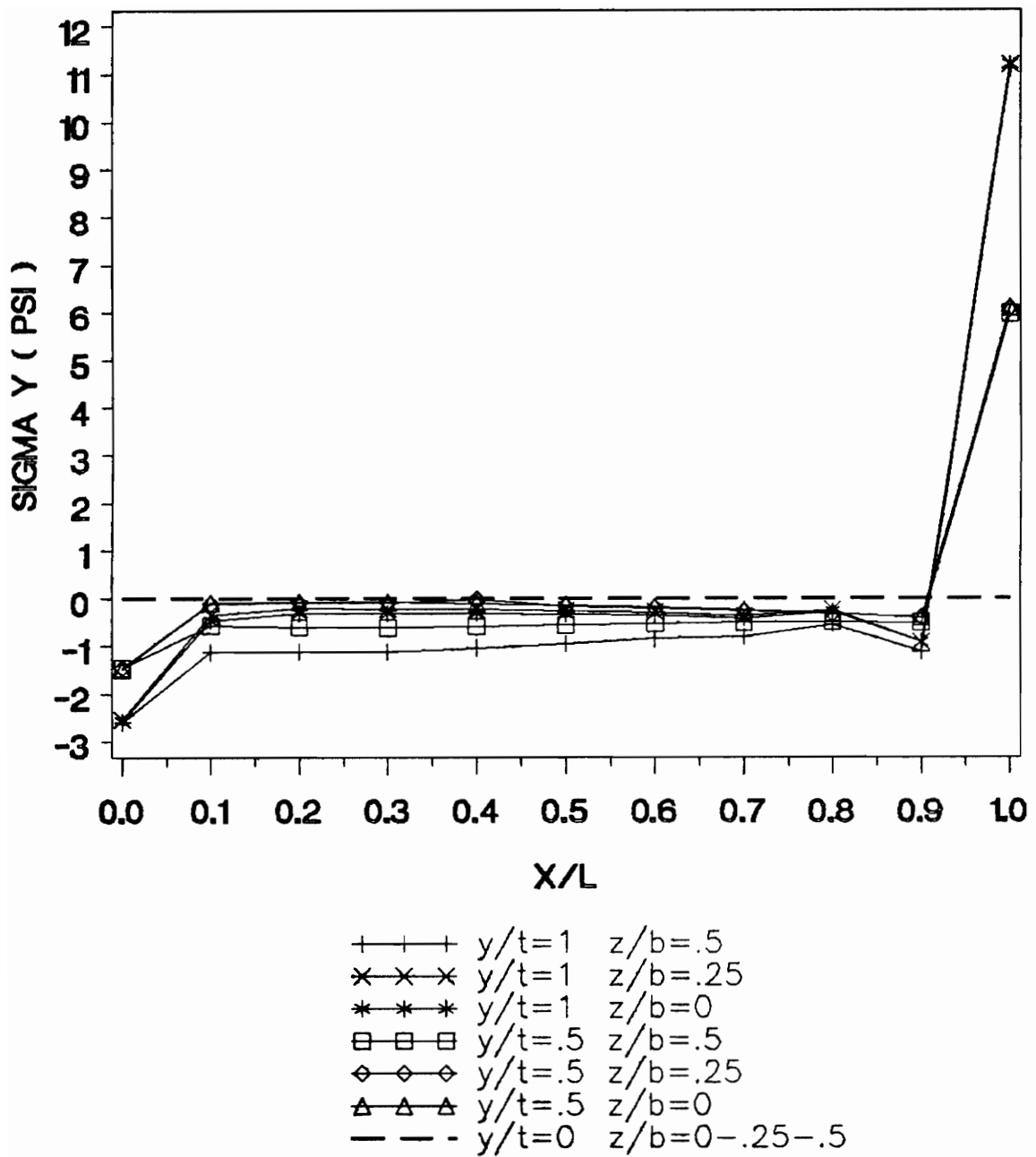


Figure 62. Tensile stress σ_y in the adhesive layer from three-dimensional analysis. $P = 100$ Lb., $E/Ga = 26000$, $l/h = 10$ and $t/h = 0.05$.

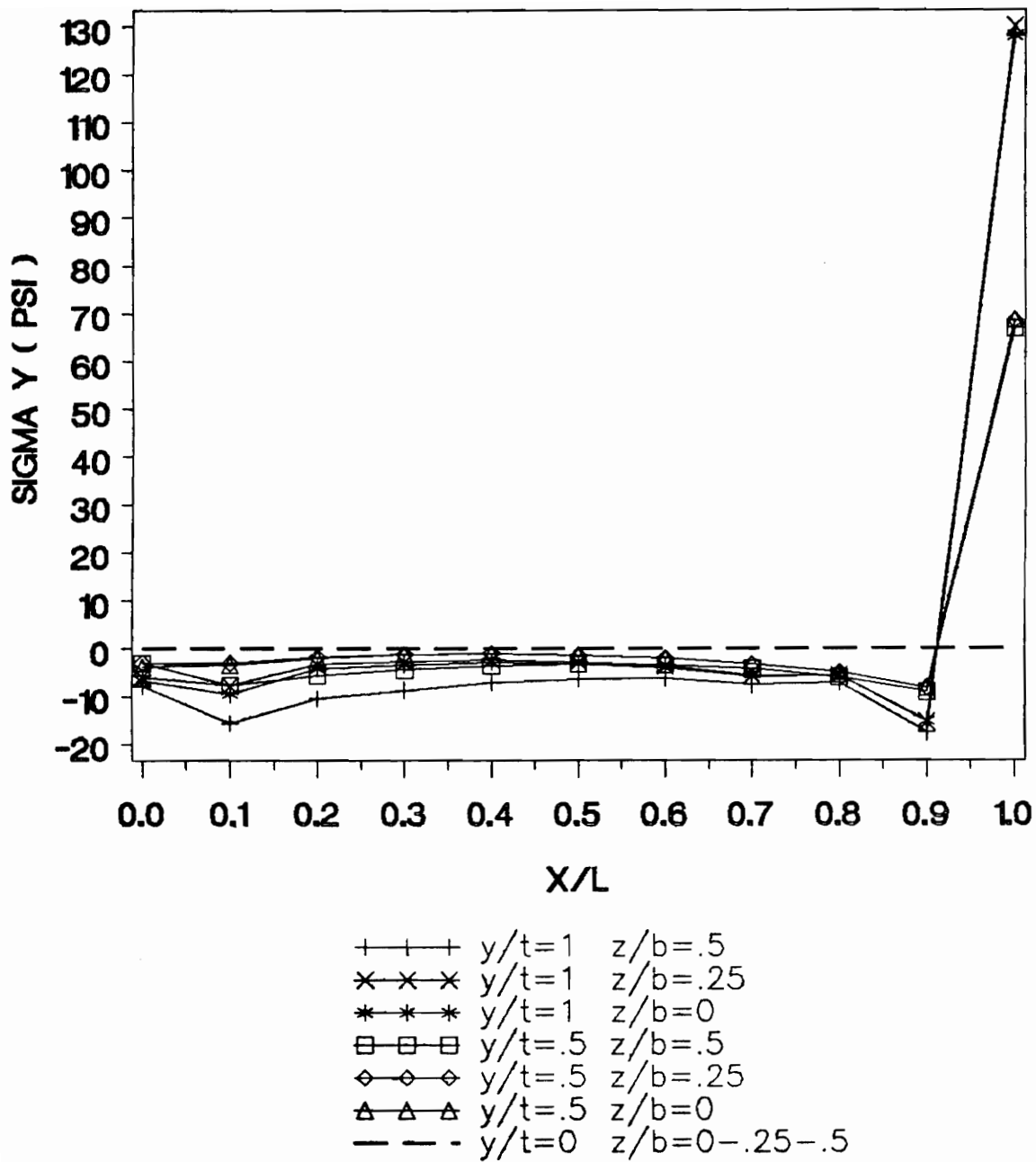


Figure 63. Tensile stress σ_y in the adhesive layer from three-dimensional analysis. $P = 100$ Lb., $E/Ga = 260$, $\ell/h = 10$ and $t/h = 0.1$.

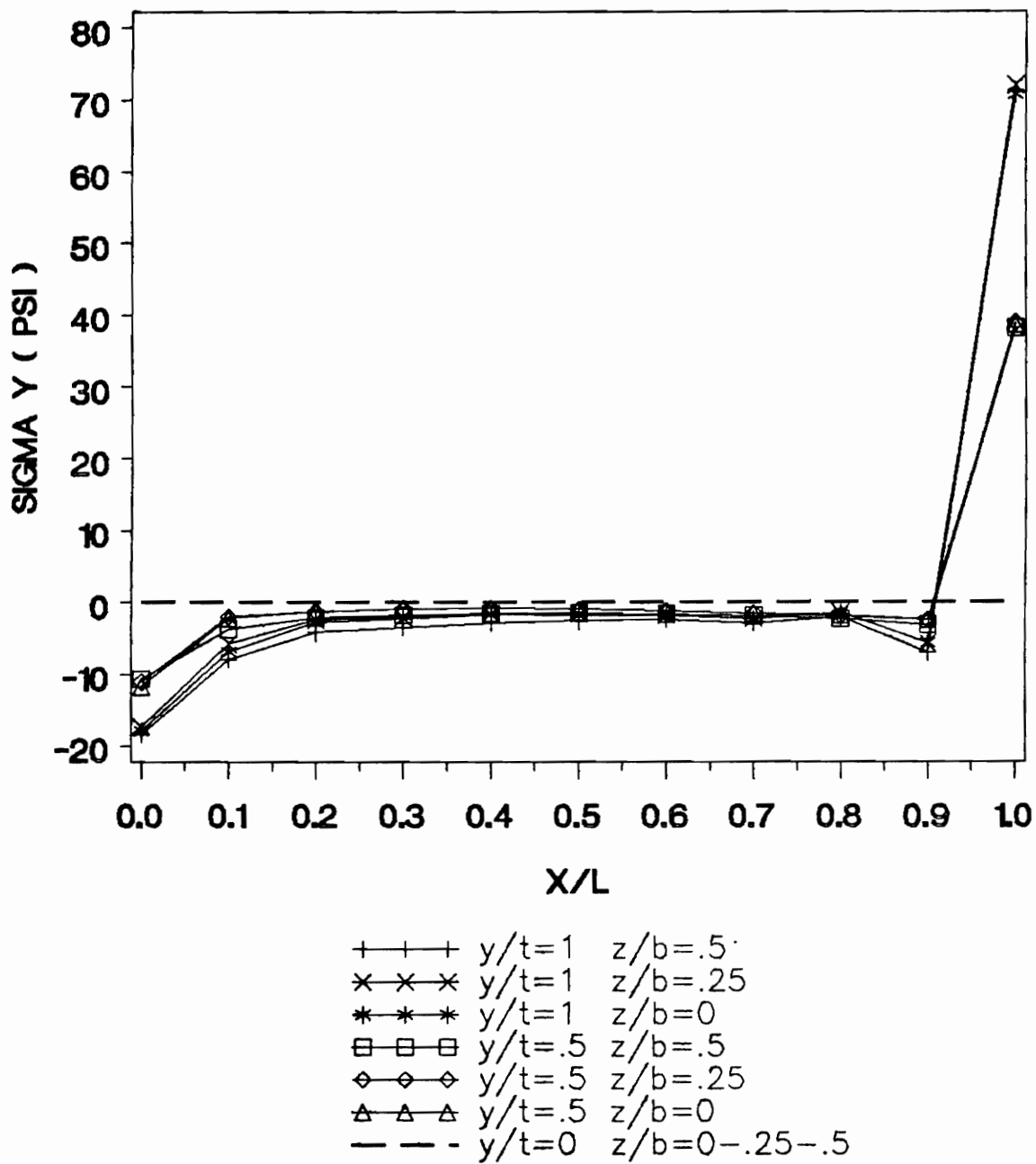


Figure 64. Tensile stress σ_y in the adhesive layer from three-dimensional analysis. $P = 100$ Lb., $E/Ga = 260$, $l/h = 10$ and $t/h = 0.05$.

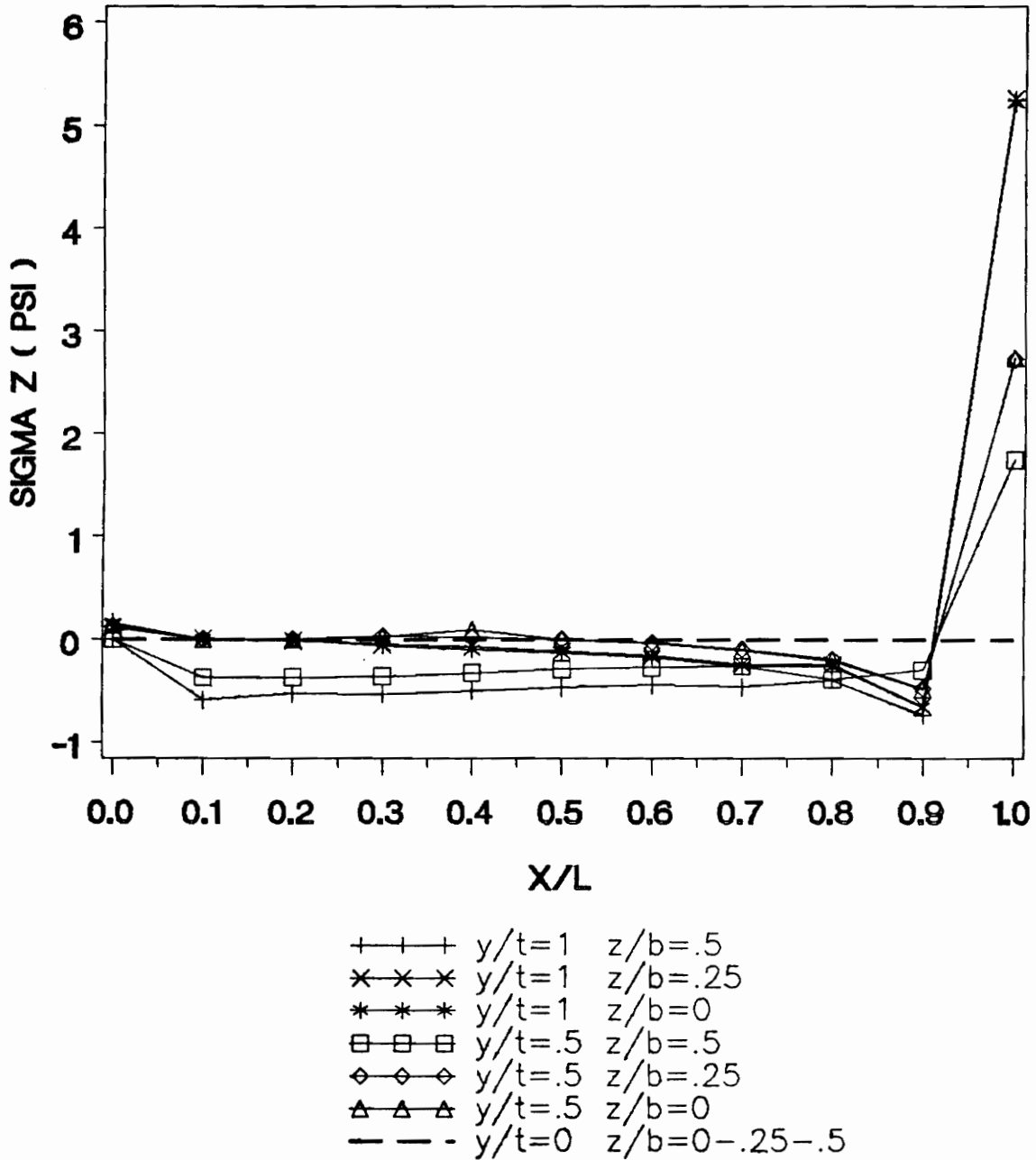


Figure 65. Tensile stress σ_z in the adhesive layer from three-dimensional analysis. $P=100$ Lb., $E/Ga=26000$, $l/h=10$ and $t/h=0.1$.

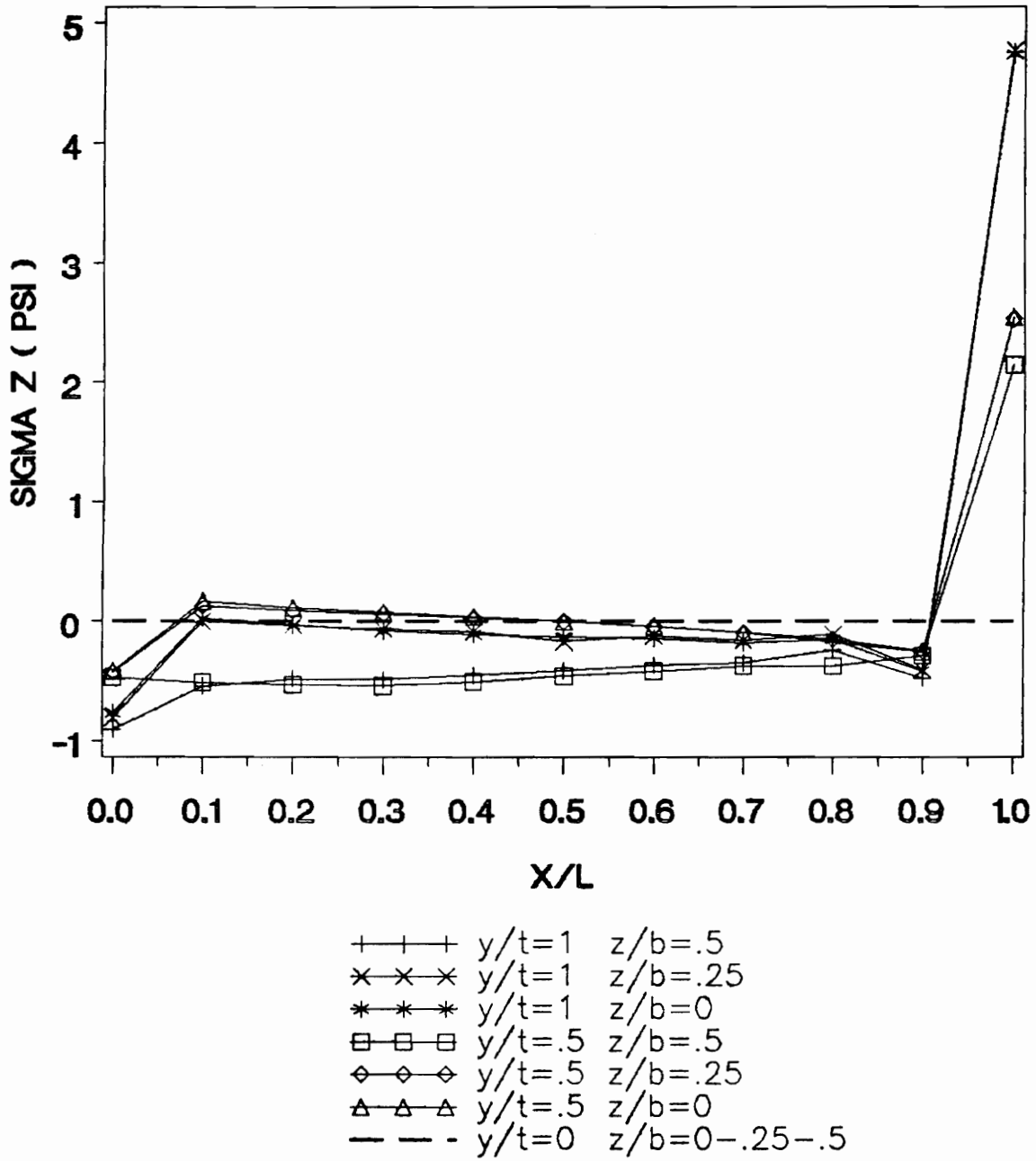


Figure 66. Tensile stress sigma z in the adhesive layer from three-dimensional analysis. P=100 Lb., E/Ga = 26000, $\ell/h = 10$ and $t/h = 0.05$.

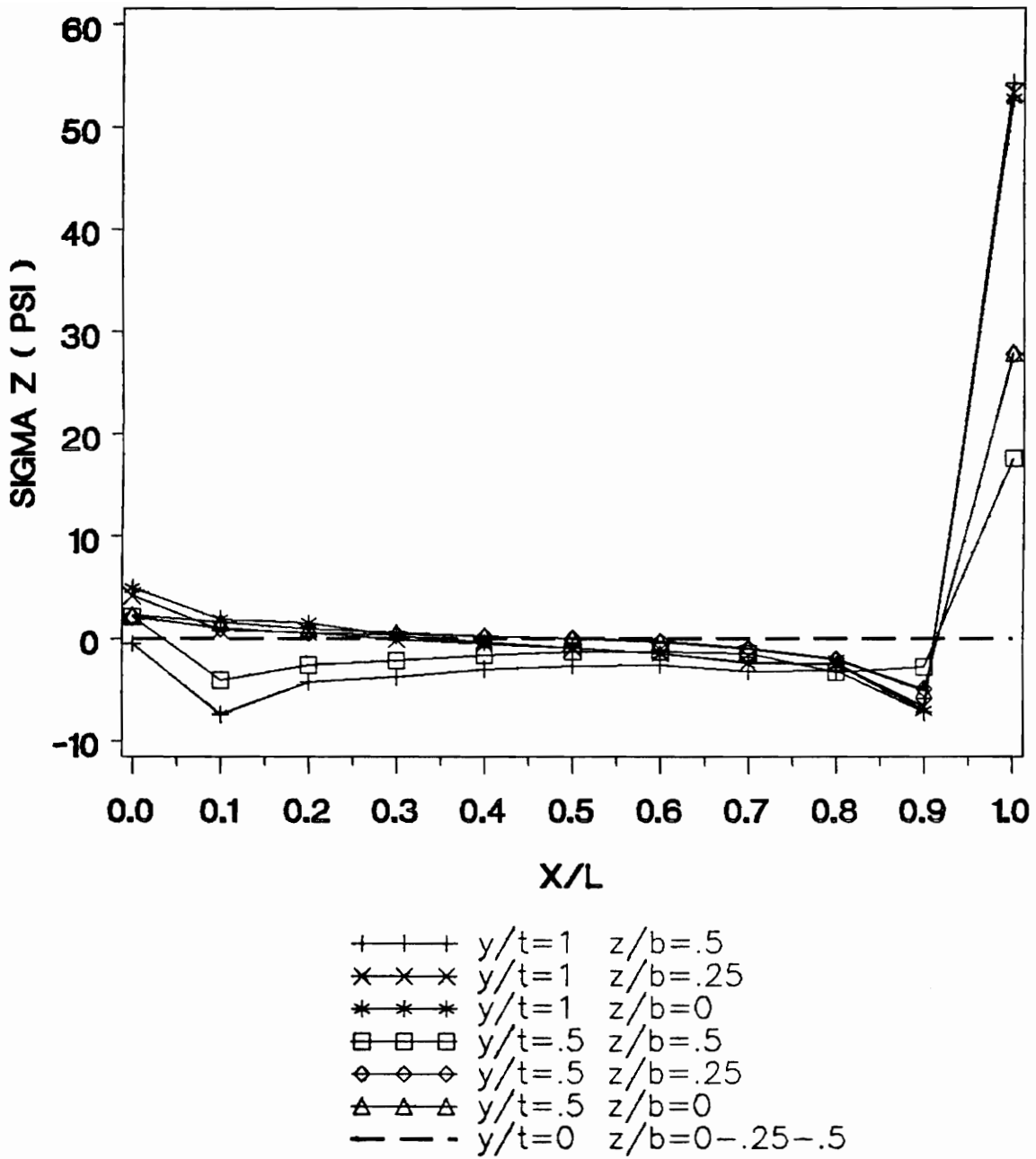


Figure 67. Tensile stress σ_z in the adhesive layer from three-dimensional analysis. $P = 100$ Lb., $E/Ga = 260$, $l/h = 10$ and $t/h = 0.1$.

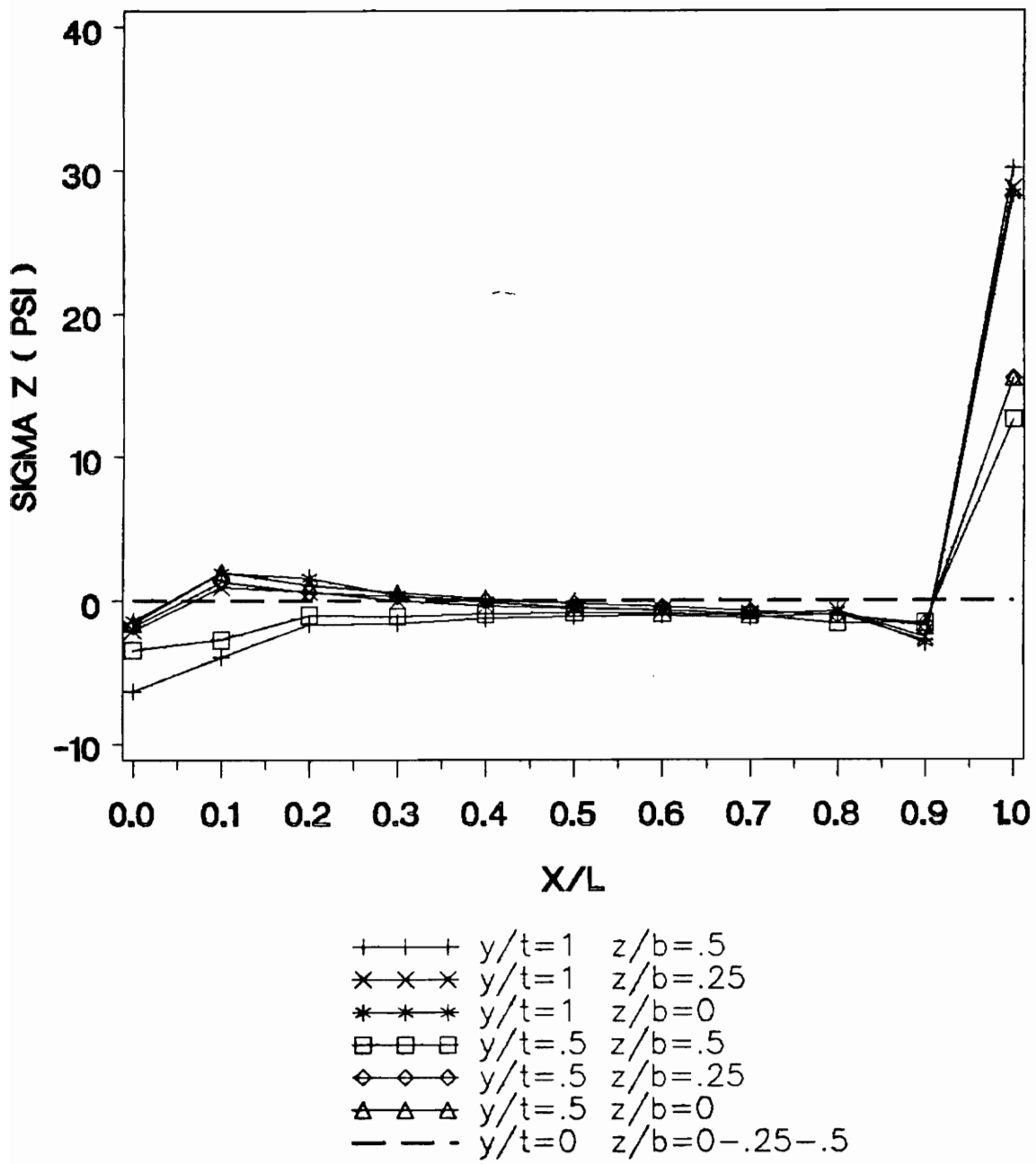


Figure 68. Tensile stress σ_z in the adhesive layer from three-dimensional analysis. $P=100$ Lb., $E/Ga = 260$, $\ell/h = 10$ and $t/h = 0.05$.

for σ_x and at the external surface of the adhesive for σ_z . These stresses approach zero as they are calculated closer to the midplane. Finally, the out-of-plane stress σ_y is a compressive stress in the upper half of the adhesive with high magnitude compared to that of the other tensile stresses. The same singularities occur at the extremities and large stress concentrations are present at the adherend-adhesive interface.

In conclusion, the three-dimensional Finite Element analysis of the BMC specimen reveals the presence of in-plane and out-of-plane stresses in the adhesive layer in addition to the shear stress. As said in the two-dimensional analysis, the magnitude of the axial stresses is negligible in comparison to that of the shear stress especially for soft adhesive, but concentrations at the loaded end occur, particularly at the interface between adherend and adhesive. Tensile stresses do not modify the state of shear because FE showed that in the cases investigated, good agreements were obtained for the shear stress distribution between theory and numerical results. The additional analysis of the beam deflection reinforced the validity of the BMC theory.

4.5.3 - Comparison of the stress state in the adhesive between the BMC test specimen and a modified BMC specimen

For stiff combinations of adherends and adhesive (aluminum-epoxy for instance), the adhesive shear deformation as well as the end point deflection resulting from the loading of the beam can be very small and can require sensitive measuring techniques to be measured. In extreme cases, the shear stress state would approach that of a monolithic beam. In chapter 2, a quantitative parametric analysis has been conducted to illustrate the situation. In order to increase the shear deformation in the adhesive layer, one option is to reduce the length of the bonded adhesive. VISTA was used to analyze the resulting state of stress in the short adhesive layer. Tensile stresses σ_x and σ_y may exist in the adhesive but as long as their magnitudes are still a few percent of that of the shear stress, the state of stress is still pure shear for all practical purposes.

4.5.3.1 - Finite Element model

We considered an adhesive layer with half the adherend length and located symmetrically between the two clamped adherends. In the adhesive layer, the mesh consisted of 112 elements with some refinement at the bond tips. The FEM mesh is depicted in fig.69.

4.5.3.2 - Results and discussion

Figure 70 represents the shear stress distributions at the adhesive mid-plane for a short adhesive of length $\ell_a = \frac{\ell}{2}$ and for an adhesive of length ℓ . For the long adhesive layer, the shear stress is that predicted by theory. For the short adhesive, the shear stress differs entirely from theory : it

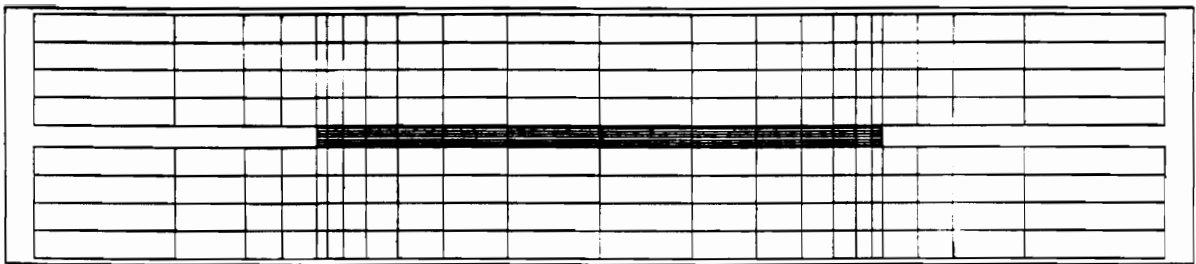


Figure 69. Finite elements mesh used with VISTA for the analysis of a short adhesive.

increases uniformly from left to right towards where the beam is loaded and it drops to zero at the tips. Fig.71 shows that the shear stress is uniform within the adhesive thickness, and that it is not uniform along the length far away from either extremity of the adhesive where the shear stress has peaks. The tensile stresses acting in the adhesive layer are shown in fig.72 and 73 and they can be compared to that depicted in the iso-stress maps for the same BMC specimen with an adhesive bonded over the entire beam length. On fig.72 and 73, one can see that high tensile stresses concentrations occur at the extremities especially at the adherend/adhesive interface for the peel stress. These stress concentrations are however limited to small lengths at the adhesive ends and the larger stress magnitudes are close to the loaded end. No other stress than the shear stress is acting at the midplane. Furthermore, when we compare the magnitude of the shear stress with that of the tensile stresses, one can see that the latter are negligible far enough from the extremities of the joint where the peaks are. Therefore, in the major part of the joint, the state of stress is still pure shear, uniform over the thickness and with an increasing magnitude along the x-location. Finally, by reducing the joint length, the shear strain is increased from 20 up to 100 % compared to the case of a long joint. This increase facilitates the measurement of the deformation for low BMC beam stiffness ratios.

In the next section, we present the results of an experimental study made in addition to the analytical and the numerical analyses of the BMC specimen.

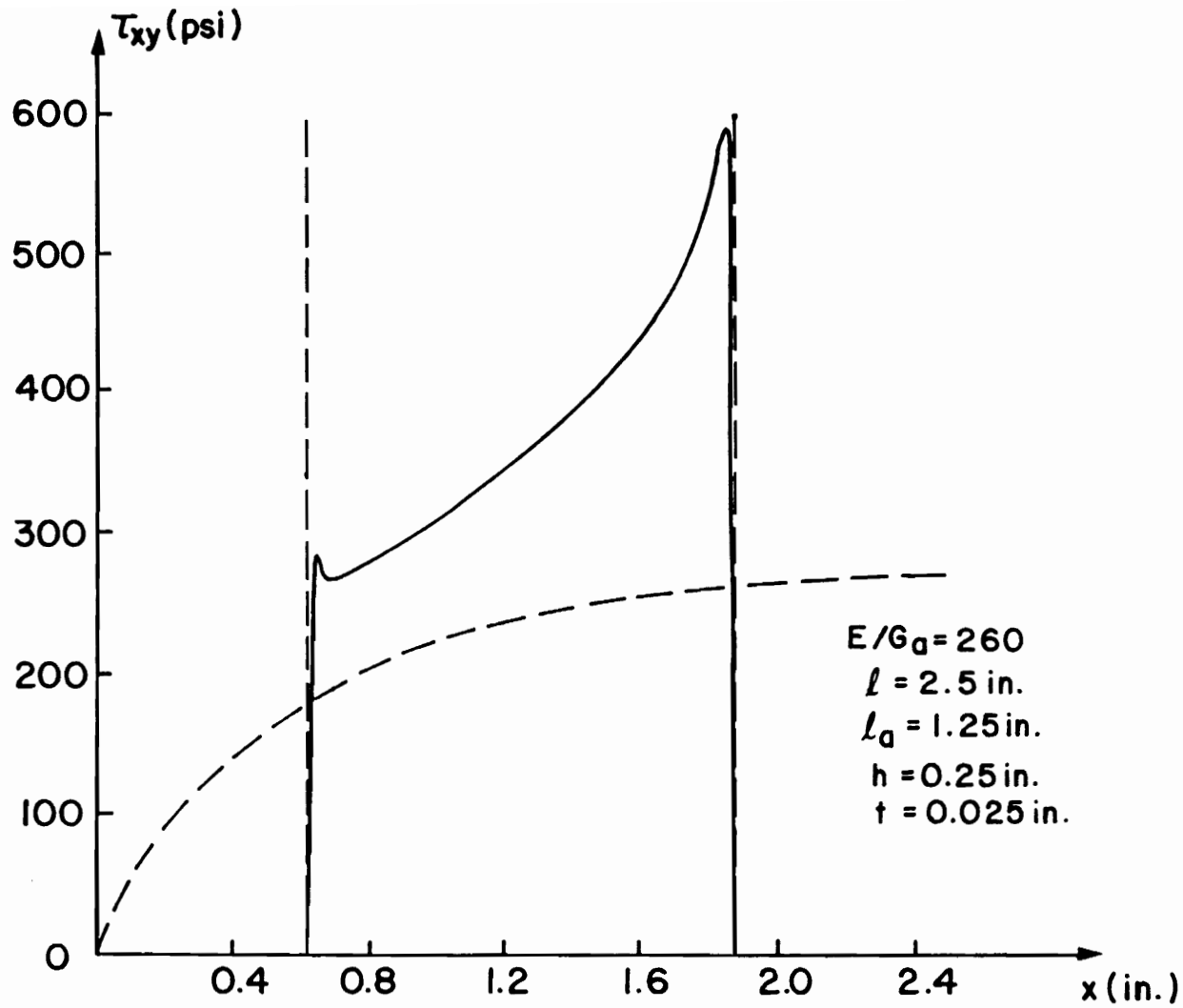


Figure 70. Comparison of the shear stress distribution between a short adhesive - plane line : results from VISTA for short adhesive - slashed line : results from theory for long adhesive .

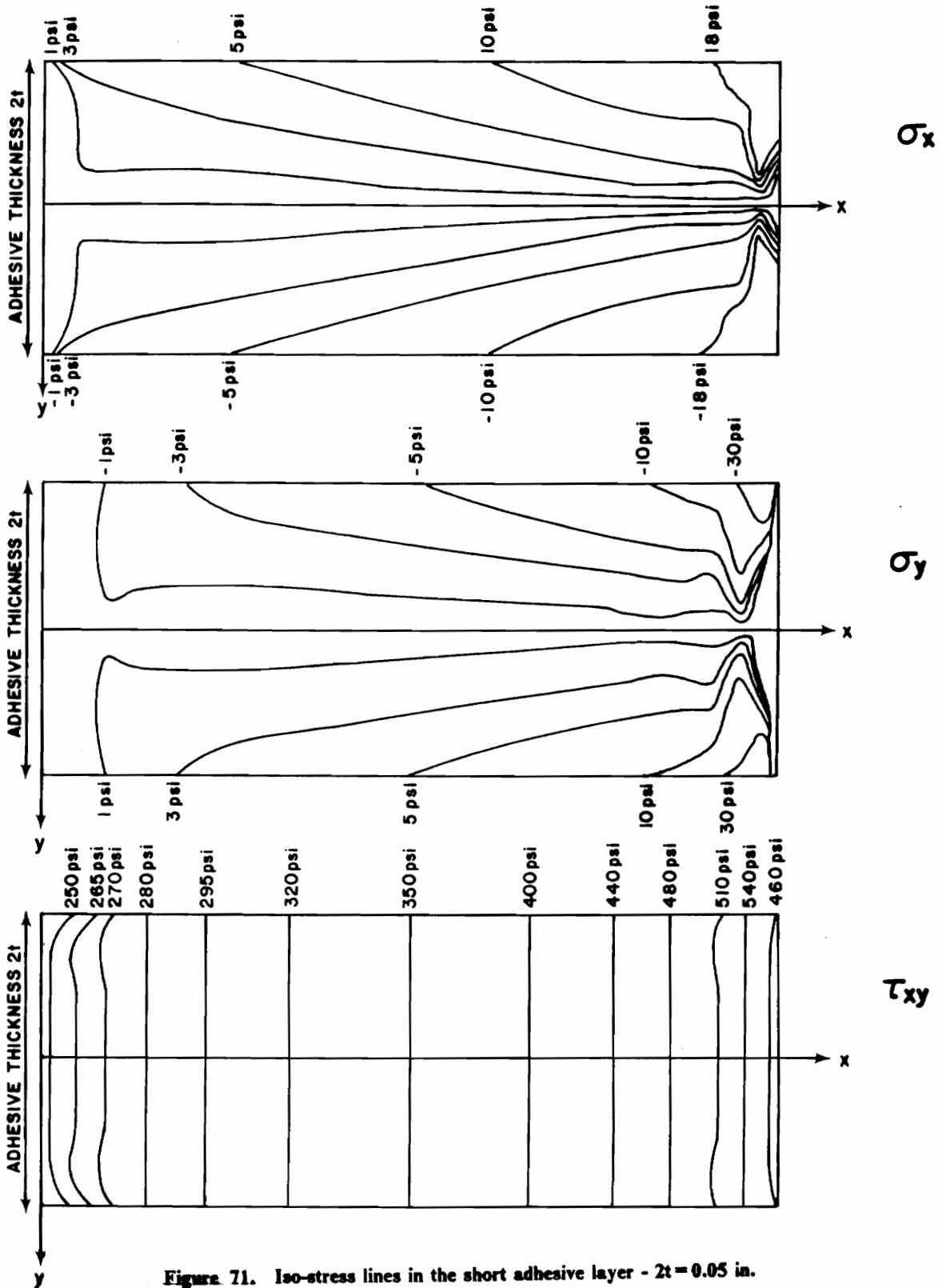


Figure 71. Iso-stress lines in the short adhesive layer - $2t = 0.05$ in.

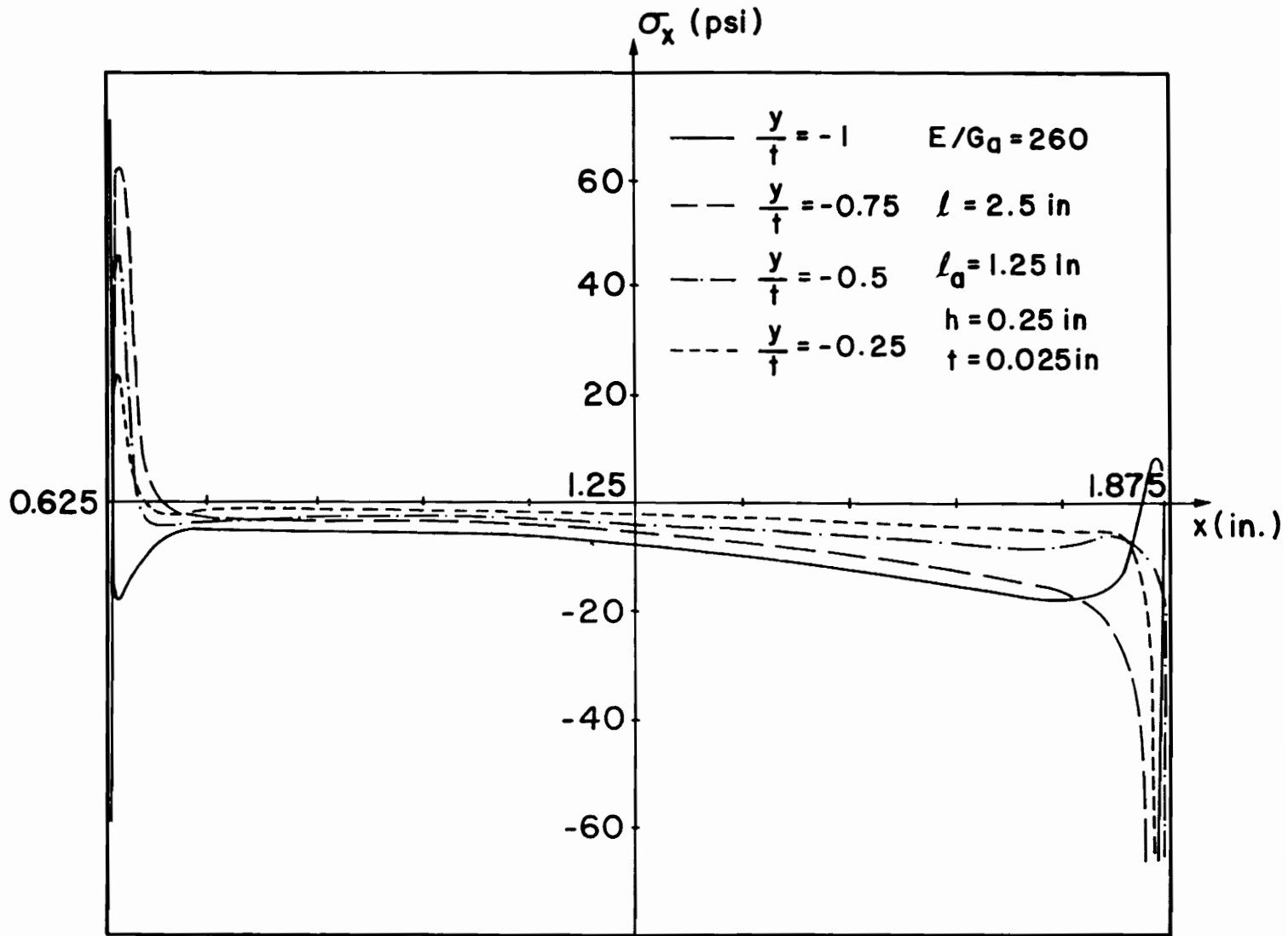


Figure 72. Tensile stress σ_x at different locations in the short adhesive layer .

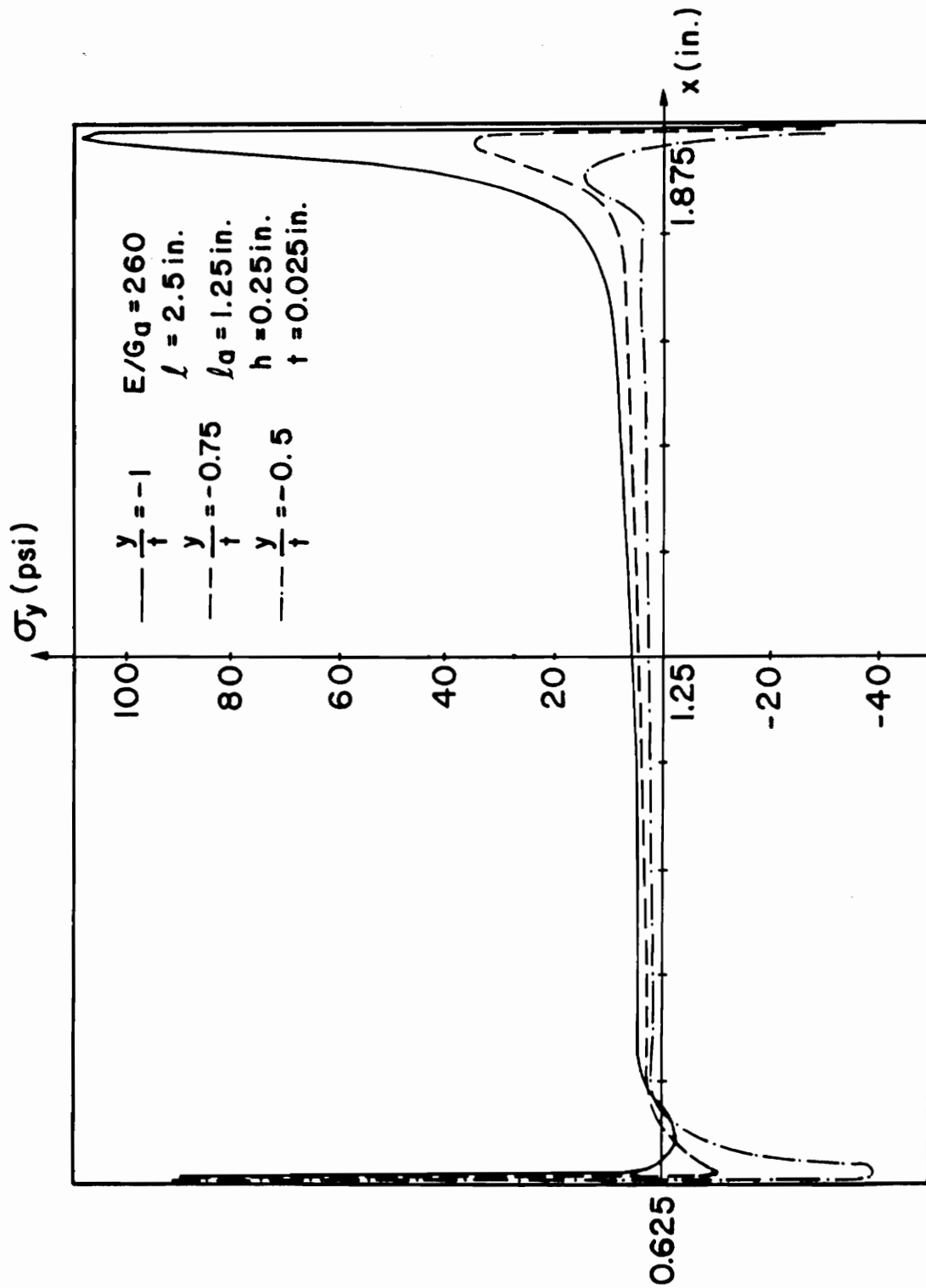


Figure 73. Tensile stress σ_y at different locations in the short adhesive layer.

5 - EXPERIMENTAL APPROACH

The experimental tests on the BMC specimen were performed in order to measure the deflection of the beam and the shear deformation. Specimen geometries were varied to compare experimental results to analytical predictions. The adherends were steel ($E = 30 \times 10^6$ PSi (207000 MPa), $\nu = 0.31$) and aluminum ($E = 10.2 \times 10^6$ PSi (70380 MPa), $\nu = 0.29$). The adhesives were Neoprene 5109S ($G_s = 130$ PSi (0.897 MPa)) and FM300-K ($G_s = 1.2 \times 10^5$ PSi (805.4 MPa)). Three types of adherend-adhesive combination were considered. Rubber-to-steel and epoxy-to-aluminum were the two extreme cases because their resulting stiffness ratios are large (2.3×10^5) and small (10^2) respectively. They also illustrate some of the most used adhesion combinations in bonded structures. A third set consisting of rubber-to-aluminum specimens provided more data for the experimental evaluation of the BMC theory.

5.1 - SPECIMEN PREPARATION

To prepare the specimens, the adherends were vapor degreased, grit-blasted with steel grit, and vapor degreased again with tri-chloroethane 1,1,1. For bonding the rubber, two coats of Chemlock 205 primer and two coats of Chemlock 220 topcoat were brushed on the adherends, allowing for

drying before applying the next layer. The mold was preheated in the platen press and the specimens were placed inside with a rubber layer sandwiched between the two adherends. The rubber was vulcanized at 163°C (325°F) for two hours at a pressure of 3.45 MPa (500 PSi). In the case of the specimens bonded with epoxy, the resin was inserted between the aluminum adherends immediately after the second vapor degreasing. Then, the specimens were cured for one hour in a preheated oven at 175°C (347°F). The shape of the specimens is shown in fig.74 and the properties of the beams are listed in tables 9, 10, 11.

5.2 - EXPERIMENTAL SET-UP

A special device had to be designed to conduct the experiments on the BMC specimen. As shown on fig.75, the beam was clamped vertically on a rigid frame that supported the loading system which consisted in a screw and a mini load cell connected to a yoke on which a pin was attached. The load was applied by pulling on one side of the specimen with the horizontal pin acting on a groove built on the constrained side of the specimen. The load was transferred to the two adherends by putting a rigid shim between both adherends at the loading point of the same thickness as the adhesive layer. The load applied with the screw was recorded with the load cell fixed between the specimen and the rigid frame device. The beam end deflection as well as the relative motion of the adherends were measured simultaneously in the manner described next.

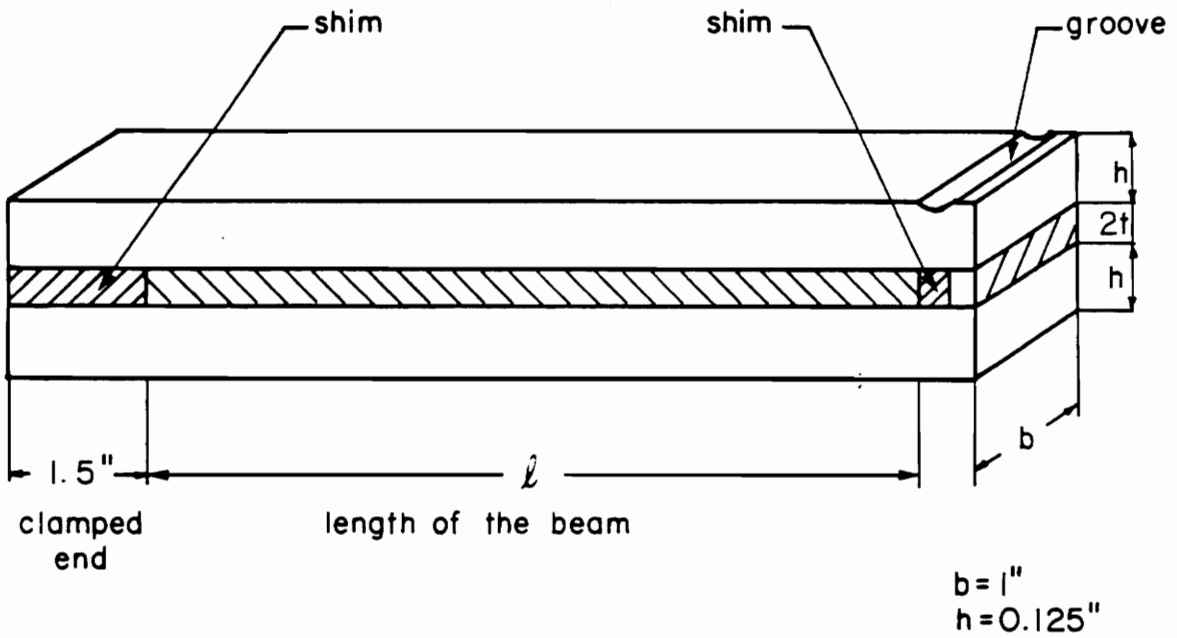


Figure 74. Specimen configuration.

Table 9. Rubber-to-steel specimens.

specimen code	adherend thickness h (in.)	adhesive thickness 2t (in.)	beam length ℓ (in.)	measurement location * x/ℓ
RB1	0.125	0.051	3.5	0.58
RB2	0.125	0.048	4.5	0.52
RB3	0.125	0.039	5.5	0.45
RB4	0.125	0.045	6.5	0.44
RB5	0.125	0.040	7.5	0.63
RB6	0.125	0.041	9.5	0.71 0.48 0.24
RB7	0.125	0.045	9.5	0.75 0.44

$E = 30 \times 10^6$ Psi , $\nu = 0.31$

$G_a = 130$ Psi

(*) for shear deformation measurements

Table 10. Rubber-to-aluminum specimens.

specimen code	adherend thickness h (in.)	adhesive thickness 2t (in.)	beam length ℓ (in.)	measurement location * x/ℓ
ARB1	0.125	0.015	3.5	0.41
ARB2	0.125	0.016	4.5	0.40
ARB3	0.125	0.041	4.5	0.43
ARB4	0.125	0.024	5.5	0.45

$E = 10.2 \times 10^6$ Psi , $\nu = 0.29$

$G_a = 130$ Psi

(*) for shear deformation measurements

Table 11. Epoxy-to-aluminum specimens.

specimen code	adherend thickness h (in.)	adhesive thickness 2t (in.)	beam length ℓ (in.)
EAL1	0.125	0.046	2.5
EAL2	0.125	0.088	2.5
EAL3	0.125	0.048	3.5
EAL4	0.125	0.043	3.5
EAL5	0.125	0.038	4.5
EAL6	0.125	0.040	4.5

$E = 10.2 \times 10^6$ Psi, $\nu = 0.29$

$G_a = 1.2 \times 10^5$ Psi

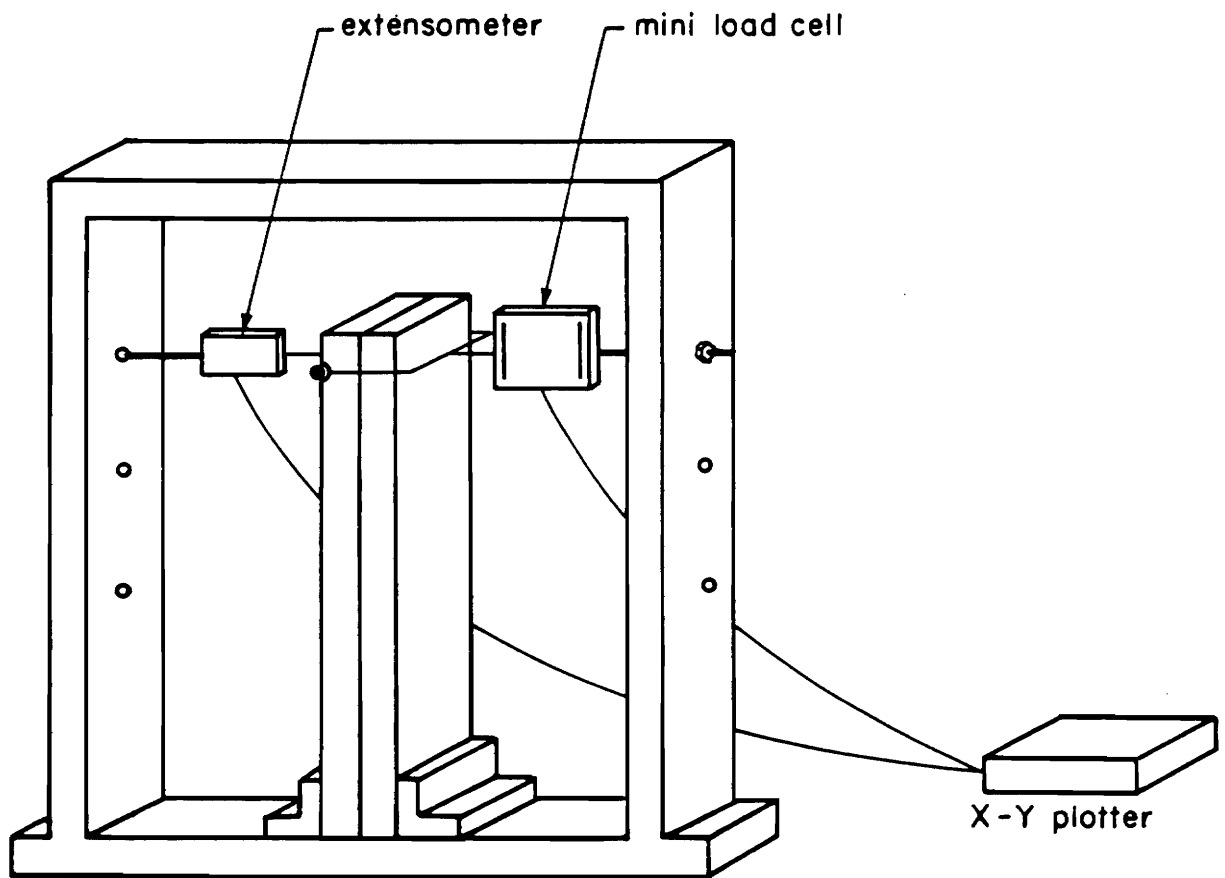


Figure 75. Experimental set-up.

5.3 - SHEAR DEFORMATION MEASUREMENTS

The measurement of the shear deformation of the beam was conducted with a Krieger gage [20] which is an extensometer initially developed to give the shear stress-strain curve for a glue line in a thick adherend lap shear specimen. The extensometer is positioned on the side of the BMC specimen as pictured in fig.76. When the beam is loaded, the extensometer records the relative motion of the adherends. The applied force and the shear deformation are then printed on a X-Y plotter and provide the data for a comparison between the experimental shear strain and that predicted from theory. The experimental results are presented on fig.77 to 87 and they are compared with the theoretical predictions. The shear strain was calculated by dividing the shear deformation by the distance separating the two hard steel points of the gage and clamped to each adherend. The theoretical curves were obtained from the shear strain approach of the BMC theory and by using the input data listed in tables 9 and 10. Comparison between experimental and analytical results shows that a good agreement is found especially when the shear deformation is measured far away from the loaded end. As demonstrated by specimens RB6 and RB7, the measured shear strain is very sensitive to the measurement location and the difference between theory and experiments increases with the quantity $\frac{x}{l}$. We expect the Krieger gage itself to be responsible for this disparity because the closer to the beam tip the shear deformation is measured, the larger is the bending deformation of the adherends. Therefore, each cross section of the adherend rotates relatively to the adhesive midplane and causes a reduction of the real deformation in shear recorded by the Krieger gage. This is illustrated for several specimens on the following figures.

For our purpose, the Krieger gage was difficult to use and is not recommended for further experiments on the BMC specimen. Vibrations occurred and the measurements lacked reproducibility on repeated loading. In particular, this happened when the shear deformation was expected to have a small magnitude relatively to the material properties of the specimen.

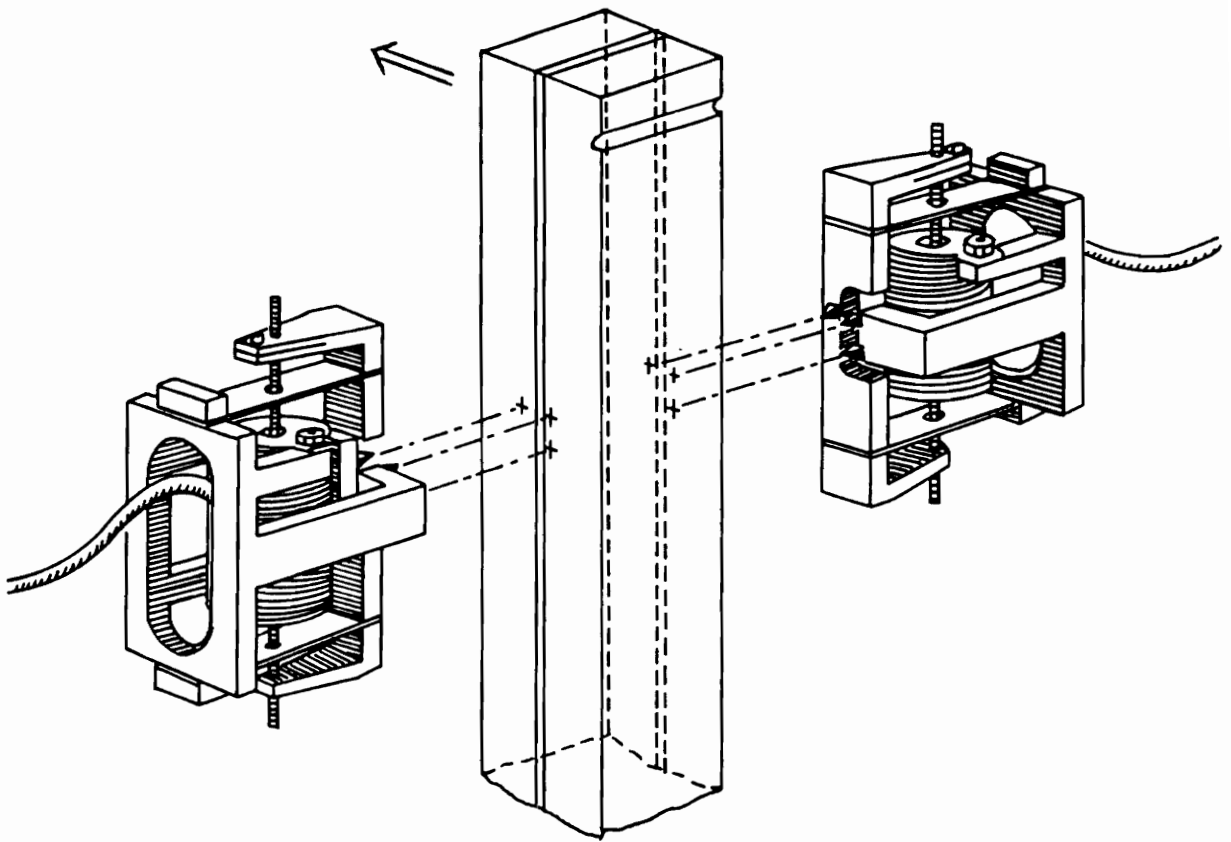


Figure 76. Krieger gage on the BMC specimen.

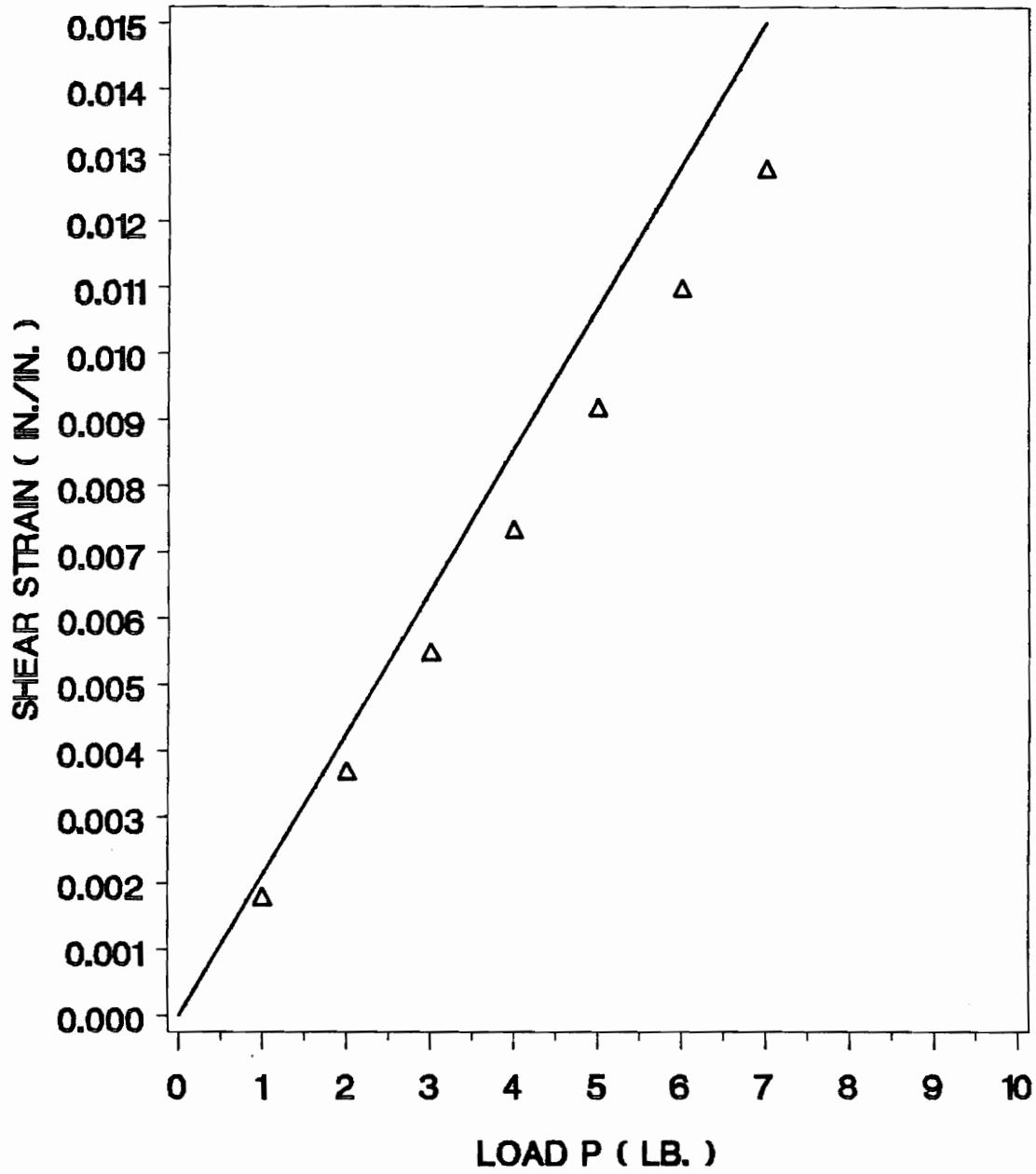


Figure 77. Shear strain versus load. Specimen RB1. Comparison of theory (solid curve) with experiments (triangles).

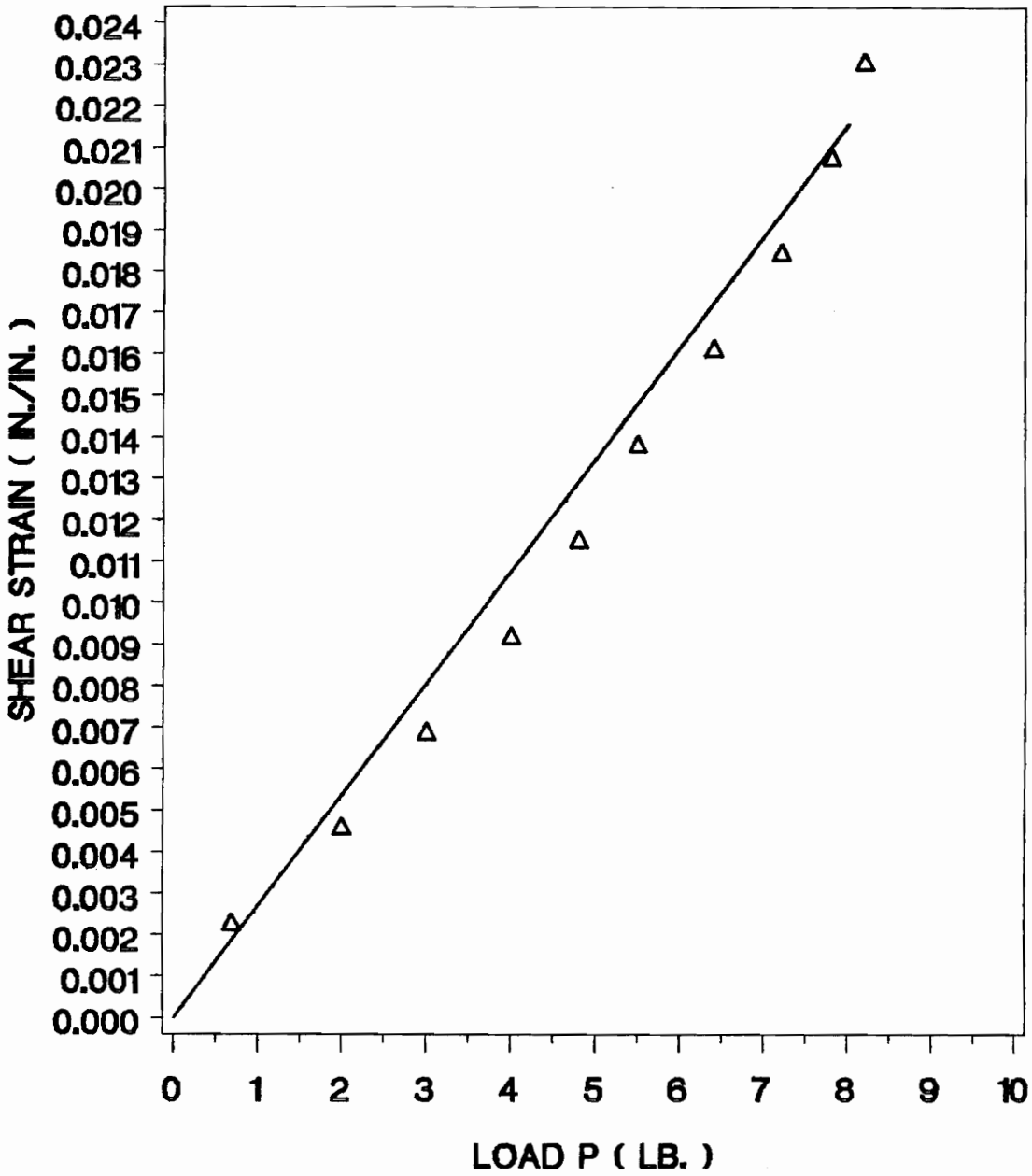


Figure 78. Shear strain versus load. Specimen RB2. Comparison of theory (solid curve) with experiments (triangles).

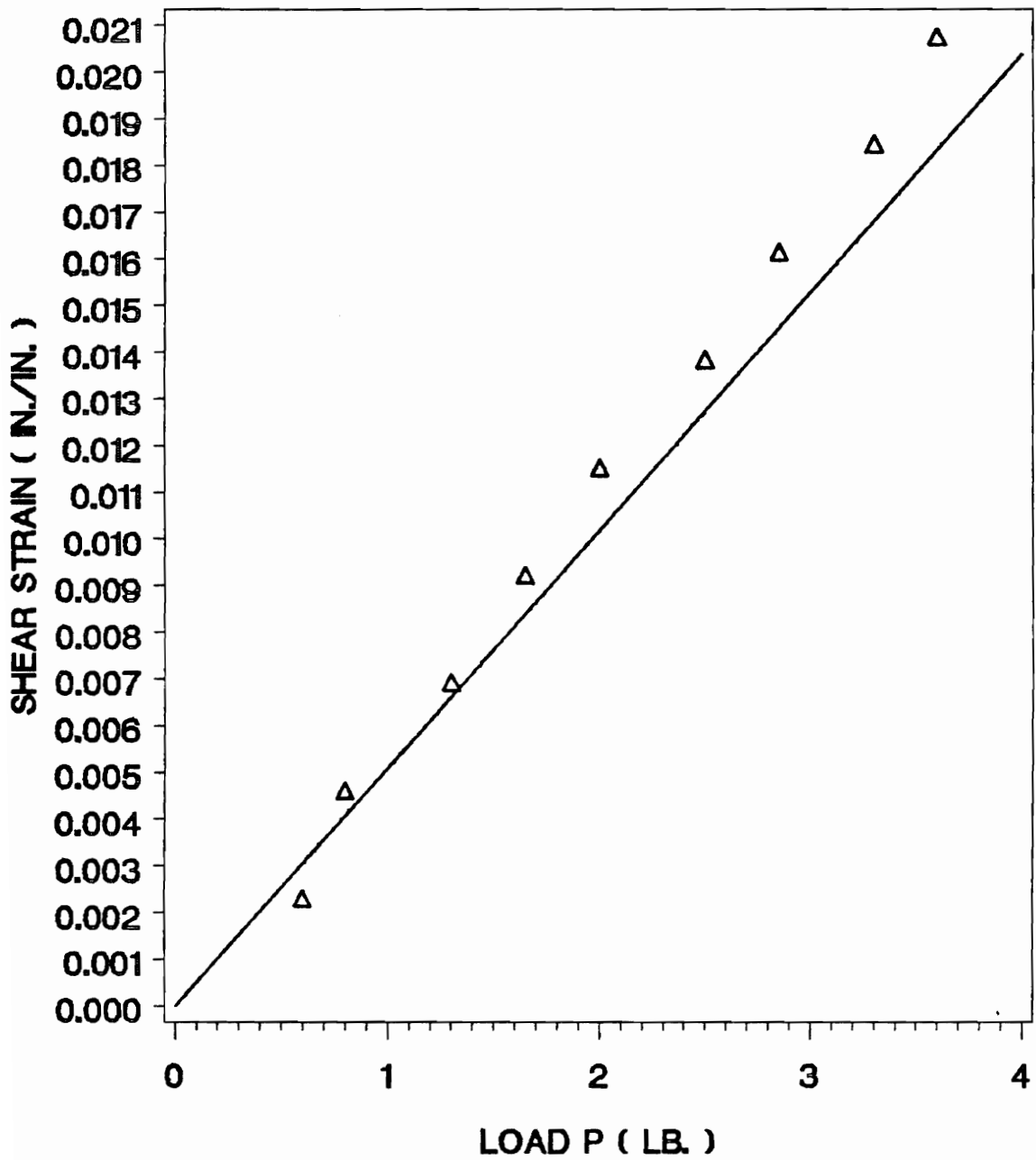


Figure 79. Shear strain versus load. Specimen RB3. Comparison of theory (solid curve) with experiments (triangles).

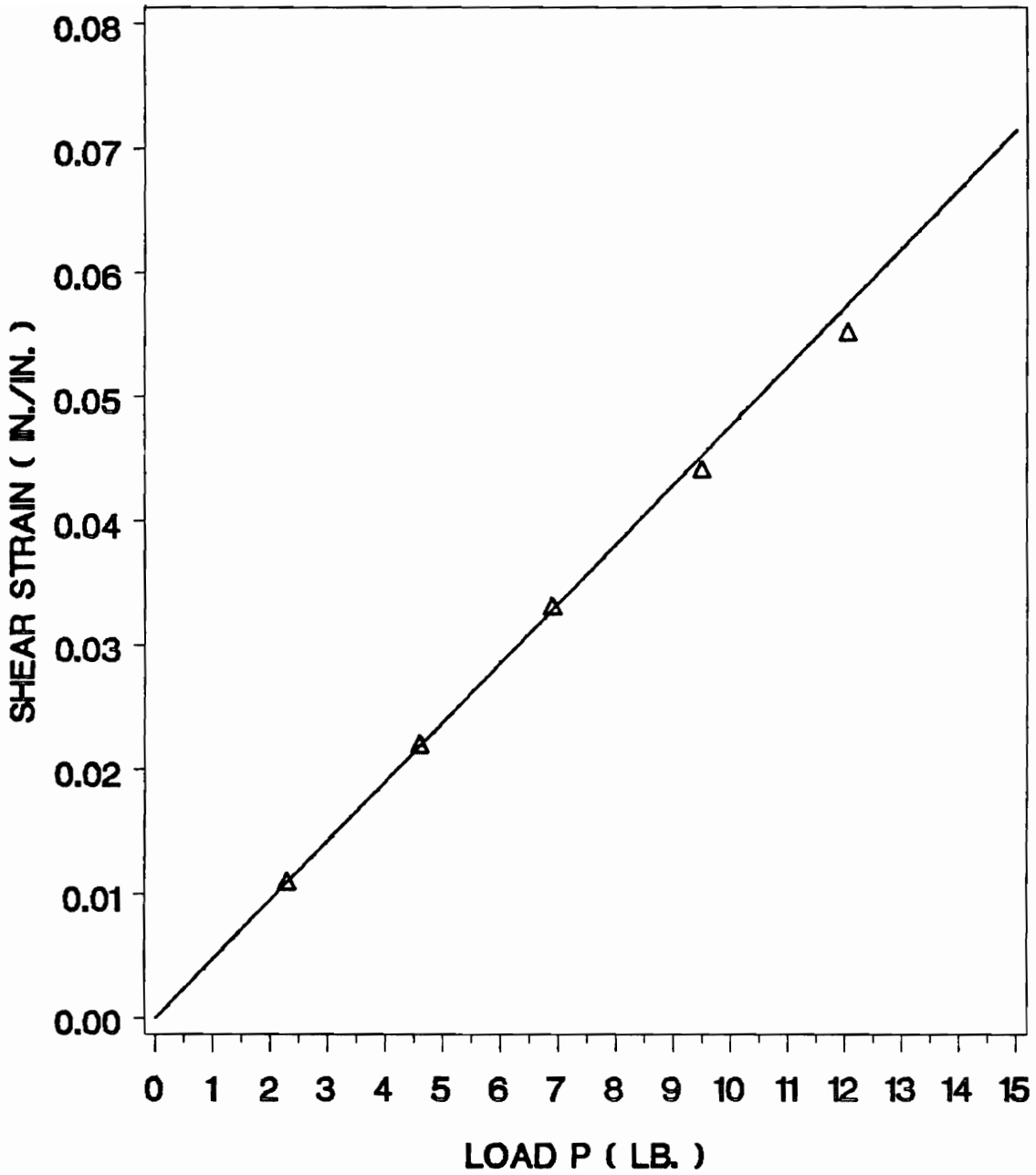


Figure 80. Shear strain versus load. Specimen RB4. Comparison of theory (plane and slashed lines) with experiments (triangles and diamonds) for two measurement locations on the beam.

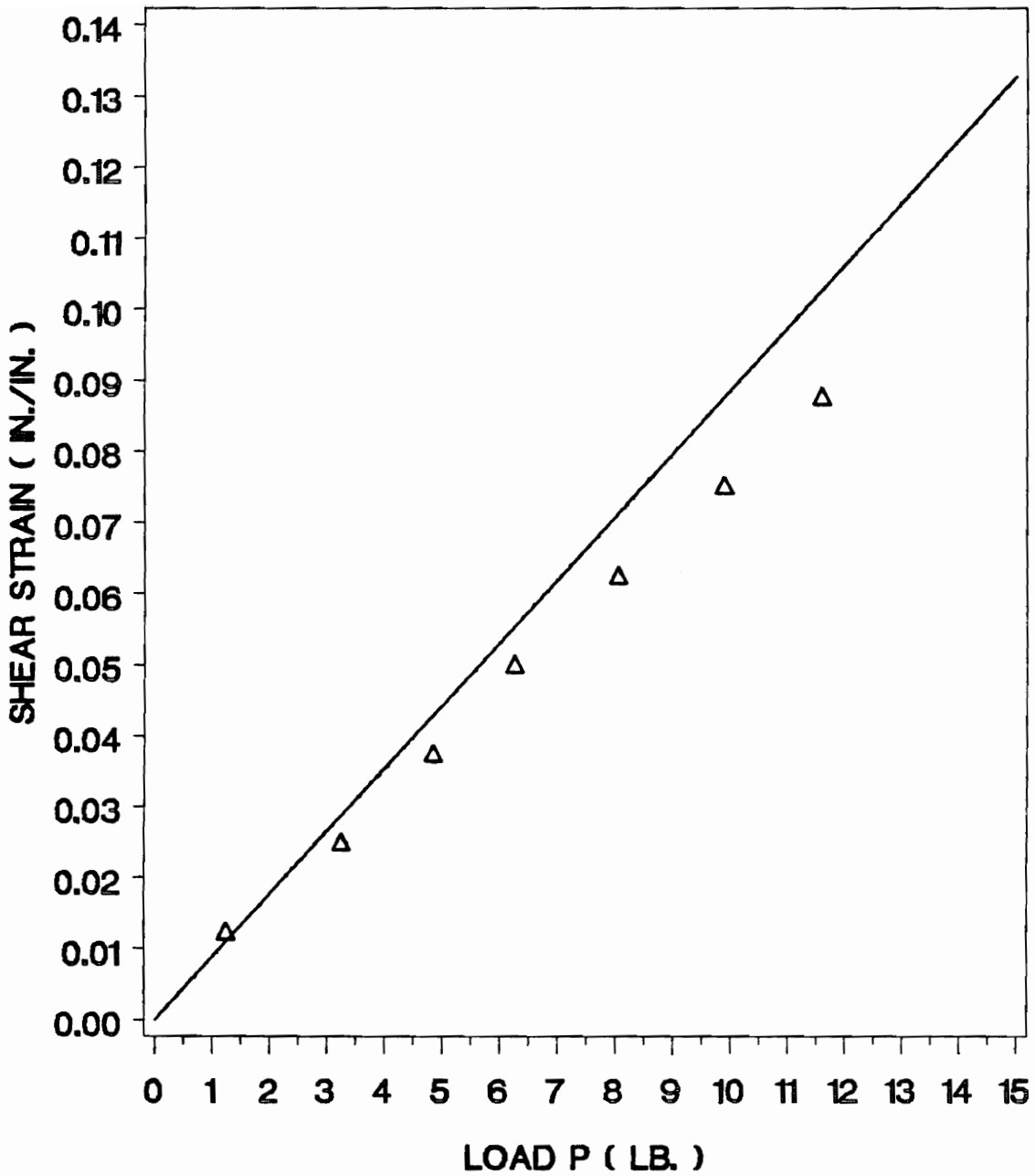


Figure 81. Shear strain versus load. Specimen RB5. Comparison of theory (solid curve) with experiments (triangles).

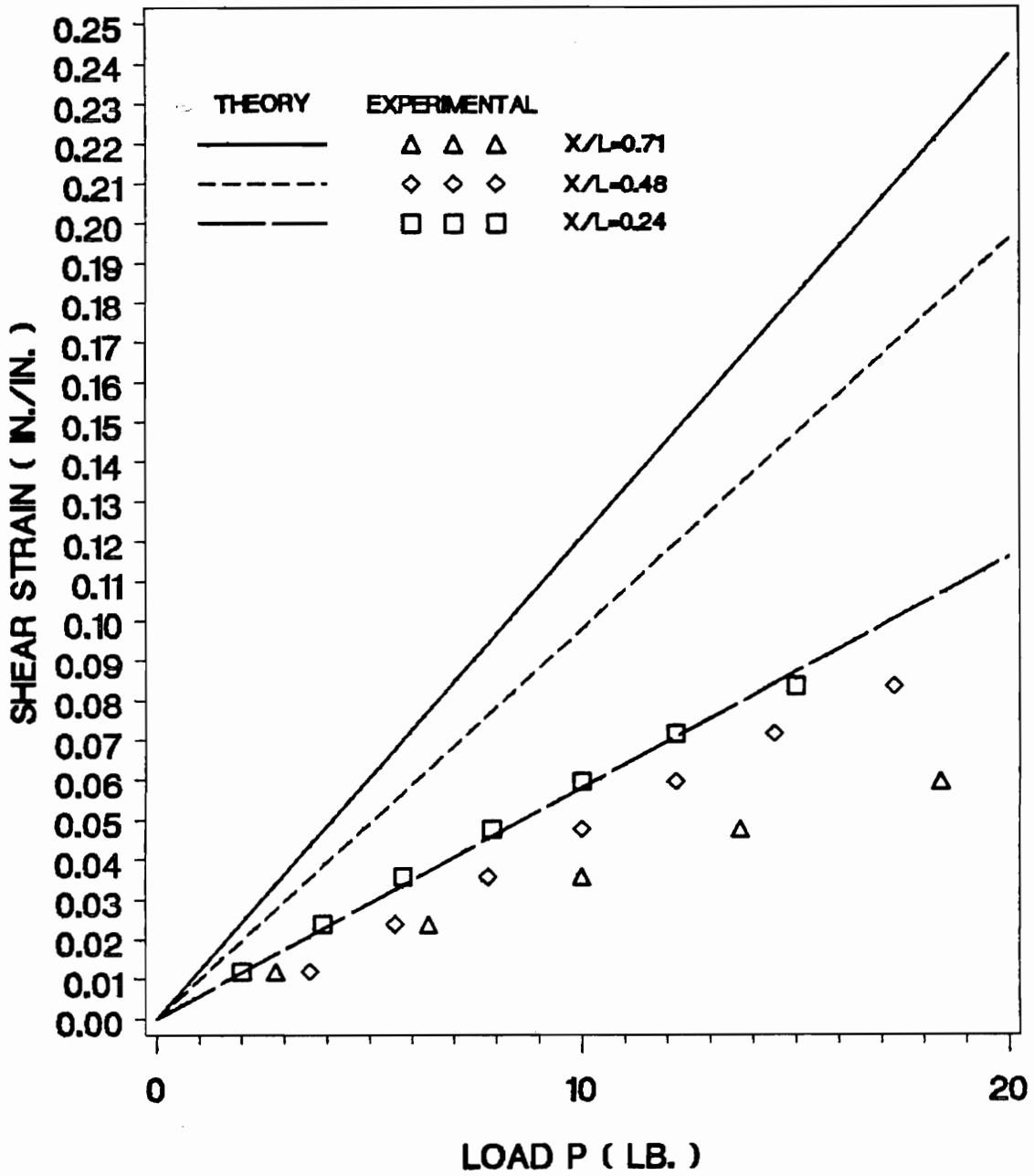


Figure 82. Shear strain versus load. Specimen RB6. Comparison of theory (solid and dashed curves) with experiments (triangles, diamonds, squares).

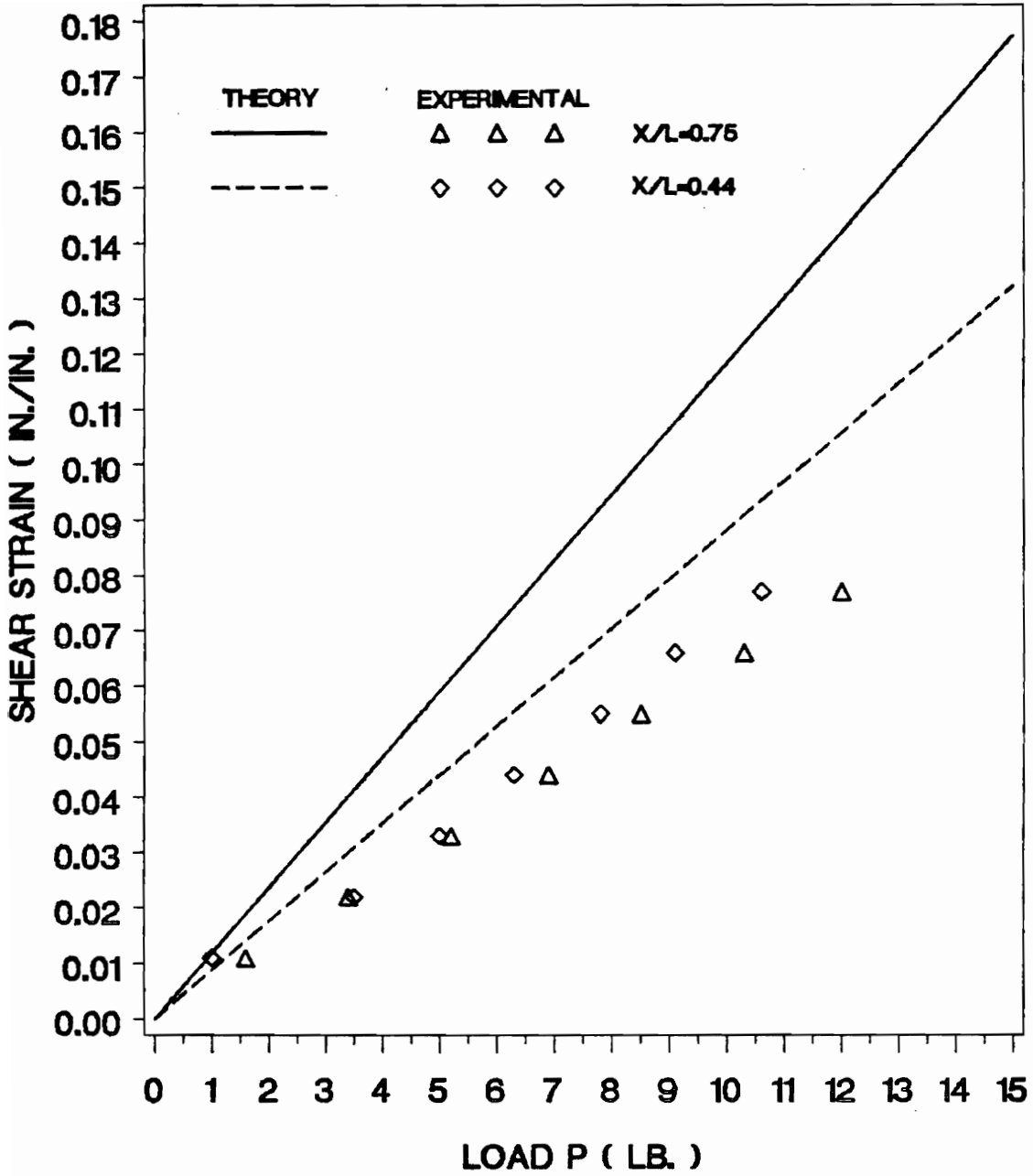


Figure 83. Shear strain versus load. Specimen RB7. Comparison of theory (solid and dashed curves) with experiments (triangles and diamonds).

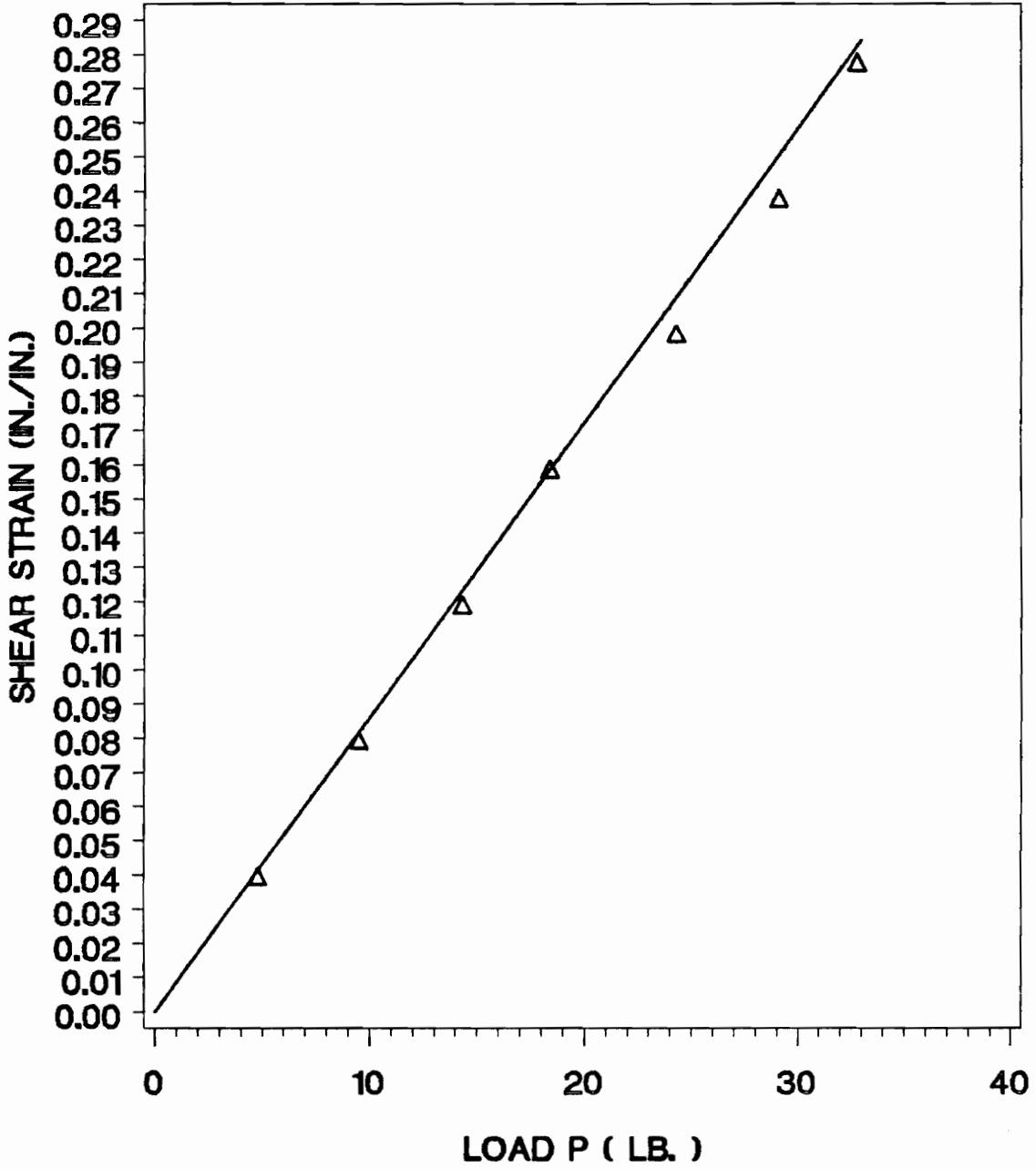


Figure 84. Shear strain versus load. Specimen ARB1. Comparison of theory (solid curve) with experiments (triangles).

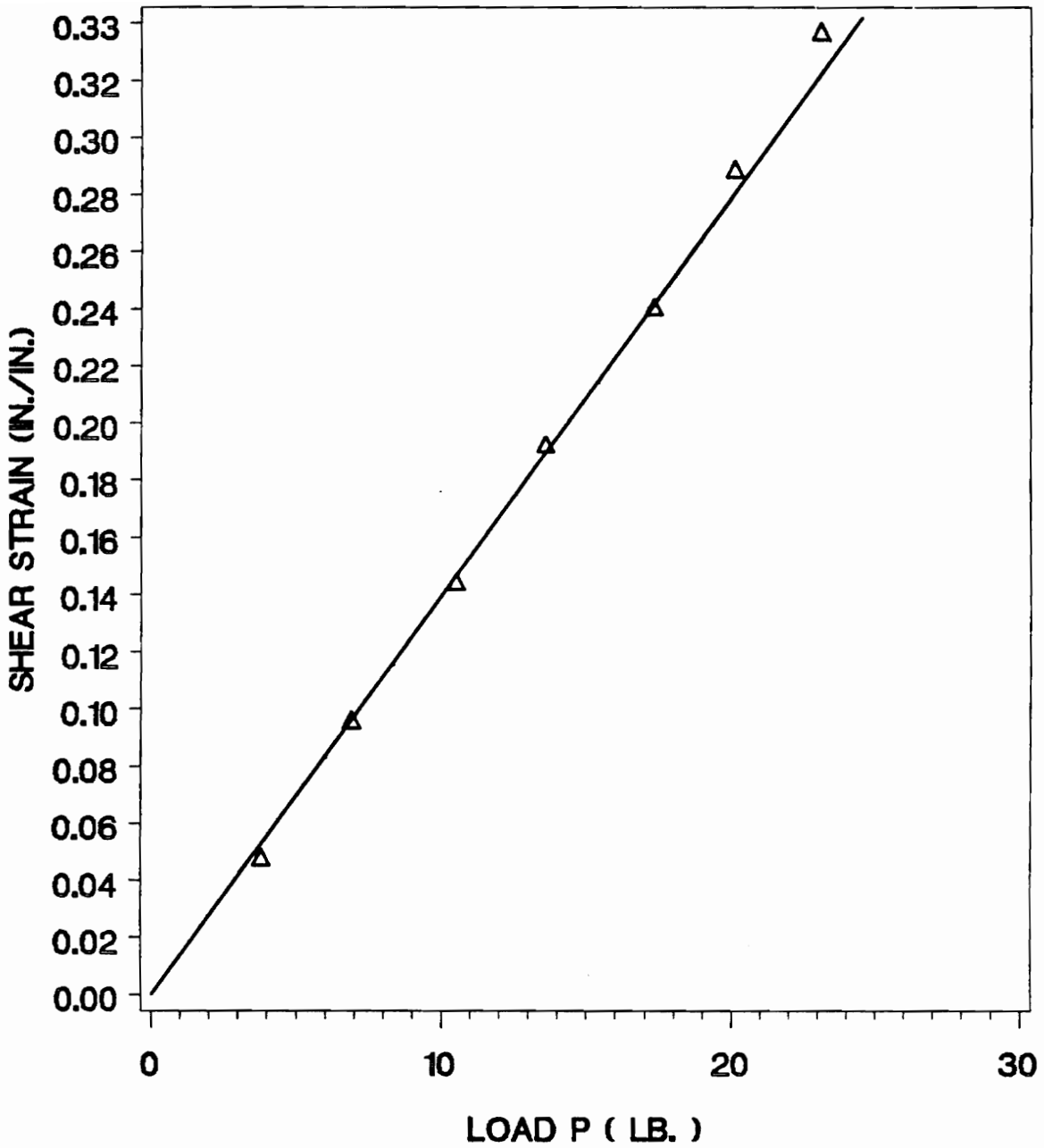


Figure 85. Shear strain versus load. Specimen ARB2. Comparison of theory (solid curve) with experiments (triangles).

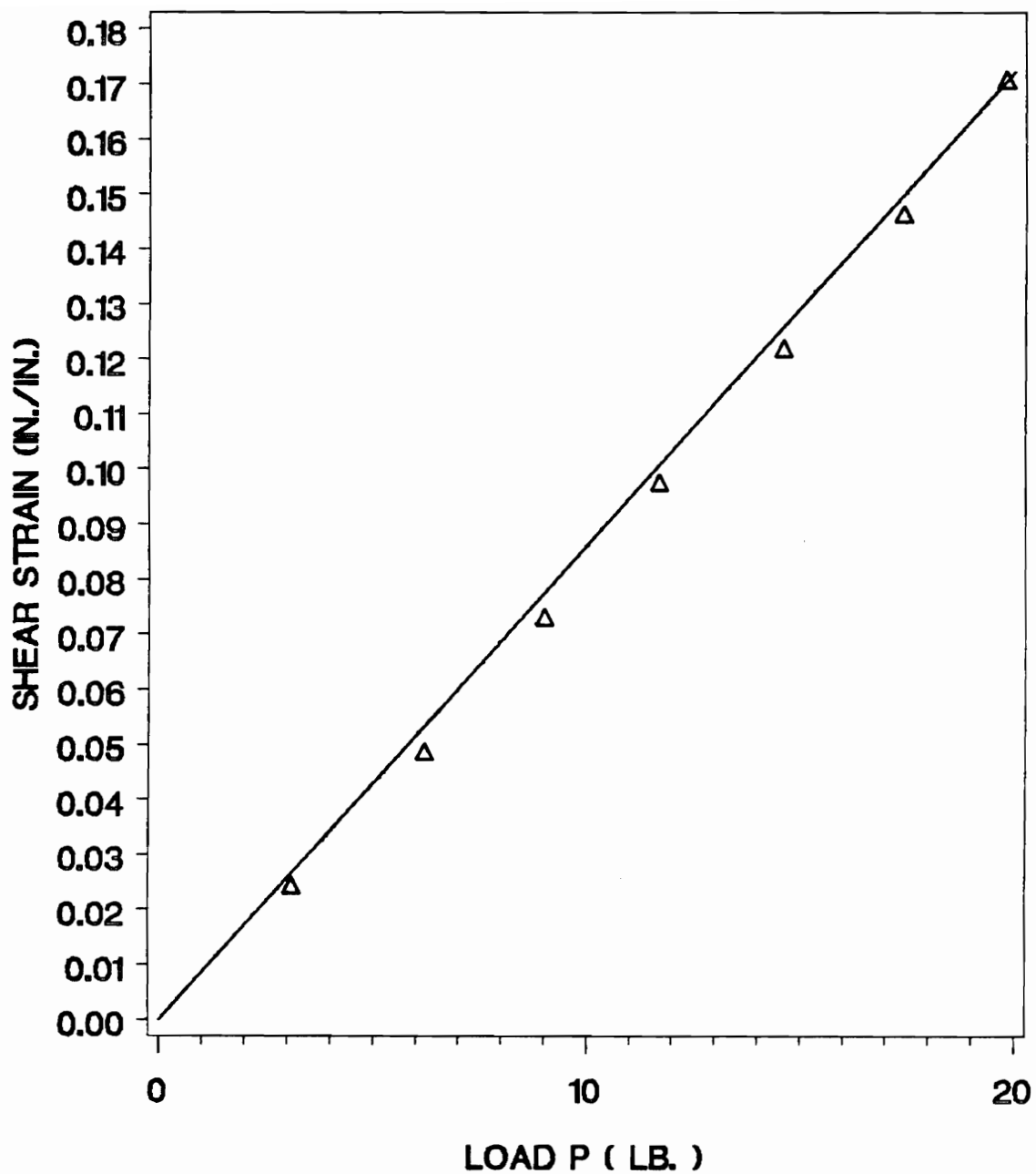


Figure 86. Shear strain versus load. Specimen ARB3. Comparison of theory (solid curve) with experiments (triangles).

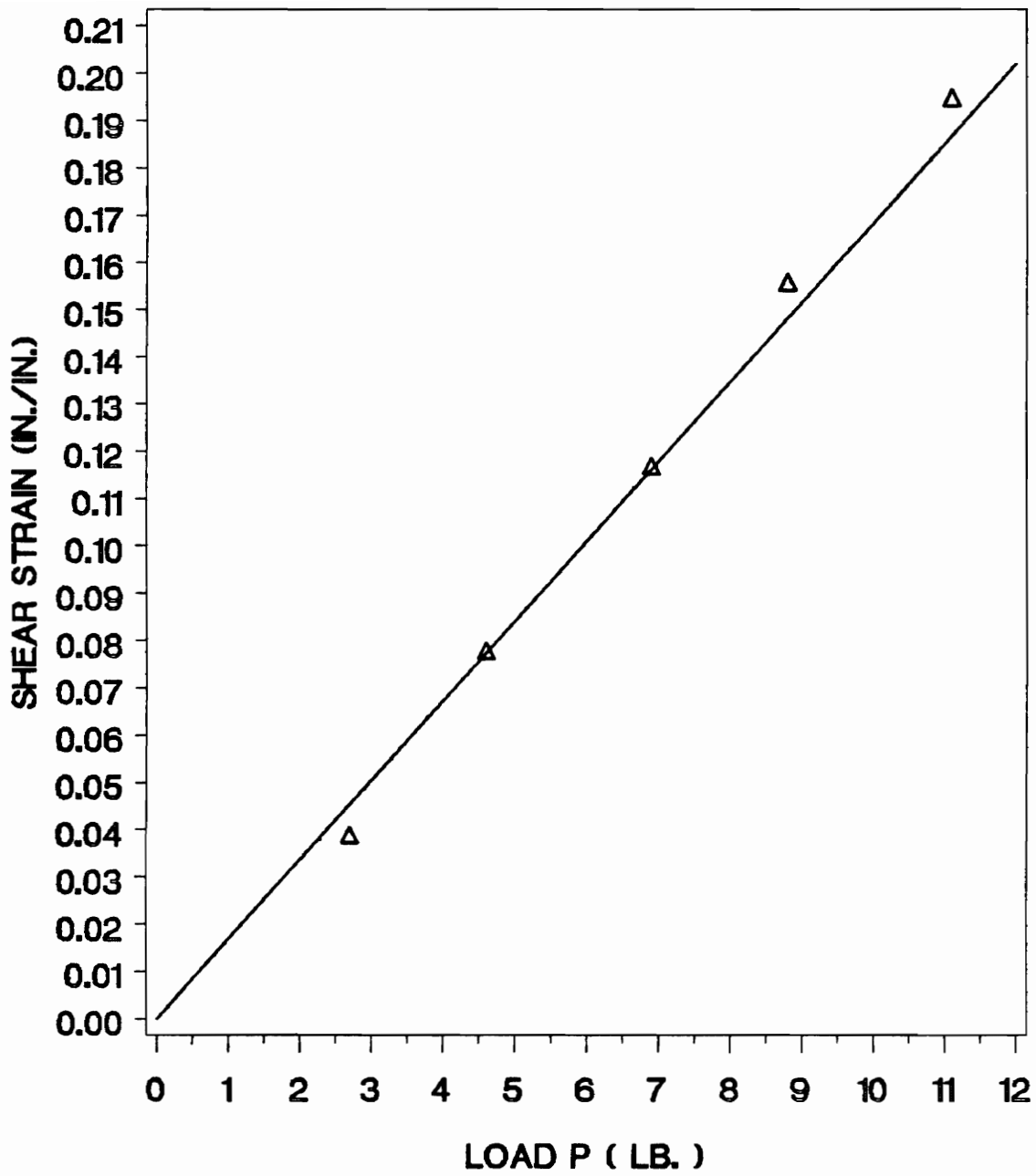


Figure 87. Shear strain versus load. Specimen ARB4. Comparison of theory (solid curve) with experiments (triangles).

5.4 - DEFLECTION MEASUREMENTS

The end deflection was measured with a MTS extensometer mounted at the loading point of the specimen. With an X-Y plotter, we simultaneously recorded the load deflection curve. Experimental results are presented on fig.88 to 101. We also have reported the theoretical data corresponding to the specimens geometrical and material properties. This allowed for a graphical comparison of experiments results with the BMC theory based on the beam deflection approach. For rubber-to-steel specimens or rubber-to-aluminum specimens, excellent agreement is obtained between the two results. Even for the epoxy-to-aluminum specimens, good agreement is found between theory and experiments. However, the loading of the epoxy-to-aluminum specimens had to be modified. When the specimens were loaded by pulling on one side and by assuming that the load was transferred to both adherends with the inserted rigid shim, deflections were 50 % larger than those predicted. The loading system was responsible for this disparity because, due to the large stiffness of the epoxy resin, the applied force on the upper adherend was actually not transferred to the lower aluminum beam. As a results the force magnitude was $\frac{P}{2}$ instead of P regardless to the initial loading conditions of the theoretical model. By designing a new loading device, we were able to apply equal forces on both aluminum beams. We set one small screw at the extremity of each adherend. The yoke was modified in order to support two pulleys on which a piano wire type cable was going around. The two extremities of the cable were attached to each small screws fixed on each adherends. By pulling on the yoke, the adherends were constrained equally. Then, experimental results matched with theory with errors inferior to 10 % which can further be attributed to a lack of rigidity of the clamping system of the specimen because the boundary conditions did not perfectly reproduced the ideal clamped BMC specimen situation. As shown in the next figures, it resulted in higher deflections for all stiff specimens bonded with epoxy. In addition, contribution of the solid loading frame is not negligible when the epoxy-to-aluminum specimens are loaded with a side load.

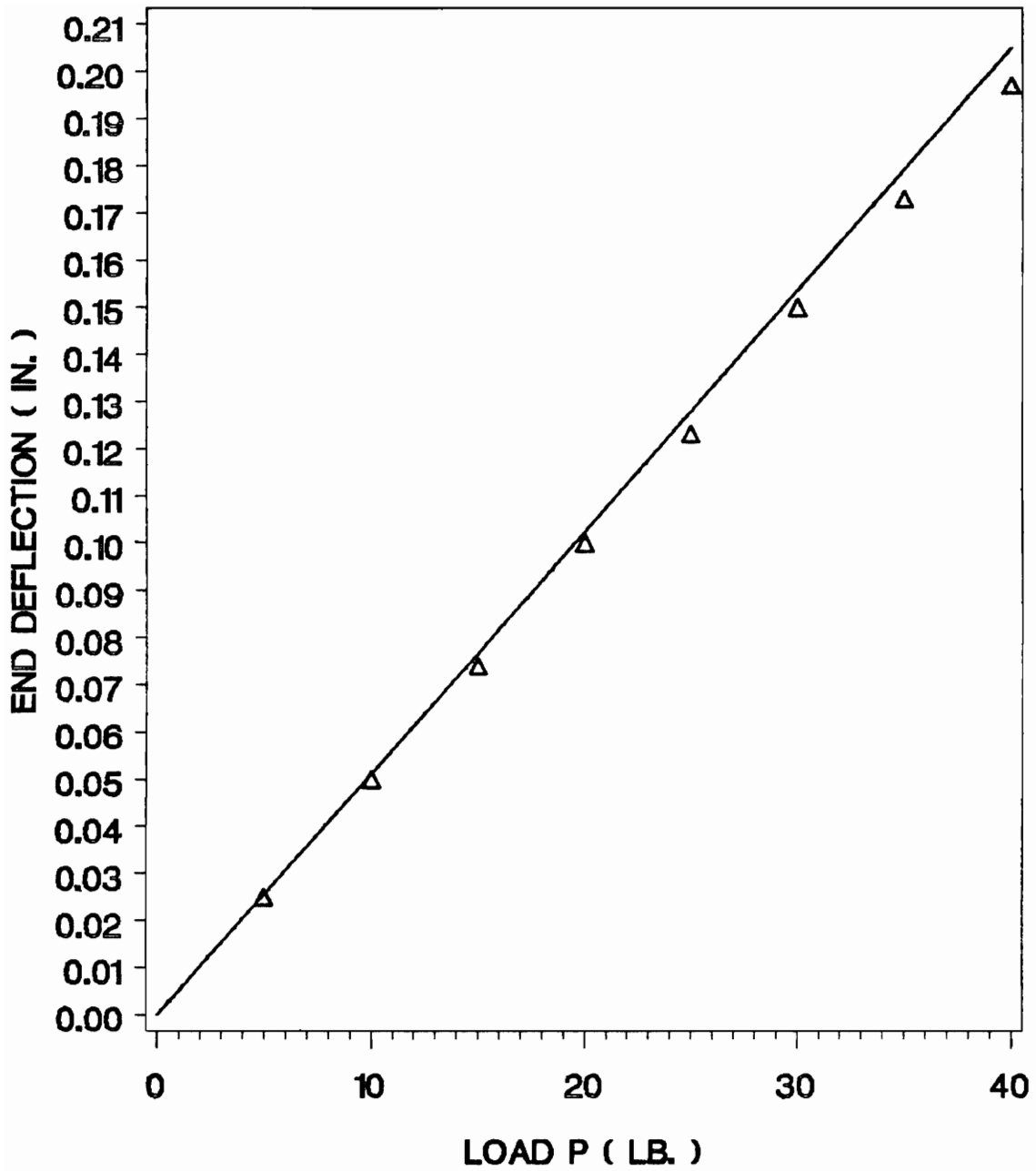


Figure 88. End deflection versus load. Specimen RB3. Comparison of theory (solid curve) with experiments (triangles).

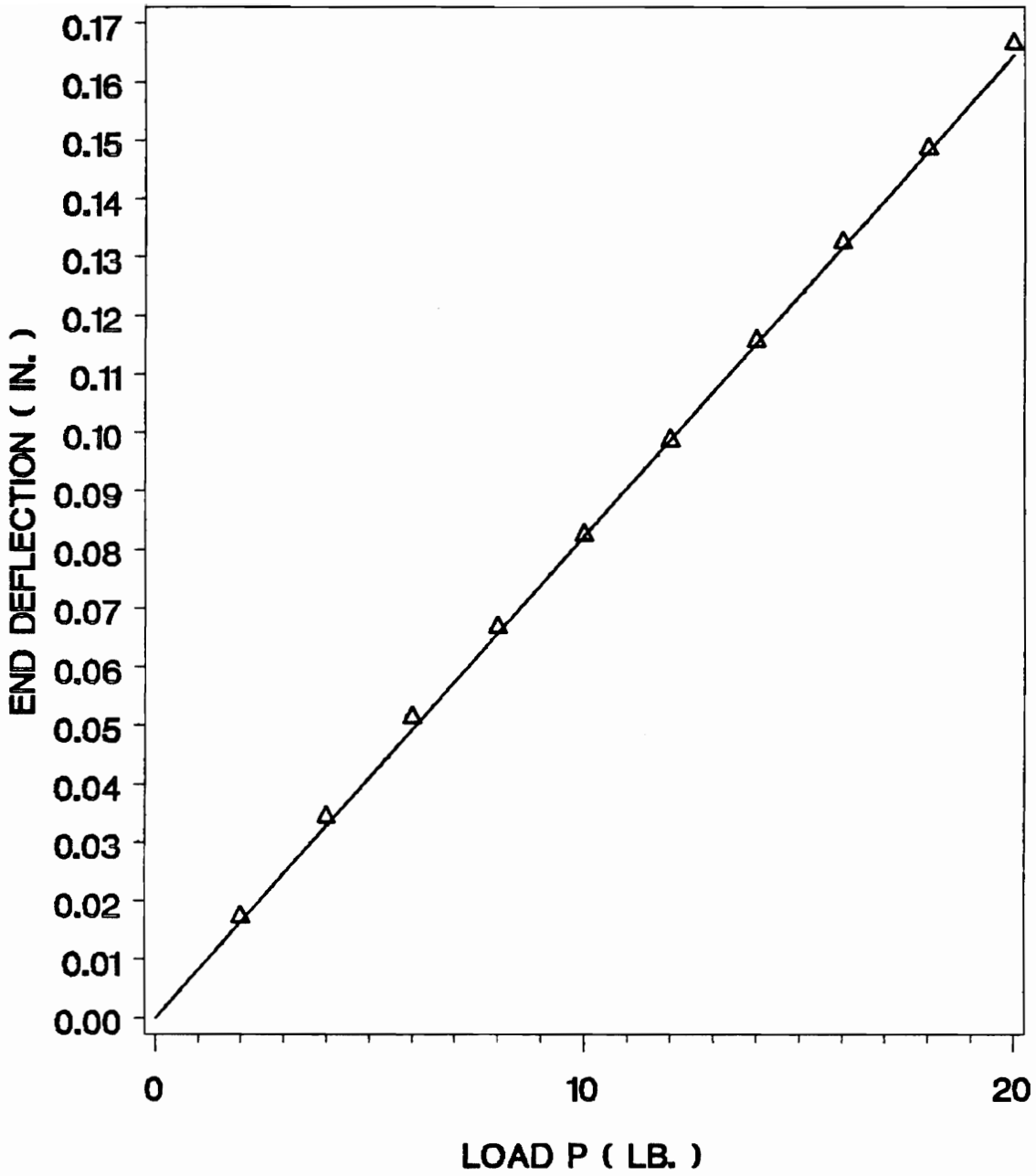


Figure 89. End deflection versus load. Specimen RB4. Comparison of theory (solid curve) with experiments (triangles).

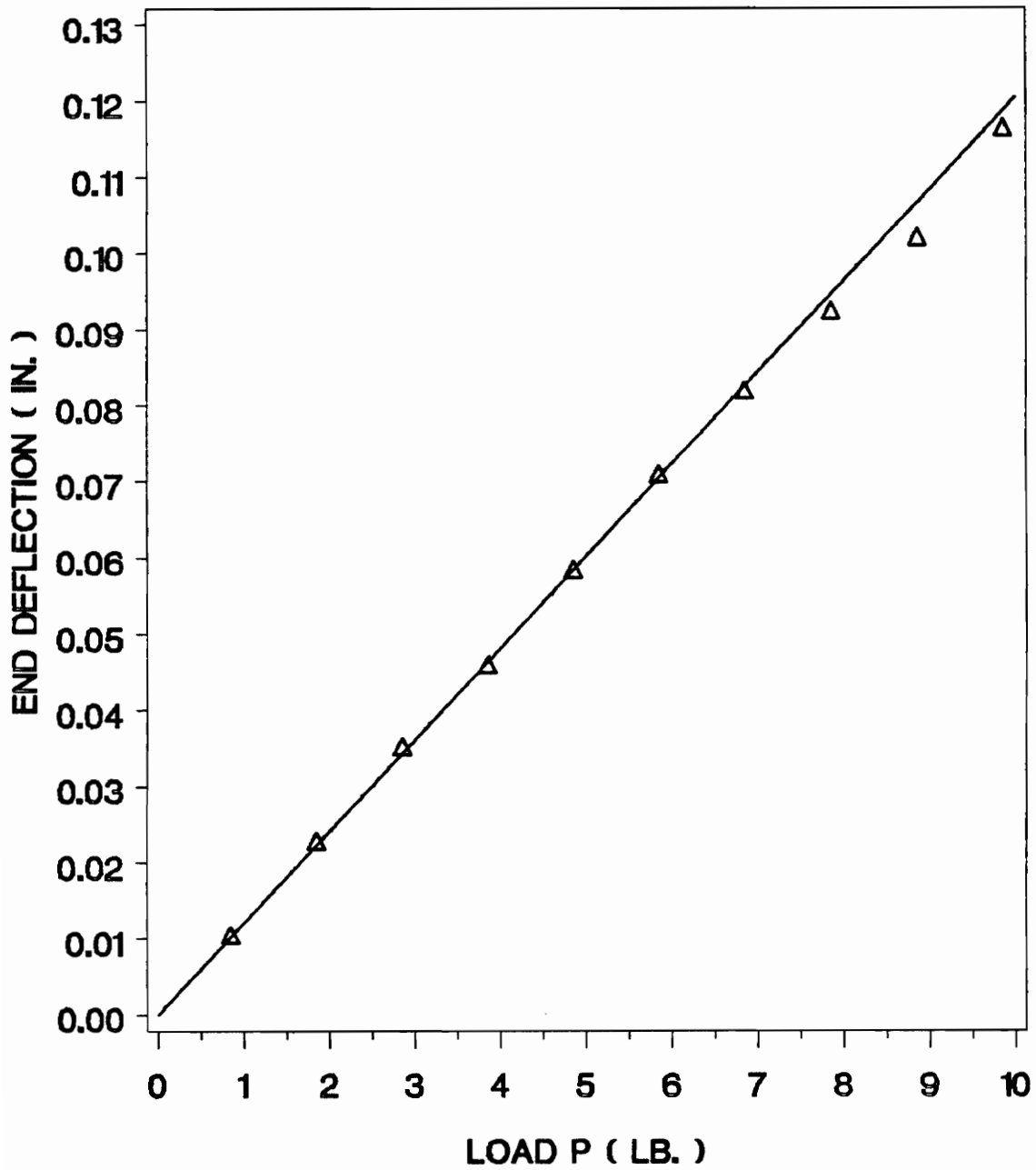


Figure 90. End deflection versus load. Specimen RB5. Comparison of theory (solid curve) with experiments (triangles).

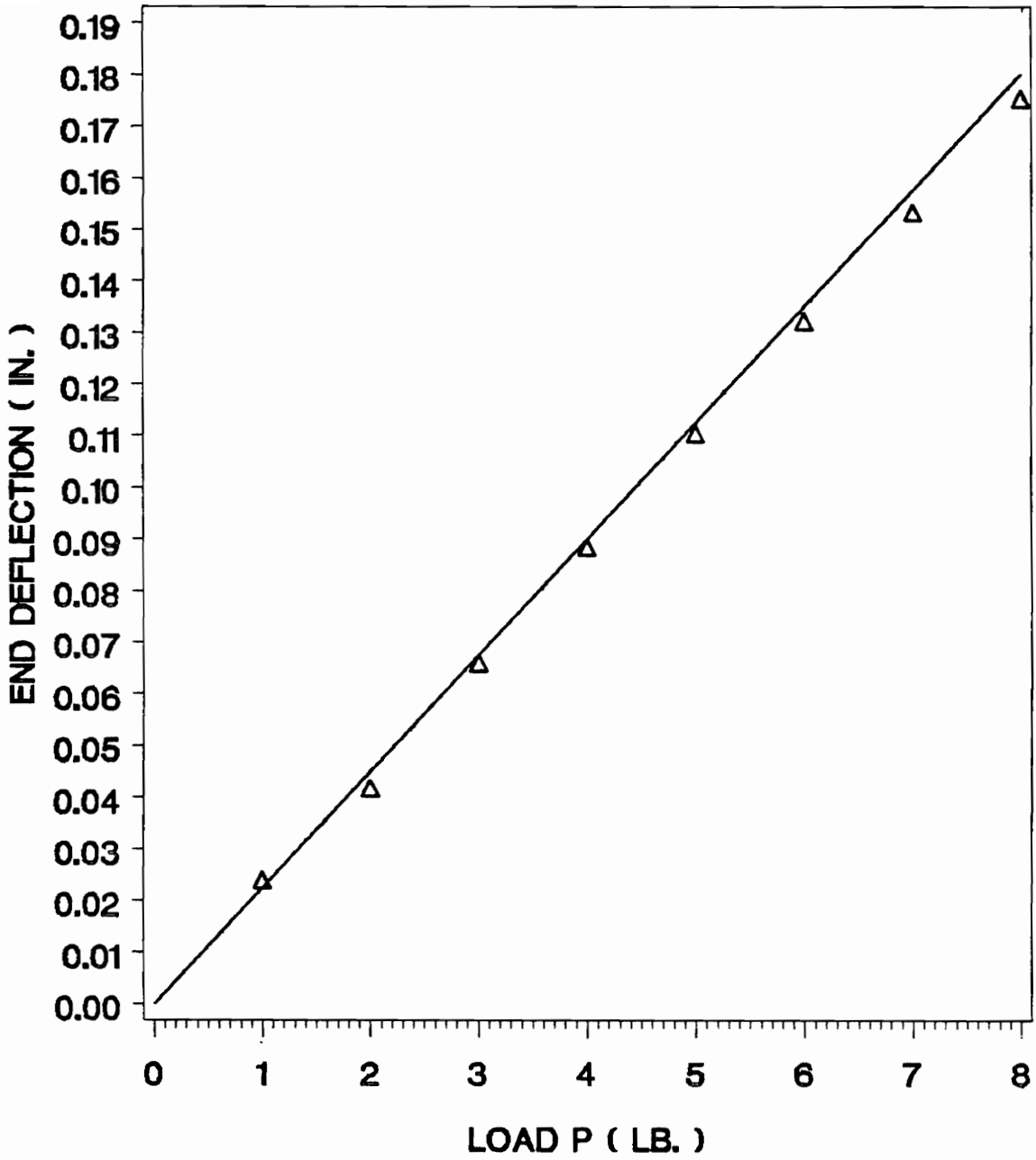


Figure 91. End deflection versus load. Specimen RB6. Comparison of theory (solid curve) with experiments (triangles).

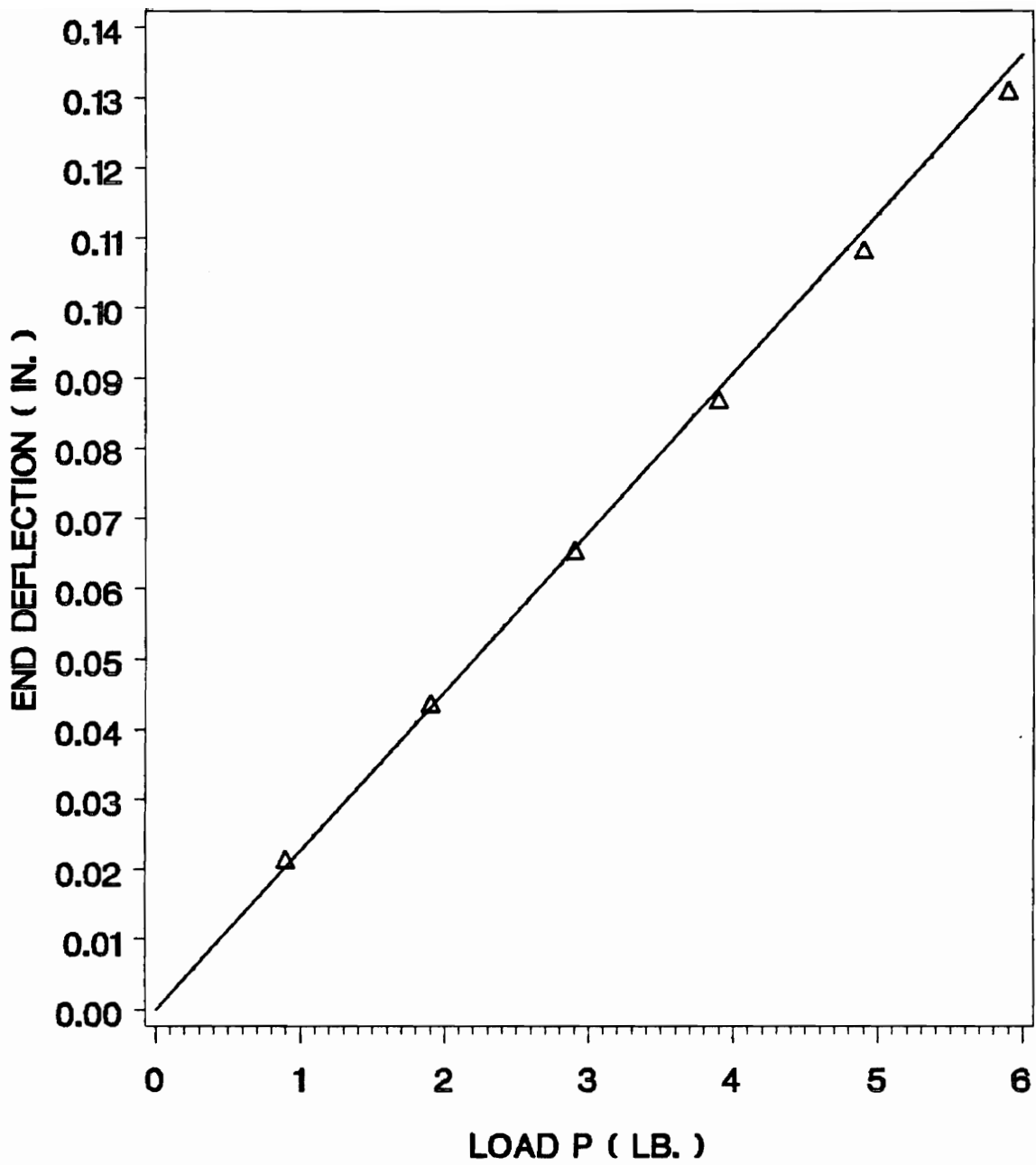


Figure 92. End deflection versus load. Specimen RB7. Comparison of theory (solid curve) with experiments (triangles).

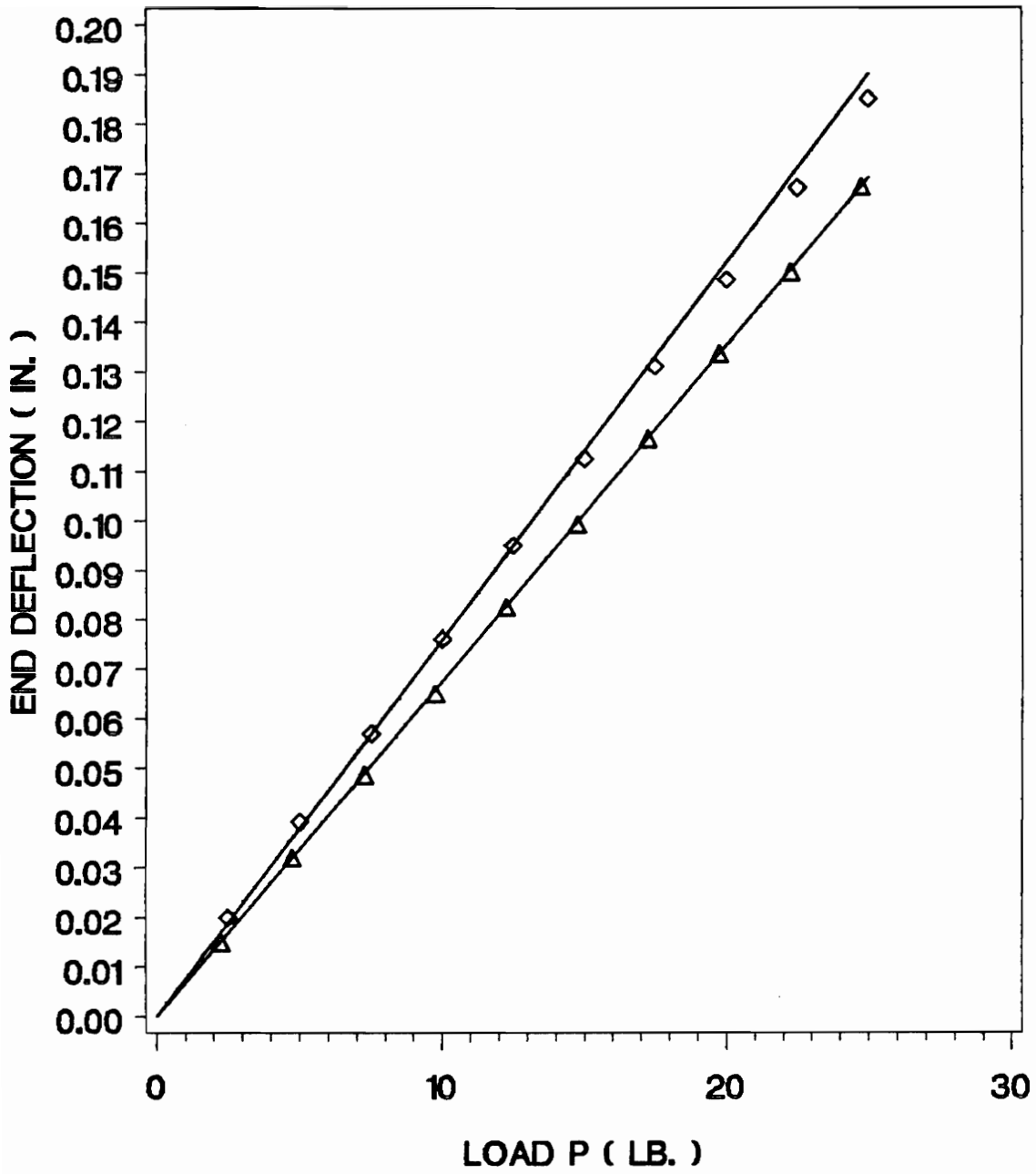


Figure 93. End deflection versus load. Specimen ARB1. Comparison of theory (solid curve) with experiments (triangles).

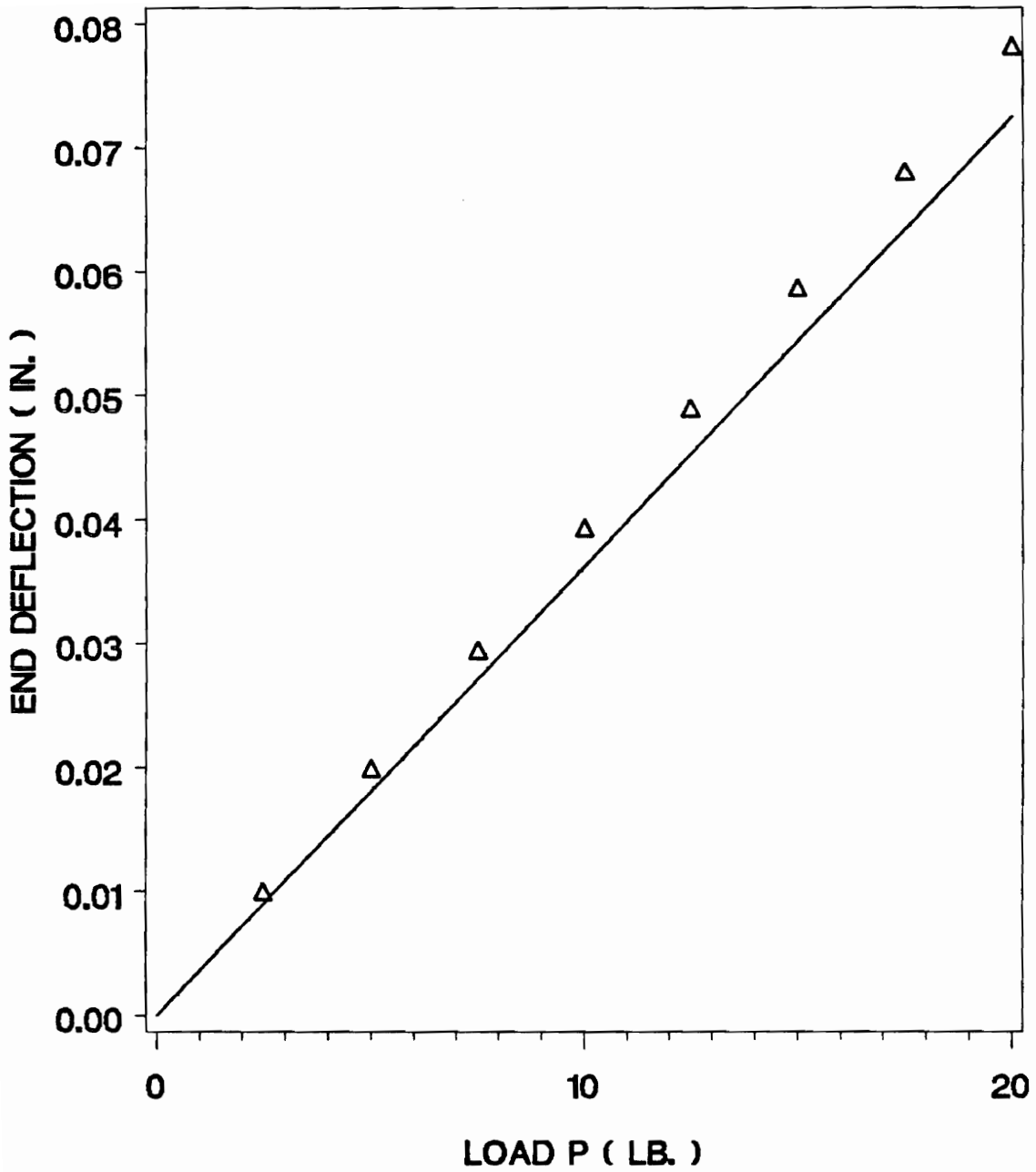


Figure 94. End deflection versus load. Comparison of theory (solid curves) with experiments for specimen ARB2 (triangles) and specimen ARB3 (diamonds).

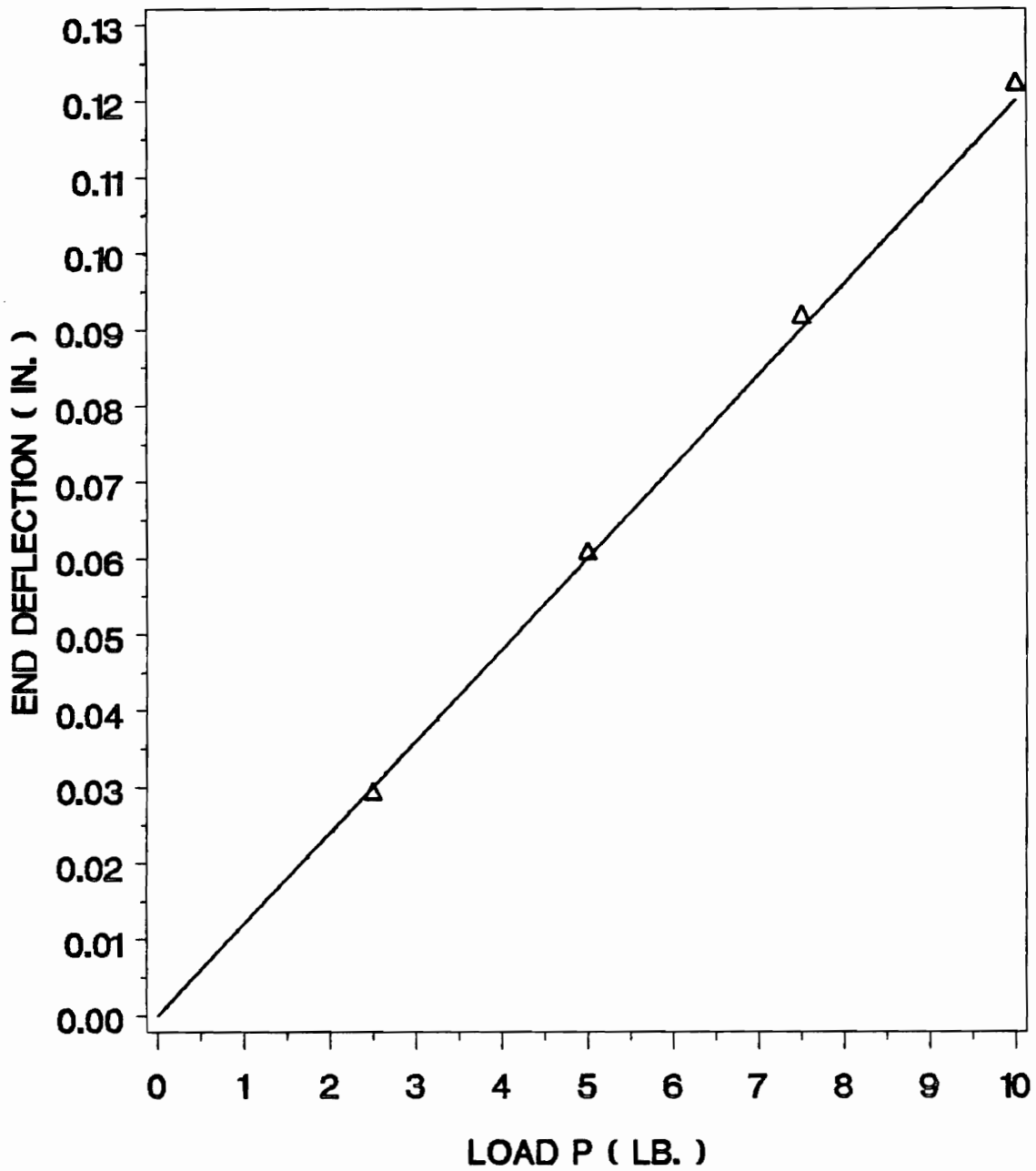


Figure 95. End deflection versus load. Specimen ARB4. Comparison of theory (solid curve) with experiments (triangles).

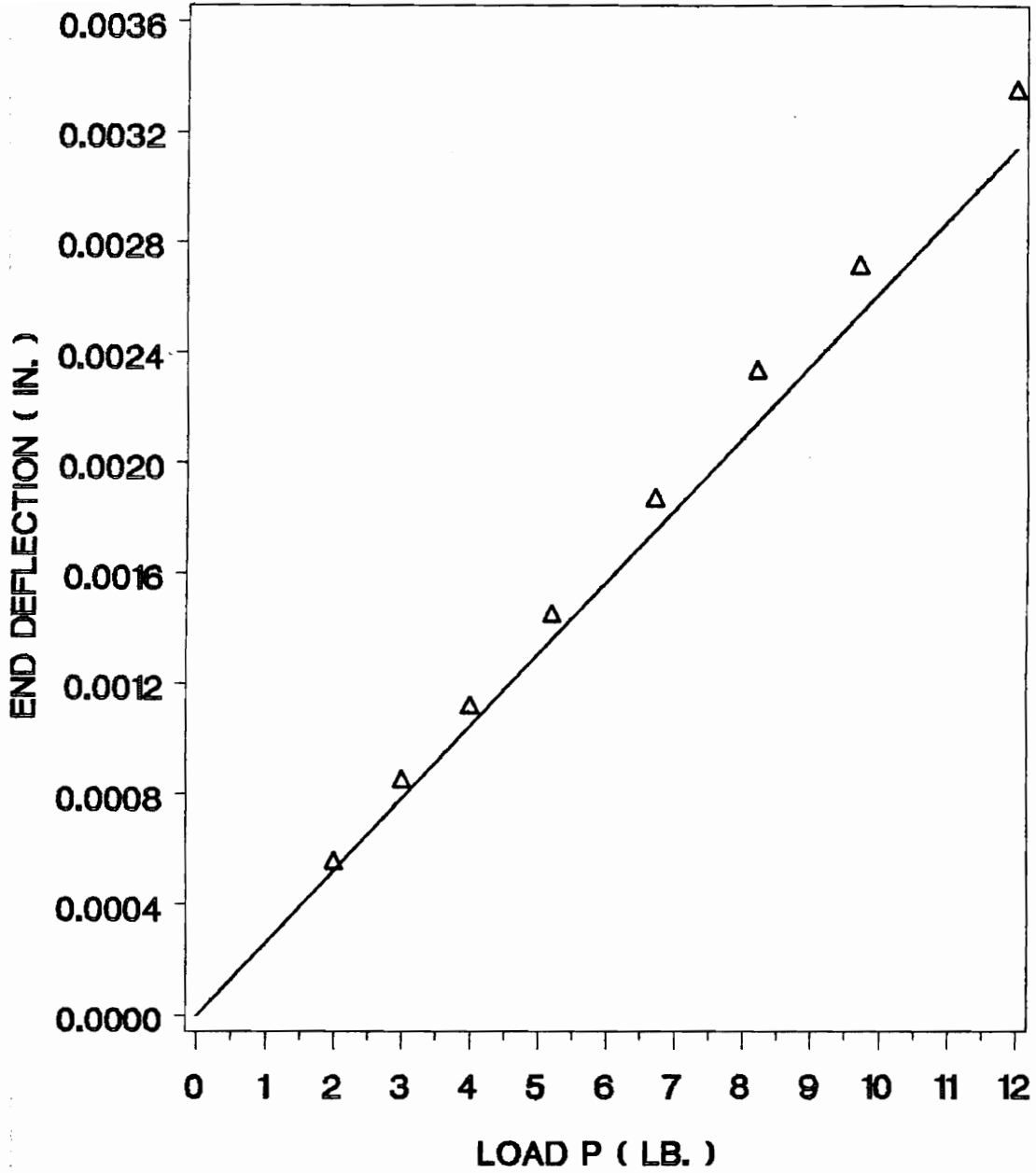


Figure 96. End deflection versus load. Specimen EAL1. Comparison of theory (solid curve) with experiments (triangles).

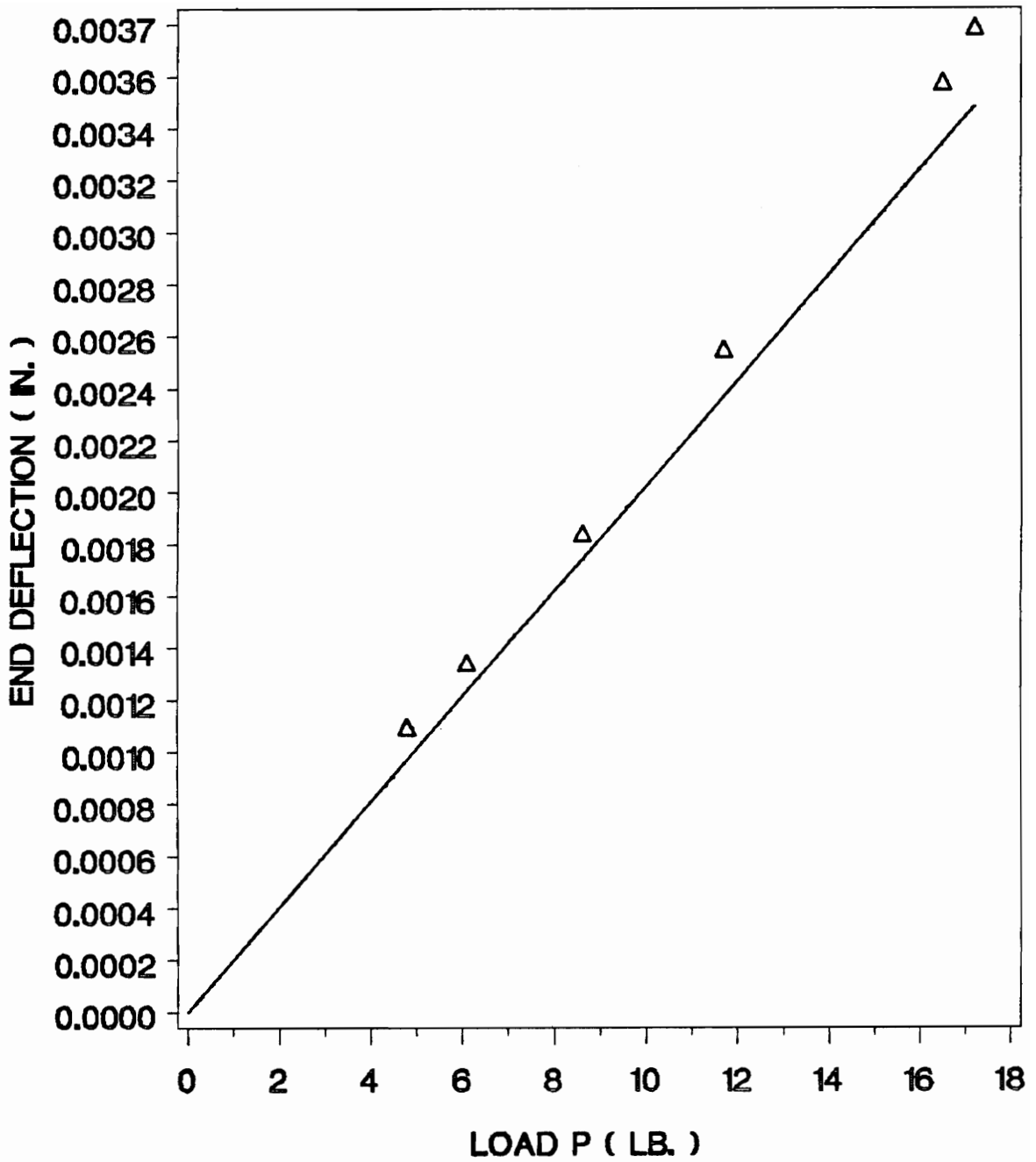


Figure 97. End deflection versus load. Specimen EAL2. Comparison of theory (solid curve) with experiments (triangles).

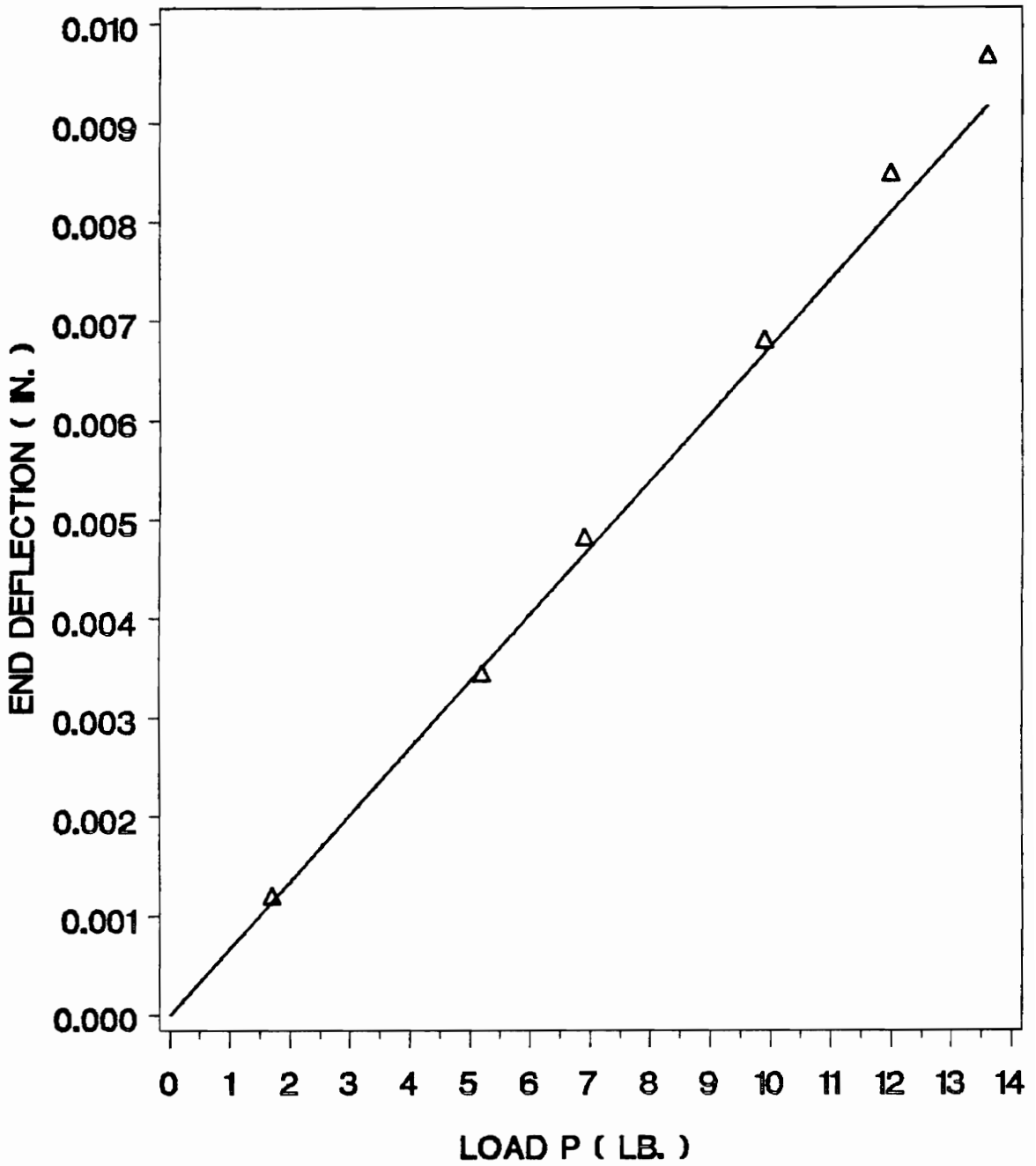


Figure 98. End deflection versus load. Specimen EAL3. Comparison of theory (solid curve) with experiments (triangles).

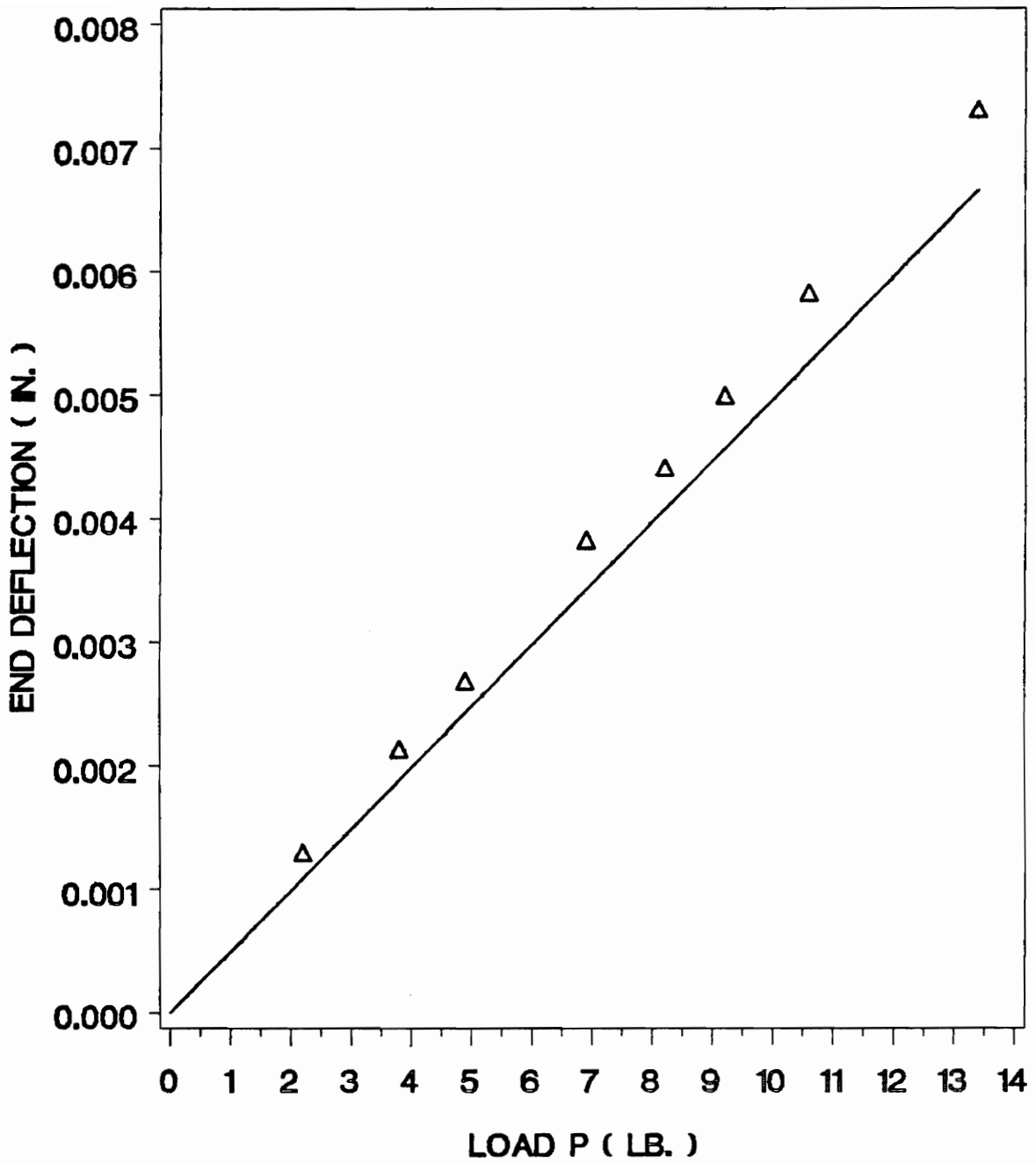


Figure 99. End deflection versus load. Specimen EAL4. Comparison of theory (solid curve) with experiments (triangles).

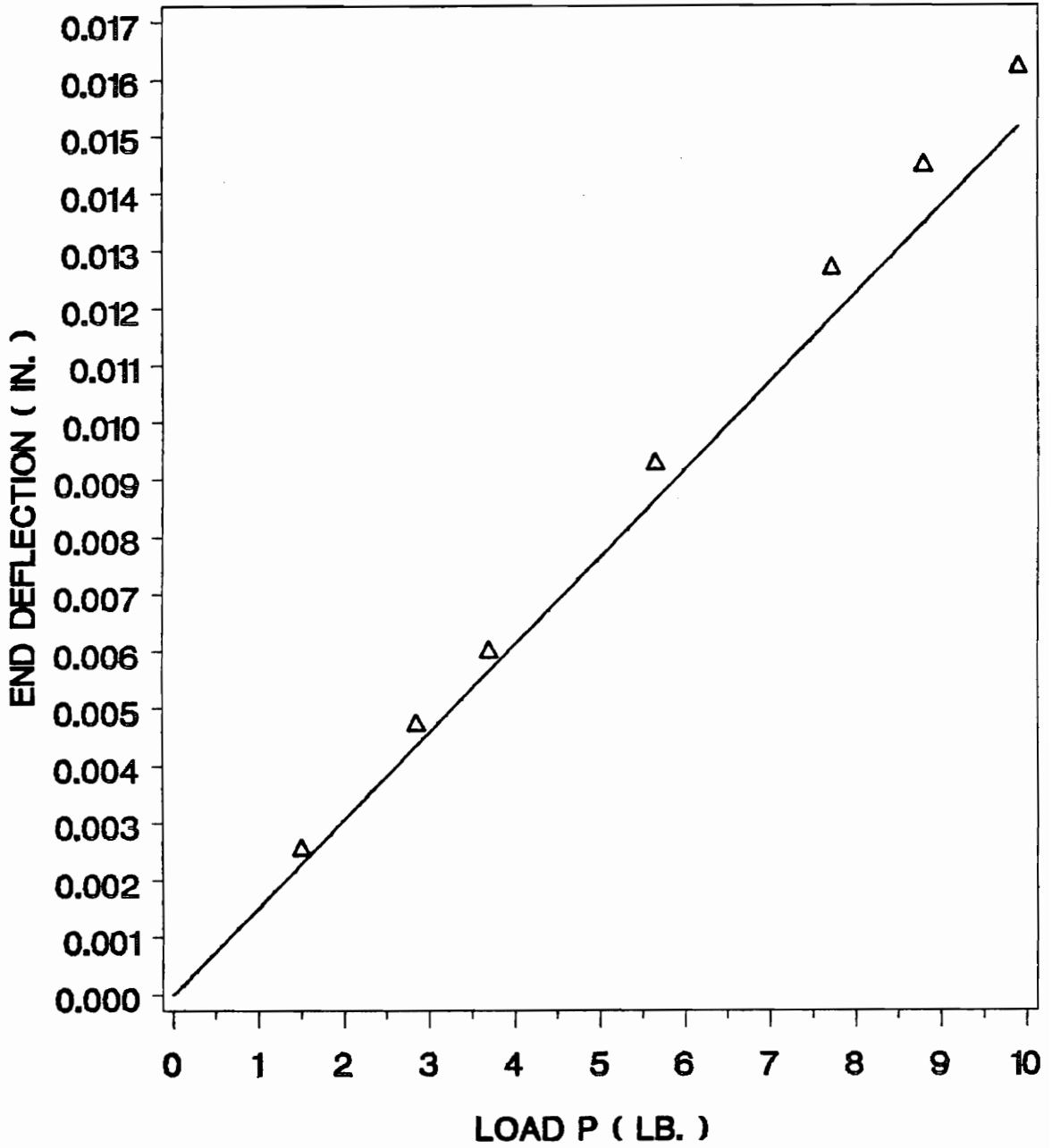


Figure 100. End deflection versus load. Specimen EAL5. Comparison of theory (solid curve) with experiments (triangles).

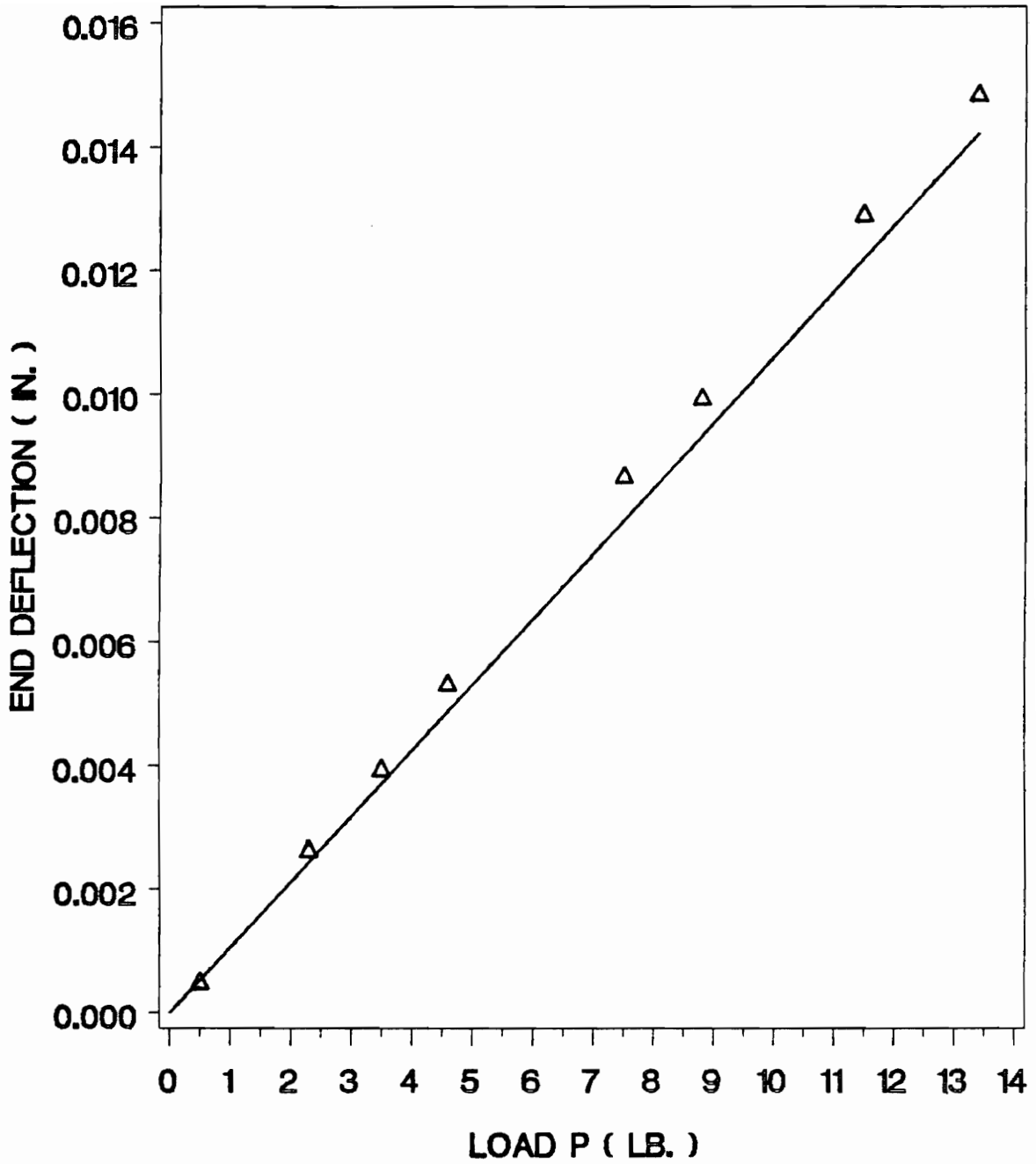


Figure 101. End deflection versus load. Specimen EAL6. Comparison of theory (solid curve) with experiments (triangles).

5.5 - DISCUSSION OF THE RESULTS

In this section, the experimental data were used to evaluate the adhesive shear modulus for each specimen tested. The results were compared to the adhesive shear moduli provided in tables 9 to 10 and the validity of the experimental data obtained from the shear deformation and the end deflection tests were discussed. The data were also used to verify the conclusions concerning the optimization of the BMC methods.

5.5.1 - Determination of the adhesive shear modulus from the shear deformation measurements

First of all, in order to derive the adhesive shear modulus from experiments, we had to evaluate the magnitude of the shear stress at the measurement location from BMC theory and by using data listed in tables 9 and 10. Then, we calculated the adhesive shear modulus as follows :

$$G_a = \frac{\tau}{\gamma_{experimental}} \quad (13a)$$

We also calculated the error generated by the evaluation of G_a in comparison with the predicted values given in tables 9 and 10. These results are presented on table 12 and one can see that the adhesive shear modulus is usually obtained with less than 10 % of error.

Another approach is now presented for the evaluation of G_a . It is based on a graphical method and its main interest consists in the verification of the conclusions developed in chapter 3. For this purpose, we plotted the variations of quantity $\gamma / (\frac{P}{Ebh})$ with increasing stiffness ratio. They are related as follows :

$$\frac{\gamma}{\frac{P}{Ebh}} = \frac{3E(1 + 2t/h)}{G_a(1 + 3(1 + 2t/h)^2)} \left(1 - \cosh \bar{\alpha} \frac{x}{\ell} + \tanh \bar{\alpha} \sinh \bar{\alpha} \frac{x}{\ell} \right) \quad (25)$$

Table 12. Comparison between experiments and theory for the calculation of the adhesive shear modulus from shear deformation measurements (P = 10 Lb.).

specimen code	theory		experiments		error on G_a %
	G_a (Psi)	$\gamma^{(1)}$ (in./in.)	$G_a^{(2)}$ (Psi)	γ (in./in.)	
RB1	130	0.0173	123	0.0182	5
RB2	130	0.0259	120	0.0281	7
RB3	130	0.0521	118	0.0576	9
RB4	130	0.0447	127	0.0458	2
RB5	130	0.0866	133	0.0847	2
RB6	130	0.0497	127	0.0596	2
RB7	130	0.0825	147	0.0727	13
ARB1	130	0.0841	129	0.0846	1
ARB2	130	0.1378	125	0.1402	4
ARB3	130	0.0826	126	0.0856	3
ARB4	130	0.1369	123	0.1442	5

$$\gamma_{theoretical}^{(1)} = \frac{\tau}{G_a}$$

$$G_a^{(2)} = \frac{\tau}{\gamma_{experimental}}$$

where the dimensionless measurement location x/ℓ is input as an experimental data.

The proper experimental value of the shear strain is indicated by an horizontal line on the strain-stiffness curve. The intersection between the horizontal line and the theoretical curve gives the corresponding stiffness ratio E/G_a . The adhesive shear modulus is calculated from the stiffness ratio and the value which is found is the estimate of the adhesive shear modulus obtained from the BMC test procedure. It can be compared with the value of the shear modulus provided in tables 9 and 10 and which have been referred as the adhesive shear modulus predicted prior to the test. Such an analysis has been conducted for every specimen tested to obtain shear strain data. The results are presented on fig.102 to 107. It is then important to notice that for rubber-to-steel specimens, for which E/G_a is 2.3×10^5 , the method is not appropriate to calculate the adhesive shear modulus because the experimental data mostly coincide with the upper horizontal plateau of the curve. Therefore, more than a unique value of the stiffness ratio can match. However, for the longest and thinnest beams, the linear part of the curve covers a larger range of stiffness ratios so that very good agreement is found between experiments and theory. For rubber-to-aluminum specimens, the stiffness ratio is smaller : $E/G_a = 7.8 \times 10^4$. The experimental data match with the theoretical input in an intermediate region located between the linear zone and the plateau. In this region, the shear stress is sensitive to the beam material properties (chapter 3) and cannot be calculated easily using equation 12a. In order to evaluate the adhesive shear modulus, the method is then to use a graphical representation of the results. However, if the BMC specimen geometry is not defined properly prior to the test, the experimental data might lies within the constant zone of the strain-stiffness curve where it is not possible to get an accurate determination of the adhesive shear modulus.

In addition, on each curve we plotted the variation of the maximum shear strain (dashed line curves), provided by the BMC theory as follows :

$$\frac{\gamma^{\max}}{\frac{P}{Ebh}} = \frac{E}{G_a \gamma^2 (1 + 2t/h)} \left(1 - \frac{1}{\cosh \bar{\alpha}} \right) \quad (26)$$

where x/ℓ was set to unity.

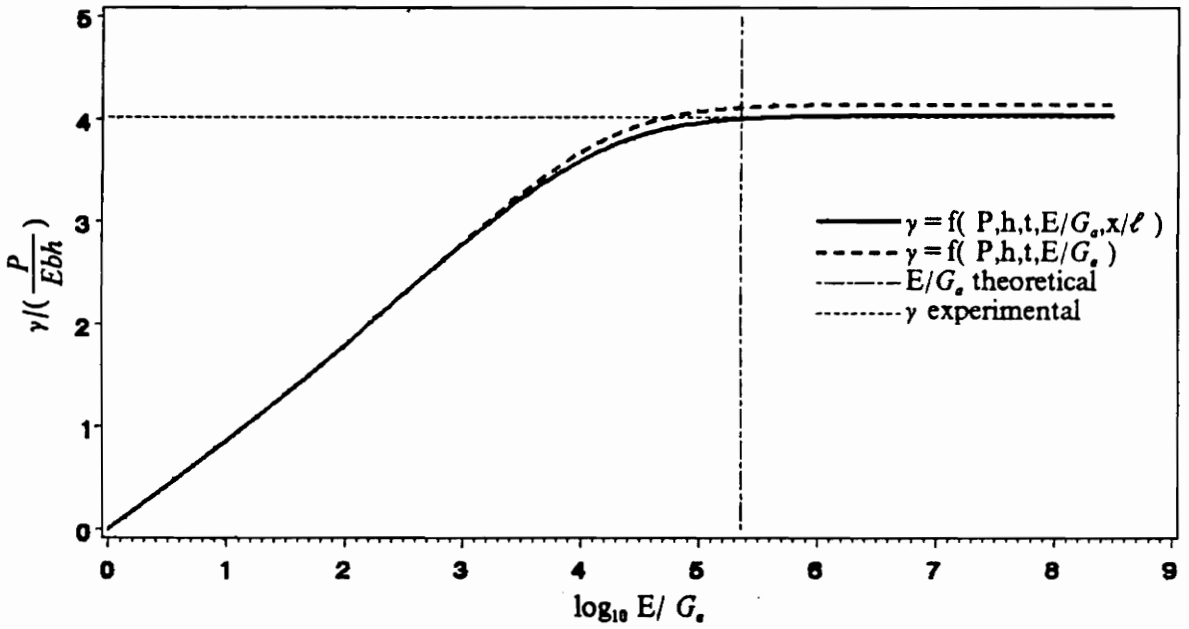
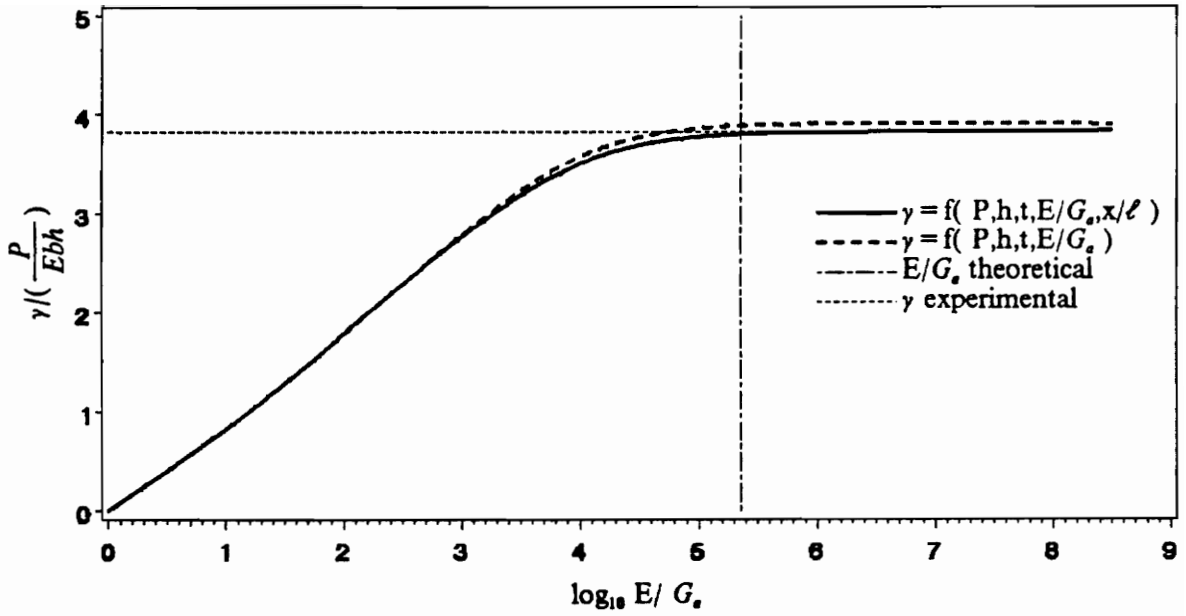


Figure 102. Shear strain versus stiffness ratio. Graphical comparison between theory and experiments. Top : specimen RB1. Bottom : specimen RB2.

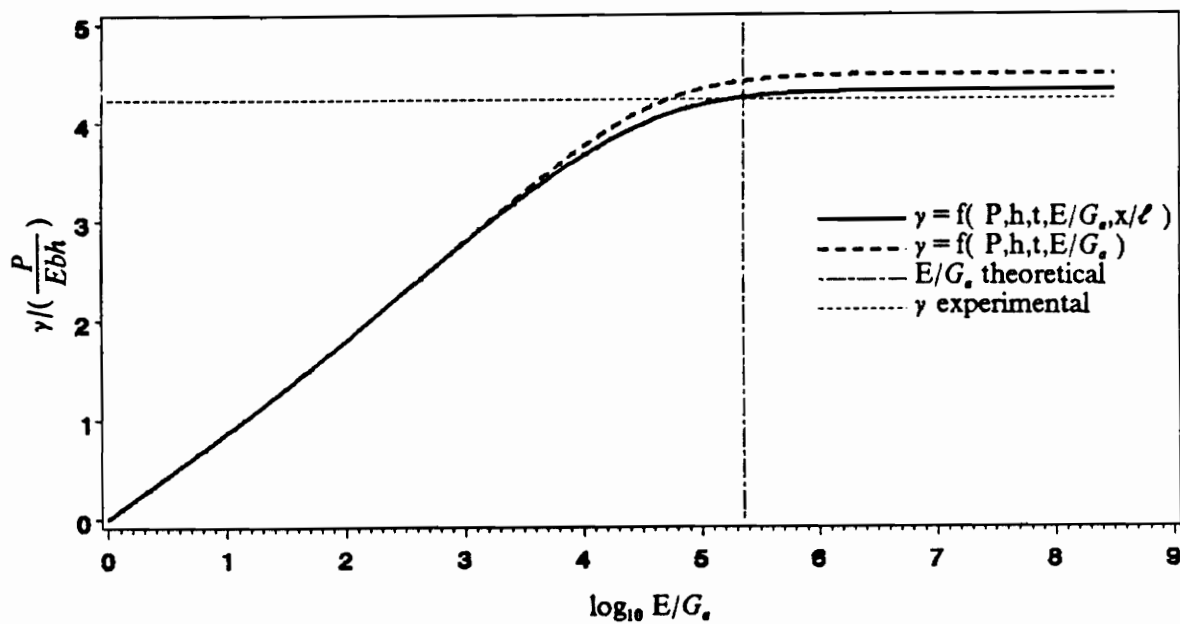
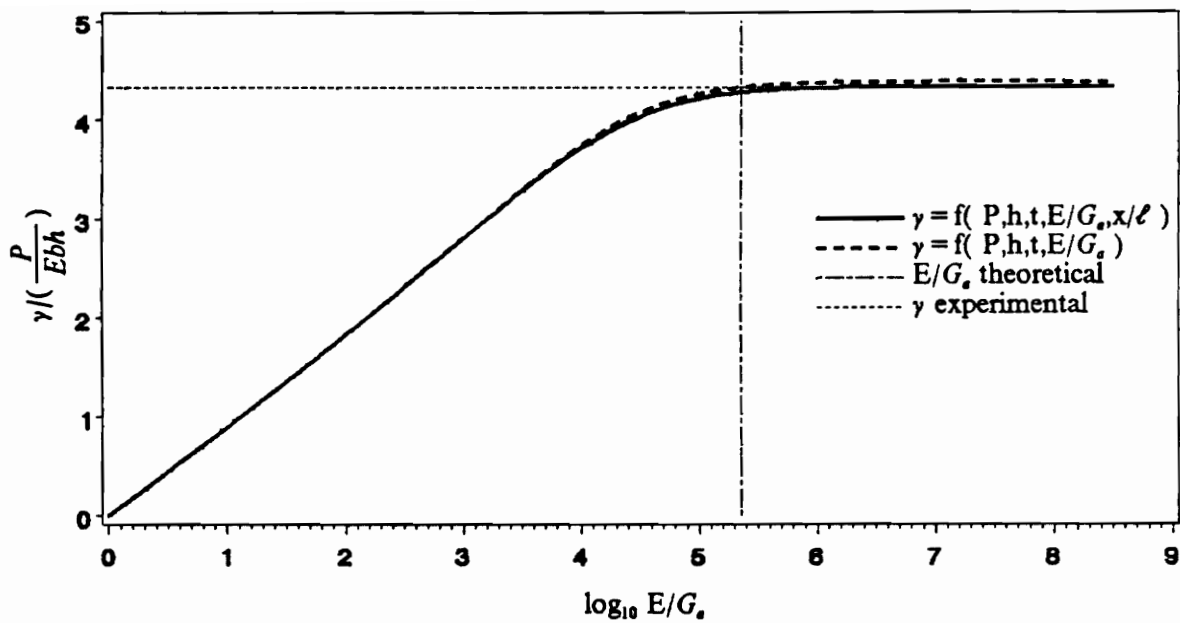


Figure 103. Shear strain versus stiffness ratio. Graphical comparison between theory and experiments. Top : specimen RB3. Bottom : specimen RB4.

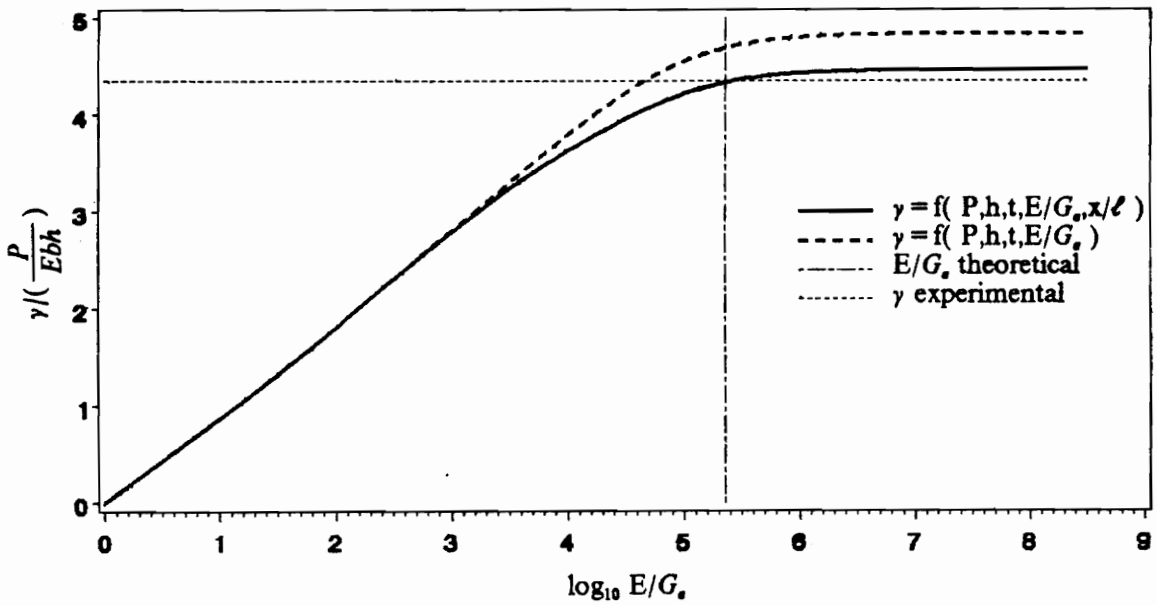
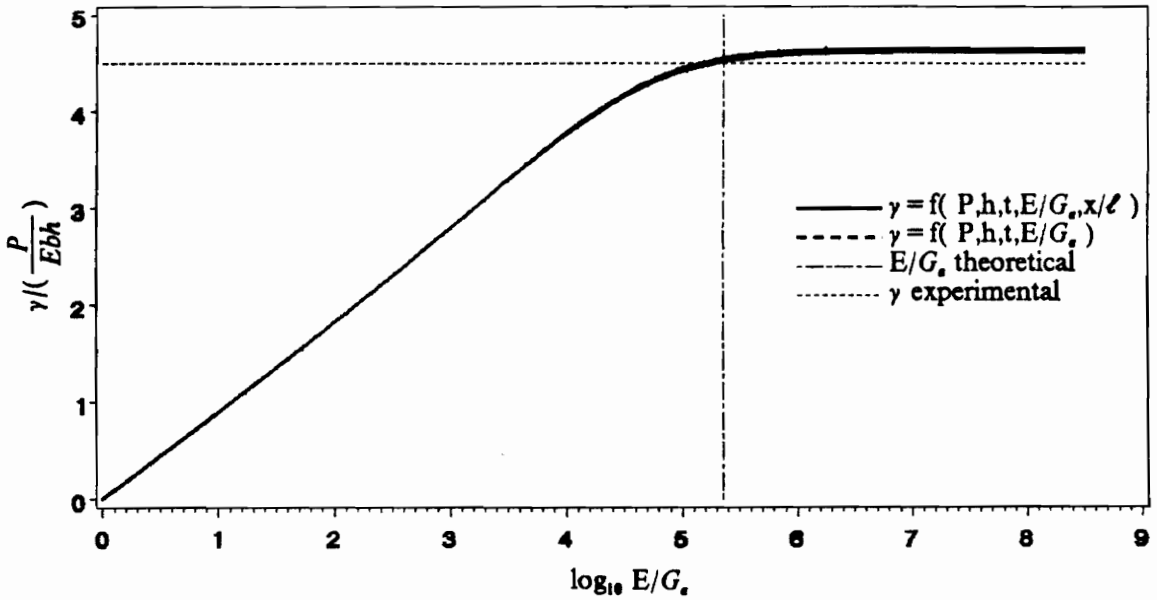


Figure 104. Shear strain versus stiffness ratio. Graphical comparison between theory and experiments. Top : specimen RB5. Bottom : specimen RB6.

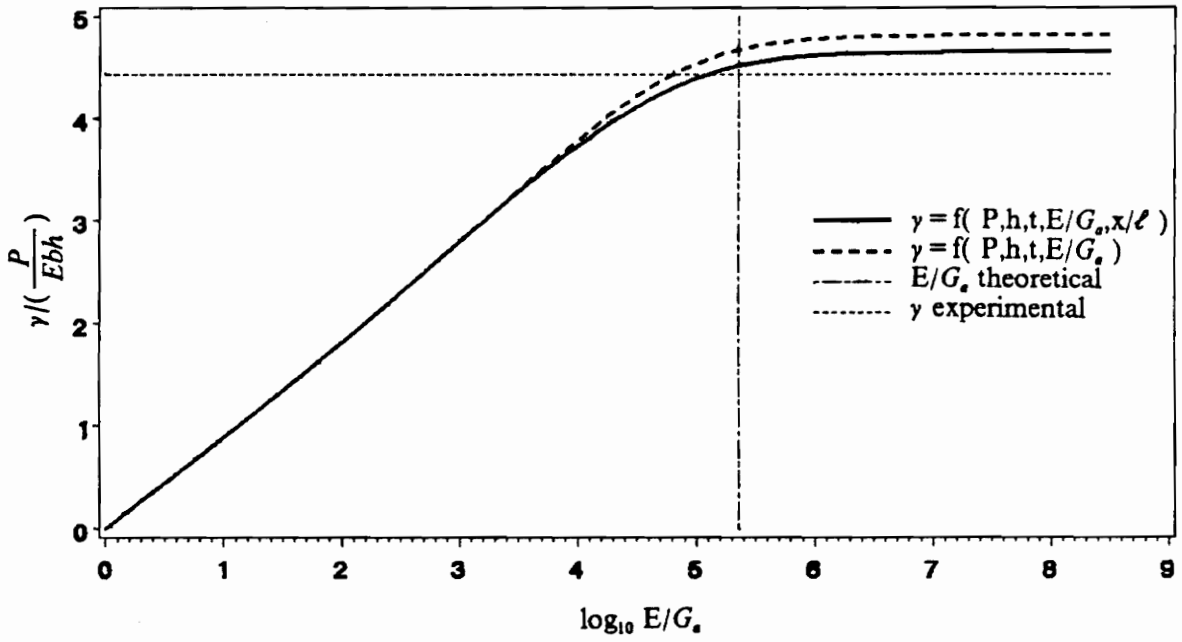


Figure 105. Shear strain versus stiffness ratio. Graphical comparison between theory and experiments for specimen RB7.

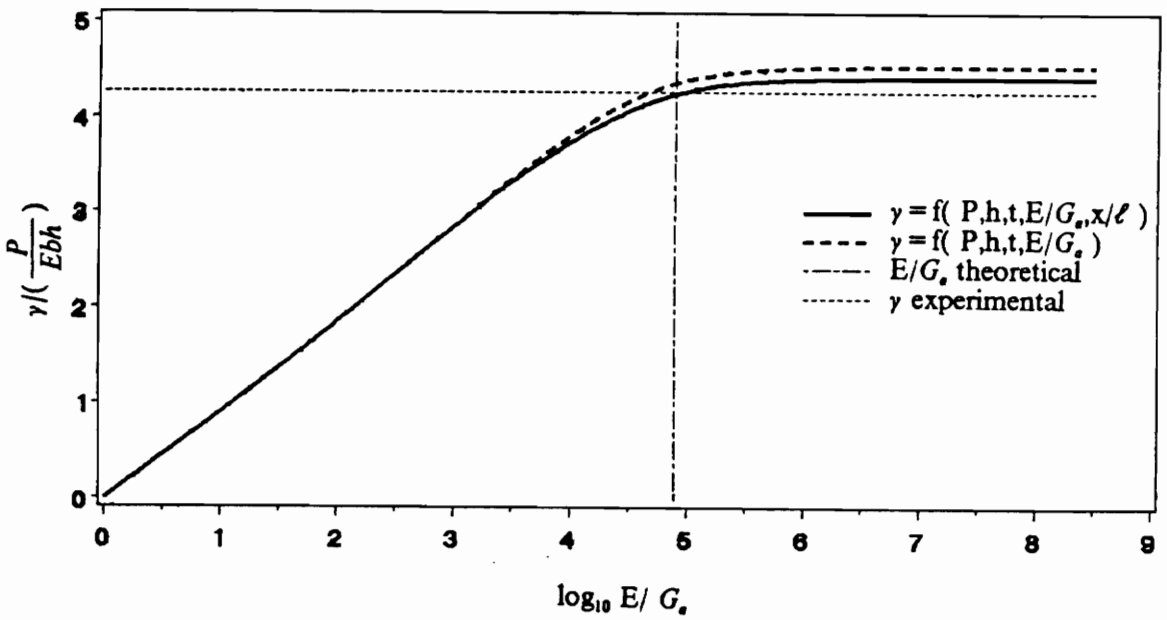
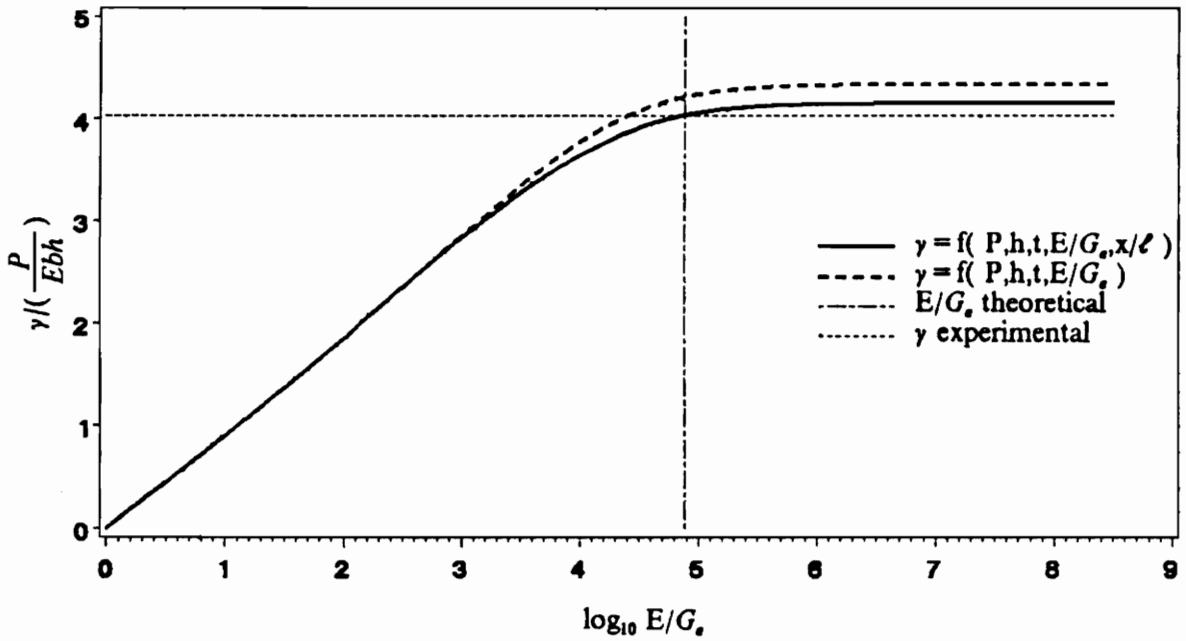


Figure 106. Shear strain versus stiffness ratio. Graphical comparison between theory and experiments. Top : specimen ARB1. Bottom : specimen ARB2.

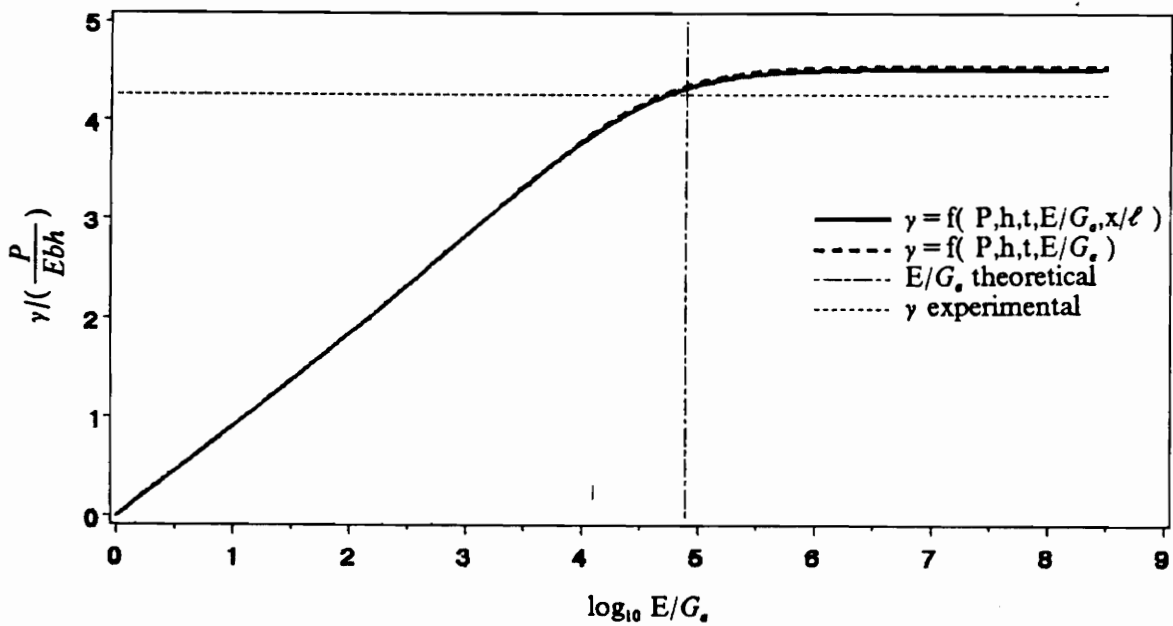
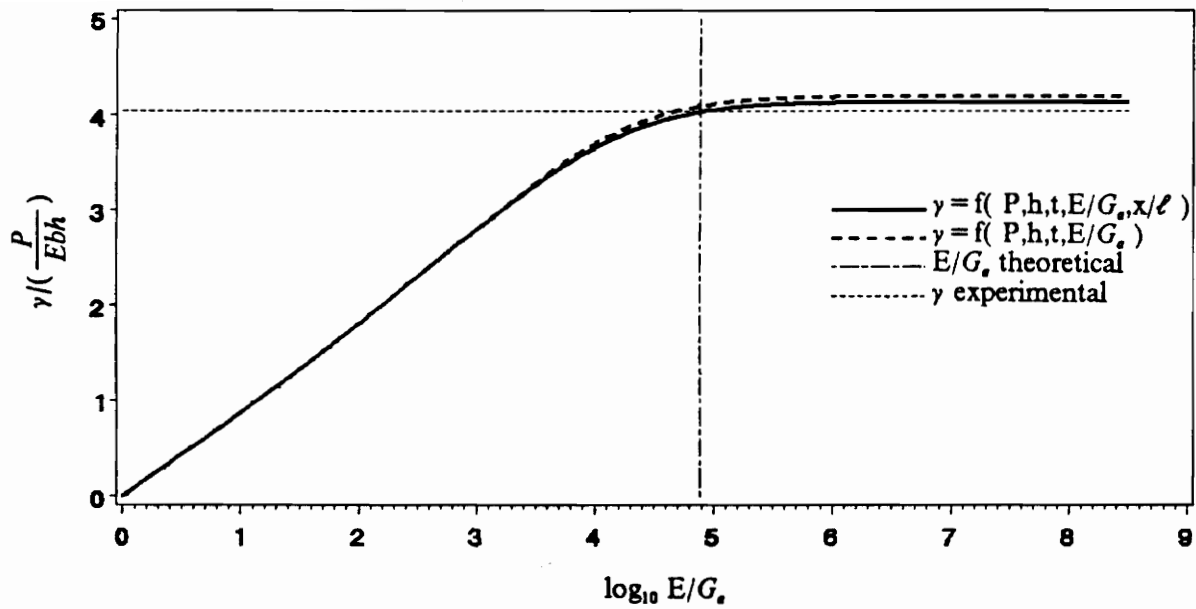


Figure 107. Shear strain versus stiffness ratio. Graphical comparison between theory and experiments. Top : specimen ARB3. Bottom : specimen ARB4.

In the case of the maximum strain versus the stiffness ratio curve, the linear variation indicates that the shear stress is only a function of loading and geometry whereas it becomes dependent on material properties if E/G_a increases. The projection of the experimental data on those curves clearly indicates that it would provide erroneous results for the stiffness ratio if the definition of γ_{xy}^{\max} was used.

The only location where the variation of the maximum shear strain could coincide with that of the strain calculated at a particular measurement location, is the linear part of the curve. It is accessible for the BMC beams whose stiffness ratio is below 10^3 but the linear shear strain zone can lie over a larger range of stiffness ratio by making the beam longer and by making the adhesive thinner. For the beams whose stiffness ratio varies linearly with the shear strain, the test is very easy because we have discussed in chapter 3 that in that situation, the shear stress can be calculated directly from the beam geometry and the loading alone. In other words, as the shear strain is determined by the experiments and because the shear stress is known, the adhesive shear modulus is computed simply as the ratio of the shear stress by the shear strain. For large specimen stiffness ratio, a long and inconvenient procedure is necessary to evaluate the adhesive shear modulus. However, the procedure does not even guarantee the accuracy of the final result, specially if prior to testing, an analysis aimed at the definition of the beam geometry has not been done. This is clearly illustrated by the contents of this section.

Hence, when we were able to calculate the adhesive shear modulus, we found a good agreement between theory and experiments. Moreover, the conclusions obtained from the optimization of the BMC shear deformation method were confirmed.

5.5.2 - Evaluation of the adhesive shear modulus from the end deflection measurements

To determine the adhesive shear modulus from the end deflection, it is recommended to use a graphical method. It consists in drawing the variation of the dimensionless end deflection "beta" versus the stiffness ratio according to the geometry of the specimen tested. The computer routine mentioned in section 3.3.2 and presented in appendix A has been written for this purpose. Then, one has to report the experimental value of beta on the β versus E/G_a curve to deduce the corresponding stiffness ratio.

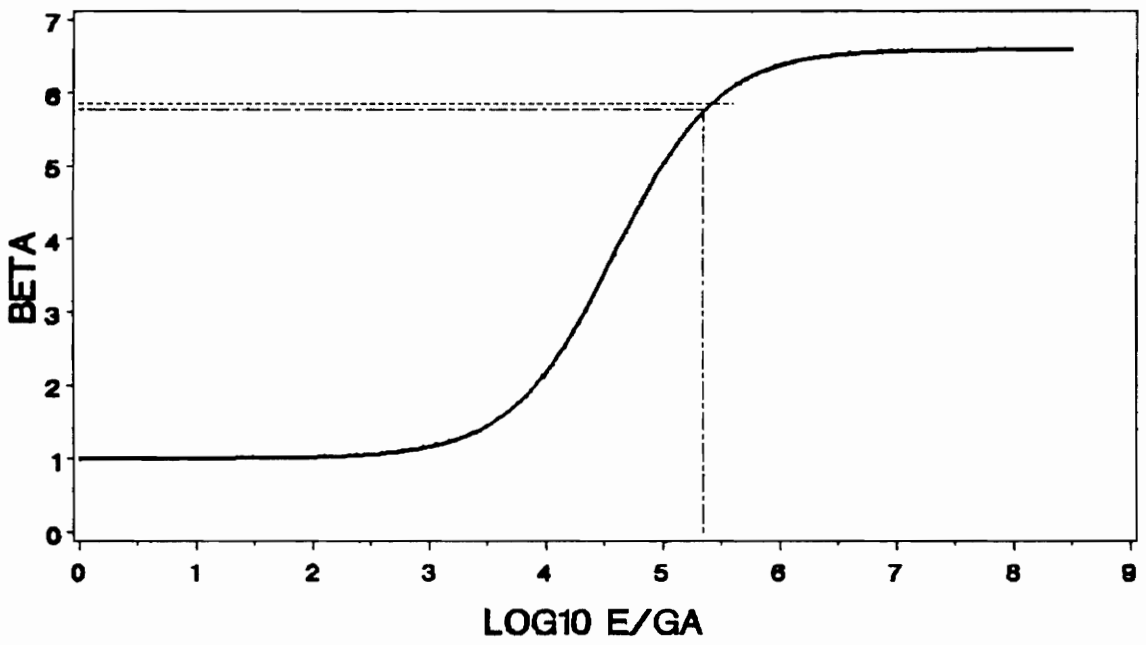
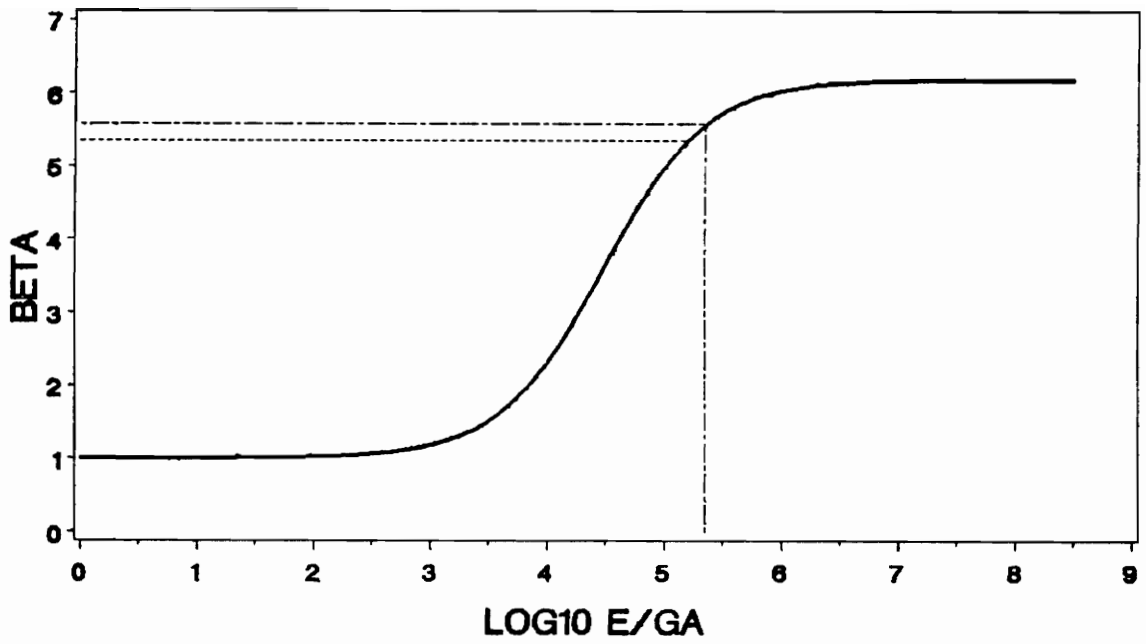
Table 13 presents the experimental results. A comparison with analytical predictions is also shown. The curves from which these data are deduced are depicted in fig.108 to 115. One can note that the results for β agree very well with theory but the error generated for the calculation of E/G_a is larger, depending on the slope of curve (β vs. E/G_a).

For rubber-to-steel and rubber-to-aluminum specimens, the fast increasing middle zone of the beta variations covers the range of stiffness ratios investigated. Therefore, results are obtained with a lot of confidence. However, the epoxy-to-aluminum specimens for which E/G_a is about 100, show that even for the shorter beams, the disparity between experiments and theory is large. The reason is that the method based on parameter β is not appropriate for stiff combinations of adherend and adhesive. For these beams, β lies in a region where it is not sensitive to the variation of the stiffness ratio.

Hence, the BMC test method based on the measurement of the beam end deflection works well with large stiffness ratios but it is limited in the case of the small ratios, even when acting on the specimen geometry. This comes to reinforce the conclusions provided from the optimization of the BMC theory.

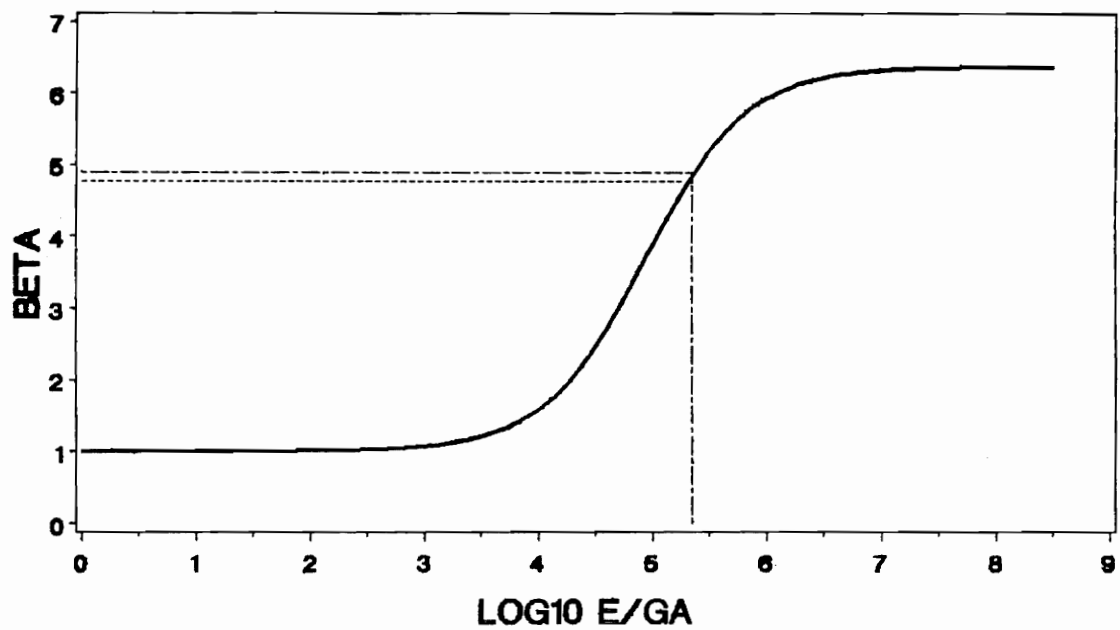
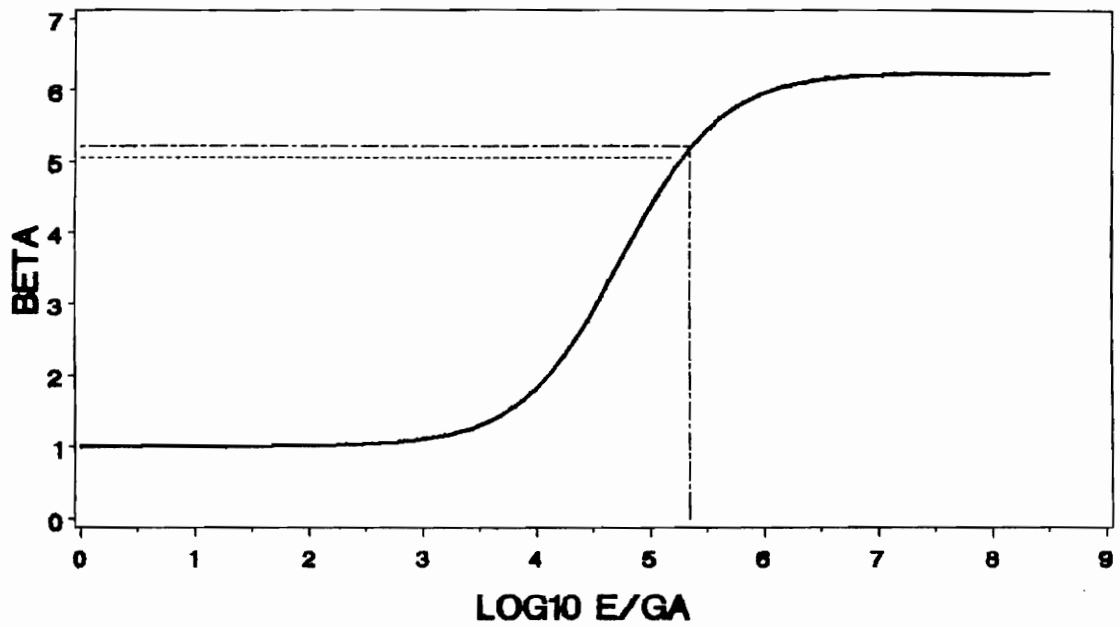
Table 13. Comparison between experiments and theory for the calculation of the adhesive shear modulus from the end deflection measurements.

specimen code	theory		experiments		error %	
	E/G_a	β	E/G_a	β	E/G_a	β
RB3	2.3×10^5	5.57	1.6×10^5	5.35	28	4
RB4	2.3×10^5	5.78	2.6×10^5	5.86	12	1
RB5	2.3×10^5	5.21	1.8×10^5	5.04	20	3
RB6	2.3×10^5	4.89	2.1×10^5	4.77	6	2
RB7	2.3×10^5	5.11	1.9×10^5	4.92	17	4
ARB1	7.8×10^4	3.87	1.0×10^5	4.03	28	4
ARB2	7.8×10^4	3.56	7.4×10^4	3.52	5	1
ARB3	7.8×10^4	5.24	7.0×10^4	5.10	9	3
ARB4	7.8×10^4	3.80	7.3×10^4	3.72	6	2
EAL1	85	1.11	108	1.19	27	8
EAL2	85	1.23	106	1.35	25	10
EAL3	85	1.06	110	1.12	29	7
EAL4	85	1.12	110	1.23	29	7
EAL5	85	1.03	123	1.10	45	5
EAL6	85	1.07	103	1.12	21	5



- - - - - theory
 - - - - - experimental

Figure 108. Dimensionless end deflection versus stiffness ratio - graphical comparison between theory and experiments - top : specimen RB3 - bottom : specimen RB4



- - - - - theory
 - - - - - experimental

Figure 109. Dimensionless end deflection versus stiffness ratio - graphical comparison between theory and experiments - top : specimen RB5 - bottom : specimen RB6

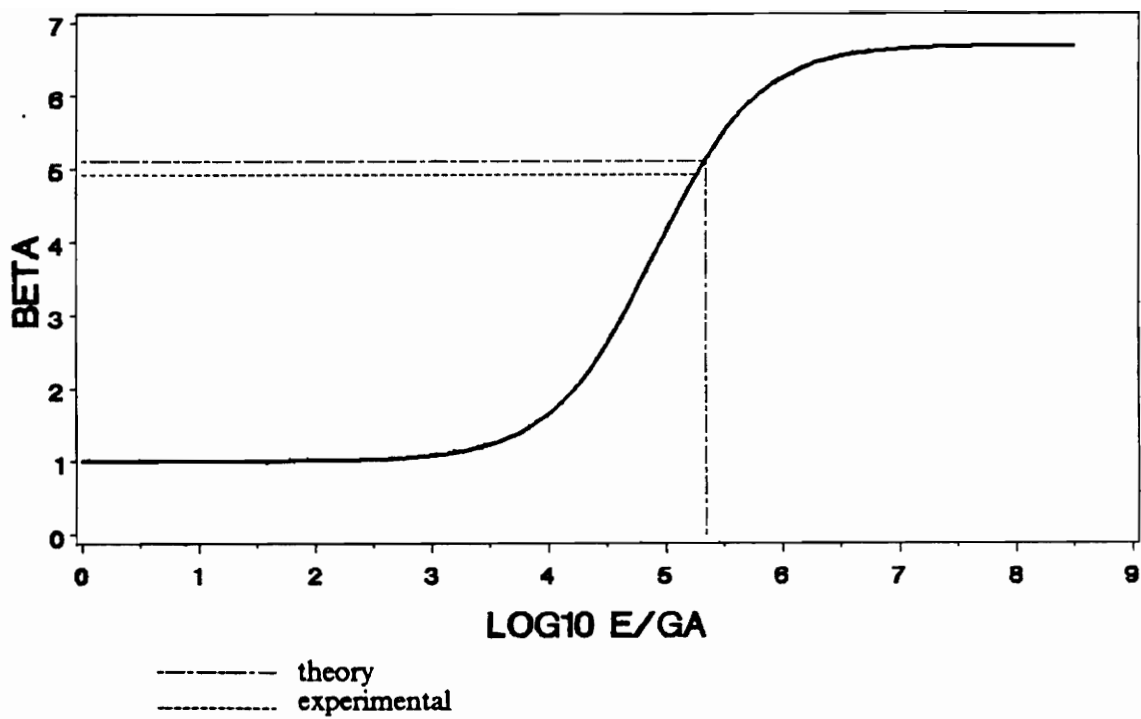
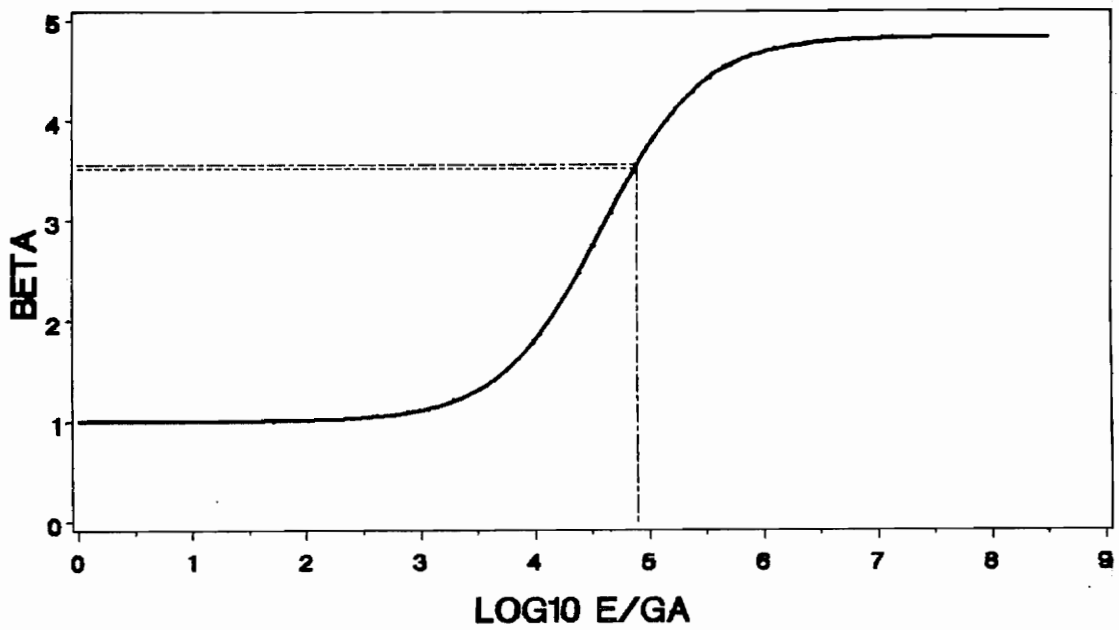
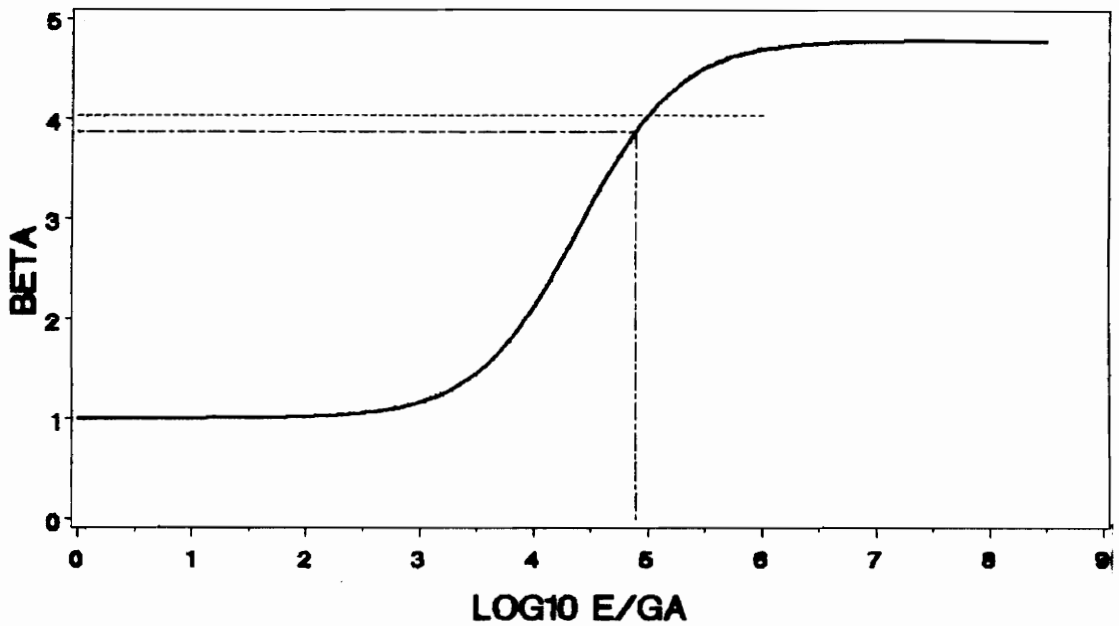
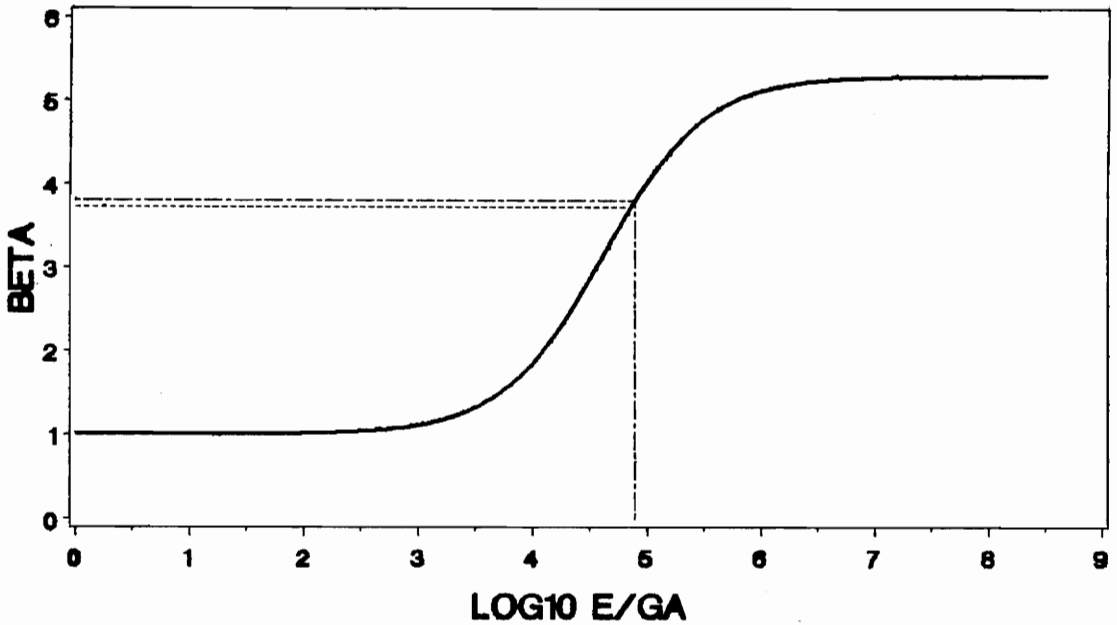
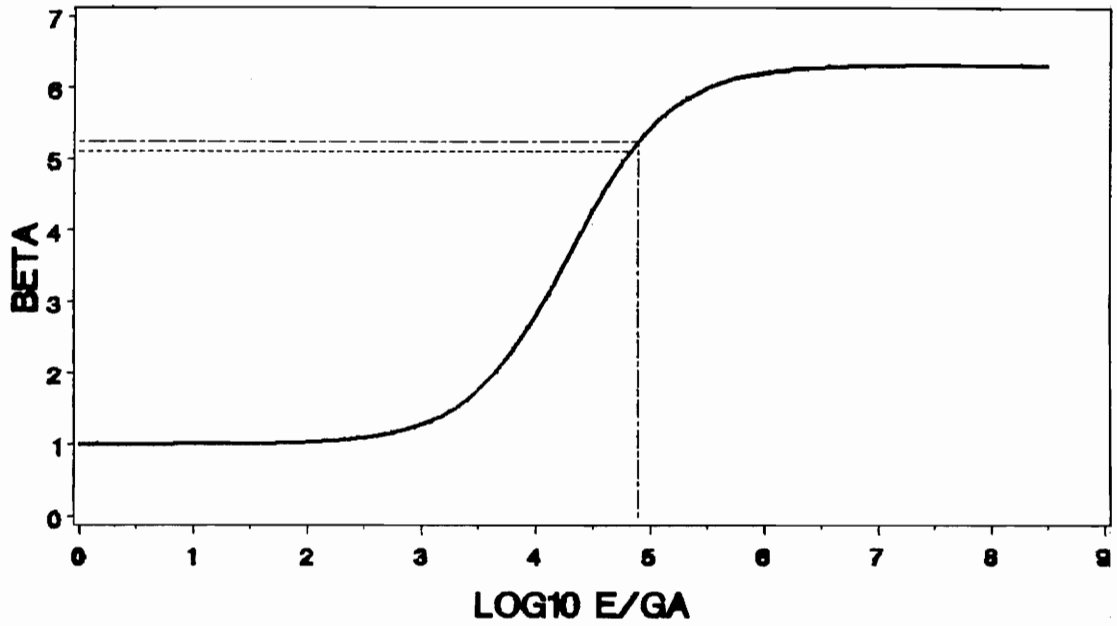


Figure 110. Dimensionless end deflection versus stiffness ratio. Graphical comparison between theory and experiments for specimen RB7.



- - - - - theory
 - - - - - experimental

Figure 111. Dimensionless end deflection versus stiffness ratio - graphical comparison between theory and experiments - top : specimen ARB1 - bottom : specimen ARB2



----- theory
 - - - - - experimental

Figure 112. Dimensionless end deflection versus stiffness ratio - graphical comparison between theory and experiments - top : specimen ARB3 - bottom : specimen ARB4

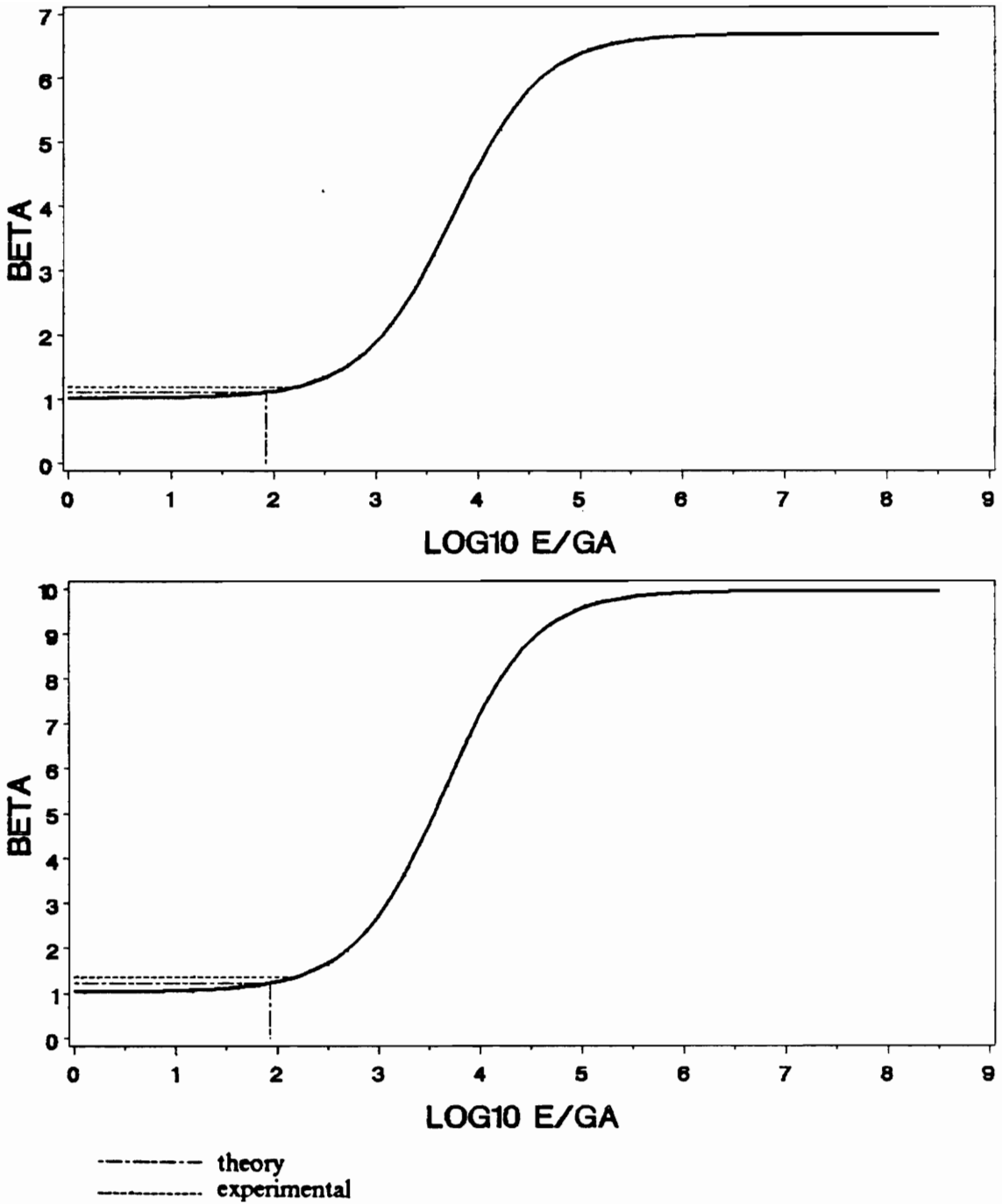
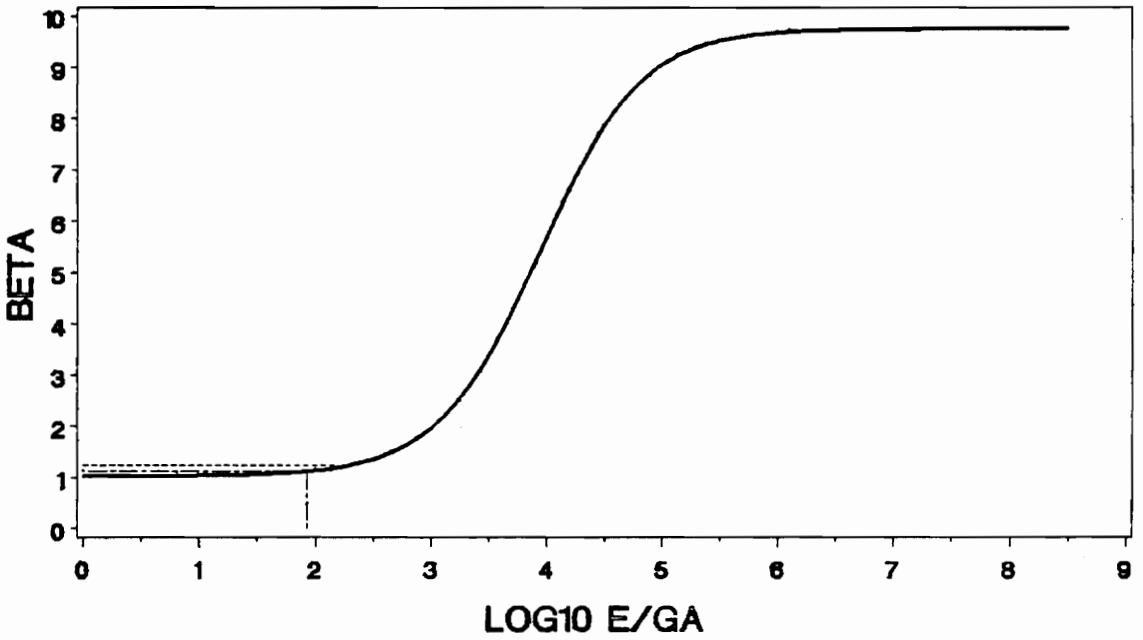
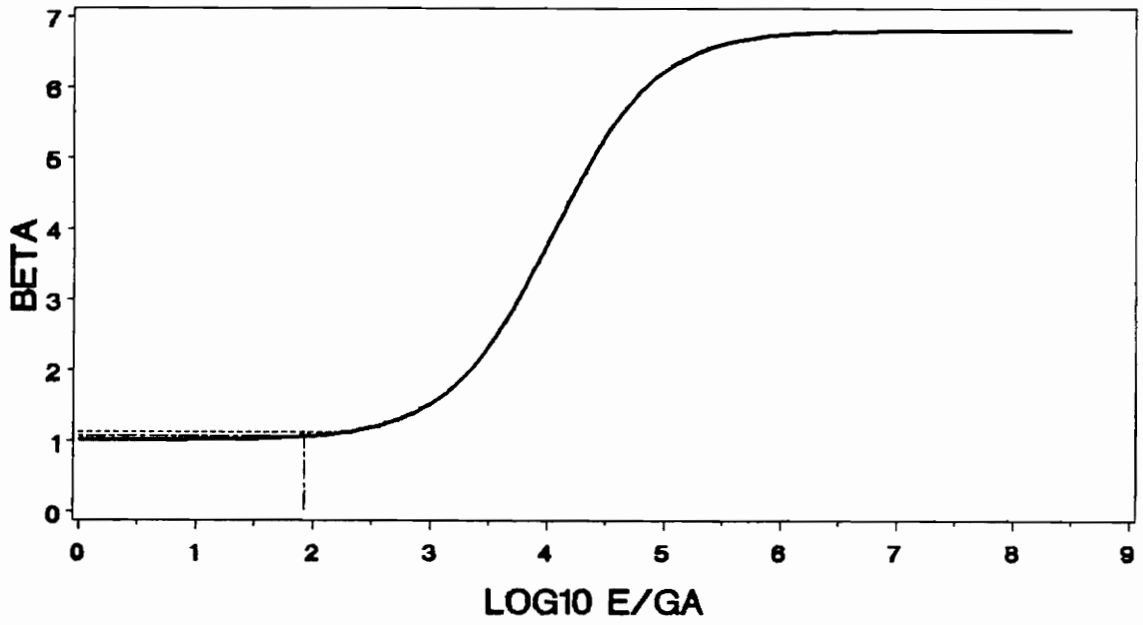


Figure 113. Dimensionless end deflection versus stiffness ratio - graphical comparison between theory and experiments - top : specimen EAL1 - bottom : specimen EAL2



- - - - - theory
 - - - - - experimental

Figure 114. Dimensionless end deflection versus stiffness ratio - graphical comparison between theory and experiments - top : specimen EAL3 - bottom : specimen EAL4

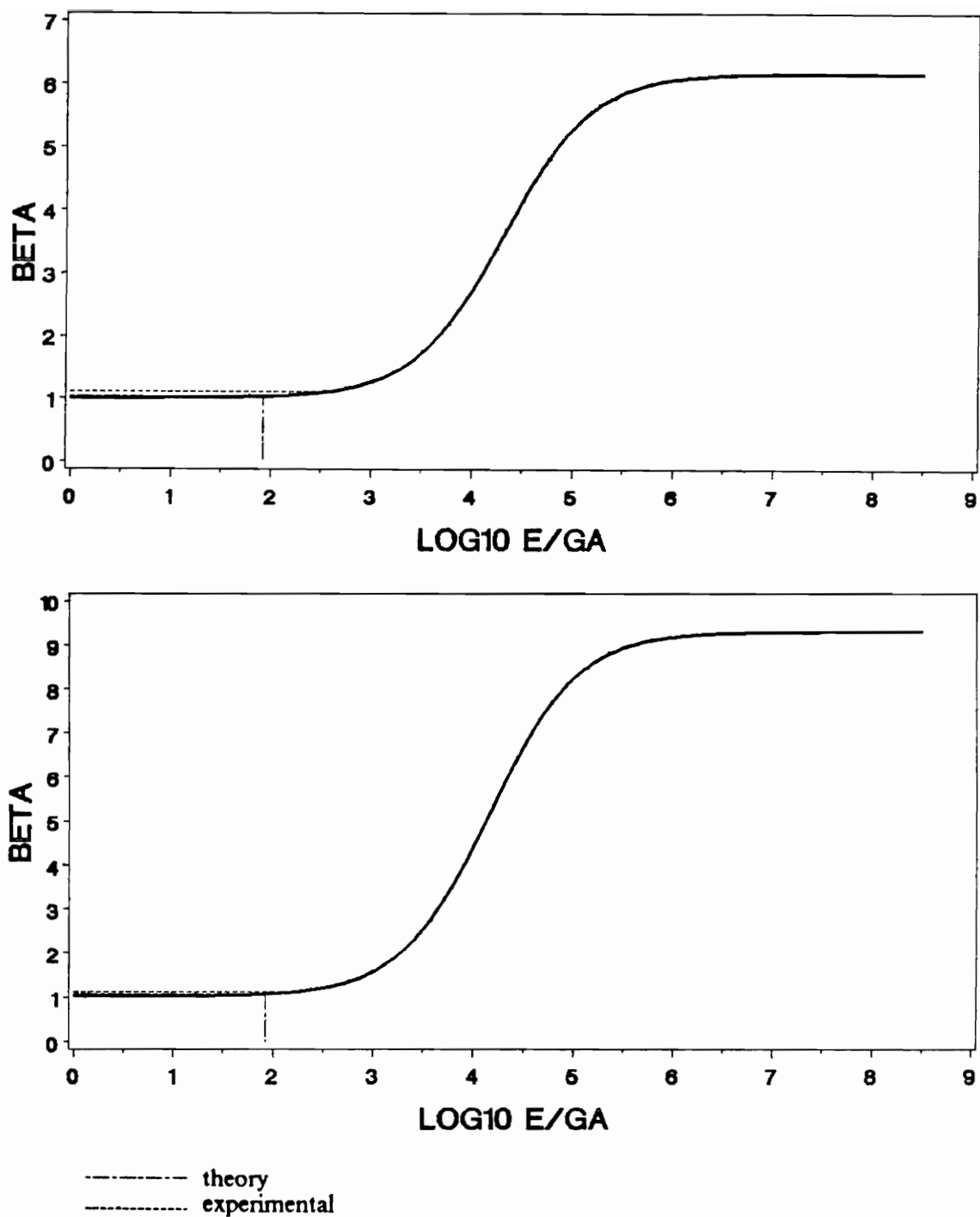


Figure 115. Dimensionless end deflection versus stiffness ratio - graphical comparison between theory and experiments - top : specimen EAL5 - bottom : specimen EAL6

6 - CONCLUSION AND RECOMMENDATIONS

In conclusion to the present report, we recall that the analysis of the BMC theory has been oriented towards three directions :

- a parametric analysis in order to study the capability of the BMC theory to provide adequate shear data on structural adhesives via relatively simple and reliable test,
- a numerical analysis developed in two and three dimensions in order to check the validity of the shear stress and the beam deflection equations from the BMC theory as well as to check the validity of the pure shear stress assumption in the adhesive layer with constant regards to practical purposes,
- an experimental study.

PARAMETRIC ANALYSIS :

Starting from the general concepts of the BMC theory, two tests of different nature were derived. These are referred as the BMC shear deformation tests and the BMC end deflection test. The parametric analysis based on the shear stress and the end deflection concepts revealed the BMC

specimen dimensions required for reliable adhesive shear property determination. Procedures and recommendations were provided to design the BMC specimen in order to calculate the adhesive stiffness and in order to make reproducible tests.

As a result from the parametric study, in the case of the BMC shear deformation test, the shear stress can be calculated easily from loading and geometry alone but only if the adhesive stiffness investigated is relatively high which requires that the stiffness ratio should not exceed 10^3 . A unique specimen geometry was proposed to characterize relatively stiff adhesives from the lecture of the shear deformation inside the bond in conjunction with the analytically predicted shear stress. A simple pure shear test with a constant shear stress inside almost the entire the bondline was also presented.

It also resulted from the parametric analysis that the characterization of the joint shear stiffness with the end deflection concept can be made only if the value of the stiffness ratio E/G_a investigated lies in the zone where the end deflection increases the most rapidly with this ratio. This condition is highly dependent on the choice of the specimen geometry.

NUMERICAL ANALYSIS :

Solutions for shear stress and for beam deflection derived from the BMC theory were compared with the Finite Element codes NOVA in plane stress and VISTA to pursue the numerical evaluation started in reference [6] which motivated the realization of the present study. The use of VISTA required to extend the BMC theory in the plane strain situation to make possible a complete comparison between numerical and analytical results. Very good agreements were found in any case of material properties and specimen geometries which constitutes a validation of the theory. Numerical analysis provided a better understanding about the stress state existing in the adhesive layer and about the conditions required for a pure shear state. Tensile stresses σ_x and σ_y do exist in the adhesive layer whose magnitudes increase with the adhesive thickness and/or stiffness. Three-dimensional analysis with the program ABAQUS showed the presence of stress concentration at the adherend/adhesive interface and both the two-dimensional and the three-dimensional

studies revealed that the magnitudes of the tensile stresses are negligible in comparison to that of the shear stress. In addition, tensile stresses do not modify the state of shear because Finite Element showed that in the cases investigated, good agreements were obtained for the shear stress distribution between theory and numerical results. In other words, the negligible magnitudes of tensile stresses confirm that the BMC specimen configuration produces a shear stress state in the adhesive layer and, the good agreement between numerical and analytical approaches constitutes a validation of the bonded cantilever beam concept as a shear test. Using VISTA, a modified BMC specimen was proposed in order to increase the deformations of stiff beams. Tensile and shear stresses peaks occurred at the adhesive ends, with axial and peel stresses concentrations at the adherend/adhesive interface, especially close to the loaded end. By comparing the stress magnitudes, stress analysis showed that in the major part of the joint, the state of stress is pure shear, uniform over the thickness and with an increasing magnitude in the x direction. These numerical results are confirmed in a recent work by K.M. Liechti which is presented in reference [21]. Finally, the fact that the shear strain increases from 20 % up to 100 % from that of the classic beam when the length of the adhesive layer is reduced between the adherends is especially appealing for experimental purpose and should be considered as a recommendation for future work.

EXPERIMENTAL ANALYSIS :

The last part of our work consisted in the experimental application and verification of the theoretical concepts. For that purpose, shear deformation and end deflection measurements were performed on BMC-method-shaped specimens which permitted to compare the experimental results to the analytical predictions. Most of the time with the shear deformation method, the adhesive shear modulus is determined with an accuracy not exceeding 10 % which satisfies the requirements for engineering errors. The evaluation of the adhesive shear modulus from the shear deformation test data required the use of a long numerical procedure because in the cases investigated, the shear stress could not be derived directly from geometry and loading alone as suggested in the parametric analysis. The use of the simplest form of the shear stress equation which does not

depend on adhesive mechanical properties was discussed and graphs showed the error generated in finding the value of the shear stiffness when the BMC theory is not used properly. Also, the development of shear deformation measurement with the Krieger gage was limited especially for stiff adhesives. We found that the shear deformation test would necessitate the development of a special deformation measurement instrumentation. The device should satisfactorily monitor the relative displacement between the adherends without being constrained by their bending.

The method based on the end deflection test is easy to perform and tests on specimens of low deformability such as epoxy-to-aluminum, revealed the importance of keeping the boundary conditions for loading similar to those used in the BMC theory. In addition, the calculation of the adhesive shear modulus is highly sensitive to the value of the dimensionless end deflection β . Consequently, sensitive equipment must be used for measuring the beam end deflection. Provided that the specimen geometry is defined prior to the test by bearing in mind the shear stiffness investigated, the test can give reliable and accurate results.

Finally, an important conclusion is that the limitations defined in terms of specimen geometry and stiffness ratio in the parametric analysis and which concerned the shear deformation test as well as the end deflection test were confirmed experimentally. For that reason, it seemed essential to recall in the present section the origin, the nature and the consequences of these limitations.

If we compare the effect of geometrical quantities such as ℓ , h and t on curves (τ_{xy}^{\max} vs. E/G_a) and (β vs. E/G_a) in fig.19 to 21 and fig.28 to 30 respectively, we see that the curves move together from left to right as the slenderness ratio increases and the thickness ratio decreases. It is thus impossible to have, at the same time, the conditions required for a constant shear in the adhesive layer and those for a deflection highly sensitive to the variation of stiffness ratio. The parametric analysis showed that a constant shear state cannot be reached for the soft adhesive unless an unrealistic experimental design of the beam is used. Conversely, a highly sensitive deflection response is more favorable for soft adhesive. Then, a deflection measurement for soft adhesives will replace a shear deformation measurement for stiff adhesives. The BMC test can work, but the specimen dimension has to be defined in regard to the adhesive tested in order to make the theory suitable for practical

use. Simple numerical codes are available to facilitate the definition of the beams geometry in each situation. Hence, in order to evaluate the shear modulus with the bonded cantilever beams for the range of soft or stiff adhesives with a testing method satisfying the conditions of simplicity, reliability and rapidity, two different types of measurements must be made which proper procedure are recalled below :

SHEAR DEFORMATION MEASUREMENTS :

The analysis of the BMC theory revealed that the influence the parameter $\bar{\alpha}$ which contains both the material and the geometrical properties of the specimen has been shown to have a very significant effect on the magnitude and the uniformity of the shear stress in the adhesive. With the curve ($\bar{\alpha}$ vs. x/ℓ), a value of parameter $\bar{\alpha}$ is defined for which the shear stress is constant over a portion of the beam. In this particular region of the beam, the shear stress has a magnitude function of geometry and loading only. This is a requirement to facilitate the use and the analysis of the data provided from the shear deformation test. Then, the shear deformation is measured at the place of known shear stress and the shear strain is derived from the shear deformation as the ratio of the latter to the adhesive thickness. Due to the choice of $\bar{\alpha}$, the shear stress is predicted from simple theoretical formula. Finally, G_a is calculated using the classical linear relationship between shear stress and strain for elastic materials.

END DEFLECTION MEASUREMENTS :

The end deflection test permits the characterization of a large range of adhesives. For proper application, the user should bear in mind that the specimen geometry must be defined in accordance with the adhesive stiffness investigated. Guidelines showing the variations of the dimensionless end deflection β versus E/G_a can help to define appropriate specimen dimensions. Then, the BMC theory combined with end deflection measurements lead to a graphical determination of the adhesive shear properties.

RECOMMENDATIONS FOR FUTURE WORK :

Our recommendations to develop further the studies about the bonded cantilever plates test method are oriented towards four directions.

First of all, is the fact that in all our work, from the BMC analysis and the Finite Element analysis to experimental verifications of predictions, we always assumed the adhesive to be a linear elastic material. This has been done on account of the fact that the BMC theory was developed by assuming both the adherend and the adhesive to be linear elastic materials in order to facilitate the mathematical analysis. In reality, most of adhesives exhibit complex material characteristics like nonlinear and/or time dependent behavior that has to be taken into account in the analytical model as well as in the Finite Element analysis.

Secondly, in addition to these complex characteristics, the chemical and mechanical bonding between adherends and adhesive is not well understood for the majority of shear tests, so more particularly for the BMC test specimen. The interface layer between adherend and adhesive is not well defined in most of the cases although it can have an important influence on the determination of the mechanical properties of the bond. Attention must thus be concentrated on that problem.

Then, experiments showed that there is a lack in pursuing accurate shear deformation measurements on stiff beams. In order to solve that inconvenience, optical methods such as Scanning Electron Microscopy or a digital imaging strain measurement system [21,22] would be probably the best candidates.

Finally, the last recommendation concerns the development of mathematical solutions to model the shear stress in the adhesive layer of the modified BMC specimen presented in chapter 4 and also to provide the BMC concept the capacity of including fracture predictions for future application of the BMC specimen in fracture mechanics.

BIBLIOGRAPHY

1. R. A. KLINE, "Stress Analysis of Adhesively Bonded Joints", Adhesive Joints p. 587, 1982
2. H.F. BRINSON, "Durability (lifetime) Predictions for Adhesively Bonded Structures", Report No. VPI-E-87-18, CAS / ESM-87-6, Center for Adhesion Science, Virginia Tech, Blacksburg, VA (July 1987), Mechanical Behavior of Adhesive Joints (A.H. CARDON and G. VERCHERY eds.), p.3-25, Pluralis, Paris, 1987
3. E. MOUSSIAUX, A. H. CARDON, H. F. BRINSON, "Bending of a Bonded Beam as a Test Method for Adhesive Properties", Adhesion Science Review 1987 (H.F. BRINSON, J.P. WIGHTMAN, T.C. WARD eds), Adhesives and Sealants Research Institute, Blacksburg, VA (1987)
4. E. MOUSSIAUX, A. H. CARDON, H. F. BRINSON, "Bending of a Bonded Beam as a Test Method for Adhesive Properties", to be published in Mechanical Behavior of Adhesive Joints (A.H. CARDON and G. VERCHERY eds)
5. E. MOUSSIAUX, A. H. CARDON, H. F. BRINSON, "Bending of a Bonded Beam as a Test Method for Adhesive Properties", Report No.VPI-E-87-9, CAS / ESM-87-2, Center for Adhesion Science, Virginia Polytechnic Institute and State University, August 1987
6. E. MOUSSIAUX, "Bending of a Bonded Beam as a Test Method for Adhesive Properties", MS Thesis, Virginia Polytechnic Institute and State University, Blacksburg, VA, (1987)
7. GOLAND and REISNER, J. App. Mech., 11, A17, March 1944
8. K.L. DE VRIES, G.P. ANDERSON, SHARON, "Evaluation of Adhesive Test Methods", Adhesive Joints p. 269, 1982
9. G. P. ANDERSON, S. J. BENNET, K. L. DE VRIES, "Analysis and Testing of Adhesive Bonds", Academic Press, 1977
10. S. ROY, J.N. REDDY, "Nonlinear Viscoelastic Analysis Adhesively Bonded Joints", Report No. VPI-E-86.28, ONR, Department of Engineering Science and Mechanics, Virginia Polytechnic Institute and State University, Blacksburg VA, November 1987
11. MC DEVITT, BAUN, "The Three-Point Bend Test for Adhesive Joints", Adhesive Joints p. 381, 1982
12. SPIGEL, PRABHAKARAN, SAWYER, "An Investigation of the Iosipescu and Asymmetrical Four-Point Bend Tests", SEM, June 1985
13. V. WEISSBERG, M. ARCAN, "A Uniform Pure Shear Testing Specimen for Adhesive Characterization", Proceeding of ASTM D-14 Symponium, September 1986, STP in press
14. J.W. GRANT, "Measurement of In-Situ Adhesive Deformation Properties " - Adhesion Science Review 1 (1988), Edited by BRINSON, WIGHTMAN, WARD
15. K.M. LIECHTI, T. FREDA, T. HASAYI, "Determining the Constitutive and Fracture Properties of Structural Adhesives", Adhesion Science Review 1, Edited by BRINSON, WIGHTMAN, WARD
16. H. BECK, "Contributions to the Analysis of Coupled Shear Walls", ACI Journals, pp.1055-1069, August 1962
17. O.C. ZIENKIEWICZ, "The Finite Element Method", 3d ed., McGraw-Hill , pp.148-171, 1977
18. J.N. REDDY, "An Introduction to the Finite Element Method", McGraw-Hill, pp.149-152, 1984

19. S.P. TIMOSHENKO, J.N. GOODIER, *"Theory of Elasticity"*, 3rd ed., McGraw-Hill, pp.15-33
20. R.B. KRIEGER, *"Stiffness Characteristics of Structural Adhesives for Stress Analysis in Hostile Environment"*, American Cyanamid Company, October 1975
21. K.M. LIECHTI, *"High Temperature Adhesive Systems"*, Interim report, Hughes Aircraft Company, Electro-Optical & Data Systems Group, El Segundo, CA 90245, pp.4-22 to 4-28, February 1988
22. C. BURGER, *"Spectral Density Indication: a New Optical Method for Full Field Strain Analysis"*, Texas A and M University, College Station, Tx 77843
23. W.F. RANSON, *"Digital Metallographic Image Technique for Measuring Micro-Deformation"*, University of South Carolina, Mechanical Engineering Department, Columbia, SC 29208

Appendix A. Supplements to the parametric analysis

Listing of the program for computing the data points of the curves alpha bar versus E/Ga.

PARAMETRIC ANALYSIS : VARIATION OF ALPHA BAR WITH E/GA

```
*****
* This program has been written for the definition of the BMC      *
* specimen dimensions. The thickness ratio must be arbitrary chosen *
* and input for the execution of the program.                      *
* The run gives the variations of the parameter beta versus the   *
* ratio E/Ga for varying l/h values. Each curves is associated to *
* a specific value of l/h. This ratio varies from 10 to 170 with a *
* step of 10. The program provides the plane stress and the plane *
* strain options.                                                 *
*****
```

```
***** NOTATION *****
*   DTR   : Thickness ratio                                     *
*   DLR   : Slenderness ratio                                 *
*   DGA   : Stiffness ratio                                  *
*   DGAL  : Decimal logarithm of the stiffness ratio         *
*   ALPHAB : Parameter alpha bar                             *
*****
```

```
WRITE(5,100)
READ(6,*) DTR
WRITE(5,200)
READ(6,*) ICHOI1
DLR=10.
DO 20 J=1,17
A3=DLR**2
DGAL=0.
DO 10 I=1,43
C=DGAL
DGA=10**C
B1=(1.+2.*DTR)**2
A1=B1/DTR
A2=1.+(1./{3.*B1})
ALPHAB=((3.*A3*A1*A2)/DGA)**0.5
IF(ALPHAB.GT.80) GO TO 30
IF(ICOI1.EQ.0) GO TO 40
WRITE(7,300) J,DGA,ALPHAB
GO TO 30
40 WRITE(7,300) J,DGAL,ALPHAB
30 DGAL=DGAL+0.2
10 CONTINUE
DLR=DLR+10.
20 CONTINUE
100 FORMAT(2X,'Enter the thickness ratio')
200 FORMAT(2X,'To compute alpha bar versus log10 E/Ga,enter 0',
* /2X,'If you prefer to compute alpha bar versus E/Ga,enter 1')
300 FORMAT(2X,I2,2X,1PE15.7,2X,1PE15.7)
STOP
END
```

Listing of the program for computing the data points of the curves beta versus E/Ga.

PARAMETRIC ANALYSIS : VARIATION OF BETA WITH E/GA

```
*****
* This program has been written for the definition of the BMC      *
* specimen dimensions. The thickness ratio must be arbitrary chosen *
* and input for the execution of the program.                    *
* The run gives the variations of the parameter beta versus the   *
* ratio E/Ga for varying l/h values. Each curves is associated to *
* a specific value of l/h. This ratio varies from 20 to 170 with a *
* step of 10. The program provides the plane stress and the plane *
* strain options.                                                *
*****
```

```
***** NOTATION *****
*   DTR   : Thickness ratio                                     *
*   DLR   : Slenderness ratio                                 *
*   DGA   : Stiffness ratio                                  *
*   DGAL  : Decimal logarithm of the stiffness ratio         *
*   ALPHAB : Parameter alpha bar                             *
*****
```

```
IMPLICIT REAL*(A-H,O-Z)
WRITE(5,100)
READ(6,*) DTR
DE=1.E+07
DA=0.3
DB=1.
DP=100.
WRITE(5,200)
READ(6,*) ICHOIC
IF(ICH0IC.EQ.0) GO TO 10
```

* PLANE STRESS ANALYSIS *****

```
WRITE(7,300)
WRITE(7,400)
DLR=20.
DO 20 J=1,16
A1=1.+2.*DTR
A2=A1**2
A3=1.+((3.*A2)**(-1))
A4=A2/DTR
A5=(DLR)**2
DGAL=0.
DO 30 I=1,18
DGA=10**DGAL
ALPHAB=(3*A5*A4*A3/DGA)**0.5
XL=150.
IF(ALPHAB.GT.XL) GO TO 40
CO=(EXP(ALPHAB)+EXP(-ALPHAB))/2.
SI=(EXP(ALPHAB)-EXP(-ALPHAB))/2.
TA=SI/CO
GO TO 50
40 TA=1.
```

** END DEFLECTION OF THE BEAM *****

```
50 F1=(1.+DTR)**3
   F3=4.*(1.-(1./A3))
   F4=3.*(1.+DA)*(DLR**(-2))
   F5=12./A3
   F6=(1.-(TA/ALPHAB))/(ALPHAB**2)
   F7=F5*F6
   BETA=(F3+F4+F7)*F1
   WRITE(7,500) J,DGAL,BETA
   DGAL=DGAL+0.5
30 CONTINUE
   DLR=DLR+1.
20 CONTINUE
   GO TO 60
```

* PLANE STRAIN ANALYSIS *****

```
10 DE=DE/(1.-(DA**2))
```

** END DEFLECTION OF THE BEAM *****

```
WRITE(7,400)
WRITE(7,600)
DLR=20.
DO 70 J=1,16
  A1=1.+2.*DTR
  A2=A1**2
  A3=1.+((3.*A2)**(-1))
  A4=A2/DTR
  A5=(DLR)**2
  DGAL=2.
  DO 80 I=1,13
    DGA=10**DGAL
    ALPHAB=(3*A5*A4*A3*(1-da**2)/DGA)**0.5
    XL=150.
    IF(ALPHAB.GT.XL) GO TO 90
    CO=(EXP(ALPHAB)+EXP(-ALPHAB))/2.
    SI=(EXP(ALPHAB)-EXP(-ALPHAB))/2.
    TA=SI/CO
    GO TO 95
90 TA=1.
```

** END DEFLECTION OF THE BEAM *****

```
95 F1=(1.+DTR)**3
   F3=4.*(1.-(1./A3))
   F4=3.*(1.+DA)*(DLR**(-2))
   F5=12./A3
   F6=(1.-(TA/ALPHAB))/(ALPHAB**2)
   F7=F5*F6
   BETA=(F3+F4+F7)*F1
   WRITE(7,500) J,DGAL,BETA
   DGAL=DGAL+0.5
80 CONTINUE
   DLR=DLR+10.
70 CONTINUE
   GO TO 60
```

* FORMATS *****

```
100 FORMAT( /2X,'Enter t/h')
200 FORMAT( /2X,'For plane stress analysis enter 1 else 0')
300 FORMAT( /2X,'Plane stress analysis')
400 FORMAT(/10X,'E/Ga',25X,'Beta')
500 FORMAT( /2X,I2,2X,1PE15.7,12X,1PE15.7)
600 FORMAT( /2X,'Plane strain analysis')
60 STOP
   END
```

Execs for plotting outputs

In order to plot the results generated by the preceding routines, the user can invoke the SAS Graphics package provided by SAS Institute Inc.. This package can be accessed by writing SAS plot commands in a plot data file such as that presented below.

```
//boxnumber JOB account number,USERID,REGION=1536K
/*PRIORITY IDLE
//STEP1 EXEC SAS
/*JOBPARM L=5
/*ROUTE PRINT VTVM1.userid
GOPTIONS DEVICE=VER80 HSIZE=6 VSIZE=6 NOTEXT82 VPOS=43;
DATA ONE;
INPUT GROUP1 X Y;
CARDS;

          **** ENTER THE OUTPUT ****

PROC GPLOT;
TITLE1 C=BLACK F=XSWISS H=1
          ' comments ';
FOOTNOTE1 C=BLACK F=XSWISS H=1
          ' comments ';
FOOTNOTE2 C=BLACK F=XSWISS H=1
          ' t/h = ... ';
AXIS1 LABEL = (A=90 F=XSWISS H=1. ' legend ')
      VALUE = (F=XSWISS H=1 )
      color = black
      MINOR = NONE;
AXIS2 LABEL =(F=XSWISS H=1 ' log10 E/Ga ')
      VALUE = (F=XSWISS H=1 )
      COLOR = BLACK;
PLOT Y*X=GROUP1/
OVERLAY FRAME NOLEGEND VAXIS=AXIS1 HAXIS=AXIS2;
SYMBOL1 C=RED L=1 I=SPLINE V=NONE;
SYMBOL2 C=RED L=1 I=SPLINE V=NONE;
SYMBOL3 C=RED L=1 I=SPLINE V=NONE;
SYMBOL4 C=RED L=1 I=SPLINE V=NONE;
/*
//
```

In the following figures are given guidelines for determining the proper BMC specimen geometry in order to perform shear deformation or end deflection tests.

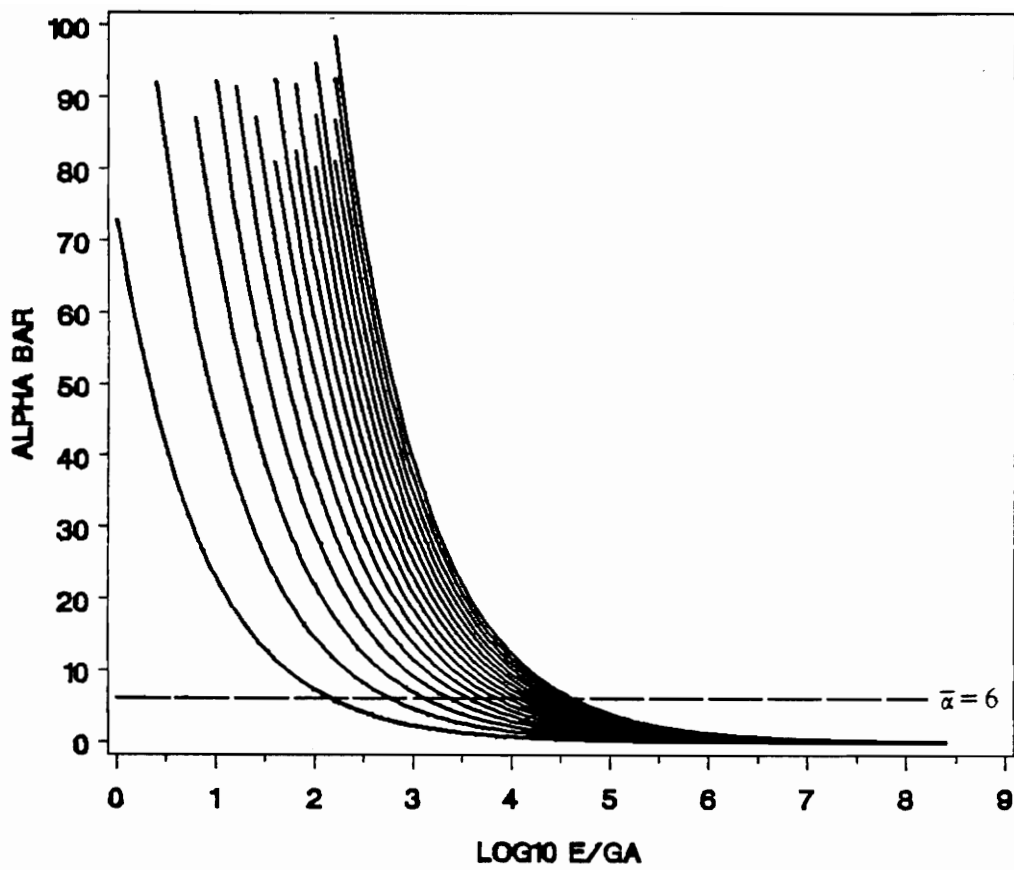


Figure 116. Parametric analysis for alpha bar versus E/Ga with t/h = 0.1. From left to right, l/h varies from 10 to 170 in steps of 10 between each curves.

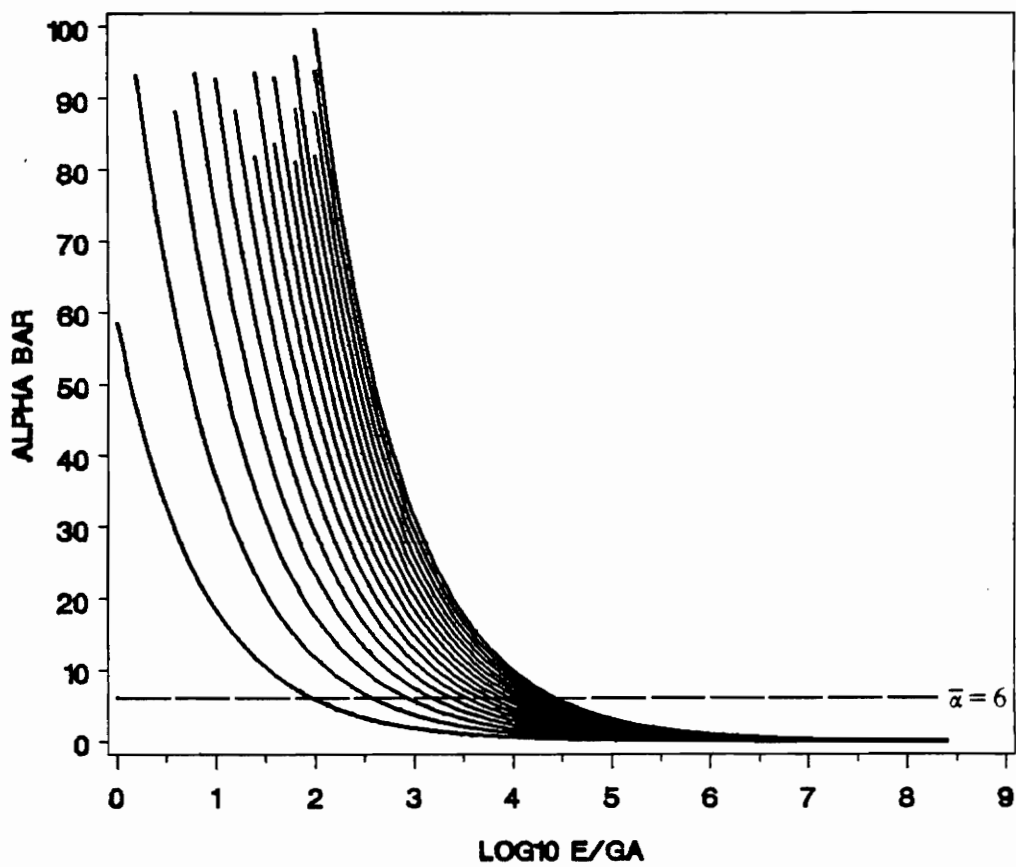


Figure 117. Parametric analysis for alpha bar versus E/Ga with $t/h = 0.2$. From left to right, l/h varies from 10 to 170 in steps of 10 between each curves.

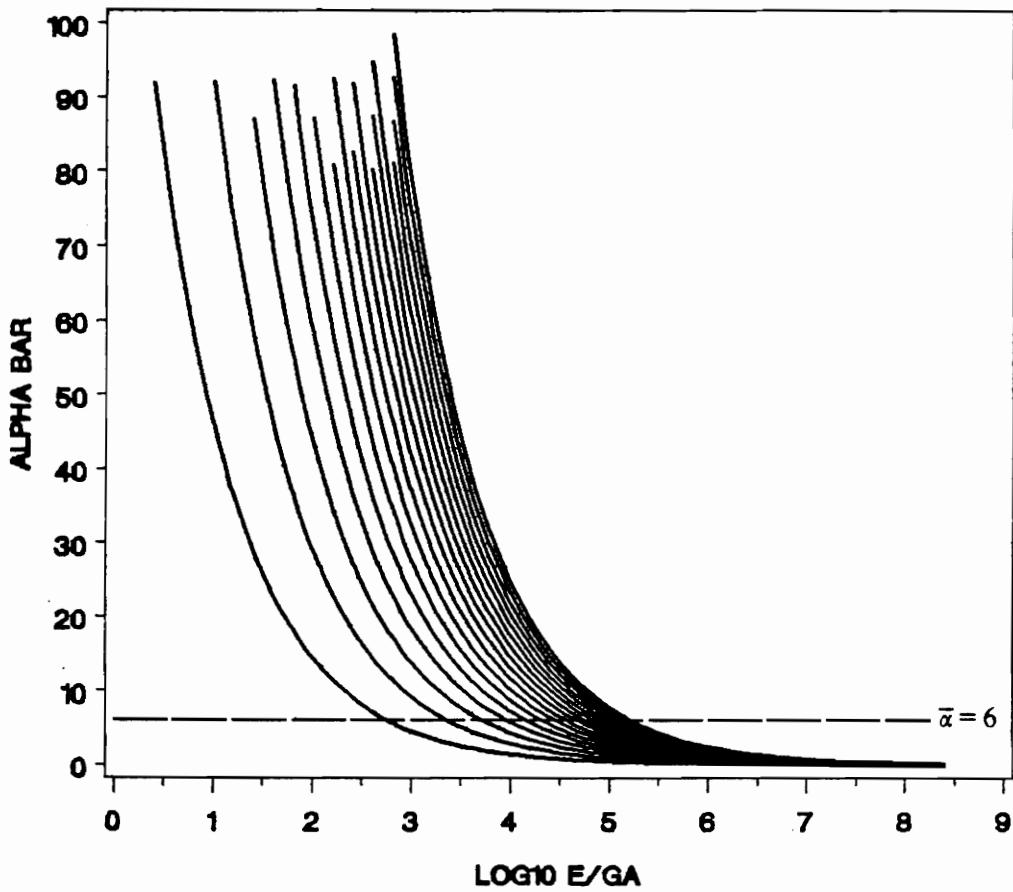


Figure 118. Parametric analysis for alpha bar versus E/Ga with $t/h = 0.02$. From left to right, l/h varies from 10 to 170 in steps of 10 between each curves.

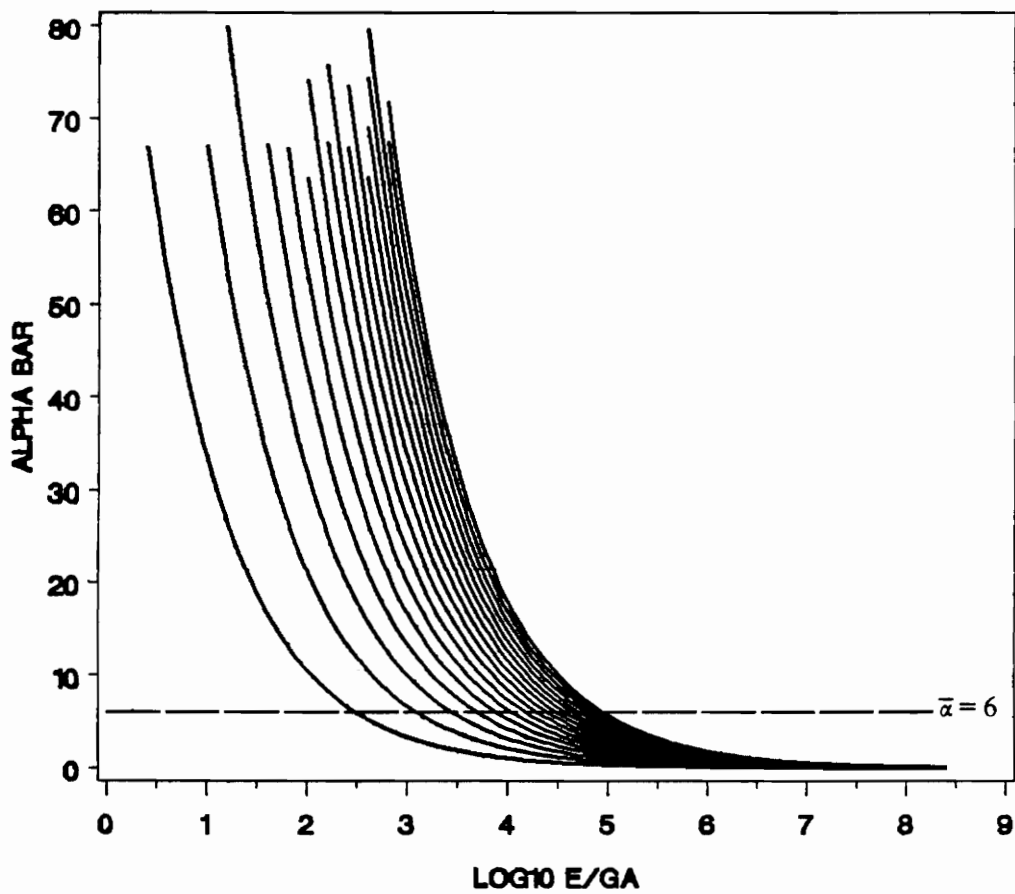


Figure 119. Parametric analysis for alpha bar versus E/Ga with $t/h = 0.04$. From left to right, l/h varies from 10 to 170 in steps of 10 between each curves.

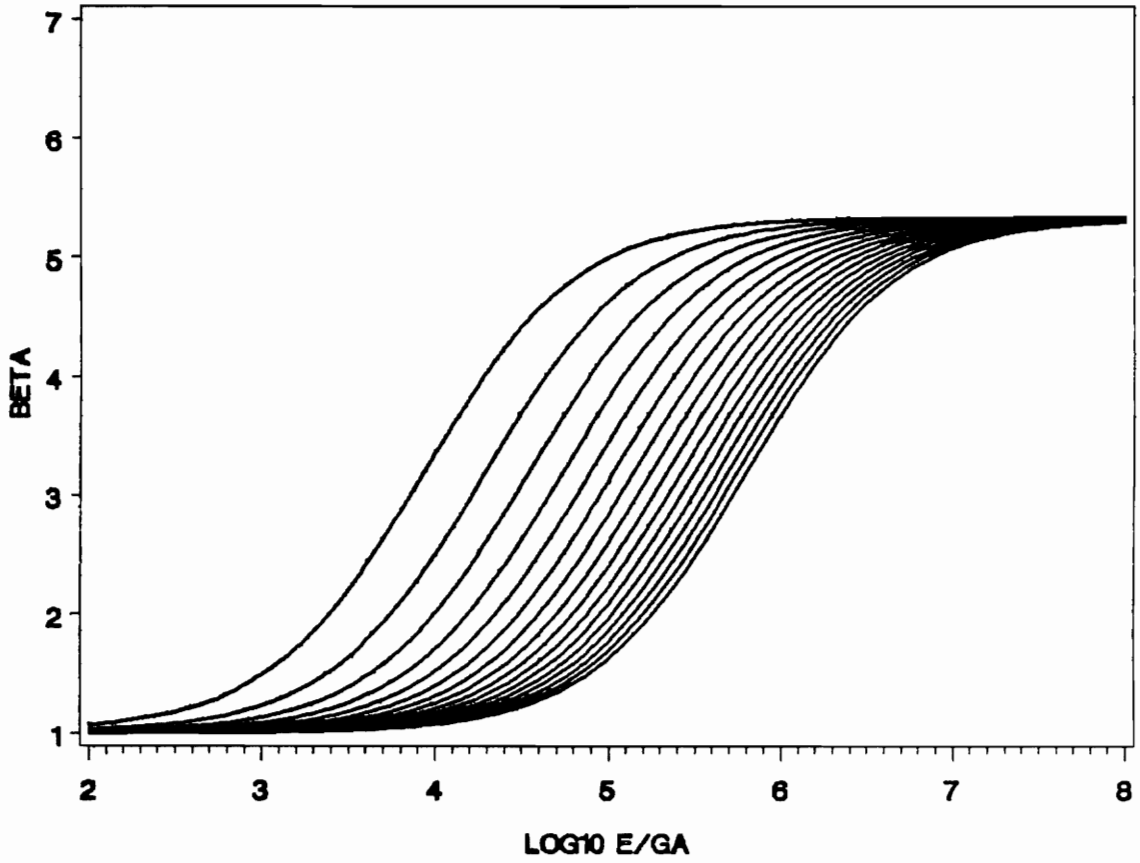


Figure 120. Parametric analysis for beta versus E/Ga with $t/h = 0.1$. From left to right, l/h varies from 20 to 170 in steps of 10 between each curves.

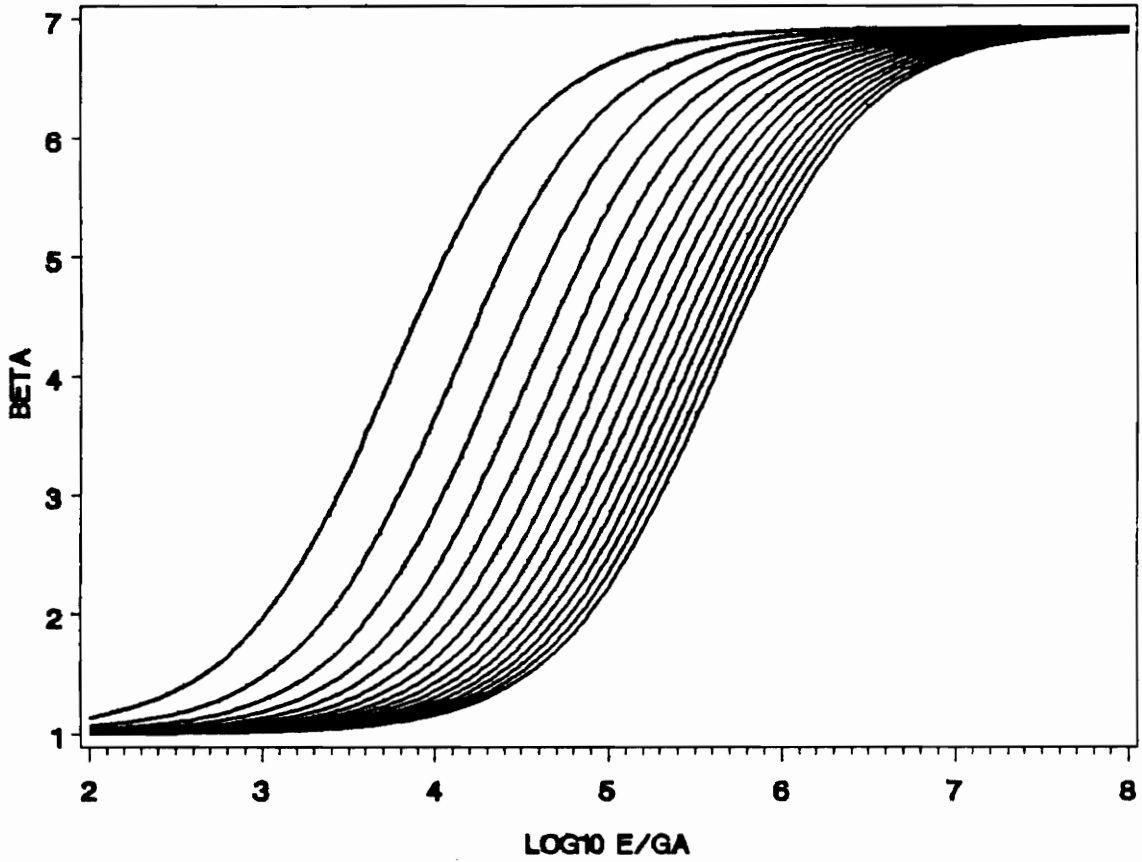


Figure 121. Parametric analysis for beta versus E/Ga with $t/h = 0.2$. From left to right, t/h varies from 20 to 170 in steps of 10 between each curves.

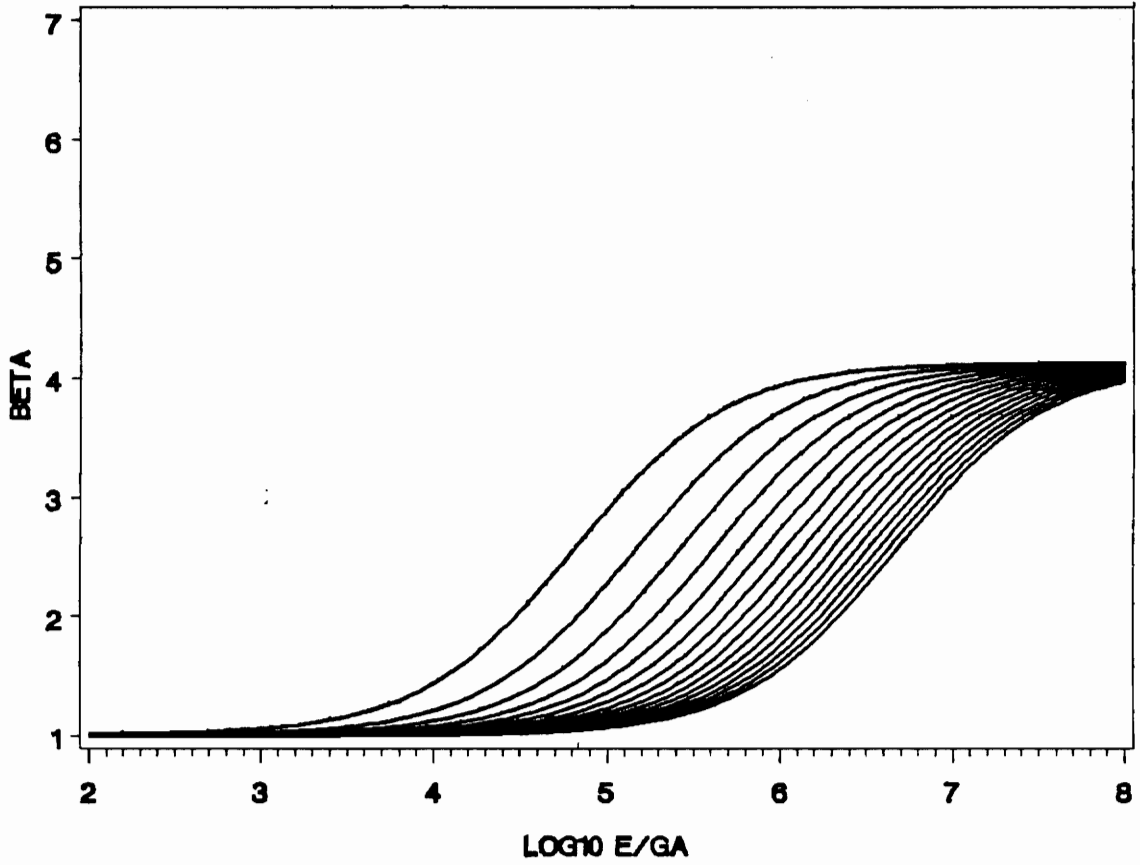


Figure 122. Parametric analysis for beta versus E/Ga with $t/h = 0.01$. From left to right, t/h varies from 20 to 170 in steps of 10 between each curves.

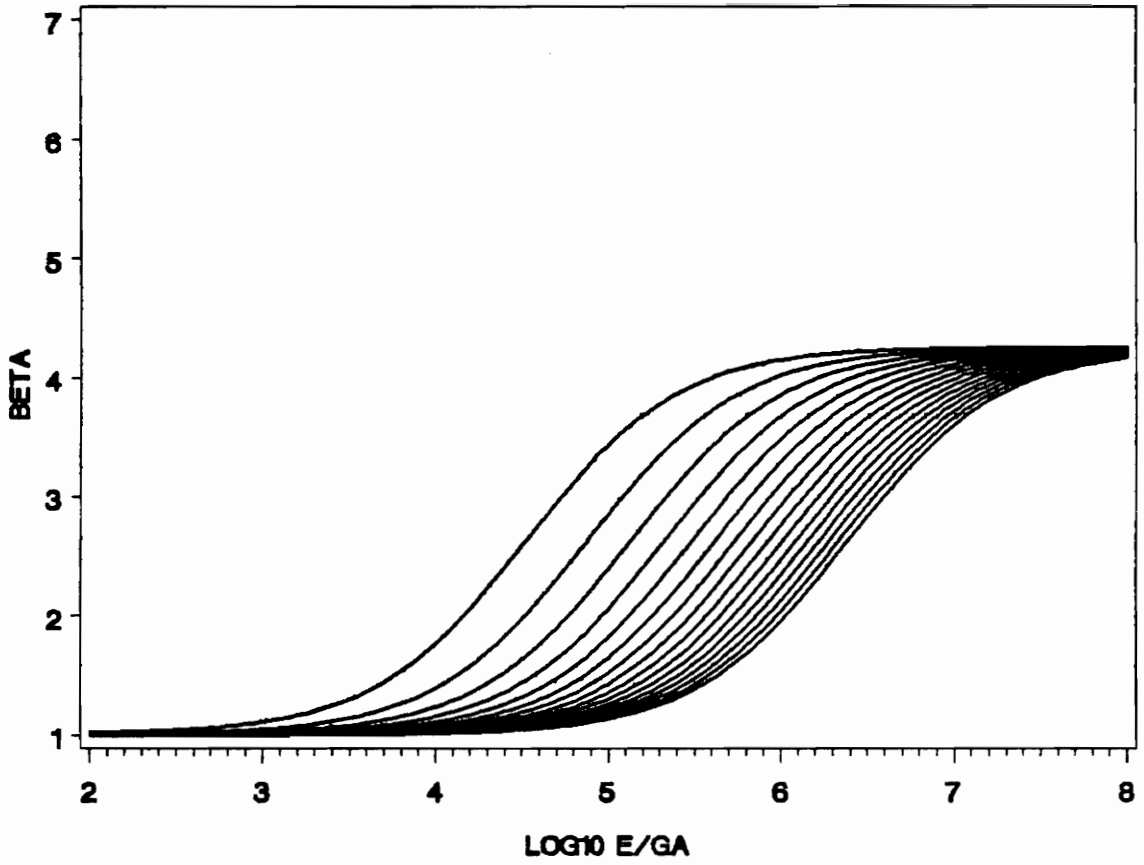


Figure 123. Parametric analysis for beta versus E/Ga with $t/h = 0.02$. From left to right, l/h varies from 20 to 170 in steps of 10 between each curves.

Vita

The author was born on January 2nd ,1965 in Paris, France. She studied at the Universite de Technologie de Compiegne (UTC) as a student in the Mechanical Engineering, majoring in materials behavior. In addition to her engineering studies and during her final year of education at the UTC, she prepared a diploma of research studies (DEA) in the area of materials damage. She moved to the United-States of America in February 1987 to undergo a 6-month training period at Virginia Polytechnic Institute and State University as part of her French degrees requirement. She then enrolled in the Engineering Science and Mechanics graduate program in September 1987 to pursue a Master of Science degree.